Materials Horizons: From Nature to Nanomaterials

Subhash Singh
Kartikey Verma
Chander Prakash *Editors*

Advanced Applications of 2D Nanostructures

Emerging Research and Opportunities

Springer

Materials Horizons: From Nature to Nanomaterials

Series Editor

Vijay Kumar Thakur, School of Aerospace, Transport and Manufacturing, Cranfield University, Cranfield, UK

Materials are an indispensable part of human civilization since the inception of life on earth. With the passage of time, innumerable new materials have been explored as well as developed and the search for new innovative materials continues briskly. Keeping in mind the immense perspectives of various classes of materials, this series aims at providing a comprehensive collection of works across the breadth of materials research at cutting-edge interface of materials science with physics, chemistry, biology and engineering.

This series covers a galaxy of materials ranging from natural materials to nanomaterials. Some of the topics include but not limited to: biological materials, biomimetic materials, ceramics, composites, coatings, functional materials, glasses, inorganic materials, inorganic-organic hybrids, metals, membranes, magnetic materials, manufacturing of materials, nanomaterials, organic materials and pigments to name a few. The series provides most timely and comprehensive information on advanced synthesis, processing, characterization, manufacturing and applications in a broad range of interdisciplinary fields in science, engineering and technology.

This series accepts both authored and edited works, including textbooks, monographs, reference works, and professional books. The books in this series will provide a deep insight into the state-of-art of Materials Horizons and serve students, academic, government and industrial scientists involved in all aspects of materials research.

More information about this series at http://www.springer.com/series/16122

Subhash Singh · Kartikey Verma · Chander Prakash
Editors

Advanced Applications of 2D Nanostructures

Emerging Research and Opportunities

Springer

Editors
Subhash Singh
Department of Production and Industrial Engineering
National Institute of Technology Jamshedpur
Jamshedpur, Jharkhand, India

Chander Prakash
School of Mechanical Engineering
Lovely Professional University
Jalandhar, Punjab, India

Kartikey Verma
Department of Chemical Engineering
Indian Institute of Technology Kanpur
Kanpur, Uttar Pradesh, India

ISSN 2524-5384 ISSN 2524-5392 (electronic)
Materials Horizons: From Nature to Nanomaterials
ISBN 978-981-16-3321-8 ISBN 978-981-16-3322-5 (eBook)
https://doi.org/10.1007/978-981-16-3322-5

This Springer imprint is published by the registered company Springer Nature Singapore Pte Ltd.
The registered company address is: 152 Beach Road, #21-01/04 Gateway East, Singapore 189721, Singapore

Series Editor's Preface

In an attempt to cover the span of research interests, the book entitled "Advanced Applications of 2D Nanostructures: Emerging Research and Opportunities" encompasses a thorough investigation on two-dimensional materials. The authors included a range of topics from the history, evolution of 2D materials, the recent advancements as well as the future prospects associated with them. The most captivating part is the simplicity with which the book is written and the spectrum of topics discussed. For scientific researchers, this book provides a platform to brush up and enhance their knowledge on the topics of two-dimensional materials, inspiring them for new discoveries in the field. For the non-scientists, this book serves as an encyclopaedia providing them with all the fundamentals, applications and the advances pertaining to two-dimensional materials. The material in the book has been clearly illustrated through written text and pictures. This book can stimulate interest in undergraduates, postgraduates and budding researchers. It is a compilation of explanatory notes on molecular structures, synthesis techniques and developments. Additionally, limitations can help students unleash the existing research opportunities by overcoming the barriers associated with them. Thus, it can be understood by pupils of any level of education. Lastly, this book gives a bird's eye view on 2D nanostructures, its wide applications in the area of supercapacitors, solar cells and biosensors, etc.

I am immensely proud of Dr. Subhash Singh and Dr. Kartikey Verma for their endeavours to compile information on this trending topic. This book is an illustration of their hard work which will be a brick in the future evolution of many intellect minds pouring across the world in this line of research. I also appreciate all the authors who made their valuable contributions to the individual chapters. I sincerely wish them the very best for their future endeavours.

Vijay Kumar Thakur
Associate Professor
Enhanced Composites and Structures Centre
School of Aerospace, Transport
and Manufacturing
Cranfield, UK

Preface

The editors are delighted to present the high-quality research content of book series *Materials Horizons: From Nature to Nanomaterials* in first edition book *Advanced Applications of 2D Nanostructures: Emerging Research and Opportunities*. Book title was chosen as it converges upcoming technologies in all science and engineering disciplines for the next decade. This book will be one of the biggest breakthroughs to bring together the researchers, scientists, engineers, scholar and students from all areas of engineering and sciences science exclusively dedicated to nanostructured 2D materials and nanocomposites. We hope that this book will be extremely useful to researchers and students working in this diversified field. Basically, this book emphasizes the current advancement in interdisciplinary research on introduction, origin, processing, morphology, structure and noble properties of nanostructured 2D materials and nanocomposites and their applications in various fields of engineering and sciences. We try our best in bringing together a panel of highly accomplished experts in the field of nanostructured 2D materials and their nanocomposites in formulation of this manuscript.

Since the exfoliation of graphene in the year 2004, a new material class comprising of sheet-like structure has come into existence. They earned their name as two-dimension (2D) materials precisely due to this structure with thickness equal to that of a single atom. The unique properties exhibited by them have garnered the attention of researchers across the world. The tremendous scope for exploitation of these characteristics has enforced rapid advancements in the field of 2D materials. The discovery of graphene (2D material having single atomic layer of carbon) opens up the possibility of other layered materials and structures. An exceptional characteristic of layered materials is their ability to accommodate various ions and molecules between their layers, a phenomenon known as intercalation. Intercalation compounds of inorganic hosts (graphite, clays, dichalcogenides and others) have also gained renewed interest owing to their unique chemical and physical properties. De-intercalation of those compounds under certain conditions (such as thermal shock) as well as sonication or volume expansion reactions in the interlayer space led to the formation of widely used exfoliated graphite and two-dimensional (2D) materials with unusual electronic properties. Recently, a large family of 2D materials, labelled MXenes,

was produced by the extraction of the A-element from the layered ternary carbides, such as Ti_3AlC_2 and other MAX phases. For developing these multifunctional materials for energy storage/generation, some renewed synthesis techniques and characterization efforts required. Further, exploration of alternative sustainable energy resources such as solar energy, geothermal power, biomass/biofuel and hydrogen energy is extremely important for the sustainable development of human civilization. Hydrogen is considered as one of the efficient and most likely future fuels, and there have been continued efforts to develop a hydrogen-based energy economy. However, the current hydrogen production mainly depends on the steam reforming technique, which is not a sustainable route, owing to the high energy involved in the process, in addition to CO_2 being the by-product. Hence, it has become extremely important to come up with breakthrough discoveries in the area of solar photovoltaics, especially on the development of highly efficient and low-cost electrocatalysts to replace the state-of-the-art precious metals—based hydrogen evolution reaction (HER) catalysts. Nanostructures of layered transition metal carbides and nitrides show promising electrocatalytic activity towards energy storage and hydrogen evolution reaction. Keeping this as the central theme, the editors/authors are proposing to explore several topics related to energy generation, conversion and storage with novel atomically thin 2D materials and their hetero-structures.

An early transition 2D nanomaterial, MXene, has recently come into the existence after graphene with so many exorbitant properties mainly related to energy storage-type material. Several scientists across the globe are working with 2D materials. This carbide belongs to the MAX phases which have a chemical formula $M_{n+1}AX_n$ where M is an early transition metal, A is an A-group element, and X is carbon or nitrogen. The crystal structure of MAX phases can be described as octahedral ternary metal carbide and/or nitride sandwiched by close-packed layers of A-element. One of the most widely studying and a promising members of this family is Ti_3AlC_2 among 70 MAX phases those are currently known. MXenes are expected to be applied extensively in many such promising anode materials for lithium-ion battery, hydrogen storage materials, high capacitors electrode materials and lead adsorption material.

The chapters included in this book highlight impactful research in the field of nanostructured 2D materials. Chapter 1 focuses on the initial developments leading to the discovery of 2D materials. A detailed description providing insights into the nature of 2D materials is broadly discussed. The classification of this new material class is listed. Moreover, the nature of growing interests in this field and the reasons behind this are reported. The research on 2D materials is still in the initial stages. Therefore, it is essential to understand the challenges and limitations in this field. A section in this chapter focuses on various prospects and challenges faced which provides the researches an idea before entering into the analytics of 2D materials. Overall, the entire chapter gives an overview on 2D materials, and it acquaints the readers to this new generation materials. Chapter 2 covers different types and intense classification of 2D materials in detail. An account of their various properties, synthesis methods, functionalization methods and applications will be given in this chapter. These materials possess unique optical, electrical and catalytic activity.

These properties have been exploited in various applications such as sensing, catalysis and in energy generation. 2D materials encompass a large family of materials which includes graphene family, oxide family and metal dichalcogenides.

In present scenario, 2D materials are attaining significant attraction from both technological and fundamental science aspect owing to their chemical, physical, magnetic and electronic characteristic differences over conventional bulk material. In Chap. 3, the author critically discussed different methods for production of 2D materials. Methods are broadly classified as mechanical and chemical exfoliation methods. The mechanical exfoliation provides versatility and low cost, whereas chemical exfoliation provides chemical homogeneity and molecular-level mixing. The synthesis and fabrication processes control the morphology and size of product which further improves the performance of 2D NSMs in different applications.

Sensors have wide application in various fields. Chapter 4 is based on the research developments regarding the synthetic background, physicochemical studies and applications in the field of sensor and catalysis. The synthetic pathway generally follows the improved hummers method and further chemical modifications as per requirement for the target applications. ^{13}C-NMR, IR, AFM, TEM, RAMAN, XPS and BET studies reveal about structure, surface topology, chemical and elemental composition of graphene oxide. The applications broadly focused in this chapter are sensing of ascorbic acid, pesticide detection and detection of diseases affected DNA. Further, its usage as a reusable heterogenous catalyst for the synthesizing important biological molecules and catalytic degradation of organic dyes.

The significance of nanocoatings is that they form a protective barrier between the material and the atmosphere serving both the aesthetics as well as preserving the material properties (chemical, mechanical and tribological). Hence, nanocoatings and thin films have a spectrum of applications in the manufacturing sector, tooling, electronics, biomedical, etc. Chapter 5 briefly explains the coating techniques entailing the properties of 2D materials correlating the relevance of 2D materials as nanocoatings and thin films.

There is a new buzz in the scientific community about a novel two-dimensional material called Mxene, which after graphene has attracted many a minds due to its unique mechanical, electrical and primarily electrochemical properties, thus predicting its widespread utility in next-generation highly efficient electrochemical devices for energy storage and delivery which are the need of the hour due to our increasing dependence on small-scale portable electronic devices, medium-scale utility in electric vehicles and large-scale standalone or grid-connected power storage units. Chapter 6 highlights these aspects of MXene for next-generation energy storage materials for batteries and supercapacitors, whereas transparent conductive electrodes have been a crucial element in interactive devices like touch panels and smart phones. MXene TCEs can be the best material for high-performance supercapacitors and transparent conductive electrodes explained in Chap. 7.

Chapter 8 emphasizes on gas detection capabilities of metal oxide (MO) species embedded in thin films engaged in the phenomena of absorption, chemical reaction and desorption of analyte gases at elevated temperatures, could confirm the importance of the nanostructured species existing at the reaction sites. For better sensitivity

of the gas detection, it became a normal practice of increasing the surface area of interaction by making the sensing film as porous as practically possible. Simultaneously, the developments of 2D material families including graphene and the related nanomaterials along with a large variety of layered metal oxide nanosheets (MO-NSs) were also found extremely useful in using them as such or in the nanocomposite forms to replace the above-mentioned species. A large variety of synthesized single-/multiple-layered MO-NS films conjugated with different types of inorganic and organic molecules have been exhibiting additional advantages due to their programmable physicochemical properties in comparison with their nanoparticulate and one-dimensional counterparts.

Chapter 9 "Modeling and Simulation of Nano-Structured 2D Materials" entails typical simulation techniques which can be used for assessing different carbonous and non-carbonous nanomaterials. It will also enable to understand the various possibilities for surface modification and evaluation of properties of the characteristic nanomaterials. The use of different molecular dynamic simulation techniques simplified the validation of possible nanostructures and evaluation of their mechanical, physical and chemical *properties.* Chapter 10 specifically focuses on corrosive nature of some nanostructured 2D materials for advanced applications in the form of nanocoatings and thin films. Fundamental strategies for corrosion protection have been briefly reviewed, followed by exploration on role of protective coatings for corrosion prevention. Keeping in view different functional requirements, essential characteristics for an ideal anti-corrosion coating have been chalked out.

Chapter 11 entitled "Nanostructured 2D materials for Biomedical, Nano Bioengineering, and Nanomechanical Devices" addresses the recent renovations and the existing studies of 2D materials for biosensing, drug/gene delivery, antimicrobial activity, bioimaging and other multimode therapeutic applications. We would put special emphasis on the extensive flexibility of various rational combinations of 2D materials superior properties for the design and construction of assorted forms of reagents or devices with highly effective simultaneous diagnostic and therapeutic functions.

In continuation to biomedical application of 2D nanomaterials, one of the most important applications is the therapeutic application through proper understanding of the toxicity profile of the material can be utilized in vitro and in vivo experimentation as explained in Chap. 12. Also, another future biomedical application is in vivo gene transformation. Various researchers found that 2D nanomaterials could serve like in vitro gene transformation vector. An application in biomolecules detection and drug delivery could be development of a latest and scalable training procedure for inerratic nanomaterials synthesis.

"Mechanical performance of 2D Nanomaterials-Based Advanced Composites" Chap. 13 highlights results associated with the mechanical properties of 2D nanomaterials and their composites for advanced structural applications. The 2D nanomaterials thus produced are extra light in weight and high in strength and stiffness. This is why these nanomaterials find application in the area of aerospace and construction works.

The book's content is multifaceted and multidisciplinary having 2D nanostructures as central theme of the book. The variety of models presented in the book are up to date and potentiality valuable to researchers, scientist, scholars in all engineering and science disciplines, such as the areas of chemical engineering, nanotechnology, mechanical engineering and medical science, electronics engineering, chemistry and physics. We are sure that everyone will be benefited with information provided in this book.

Jharkhand, India — Subhash Singh
Kanpur, India — Kartikey Verma
Phagwara, India — Chander Prakash

Acknowledgements

We express our heartfelt gratitude to *Springer Nature Singapore* and the editorial team for their aspiring guidance and support during the preparation of this book. We are sincerely grateful to reviewers for their suggestions and illuminating views on research content presented in this book *Advanced Applications of 2D Nanostructures: Emerging Research and Opportunities.*

We are thankful to Prof. Karunesh Kumar Shukla, Director, National Institute of Technology, Jamshedpur, and Prof. S. B. Prasad, Head, Department of Production and Industrial Engineering, National Institute of Technology, Jamshedpur, for encouragement and their support. Our sincere thanks to Prof. Vijay Kumar Thakur, Enhanced Composites and Structures Centre, School of Aerospace, Transport and Manufacturing, Cranfield University, Cranfield, UK, for guiding us at different stages of this project. Our gratitude to Prof. Raju Kumar Gupta, Associate Professor, Department of Chemical Engineering, Indian Institute of Technology, Kanpur, Uttar Pradesh, India, for encouragement and support throughout working on this book. Our sincere thanks to Prof. Kaushik Pal, Department of Mechanical and Industrial Engineering, Joint Faculty Centre of Nanotechnology, Indian Institute of Technology, Roorkee, Uttarakhand, India, for providing constant ideas of innovation for chapters. Special thanks to Dr. Ashwani Kumar, Department of Technical Education (Ministry of Technical Education) Government of Uttar Pradesh, India, for sharing his research experience and views on final draft of this book project.

Jharkhand, India — Subhash Singh
Kanpur, Uttar Pradesh, India — Kartikey Verma
Phagwara, India — Chander Prakash

Introduction

In the present era of modern science and engineering, when technology is discussed, the roots go back to the understanding of material systems. It is often debated that properties of materials are based on what the material is made of. However, it is not only the composition but also the size and dimensionality of the materials that decides its behaviour. This is substantially true for some materials when their dimensions are reduced to nano-scale; i.e., their size can be expressed in nanometres. In the prevailing times of nanotechnology, materials can be easily engineered in the nano-scale. The analysis on materials is done by having at least one of the dimensions at nano-scale. The materials synthesised at nano-scale may be classified based on their dimensionality restraint on one of the dimensions produces a 2D material with sheet structure. Restraining two dimensions in terms of their size, 1D material is obtained, and when all the dimensions are restrained to nano-scales, 0D materials are produced. Structures with nano-metric dimensions shaped into zero-, one- or two- dimensional materials have radically different properties. Hence, it can be authoritatively established that apart from a material's atomic structure its material characteristics are also influenced by its dimensions.

In this context, it can be said that the nanostructures of carbon are an integral and a vital part of nanotechnology. It is the initially discovered carbon nanotubes (CNTs) and fullerene that enforced research development in the direction of 2D materials. It is post this discovery that attempts have been made to isolate the two-dimensional materials of graphite. Finally, in the year 2004, the attempts paved way and a breakthrough was achieved in successfully isolating graphene. Graphene possessed distinctive characteristics which initially elicited unmatched attention towards its two-dimensional sheet like structure and characterizations. Subsequently, research on remaining non-carbon-based elements grew. Therefore, the 2D materials gathered much interest within the recent past rendering outstanding electronic, mechanical and optical properties for various practical applications. Their unique features with emerging prospects in various engineering fields have inclined the interests of researchers across the world towards 2D materials. This eventually guided to the isolation of many 2D materials in the span of a decade.

The research advancements extended the discovery of 2D materials in carbides and nitrides. Rare characteristics (physical) are observable in the nanostructured 2D materials when charge and heat transmission are established to one single plane. Hence, the structure of 2D materials is extensively reviewed. It is in the field of electronics that 2D materials exhibit encouraging prospects. It is deemed that 2D materials are capable enough to replace silicon in various photonics, electronics and nano-electromechanical systems in the coming years. This is due to the fact that 2D materials unveil an exceptional range of optical, thermal as well as electronic characteristics. A whole new system of electronic devices can be generated through the 2D materials.

This book focuses on the initial developments leading to the discovery of 2D materials. A detailed description providing insights into the nature of 2D materials is broadly discussed. The classification of this new material class is listed. Moreover, the nature of growing interests in this field and the reasons behind this are reported. Therefore, it is essential to understand the challenges and limitations in this field. A section in this book focuses on various prospects and challenges faced which provides the researcher an idea before entering into the analytics of 2D materials. The applications of 2D materials have gained popularity in electronics, biomedicine, biosensors, water purification, energy storage devices and electrochemical sensors, etc. Overall, the entire book gives an in-depth knowledge on 2D materials and their applications which acquaint the readers to this new generation materials.

Contents

Editors and Contributors

About the Editors

Dr. Subhash Singh is currently working as Assistant Professor in Department of Production & Industrial Engineering, NIT Jamshedpur. He completed his PhD from Indian Institute of Technology Roorkee in 2017. He has over 8 years of teaching experience in various institutions/universities. He specializes in the areas of modification of nano materials, thin coating, Synthesis of nanocrystalline spinel, metal matrix composites (MMCs), synthesis of 2D materials, friction stir processing (FSP), and unconventional machining of biodegradable materials. He has over twenty research publications in various prestigious international journals and authored eight book chapters. Currently, two research projects are running under his supervision funded by SERB (DST) and IUSSTF.

Dr. Kartikey Verma has been working as Young Scientist Fellow (DST Young Scientist Fellow) in Department of Chemical Engineering at Indian Institute of Technology, Kanpur, India. He received his Ph.D. in Physics from University of Lucknow, Lucknow, Uttar Pradesh, India. His research interests include processing and characterization of thin films, polymer matrix composites, nanocomposites, bio-based polymers and carbon based materials for barrier properties, packaging and energy storage material. He has published more than 20 research papers in several international journals, along with more than 25 publications in proceedings of international/national conferences.

Dr. Chander Prakash is Associate Professor in the School of Mechanical Engineering, Lovely Professional University, Jalandhar, India. His area of research is biomaterials, rapid prototyping & 3-D printing, advanced manufacturing, modeling, simulation, and optimization. He has more than 12 years of teaching experience and 6 years research experience. He authored 60 research papers and 25 book chapters. He has written more than 150 research articles for various journals and conferences. He has edited 19 Books for Springer, Elsevier, and CRC Press. He has authored 1

book with World Scientific Publisher. He is also the series editor of "Sustainable Manufacturing Technologies: Additive, Subtractive, and Hybrid" with CRC Press.

Contributors

Neha Ahlawat Department of Mathematics, Jaypee Institute of Information Technology, Noida, Uttar Pradesh, India

Faisal Ahmad Iris Worldwide, Gurugram, Haryana, India

Shamim Ahmad JCB University of Science and Technology, YMCA, Faridabad, Haryana, India

Nazish Alam Department of Production and Industrial Engineering, National Institute of Technology Jamshedpur, Jharkhand, India

Tushar Banerjee Department of Production and Industrial Engineering, National Institute of Technology Jamshedpur, Jharkhand, India

Sanjay K. Behura The University of Arkansas at Pine Bluff, Pine Bluff, AR, USA

Majid Beidaghi Department of Mechanical Engineering, Auburn University, Auburn, USA

Karan Chaudhary Department of Chemistry, University of Delhi, Delhi, India

Mayank Garg CSIR-Central Scientific Instruments Organisation, Chandigarh, India;
Academy of Scientific and Innovative Research (AcSIR), Ghaziabad, India

Swati Gupta Department of Production and Industrial Engineering, National Institute of Technology Jamshedpur, Jharkhand, India

Md. Manzar Iqbal Department of Production and Industrial Engineering, National Institute of Technology Jamshedpur, Jharkhand, India

Amaresh Kumar Department of Production and Industrial Engineering, National Institute of Technology Jamshedpur, Jharkhand, India

Vikas Kumar Department of Automotive Technology, Mechanical Department Division, Federal TVET Institute, Addis Ababa, Ethiopia

Chandan Kumar Maity Department of Chemistry, IIT (ISM), Dhanbad, Dhanbad, India

Dhanraj T. Masram Department of Chemistry, University of Delhi, Delhi, India

Mayank Mishra Department of Production and Industrial Engineering, National Institute of Technology Jamshedpur, Jamshedpur, Jharkhand, India

Raghvendra Kumar Mishra Enhanced Composites and Structures Center, School of Aerospace, Transport, and Manufacturing, Cranfield University, Bedfordshire, UK

Vinay Panwar Mechanical Engineering Department, Netaji Subhas University of Technology, Dwarka, New Delhi, India

A. V. Pradeep Department of Mechanical Engineering, Vignan's Institute of Engineering for Women, Visakhapatnam, India

Chander Prakash School of Mechanical Engineering, Lovely Professional University, Phagwara, India

S. B. Prasad Department of Production and Industrial Engineering, National Institute of Technology Jamshedpur, Jamshedpur, Jharkhand, India

Arpita Roy Department of Chemistry, IIT (ISM), Dhanbad, Dhanbad, India

S. V. Satya Prasad Department of Production and Industrial Engineering, National Institute of Technology Jamshedpur, Jamshedpur, Jharkhand, India

Amit L. Sharma CSIR-Central Scientific Instruments Organisation, Chandigarh, 160030 India;
Academy of Scientific and Innovative Research (AcSIR), Ghaziabad, India

Dharmendra Pratap Singh Unité de Dynamique et Structure des Matériaux Moléculaires (UDSMM), Université du Littoral Côte d'Opale (ULCO), Calais, France

Subhash Singh Department of Production and Industrial Engineering, National Institute of Technology Jamshedpur, Jamshedpur, Jharkhand, India

Suman Singh CSIR-Central Scientific Instruments Organisation, Chandigarh, India;
Academy of Scientific and Innovative Research (AcSIR), Ghaziabad, India

Sunpreet Singh Department of Mechanical Engineering, National University of Singapore, Singapore, Singapore

Kartikey Verma Department of Chemical Engineering, Indian Institute of Technology, Kanpur, India

Neelam Vishwakarma CSIR-Central Scientific Instruments Organisation, Chandigarh, India

Chapter 1
Introduction, History, and Origin of Two Dimensional (2D) Materials

S. V. Satya Prasad, Raghvendra Kumar Mishra, Swati Gupta, S. B. Prasad, and Subhash Singh

1 Introduction

In the present era of modern science and engineering, when technology is discussed, the roots go back to the understanding of material systems. It is often debated that properties of materials are based on what the material is made of. However, it is not only the composition but also the size and dimensionality of the materials that decide its behaviour. This is substantially true for some materials when their dimensions are reduced to nanoscale, i.e., their size can be expressed in nanometres. In the prevailing times of nanotechnology, materials can be easily engineered in the nano-scale. The analysis of materials is done by having at least one of the dimensions at nano-scale. The materials synthesized at nanoscale may be classified based on their dimensionality (Gupta et al., 2015). This categorization is tabulated in Table 1. A restraint on one of the dimensions produces a 2D material with sheet structure. Restraining 2 dimensions in terms of their size, 1D material is obtained and when all the dimensions are restrained to nano-scales 0D materials are produced (Ozin et al., 2008). Structures with nanometric dimensions shaped into zero- one- or two- dimensional materials have radically different properties. Hence, it can be authoritatively established that apart from a material's atomic structure, its material characteristics are also influenced by its dimensions.

In this context it can be said that the nano-structures of carbon are an integral and a vital part of nanotechnology. It is the initially discovered CNTs (carbon nanotubes) and fullerene that enforced research development in the direction of 2D materials.

S. V. S. Prasad · S. Gupta · S. B. Prasad · S. Singh (✉)
Department of Production and Industrial Engineering, National Institute of Technology Jamshedpur, Jharkhand 831014, India

R. K. Mishra
Enhanced Composites and Structures Center, School of Aerospace, Transport, and Manufacturing, Cranfield University, Bedfordshire MK43 0AL, UK

S. Singh et al. (eds.), *Advanced Applications of 2D Nanostructures*,
Materials Horizons: From Nature to Nanomaterials,
https://doi.org/10.1007/978-981-16-3322-5_1

Table 1 Dimensional categorization of materials

Dimensional category	Examples
Zero Dimensional (0D)	Fullerene, Quantum Dots
One Dimensional (1D)	Nanotubes, nanowires and nanoribbons
Two Dimensional(2D)	Materials with thickness of a single atom
Three Dimensional (3D)	Nanocones and nanoballs

Gupta et al., (2015)

It posted this discovery that attempts have been made to isolate the two dimensional materials of graphite. Finally, in the year 2004 the attempts paved way and a breakthrough was achieved in successfully isolating graphene. Graphene possessed distinctive characteristics which initially elicited unmatched attention towards its two-dimensional, sheet-like structure and characterizations. Subsequently, research on remaining non-carbon-based elements grew. Therefore, the 2D materials gathered much interest within the recent past rendering outstanding electronic, mechanical, and optical properties for various practical applications. Their unique features with emerging prospects in various engineering fields have inclined the interests of researchers across the world towards 2D materials. This eventually guided to the isolation of many 2D materials in the span of a decade.

The research advancements extended the discovery of 2D materials in carbides and nitrides. Rare characteristics (physical) are observable in the nanostructured 2D materials when charge and heat transmission are established to one single plane. Hence, the structure of 2D materials is extensively reviewed. It is in the field of electronics that 2D materials exhibit encouraging prospects. It is deemed that 2D materials are capable enough to replace silicon in various photonics, electronics and nano-electromechanical systems in the coming years. This is due to the fact that 2D materials unveil an exceptional range of optical, thermal as well as electronic characteristics. A whole new system of electronic devices can be generated through the 2D materials.

Presently, apart from the materials of carbon, the family of 2D materials is inclusive of metal oxides (layered) and TMDs (transition metal dichalcogenides). The entire family of 2D materials is represented in Fig. 1 (Geim & Grigorieva, 2013; Huang et al., 2014). One of the most crucial aspects of 2D materials is their stability. Among the existing 2D materials, monolayers of the graphene family, Micas, BSCCO and the TMDs (MoS_2, WS_2, $MoSe_2$, and WSe_2) under atmospheric conditions are stable. Stability may be observed in case of MoO_3, WO_3, the semiconducting dichalcogenides and the layered oxides of copper in atmospheric conditions. But the stability of layered semiconductors and metallic dichalcogenides is only possible in inert conditions. Though the exfoliation of 2D perovskite oxides and hydroxides is complete, not much data is available on these.

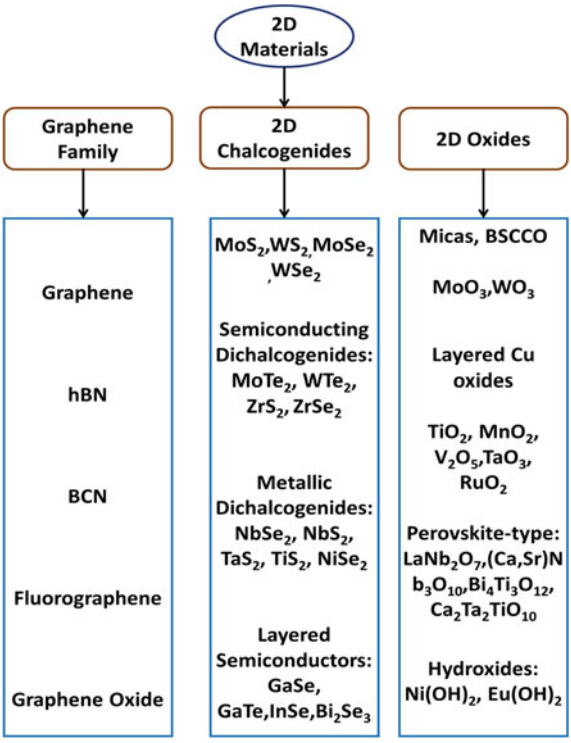

Fig. 1 The family of 2D materials (Geim & Grigorieva, 2013; Huang, 2014)

2 Evolution of 2D Materials

Many years ago, scientists believed that the two-dimensional materials cannot exist in nature due to their environmental instability. But presently, the theoretically recognized number of stable 2D materials is around 700. Although some of them are yet to be synthesized. The initial analyses on the electronic as well as the atomic structures of germanene and silicene were carried out in the year 1994, i.e. 10 years prior to the discovery of graphene. In the year 1962, Boehm coined the suffix "ene" to the foils of carbon with one layer. When the various discoveries related to carbon are studied in a sequential manner, it will be surprising to know that Graphite is quite familiar among the researchers for a very long time (specifically dating back to sixteenth century). The industrial applications of graphite also have been widespread especially in making steel or as dry lubricants and brake linings. But only when the fullerenes were discovered in 1985, the existence of many other allotropes of carbon came into limelight (Kroto, 1985). This also established the presence of carbon nanotubes of one-dimensional structure. The findings related to nanotubes of carbon were initially reported in the year 1991 (Iijima, 1991). These findings fuelled huge quantities of research encouraging the researchers to produce one-dimensional nanoribbons or isolate the two-dimensional materials of graphite from the two-dimensional crystals

(Gupta et al., 2015). Considering graphite (solitary layered) to be the initial material, multiple reports on fullerenes, graphite and nanotubes were presented since then. But only in the year 2004, the isolation of monolayer sheet of graphene was possible as an initiative (Novoselov, 2004). This was a great leap forward to a new class of materials. The solitary graphite layers obtained from graphite (in bulk form) post isolation were termed as graphene.

The graphene sheet is the primitive 2D material (thickness equal to single atom) that has been isolated. Multiple endeavours in the last 50 years have been towards achieving the sheets of graphene. This is to envisage the characteristics of single-atom thick, closely packed layer consisting of sp^2 carbon. The success achieved for previous attempts was modest and the nature of work till 1990s was intercalation of graphitic compounds. The process involves the atom to be sandwiched amid the layers of graphite due to which the inter-planar forces become weak and expedite the layer separation (Mas-Ballesté, 2011). Moreover, expandable graphite was extensively used which has the ability to expand in terms of its volume when heated quickly. The success in obtaining outstanding results was limited (about 10–50 layers). This trend was prevalent in 1960s. In the subsequent years, multiple attempts were made with various other complex processes with no much success. At last, success befriended the Andre Geim's group in 2004 that successfully isolated the solitary graphite layers at Manchester University (Novoselov et al., 2005). The scotch tape process was employed in which layers of graphene were pulled and transmitted to SiO_2 (thin layer) over silicon wafer (Novoselov et al., 2004). The new material obtained was extremely thin compared to a paper and had strength higher than that of a diamond with an electrical conductance much higher than Cu.

Now, the researchers have developed many methods for the preparation of graphene. Thus, graphene was the first modern carbon-based 2D material and its success revealed that stable, single and few-atom-thick layers materials are possible exhibiting exceptional technologically useful properties. The discovery of graphene also made researchers to switch to study and synthesis of non-carbon-based 2D materials. Since then there have been many other 2D materials that are identified. Among the entire family of two-dimensional materials, the initial and extended lineage that evoked research interests is the TMDs (Choi, 2017). The world's attention has been gathered by TMDs due to their exceptional electronic characteristics. They have good flexibility, are extremely thin and exhibit transparency. Due to their semiconductor nature, TMDs find their applications in memory devices, transistors, photovoltaic devices, photo detectors, Li-ion batteries and catalysis of HE (H_2 evolution). The TMDs structure is different to that of graphene, as TMDs possess sandwich structure with two chalcogens sandwiching the transition layer of metal. In contrast, graphene possesses carbon layer of sole-atom thickness (Lv, 2015). The transition metals include Mo, Nb, W whereas the chalcogens include elements like S, Te, Se, etc. TMDs possess strong covalent bonds within the plane and weak interlayer non-covalent bonds. Hence, either of the chemical/physical exfoliation methods can be employed to isolate TMDs 2D structures. The isolating methods include Li intercalation, exfoliation by adhesive tape, chemical or solvent aided exfoliation (Nicolosi, 2013; Zeng, 2011, 2012).

Thereafter, first MXene, generalized as $M_{n+1}X_nT_x$ was discovered at Drexel University in 2011 by selectively etching MAX phases (Naguib, 2011). The first reported Mxene was $Ti_3C_2T_x$. Within few months, many other 2-D materials were obtained through exfoliated compounds like Ta_4AlC_3,Ti_2AlC, $(V_{0.5}Cr_{0.5})_3AlC_2$, Ti_3AlCN and $(Ti_{0.5}Nb_{0.5})_2AlC$ (Naguib et al., 2012). So far more than 30 variations of Mxenes are fabricated. Many more have been theoretically predicted, making it one of the fastest-growing 2D material families (Anasori et al., 2017).

Later in 2012, Silicene, a 2D allotrope of silicone was discovered on a silver (111) single crystal in prevailing situations of ultrahigh vacuum through the process of molecular beam epitaxy (MBE) (Vogt, 2012). The fabrication of silicene triggered a concentrated search for similar 2D materials fabricated using equivalent techniques like the MBE. The characteristics of silicine are largely contrasting to that of graphene. The only similarity lies in their two-dimensional structure. These elements do not naturally exist nor do they have parental crystal having a 3D layer. Therefore, the possibility of exfoliation is eliminated and chemical fabrication is the available option. The fabrication may also be carried on a substrate by the process of epitaxial growth. Hence, the electronic and structural characteristics may be dependent on substrate.

After generation of silicene, researchers estimated that borophene can be achieved on similar lines by utilizing support extended by metal surface. Finally, in 2015, successful synthesis of three different borophene phases was achieved on the surfaces of silver (111) surfaces in the prevailing surroundings of ultrahigh-vacuum (Mannix, 2015). This 2D boron structure is metallic in nature despite its bulk boron being semiconductor (Wu, 2012).

Further in 2014, germanene (2D germanium) was reported by an international team of researchers led by Guy Le Lay at France's Aix-Marseille University (Dávila, 2014). In 2016, 2D tin known as stanene was discovered (Zhu, 2015). Survey of the 3D materials that can be exfoliated has shown that there may be many 2D materials that are yet to be discovered. Among the new system researchers have worked with hexagonal boron nitride, different transition metals chalcogenide.

3 Growing Interest in 2D Materials

The emerging field of 2D materials has become an area of great interest both in the field of fundamental science and technological aspect and without any doubt it could be presumed that over the next few years this field will lead to many new and exciting discoveries. The 2D materials maybe considered as the suitable section of emerging materials for engineering applications. The sheet-like structure possessed by 2D materials allows the flexibility to customize its characteristics through the surface treatments like chemical functionalization (Xu, 2009). Moreover, it is an extremely effortless process to get the 2D materials as dispersed nano-flakes (Hernandez, 2008). The characteristics of 2D materials include high strength, extreme lightweight nature,

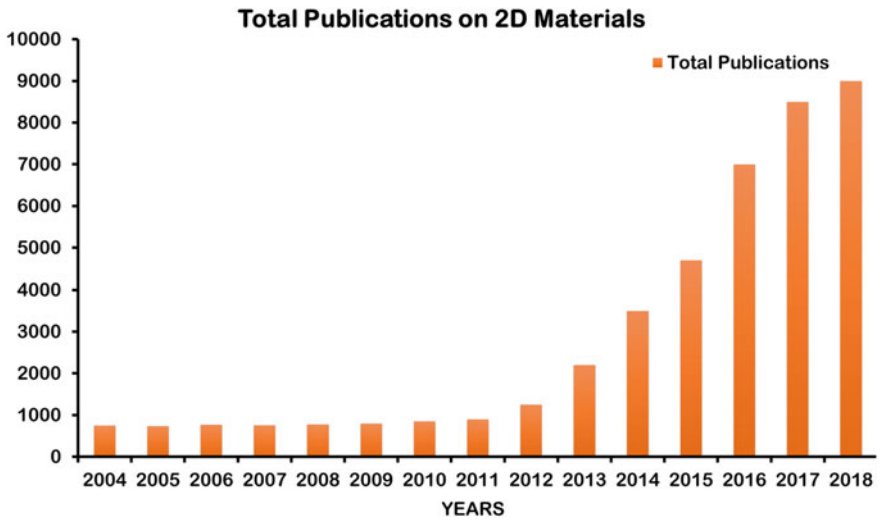

Fig. 2 Increasing trend of the total 2D material publications per year (Choi et al., 2017; Donarelli & Ottaviano, 2018)

good mobility of carriers, great modulus of elasticity, high optical, high UV adsorption, and superconductivity. These distinctive characteristics are restored. Hence, these may be thoroughly exploited in the fabrication of high-performance composites (Coleman, 2011). Also, the electronic band structures of these materials are a field of attention. Their zero band gap allows absorption of wide light span within the region of electromagnetic band (Reina, 2009). Among various reasons, the prime reason for the extreme growth in 2D material research is due to the unmatchable characteristics spotted in them. An appealing fact is that there is an increasing trend in the documentation of 2D material research every year as represented in Fig. 2. Approximately there are over 150 sheet structured materials that can be synthesized at nano levels. The list incorporates graphene family, 2D chalcogenides, 2D oxides as well as 2D carbides or nitrides (Choi et al., 2017).

The sheet structured materials are ideal for electronic applications since they are accessible to charge carriers enabling extraordinary mobility of carriers in all atmospheric conditions. Also, they possess excellent thermal conductivity. The strength (breaking) possessed by 2D materials (like graphene) is abnormally high because in comparison to steel their strength is greater by 200 fold (Lee, 2008). They also exhibit exceptional flexibility apart from the strength. The extremely thin membrane and its stretchable nature have the ability to overcome elastic deformation over 20%. These properties make 2D materials desirable prospects for lightweight applications. They are added to light weight polymers to enhance mechanical characteristics. The 2D materials have a slight disadvantage that they are brittle in nature and crack at higher strains. The 2D structured materials are an attractive prospect for mechanical applications in terms of the strength of their chemical bond. There is a possibility of

modifying sheet structured elements chemically. The mechanical characteristics can be altered due to the existence of functional compounds (Yazyev & Louie, 2010). The best illustration of this is converting metals into insulators by the process of functionalization (Gierz, 2008). These functional characteristics can be produced in local regions and facilitate the fabrication of 2D material gadgets with multiple characteristics in different areas. Therefore, the 2D materials are the most sought after for their extraordinary range of exhibited properties which may be exploited for various applications (Gao, 2015).

4 Challenges and Opportunities

Currently, the research interest on 2D materials other than graphene is extremely high in the field of nanomaterials. The pursuit of other 2D materials signifies the characteristic similarities with graphene. But it is essential to thoroughly comprehend the behavioural aspects under testing conditions before they are applied for everyday use. For instance, the electronic characteristics of TMDs layers are known based on academic reports but the remaining mechanical, thermal and chemical characteristics are yet to be learnt. The research analysis on TMDs is currently limited. Hence, many endeavours are to be put in towards the analysis on how reliable the sheet structured materials are. Their performance needs to be evaluated to identify longevity under thermal or electrical stress examinations. The sheet-like structure of 2D materials is bound with issues like surface passivation especially for electronic applications. Moreover, only techniques like exfoliation or flake transmission are the commonly employed for bulk production. This is feasible to graphene or BN. As such no proper methods are available which would yield high productivity. Hence it is of top-most priority to discover advanced techniques which would be suitable for large-scale production of 2D nanomaterials. If not the applications of other 2D-based materials shall be extremely difficult and expensive for practical aspects.

Similar issues are persistent with active materials like silicene/germanene. The theoretical findings stress upon resemblance of their properties (electronic) with graphene but practical investigations are still inadequate. The layers of silicene/germanene currently are formed on substrates that are metals. But in the production of electronic devices these substrates are inappropriate. Hence, endeavours towards generation of silicene/germanene on substrates that are insulators or non-metallic are indispensable.

The research on sheet structured materials is taking baby steps but developing at an extremely rapid rate. It is the unmatched characteristics exhibited by 2D materials that stimulate the researchers to take interest in this briskly progressing field. Large advancement scopes are available in terms of formulating newer techniques for producing 2D materials on mass scale. It is also essential to achieve superiority in the structural development of existing layers. Further research is required in determining physiochemical characteristics of multi/single-layered nano-sheets. Material characteristic advancements through doping, functionalization and strain effect can

be done as a part of forthcoming research. Additionally, the possibility of fabricating newer 2D materials with enhanced properties is always present which can further broaden the scope of these unique materials.

References

Anasori, B., Lukatskaya, M. R., & Gogotsi, Y. (2017). 2D metal carbides and nitrides (MXenes) for energy storage. *Nature Reviews Materials*. https://doi.org/10.1038/natrevmats.2016.98

Choi, W., et al. (2017). Recent development of two-dimensional transition metal dichalcogenides and their applications. *Materials Today*. https://doi.org/10.1016/j.mattod.2016.10.002

Coleman, J. N., et al. (2011). Two-dimensional nanosheets produced by liquid exfoliation of layered materials. *Science*. https://doi.org/10.1126/science.1194975

Dávila, M. E., et al. (2014). Germanene: A novel two-dimensional germanium allotrope akin to graphene and silicene. *New Journal of Physics*. https://doi.org/10.1088/1367-2630/16/9/095002

Donarelli, M., & Ottaviano, L. (2018). 2D materials for gas sensing applications: A review on graphene oxide, MoS_2, WS_2 and Phosphorene.*Sensors (Basel, Switzerland)*. https://doi.org/10.3390/s18113638

Gao, W. (2015). The chemistry of graphene oxide. In *Graphene Oxide: Reduction recipes, spectroscopy, and applications*. https://doi.org/10.1007/978-3-319-15500-5_3

Geim, A. K., & Grigorieva, I. V. (2013). Van der Waals heterostructures.*Nature*. https://doi.org/10.1038/nature12385

Gierz, I., et al. (2008). Atomic hole doping of graphene. *Nano Letters*. https://doi.org/10.1021/nl802996s

Gupta, A., Sakthivel, T., & Seal, S. (2015). Recent development in 2D materials beyond graphene. *Progress in Materials Science*. https://doi.org/10.1016/j.pmatsci.2015.02.002

Hernandez, Y., et al. (2008). High-yield production of graphene by liquid-phase exfoliation of graphite. *Nature Nanotechnology*. https://doi.org/10.1038/nnano.2008.215

Huang, Y. H., et al. (2014). Transport properties in semiconducting NbS_2 nanoflakes. *Applied Physics Letters, 105*. https://doi.org/10.1063/1.4894857

Iijima, S. (1991). Helical microtubules of graphitic carbon. *Nature*. https://doi.org/10.1038/354056a0

Kroto, H. W., et al. (1985). C60: Buckminsterfullerene. *Nature, 318*(6042), 162–163. https://doi.org/10.1038/318162a0

Lee, C., et al. (2008). Measurement of the elastic properties and intrinsic strength of monolayer graphene. *Science*. https://doi.org/10.1126/science.1157996

Lv, R., et al. (2015). Transition metal dichalcogenides and beyond: Synthesis, properties, and applications of single- and few-layer nanosheets. *Accounts of Chemical Research*. https://doi.org/10.1021/ar5002846

Mannix, A. J., et al. (2015). Synthesis of borophenes: Anisotropic, two-dimensional boron polymorphs. *Science*. https://doi.org/10.1126/science.aad1080

Mas-Ballesté, R., et al. (2011). 2D materials: To graphene and beyond. *Nanoscale, 3*(1), 20–30. https://doi.org/10.1039/c0nr00323a

Naguib, M., et al. (2011). Two-dimensional nanocrystals produced by exfoliation of Ti_3AlC_2. *Advanced Materials, 23*, 4243–4253. https://doi.org/10.1002/adma.201102306

Naguib, M., et al. (2012). Two-dimensional transition metal carbides. *ACS Nano*. https://doi.org/10.1021/nn204153h

Nicolosi, V., et al. (2013). Liquid exfoliation of layered materials. *Science*. https://doi.org/10.1126/science.1226419

Novoselov, K. S., et al. (2004). Electric field effect in atomically thin carbon films, *Science. American Association for the Advancement of Science, 306*(5696), 666–669. https://doi.org/10.1126/science.1102896

Novoselov, K. S., et al. (2005). Two-dimensional atomic crystals. In*Proceedings of the National Academy of Sciences of the United States of America.* https://doi.org/10.1073/pnas.0502848102

Ozin, G. A., Arsenault, A., & Cademartiri, L. (2008). *Nanochemistry*. The Royal Society of Chemistry.

Reina, A., et al. (2009). Large area, few-layer graphene films on arbitrary substrates by chemical vapor deposition. *Nano Letters.* https://doi.org/10.1021/nl801827v

Vogt, P., et al. (2012). Silicene: Compelling experimental evidence for graphenelike two-dimensional silicon. *Physical Review Letters.* https://doi.org/10.1103/PhysRevLett.108.155501

Wu, X., et al. (2012). Two-dimensional boron monolayer sheets. *ACS Nano.* https://doi.org/10.1021/nn302696v

Xu, Y., et al. (2009). A graphene hybrid material covalently functionalized with porphyrin: Synthesis and optical limiting property. *Advanced Materials.* https://doi.org/10.1002/adma.200801617

Yazyev, O. V., & Louie, S. G. (2010) Topological defects in graphene: Dislocations and grain boundaries. *Physical Review B - Condensed Matter and Materials Physics.* https://doi.org/10.1103/PhysRevB.81.195420

Zeng, Z., et al. (2011). Single-layer semiconducting nanosheets: High-yield preparation and device fabrication. *Angewandte Chemie - International Edition.* https://doi.org/10.1002/anie.201106004

Zeng, Z., et al. (2012). An effective method for the fabrication of few-layer-thick inorganic nanosheets. *Angewandte Chemie - International Edition.* https://doi.org/10.1002/anie.201204208

Zhu, F. F., et al. (2015). Epitaxial growth of two-dimensional stanene. *Nature Materials.* https://doi.org/10.1038/nmat4384

Chapter 2
Different Types and Intense Classification of 2D Materials

Mayank Garg, Neelam Vishwakarma, Amit L. Sharma, and Suman Singh

1 Introduction

Based on the dimensionality, the materials can be classified as zero dimensional (0D), one dimensional (1D), two-dimensional (2D) and three dimensional (3D) (Dolez, 2015). As the name suggests, 0D materials don't possess any finite dimension. Quantum dots and nano-dispersions are examples of these class of material (Tiwari et al., 2012). 1D materials have finite length for example nanotubes and nano-fibres. 2D materials possess both length and breadth for example nanosheets. 3D materials are complex materials having 0D, 1D and 2D in close proximity to each other interacting in specified manner. The 2D materials are thin sheets on atomic-scale which have unique properties as compared to other known materials (Zeng et al., 2015). These materials exhibit electronic, physical, optical, thermal and mechanical properties which are very helpful for various applications. The most exciting feature of this class of materials is the flexibility we get with these materials. The properties of the material can be modulated easily which helps in various applications. The bonding within each layer of the 2D material is quite strong because of ionic or covalent bonds. This provides mechanical strength to these materials (Gould et al., 2016). The different layers of the material are held together by weak forces such as Vander Waal forces (Mannix et al., 2017). Since 2004 when the graphene was discovered at The University of Manchester, many 2D materials have been discovered (Mas-Ballesté et al., 2011). Nobel prize in physics for the discovery of graphene was awarded to Andre Geim and Konstantin Novoselov in the year 2010 (Zhang, 2018). After the discovery of graphene, there are now a plethora of 2D materials

M. Garg · N. Vishwakarma · A. L. Sharma · S. Singh (✉)
CSIR-Central Scientific Instruments Organisation, Sector 30-C, Chandigarh 160030, India
e-mail: ssingh@csio.res.in

M. Garg · A. L. Sharma · S. Singh
Academy of Scientific and Innovative Research (AcSIR), Ghaziabad 201002, India

S. Singh et al. (eds.), *Advanced Applications of 2D Nanostructures*,
Materials Horizons: From Nature to Nanomaterials,
https://doi.org/10.1007/978-981-16-3322-5_2

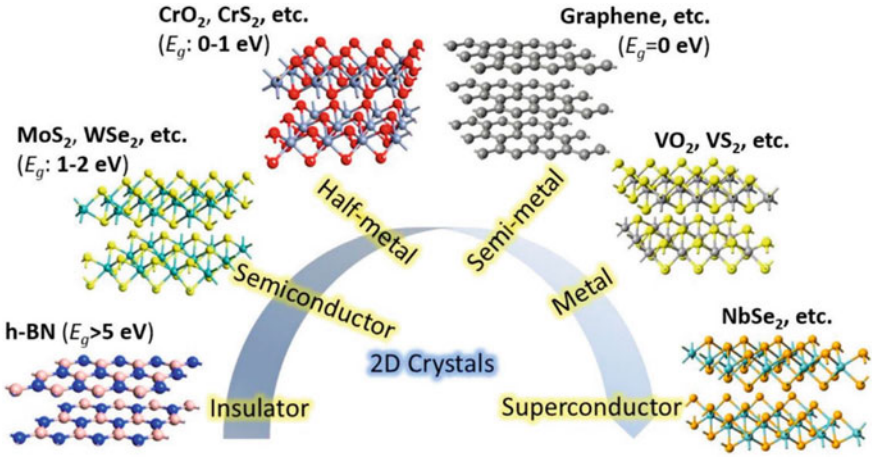

Fig. 1 Different 2D material with different properties (conductors, super conductors and insulators). Reproduced with permission from SPIE publications, Jiahai Kang, Wei Cao, Xuejun Xie, Deblina Sarkar, Wei Liu and Kaustav Banerjee, *Graphene and Beyond-Graphene 2D Crystals for Next-Generation Green Electronics*, 908305, 2014, p. 1–7 (Kang et al., 2014)

known to us (Osborne, 2016). These include many graphene analogues such as 2D oxides and 2D chalcogenides which will be discussed in detail in the coming sections (Das et al., 2015) (Fig. 1).

As mentioned, these materials have unique properties. These are optically and electrochemically active, apart from having good thermal and mechanical properties (Akinwande et al., 2017; Gupta et al., 2018; Kim et al., 2018). These properties have been used for different applications. Typical applications of 2D material are use in catalysis, energy generation and storage, photonics, optics, electronic devices and in biomedical field (Butler et al., 2013, 2016; Kostarelos, 2016).

A more detailed account of the types, properties and applications of the 2D materials will be provided in the coming sections. The different types of the 2D materials will be discussed giving description of their properties, synthesis methods, and applications. All the general applications will be briefly discussed.

2 Types

As seen above, all the 2D materials are fundamentally similar in structure, i.e. layers of atoms stacked on top of one another, held by various forces. However, these materials can be classified into 3 types:

- Graphene family
- 2D oxides
- 2D Chalcogenides

All these types will be discussed individually in the following sections.

2.1 Graphene Family

Carbon's peculiar properties have long piqued the interest of scientists. This interest has risen in recent years due to advances in material science in carbon allotropes such as graphite, fullerenes, Buckyballs, and other carbon allotropes at the nanoscale. These structures not only hold advanced electrical and mechanical properties but also follow quantum confinement rules to enhance their optical, chemical and bio-interfacing properties.

2.1.1 Types of 2Dimensional Graphene Family Materials

Following are various 2D materials classified under graphene family:

1. Graphene: Graphene holds the crown of being most advanced material with applications in almost every major area due to its 1-atom thick, 2-dimensional hexagonal honeycomb structure, allowing it to be not only the thinnest but also the strongest material is known to humankind. Graphene is extremely transparent (as high as 96% through some synthesis methods (Wassei & Kaner, 2010) and highly conducting towards both heat and electricity. Owing to these remarkable properties, graphene-based materials have been employed for vast range of applications like sensors, energy, coating of materials, etc.

2. Graphene oxide: Even though graphene has several advantages, synthesis of pristine graphene is not easy since the single atomic layers are extremely unstable during synthesis. When a powerful oxidizing agent is used during graphene synthesis, it oxidizes graphite such that the material becomes hydrophilic and thus expanding the layers spacing. This phenomenon makes exfoliation of graphite into graphene layers more convenient and stable. This solution can be further sonicated in aqueous medium to give single to few layers' graphene oxide which can be easily dispersed in any medium. The properties of graphene oxide change slightly from pristine graphene due to presence of oxidizing species. For example, due to the disturbance of sp^2 bonds in layers, GO acts as electric insulator. Hence it becomes important to reduce graphene oxide to regain its original properties and hexagonal structure.

3. Fluorographene: Even though graphene has exceptional properties, shortcomings like hydrophobicity and structural deformities while synthesis shadowed its several benefits. To overcome this, several functionalization methods were evolved along the years by researchers. Fluorographene (FG) can be prepared by fluorination of graphene (Robinson et al., 2010). FG is highly researched, promising material which is a rising topic of interest which could lead to efficient graphene derivative.

4. Hexagonal Boron Nitride (hBN): hBN is a layered ultra-flat structure isomorphic to graphene and is attracting the interest of more and more researchers due to it tremendous electrical-optical properties, structural uniqueness, thermal stability and

chemical behaviour, etc. hBN can make composites with several other materials like metal chalcogenides, graphene oxide sheets, etc.

5. Boron Carbon Nitride (BCN): BCN is relatively new compared to other carbon composites. With controllable band gaps (0–5.5 eV), the Carbon-Boron nitride hybrid exhibits several advanced properties like optical absorptivity, electrochemical activities and cathodoluminescence, etc. (Wu et al. 2016a). The structural configuration of BCN varies with variation in bonds between three atom, i.e., B, C and N (Lei et al., 2011). Such doping in material provides superiority for applications in several fields like energy storage, capacitors, photocatalytic processes and gas storage devices, etc. Different stimulation methods demonstrate that for increased stability, atoms in lowest energy states favour the B-N and C–C bonds. The BCN system forms phase separation to single-layered BN and graphene if B–C, C–N, B–B and N–N bond are prevalent (Yuge, 2009). BCN can occur in 0D, 1D, or 2D forms.

2.1.2 Properties of Graphene Which Makes It Unique and Advanced Material

(i) **Electronic Properties**: Graphene has a zero-overlap conduction and valance band structure with a s^2p^4 electron distribution, leaving $4e^-$ exclusively for chemical bonding. Although in case of sheets, there is sp^2 hybridization using 3 out of 4 electrons, leaving only one highly active electron (π e^-) delocalized, left below and above the planer structure, resulting in properties like super-high conductivity exhibited by graphene or graphene-based materials (GBM).
The electronic mobility of graphene at room temperature reported is very high ~250,000 cm^2/Vs (Cui et al., 2011; Zhu et al., 2010), helping it to act like photons. It also has low intrinsic electrical noise which is why it exhibits high sensitivity towards even smallest changes in chemical, electrical or mechanical properties of material. It provides high electrical conduction with least resistivity (lesser than Ag wires at room conditions). Since electrons and holes here behave like quasi-particles (also referred to as massless Dirac fermions), graphene also shows Quantum Hall effect (Geim, 2009; Geim & Novoselov, 2007) i.e. quantization of graphene energy into discrete level (Landau levels) levels due to quantum confinement in sheet.

(ii) **Mechanical Properties**: With 0.142 nm long carbon bonds, graphene holds the title of strongest material knows to humans. It has huge intrinsic tensile strength (~130 GPa) (Qiu et al., 2015) and Young's modulus ~1TPa (Lee et al., 2008), also being one of the lightest material (~0.77 mg/m^2). Graphene has breaking strength ~42 N/m (Huang et al., 2012) and these qualities make graphene most suitable candidate for making composites, fabrication of high stiffness and strong materials, etc. High Flexibility as a result of sp^2 hybridization and still holding enough rigidity to withstand conformational changes is also a very rare combination in materials.

(iii) **Optical properties**: Graphene is a highly transparent conducting material with nearly 98% transmittance (Wassei & Kaner, 2010). In past, it was proved that the white light absorbance is dependent on Fine structure constant and not on material properties. Therefore, graphene being single atom thick has only about 2.3% white light absorption. With universal dynamic conduction value $G = e2/4\hbar$ (±2–3%) over visible spectra, graphene is the star material for mode-locking fibre lasers.

(iv) **Thermal Properties**: Graphene shows in-plane and inter-plane thermal conductivity. On one hand where in-plane conductivity varies 4000–5000 W/mK (Zhu et al., 2012), the inter-plane conductivity can be as low as 6 W/mK, because of weak van Der Walls interactions.

2.1.3 Synthesis Methods

Graphene is rarely used in its pure due to several structural deformities formed during synthesis and is therefore preferred in the form of reduced graphene oxide (rGO), fluorographene, graphene oxide (GO), etc.

For the synthesis of graphene-based materials (GBMs), either Top-Down or Bottom-Up methods are used. The methods which reduces the size of graphite material from bulk to single-layered graphene are grouped into top-down methods, for example, mechanical exfoliation, chemical exfoliation, liquid-phase reduction, etc. When single atoms are arranged one by one to create an even carbon layer, it is categorized into Bottom-Up approach, for example, chemical vapor deposition (CVD), epitaxy, lithography etc.

Top-Down Synthesis:

(i) Material Exfoliation: With the multi-layered graphite in hand, which is nothing but layers and layers of graphene bound together by weak bonds, exfoliation by physical, chemical or mechanical forces is one of the widely used methods to produce graphene-based materials.

a. Liquid–phase exfoliation:

This type of exfoliation involves chemical agents used for weakening intra-layer bonds which can be later separated using ultrasonication. To ease the layering and reduce structural defects, nanoparticles can be introduced between layers as "particle wedges" (Hong et al., 2018). Chemical exfoliation can be preferred for preparing 1–4 layered graphene structures and would have been a highly potential option for up-scaling if not for drawbacks like immense purification steps to remove the by-products (Fig. 2).

b. Electrochemical Exfoliation: Electrochemical method of GBM preparation uses a carbon source as one of the electrodes in either aqueous or organic solutions. Several methods using acids like sulphuric acid (H_2SO_4) (Su et al., 2011) or alkalis like potassium hydroxide (Tripathi et al., 2013) are reported. The size and exfoliation levels can be varied by changing electrochemical parameters.

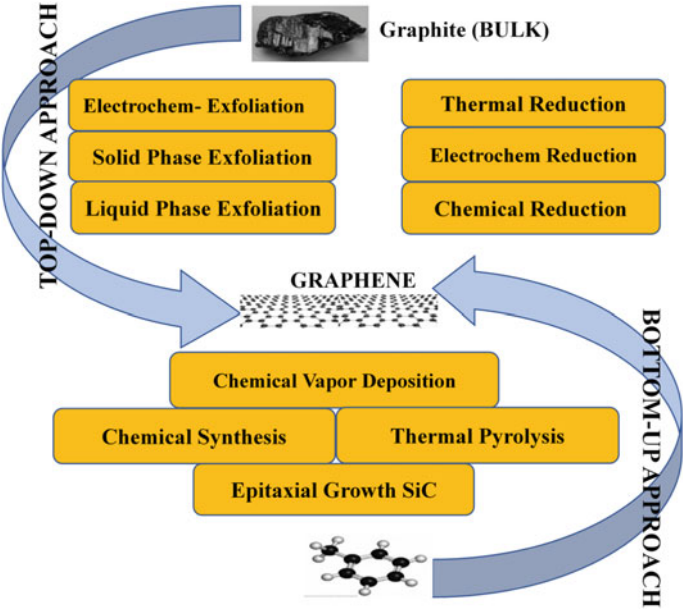

Fig. 2 Synthesis approaches for graphene family materials

(ii) Reduction of carbon material: Reducing carbon material like graphite flakes is an efficient and cost-effective method which can be upscaled to produce high-quality Graphene oxide layers. GO films can also be converted into reduced graphene oxide (rGO) by thermal or chemical reduction using a wide range of reducing agents.

a. Chemical reduction: It is one of the major methods to prepare GO, rGO and other graphene derivatives. Several oxidizing agents like H_2SO_4, HNO_3 and $KMnO_4$ etc. are used for chemical exfoliation of graphite sheets to produce single-layer graphene sheets (Hummers & Offeman, 1958). Since Hummer's method used toxic and harsh chemicals, there have been several modifications to efficiently produce GO and rGO. Several other chemical compounds like sodium borohydride and hydrazine (Eda et al., 2008) etc. are also extensively researched as potential reducing agents for GO and rGO synthesis.

b. Thermal reduction: Methods like thermal annealing and hydrothermal methods can be used to prepare graphene-based materials like rGO, GQDs, fluorographene, etc. Mei et al, (Mei et al., 2015) reported that high temperature can actually increase the reduction of graphene oxide (Mei et al., 2015), to synthesize rGO. GO is exposed to high temperature (~1000 °C) so that H_2O and oxygen molecules will evaporate creating reduction of GO (Gao et al., 2009).

Other than these, there is also electrochemical reduction method which reduces GO to produce rGO (Feng et al., 2016). Chemical reduction method is the most widely used of all the methods due to its lower cost and higher yield as compared to other methods like mechanical exfoliation, lithography, etc.

Bottom-up approach:

This process entails attaching smaller molecules, such as hydrocarbons, to a substrate in order to produce graphene or its derivatives.

(i) Chemical Vapor deposition (CVD): CVD is one of the most enthusiastically opted method by researcher for fabrication of single to few layers of nanosheets in either crystalline or amorphous configurations in large sizes which are otherwise difficult using chemical methods. CVD targets molecules from conducting materials with high precision and extremely controlled parameters like temperature, pressure, flow rates, etc., producing high-quality, defect-free graphene nanosheets. CVD graphene has enormous applications like in electronic transistors, conducting electrodes, anti-corrosion layering on substrate and high sensitivity sensing devices (Kobayashi et al., 2013; Schriver et al., 2013; Wu et al., 2016b; Xu et al., 2017). Gases like ethane, methane and propane and other dopants can be dissolved into heated substrates like Cu or Ni to make a platform for graphene sheet to deposit. Materials like nickel, platinum cobalt and ruthenium (Kim et al., 2009) are the most preferred precursors for CVD synthesis of graphene.

(ii) Epitaxial growth (EG): Epitaxial growth on silica carbide (SiC) is another widely used method for graphene sheet fabrication. In this method, Silicon Carbide is exposed to extreme high temperature 1200–1500 °C and high vacuum which in turn sublimates silicon ions, hence giving is layers of Carbon atoms on the surface. Epitaxial growth method used highly controlled systems creating self-assembled hexagonal sheets of carbon atoms which are transferrable onto other substrates. There are several reports where there is change in electronic properties in epitaxial graphene (EG) like band gap of 260 meV and Fermi level shifting to 400 meV (Unarunotai et al., 2009; Zhou et al., 2007). EG offers advanced electroanalytical mechanism for different biosensors and compare to CNTs, B-doped diamonds, etc. EG biosensors are seen to have high selectivity and sensitivity and are able to differentiate between different analytes, thereby giving an edge for sensing applications.

2.2 2D Oxides

An arrangement in the form of layers or sheets wherein a metal is bound to an oxygen is referred to as 2D oxides. Many 2D oxides have been reported. For example, metal oxides in which the metal can be titanium, cobalt, copper, tungsten, etc. (Gupta et al., 2015). Iron oxide is a new member to the 2D oxide family which was recently added (Larionov et al., 2018). These possess remarkable electronic properties because of the presence of oxygen ions (Rasmussen & Thygesen, 2015). Applications of these materials include usage in electronic devices (Azadmanjiri et al., 2018). The synthesis procedure involves self-assembly method (Osada & Sasaki, 2013). Ion layer adsorption and reactions (Gao et al., 2017), lasers (Mulenko et al., 2016) or molten salts method (Hu et al., 2017) are also used for the material synthesis. Since these materials possess excellent electronic properties and hence these have been mostly used in electronic devices like batteries, transistors and as supercapacitors (Peng et al., 2017;

Yin et al., 2018; Yang et al., 2019). Their high electron mobility also helps in catalytic activity and hence catalytic and photocatalytic applications of 2D oxides have also been reported (Loh et al., 2016; Haque et al., 2017; Heard et al., 2019). These have been used for the sensing of nitrogen dioxide, acetone, ethanol, formaldehyde, etc. (Dral and ten Elshof 2018). Materials such as manganese dioxide, zinc oxide and copper oxide have been extensively used for the biosensing applications. These have been used for the biosensing of analytes such as glucose, hydrogen peroxide, DNA and various proteins such as BSA (Shavanova et al., 2016).

2.3 2D Chalcogenides

2D Chalcogenide is similar in properties to the other 2D materials discussed in above sections. It is formed when a transition metal (M) is bound covalently to two chalcogens (X). The different layers of these materials are held by weak Vander Waal forces. Examples of these materials include molybdenum disulphide, tungsten disulphide, tungsten ditelluride, etc. (Chernozatonskii & Artyukh, 2018; Lv et al., 2015; Zhou et al., 2018). The crystal structure of TMDs change when they are converted from bulk form to a monolayer form. It changes from a metallic state (1T) to a semiconducting state (2H) (Yu et al. 2018) (Fig. 3).

These materials have very exciting properties depending on the crystal structure they are currently in. These materials are optically, electrochemically active and

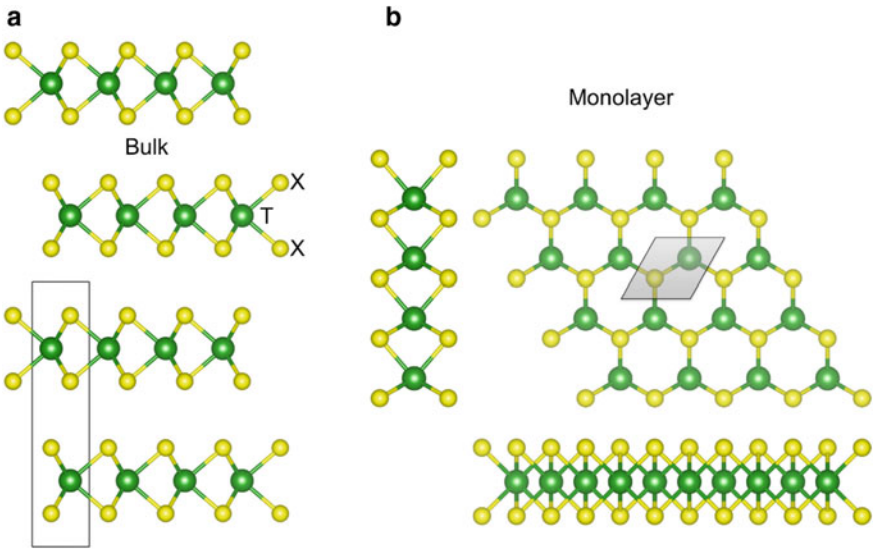

Fig. 3 The two forms of TMDs. Based on application either their bulk form (**a**) or monolayer form can be used (**b**). Reproduced with permission from ref (Kuc & Heine, 2016)

also known to possess thermos-electronic properties. When the energy bandgaps of the TMDs cover the visible and near-infrared regions of the light, these gives rise to many potential applications. This property can be explored for photonic devices such as LEDs, transistors, lasers, etc. These materials have been deeply explored for the optical based applications (Berkelbach & Reichman, 2018; Zheng et al., 2018). The modulation of band gap also alters the electronic properties of the TMDs (Jung et al., 2014). These have also been extensively studied for use as an electronic devices such as in case of FET and other energy storage devices (Huang et al., 2016; Schmidt et al., 2015). The optical and electronic properties have been combined to yield opto-electronic devices (Lee et al., 2017). These have been used for energy generation, storage, catalytic activities, transistors, solar cells and in photodetectors (Choi et al., 2016; Khan & Leuenberger Michael, 2018; Xia & Li, 2016; Xie & Cui, 2016). These marterials have been used for the thermal energy generation and heat management (Zhang & Zhang, 2017). All these properties make TMDs an exciting material to work with.

2.3.1 Synthesis

There are broadly 3 classifications for the synthesis of TMDs. These are mechanical exfoliation, wet chemical methods and the vapour deposition method (Wang et al., 2015; Lin et al., 2016; Zhang et al., 2016, Yu et al., 2018).

1. Mechanical exfoliation

As mentioned in the above sections, TMDs exist in the form of layers. Hence to obtain individual layers for specific applications, mechanical exfoliation is an option. It is quick, simple and easily scalable method for the synthesis of this material. In this method, mechanical energy is provided to break the bulk material into smaller pieces. This is mostly done using sonication process in which high-frequency sonic waves are passed through the solution containing the bulk material. The time and energy of the exposure to sonic waves govern the size of the final material. This method provides flexibility for many modulations. However, when the energy is removed, these sheets or layers tend to re-aggregate because of weak interactions between them. To prevent this from happening, usually some chemicals are used so as to keep these sheets apart (Guan et al., 2015). For instance, authors have used dilute solution of household detergent for the synthesis of MoS_2 and WS_2 nanosheets (Mishra et al., 2015). Figure 4 shows this process. Mechanical exfoliation suffers from disadvantages such as the number of layers in synthesis cannot be controlled, difficulty in achieving required particle size and low yields.

2. Wet chemical method

This is a bottom-up approach for the synthesis of TMDs. In this, the constituents of the TMDs, are reacted together in a liquid in the presence of electric current (Wan et al., 2017) or heat (Ren et al., 2015) so as to obtain TMDs. This method is better as compared to the mechanical exfoliation as particle size can be controlled but the drawbacks of this method is that the yields are lower than the mechanical exfoliation

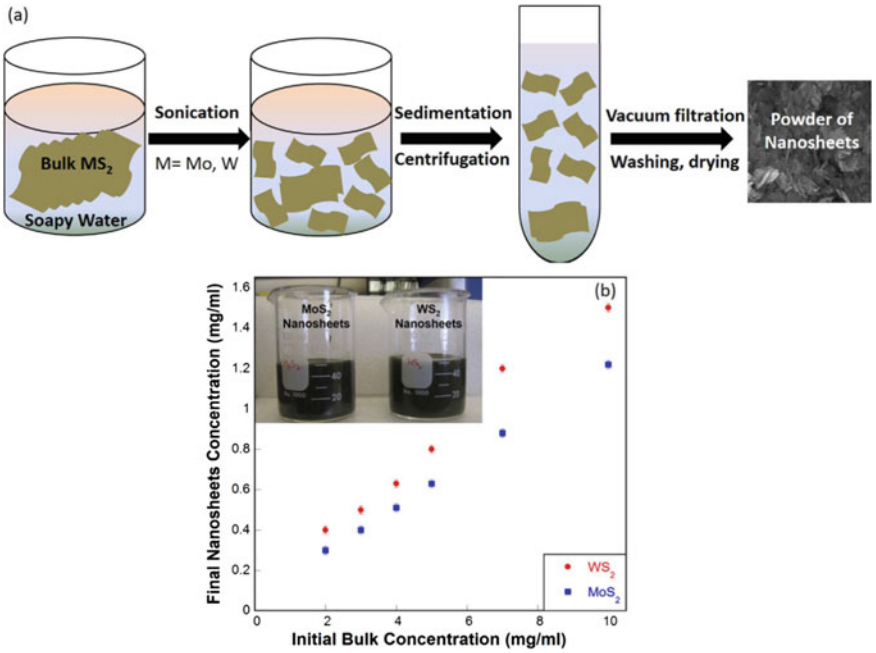

Fig. 4 Use of soapy water for the synthesis of MoS_2 and WS_2 nanosheets via mechanical exfoliation method. Reproduced with permission from ref (Mishra et al., 2015)

method and this method produces particles with very high defects. The scale-up of this method is also difficult.

3. Vapor deposition method

This is the more sophisticated process for the controlled synthesis of TMDs (Giri et al., 2018; Song et al., 2015). This process involves use of either physical vapour deposition in which the material is sprayed over the substrate to obtain a controlled thickness of the layers of the material or use of chemical vapour deposition which involves use of chemical for the similar purpose. This method is most beneficial over the other methods in obtaining a controlled growth and morphology of the material (You et al., 2018). However, this method requires very sophisticated and expensive instruments for the synthesis. The material produced by this method is expensive as compared to other two methods discussed above.

2.3.2 Applications of TMDs

Because of their properties, tunability and chemical diversities, these materials have been extensively been used in areas such as catalysis, photocatalysis, energy generation and storage devices and as electronic devices (Choi et al., 2017). There is ample literature on the applications of these materials. In our discussion, we shall only be

highlighting the various applications. As mentioned above, different structures of this material give different properties which lead to many applications (Wei et al., 2018). The tunable band gap makes the TMDs as suitable candidates for catalytic activities. These materials possess good catalytic activities which is well highlighted in literature (Haque et al., 2018). These have been used in hydrogen evolution reactions and in remediation of many environmental pollutants (Peng et al., 2017; Rosman et al., 2018).

As an example, WS_2/WO_3 heterostructures (Ma et al., 2017), Al_2O_3 coated MoS_2 (Vattikuti & Byon, 2015), and MoS_2 nanosheets with embedded TiO_2 nanoparticles (Ren et al., 2016) have shown excellent photocatalytic activity. Other application in which TMDs find their use is for electronic and photoelectronic applications (Gong et al., 2017). Due to its high carrier mobility property, these have been used as field effect transistors (FETs) (Ahmed & Yi, 2017). The catalytic activity allows the water molecules to be split for the generation of hydrogen which can be used as a source of energy (Li et al., 2018). Researchers are trying to develop various devices such as LEDs, solar cells and other photovoltaic devices from TMDs exploiting their semiconducting nature (Jariwala et al., 2014). Composites of conducting polymers and TMD have also shown great potential for applications mentioned above (Sajedi-Moghaddam et al., 2017).

TMDs have also been exhaustively studied for their application in biomedical domain like photothermal therapy, biosensors, cellular imaging, etc. (Agarwal & Chatterjee, 2018; Chimene et al., 2015; Wen et al., 2018). Modulating the structure of TMDs also helps with the biomedical applications. In one such case, the authors created vacancies on 2D MoS_2 using PEG-SH to improve the biocompatibility of 2D MoS_2 which finally can be used for encapsulating the cells for potential tissue engineering or other biomedical applications (Jaiswal et al., 2017). The most widely developed application of TMDs is the use as biosensor. As mentioned in previous sections also, TMDs have been used as both optical and electrochemical sensors. The small size in case of TMD based quantum dots provides a highly fluorescent platform for the optical detection of analytes and the large surface area along with high electron mobility makes them a highly seeked platform for the electrochemical based bio detections (Li et al., 2017). TMDs have been used for the detection of various analytes such as nucleic acids (DNA or RNA), small molecules such as glucose, hydrogen peroxide, cholesterol, various disease biomarkers and many more (Hu et al., 2017). Among various TMDs, the most extensively studied material MoS_2. It has been reported to be used in all potential applications of biosensor. The work on MoS_2 is so extensive that there are multiple reviews to recollect the work done (Barua et al., 2018). These have been reported to be used for the detection of analytes such as glucose, DNA, dopamine, hydrogen peroxide, and various cancer antigens, etc. (Barua et al., 2018; Liu & Liu, 2018) (Fig. 5).

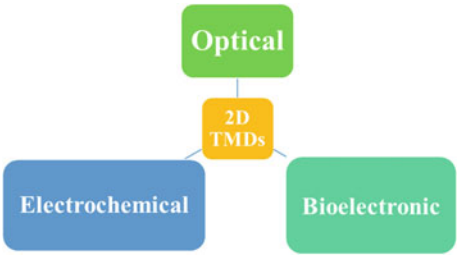

Fig. 5 Use of 2D TMD materials as different sensors

3 Conclusion

2D materials have been shown to be very promising candidates for various applications. This material is better as compared to others because of simple synthesis methods, high yields and easy to control properties. This material stands out from the other materials because of its optical, electrical and catalytic applications. These properties have been exploited for various applications such as biosensing, catalysis and energy generation. This chapter tried to highlight the various 2D materials available while mentioning their properties, synthesis methods, functionalizing agents and applications. Due to their immense potential, more and more research is going on with the 2D materials and their composites to achieve real-life applications.

Acknowledgements The authors acknowledge the support of Director, CSIR-CSIO, Chandigarh for his constant encouragement. M.G acknowledges the SRF-GATE fellowship from Council of Scientific and Industrial Research (CSIR-HRDG), New Delhi. N.V acknowledges JRF fellowship received from Council of Scientific and Industrial Research (CSIR), New Delhi, through project HCP 0012.

References

(2016). *Expanding our 2D vision*. Nature Reviews Materials 1: 16089.

Agarwal, V., & Chatterjee, K. (2018). Recent advances in the field of transition metal dichalcogenides for biomedical applications. *Nanoscale, 10*(35), 16365–16397.

Ahmed, S., & Yi, J. (2017). Two-dimensional transition metal dichalcogenides and their charge carrier mobilities in field-effect transistors. *Nano-Micro Letters, 9*(4), 50.

Akinwande, D., Brennan, C. J., Bunch, J. S., Egberts, P., Felts, J. R., Gao, H., Huang, R., Kim, J.-S., Li, T., Li, Y., Liechti, K. M., Lu, N., Park, H. S., Reed, E. J., Wang, P., Yakobson, B. I., Zhang, T., Zhang, Y.-W., Zhou, Y., & Zhu, Y. (2017). A review on mechanics and mechanical properties of 2D materials—Graphene and beyond. *Extreme Mechanics Letters, 13*, 42–77.

Azadmanjiri, J., Srivastava, V. K., Kumar, P., Wang, J., & Yu, A. (2018). Graphene-supported 2D transition metal oxide heterostructures. *Journal of Materials Chemistry A, 6*(28), 13509–13537.

Barua, S., Dutta, H. S., Gogoi, S., Devi, R., & Khan, R. (2018). Nanostructured MoS2-based advanced biosensors: A review. *ACS Applied Nano Materials, 1*(1), 2–25.

Berkelbach, T. C., & Reichman, D. R. (2018). Optical and excitonic properties of atomically thin transition-metal dichalcogenides. *Annual Review of Condensed Matter Physics, 9*(1), 379–396.

Butler, S. Z., Hollen, S. M., Cao, L., Cui, Y., Gupta, J. A., Gutiérrez, H. R., Heinz, T. F., Hong, S. S., Huang, J., Ismach, A. F., Johnston-Halperin, E., Kuno, M., Plashnitsa, V. V., Robinson, R. D., Ruoff, R. S., Salahuddin, S., Shan, J., Shi, L., Spencer, M. G., … Goldberger, J. E. (2013). Progress, challenges, and opportunities in two-dimensional materials beyond graphene. *ACS Nano, 7*(4), 2898–2926.

Chernozatonskii, L. A., & Artyukh, A. A. (2018). Quasi-two-dimensional transition metal dichalcogenides: Structure, synthesis, properties, and applications. *Physics-Uspekhi, 61*(1), 2–28.

Chimene, D., Alge, D. L., & Gaharwar, A. K. (2015). Two-dimensional nanomaterials for biomedical applications: Emerging trends and future prospects. *Advanced Materials, 27*(45), 7261–7284.

Choi, J., Zhang, H., & Choi, J. H. (2016). Modulating optoelectronic properties of two-dimensional transition metal dichalcogenide semiconductors by photoinduced charge transfer. *ACS Nano, 10*(1), 1671–1680.

Choi, W., Choudhary, N., Han, G. H., Park, J., Akinwande, D., & Lee, Y. H. (2017). Recent development of two-dimensional transition metal dichalcogenides and their applications. *Materials Today, 20*(3), 116–130.

Cui, X., Zhang, C., Hao, R., & Hou, Y. (2011). Liquid-phase exfoliation, functionalization and applications of graphene. *Nanoscale, 3*(5), 2118–2126.

Das, S., Robinson, J. A., Dubey, M., Terrones, H., & Terrones, M. (2015). Beyond graphene: Progress in novel two-dimensional materials and van der Waals solids. *Annual Review of Materials Research, 45*(1), 1–27.

Dolez, P. I. (2015). Chapter 1.1—Nanomaterials definitions, classifications, and applications. In P. I. Dolez (Ed.), *Nanoengineering* (pp. 3–40). Amsterdam: Elsevier.

Dral, A. P., & ten Elshof, J. E. (2018). 2D metal oxide nanoflakes for sensing applications: Review and perspective. *Sensors and Actuators B: Chemical, 272*, 369–392.

Eda, G., Fanchini, G., & Chhowalla, M. (2008). Large-area ultrathin films of reduced graphene oxide as a transparent and flexible electronic material. *Nature Nanotechnology, 3*(5), 270.

Feng, X., Chen, W., & Yan, L. (2016). Electrochemical reduction of bulk graphene oxide materials. *RSC Advances, 6*(83), 80106–80113.

Gao, L., Li, Y., Xiao, M., Wang, S., Fu, G., & Wang, L. (2017). "Synthesizing new types of ultrathin 2D metal oxide nanosheets via half-successive ion layer adsorption and reaction. *2D Materials, 4*(2): 025031.

Gao, X., Jang, J., & Nagase, S. (2009). Hydrazine and thermal reduction of graphene oxide: Reaction mechanisms, product structures, and reaction design. *The Journal of Physical Chemistry C, 114*(2), 832–842.

Geim, A., & Novoselov, K. (2007). The rise of graphene. *Naturematerials, 6*, 183–191.

Geim, A. K. (2009). Graphene: Status and prospects. *Science, 324*(5934), 1530–1534.

Giri, A., Park, G., Yang, H., Pal, M., Kwak, J., & Jeong, U. (2018). Synthesis of 2D metal chalcogenide thin films through the process involving solution-phase deposition. *Advanced Materials, 30*(25), 1707577.

Gong, C., Zhang, Y., Chen, W., Chu, J., Lei, T., Pu, J., Dai, L., Wu, C., Cheng, Y., Zhai, T., Li, L., & Xiong, J. (2017). Electronic and optoelectronic applications based on 2D novel anisotropic transition metal dichalcogenides. In *Advanced Science (Weinheim, Baden-Wurttemberg, Germany), 4*(12), 1700231–1700231.

Gould, T., Lebègue, S., Björkman, T., & Dobson, J. F. (2016). Chapter One—2D structures beyond graphene: The brave new world of layered materials and how computers can help discover them. In F. Iacopi, J. J. Boeckl & C. Jagadish (Eds.), *Semiconductors and semimetals* (Vol. 95, pp. 1–33). Elsevier.

Guan, G., Zhang, S., Liu, S., Cai, Y., Low, M., Teng, C. P., Phang, I. Y., Cheng, Y., Duei, K. L., Srinivasan, B. M., Zheng, Y., Zhang, Y.-W., & Han, M.-Y. (2015). Protein induces layer-by-layer exfoliation of transition metal dichalcogenides. *Journal of the American Chemical Society, 137*(19), 6152–6155.

Gupta, A., Sakthivel, T., & Seal, S. (2015). Recent development in 2D materials beyond graphene. *Progress in Materials Science, 73*, 44–126.

Gupta, S., Shirodkar, S. N., Kutana, A., & Yakobson, B. I. (2018). In pursuit of 2D materials for maximum optical response. *ACS Nano, 12*(11), 10880–10889.

Haque, F., Daeneke, T., Kalantar-zadeh, K., & Ou, J. Z. (2017). Two-dimensional transition metal oxide and chalcogenide-based photocatalysts. *Nano-Micro Letters, 10*(2), 23.

Haque, F., Daeneke, T., Kalantar-zadeh, K., & Ou, J. Z. (2018). Two-dimensional transition metal oxide and chalcogenide-based photocatalysts. *Nano-Micro Letters, 10*(2), 23.

Heard, C. J., Čejka, J., Opanasenko, M., Nachtigall, P., Centi, G., & Perathoner, S. (2019). 2D oxide nanomaterials to address the energy transition and catalysis. *Advanced Materials, 31*(3), 1801712.

Hong, S. B., Jeong, J.-M., Kang, H. G., Seo, D., Cha, Y., Jeon, H., Lee, G. Y., Irshad, M., Kim, D. H., & Hwang, S. Y. (2018). Fast and scalable hydrodynamic synthesis of MnO_2/defect-free graphene nanocomposites with high rate capability and long cycle life. *ACS Applied Materials & Interfaces, 10*(41), 35250–35259.

Hu, Y., Huang, Y., Tan, C., Zhang, X., Lu, Q., Sindoro, M., Huang, X., Huang, W., Wang, L., & Zhang, H. (2017). Two-dimensional transition metal dichalcogenide nanomaterials for biosensing applications. *Materials Chemistry Frontiers, 1*(1), 24–36.

Hu, Z., Xiao, X., Jin, H., Li, T., Chen, M., Liang, Z., Guo, Z., Li, J., Wan, J., Huang, L., Zhang, Y., Feng, G., & Zhou, J. (2017). Rapid mass production of two-dimensional metal oxides and hydroxides via the molten salts method. *Nature Communications, 8*, 15630.

Huang, W., Gan, L., Li, H., Ma, Y., & Zhai, T. (2016). 2D layered group IIIA metal chalcogenides: Synthesis, properties and applications in electronics and optoelectronics. *CrystEngComm, 18*(22), 3968–3984.

Huang, X., Qi, X., Boey, F., & Zhang, H. (2012). Graphene-based composites. *Chemical Society Reviews, 41*(2), 666–686.

Hummers, W. S., & Offeman, R. E. (1958). Preparation of Graphitic Oxide. *Journal of the American Chemical Society, 80*(6), 1339–1339.

Jaiswal, M. K., Carrow, J. K., Gentry, J. L., Gupta, J., Altangerel, N., Scully, M., & Gaharwar, A. K. (2017). Vacancy-driven gelation using defect-rich nanoassemblies of 2D transition metal dichalcogenides and polymeric binder for biomedical applications. *Advanced Materials, 29*(36), 1702037.

Jariwala, D., Sangwan, V. K., Lauhon, L. J., Marks, T. J., & Hersam, M. C. (2014). Emerging device applications for semiconducting two-dimensional transition metal dichalcogenides. *ACS Nano, 8*(2), 1102–1120.

Jung, Y., Shen, J., & Cha, J. J. (2014). Surface effects on electronic transport of 2D chalcogenide thin films and nanostructures. *Nano Convergence, 1*(1), 18.

Kang, J., Cao, W., Xie, X., Sarkar, D., Liu, W., & Banerjee, K. (2014). *Graphene and beyond-graphene 2D crystals for next-generation green electronics*, SPIE.

Khan, M. A., & Leuenberger Michael, N. (2018). Optoelectronics with single layer group-VIB transition metal dichalcogenides. *Nanophotonics., 7*, 1589.

Kim, J. H., Jeong, J. H., Kim, N., Joshi, R., & Lee, G.-H. (2018). Mechanical properties of two-dimensional materials and their applications. *Journal of Physics D: Applied Physics, 52*(8), 083001.

Kim, K. S., Zhao, Y., Jang, H., Lee, S. Y., Kim, J. M., Kim, K. S., Ahn, J.-H., Kim, P., Choi, J.-Y., & Hong, B. H. (2009). Large-scale pattern growth of graphene films for stretchable transparent electrodes. *Nature, 457*(7230), 706.

Kobayashi, T., Bando, M., Kimura, N., Shimizu, K., Kadono, K., Umezu, N., Miyahara, K., Hayazaki, S., Nagai, S., & Mizuguchi, Y. (2013). Production of a 100-m-long high-quality graphene transparent conductive film by roll-to-roll chemical vapor deposition and transfer process. *Applied Physics Letters, 102*(2), 023112.

Kostarelos, K. (2016). Translating graphene and 2D materials into medicine. *Nature Reviews Materials, 1*, 16084.

Kuc, A., & Heine, T. (2016). On the stability and electronic structure of transition-metal dichalcogenide monolayer alloys Mo1−xXxS2−ySey with X = W, Nb. *Electronics, 5*(1), 1.

Larionov, K. V., Kvashnin, D. G., & Sorokin, P. B. (2018). 2D FeO: A new member in 2D metal oxide family. *The Journal of Physical Chemistry C, 122*(30), 17389–17394.

Lee, C., Wei, X., Kysar, J. W., & Hone, J. (2008). Measurement of the elastic properties and intrinsic strength of monolayer graphene. *Science, 321*(5887), 385–388.

Lee, J., Huang, J., Sumpter, B. G., & Yoon, M. (2017). Strain-engineered optoelectronic properties of 2D transition metal dichalcogenide lateral heterostructures. *2D Materials, 4*(2), 021016.

Lei, W., Portehault, D., Dimova, R., & Antonietti, M. (2011). Boron carbon nitride nanostructures from salt melts: Tunable water-soluble phosphors. *Journal of the American Chemical Society, 133*(18), 7121–7127.

Li, H., Jia, X., Zhang, Q., & Wang, X. (2018). Metallic transition-metal dichalcogenide nanocatalysts for energy conversion. *Chemistry, 4*(7), 1510–1537.

Li, X., Shan, J., Zhang, W., Su, S., Yuwen, L., & Wang, L. (2017). Recent advances in synthesis and biomedical applications of two-dimensional transition metal dichalcogenide nanosheets. *Small (weinheim an Der Bergstrasse, Germany), 13*(5), 1602660.

Lin, Z., McCreary, A., Briggs, N., Subramanian, S., Zhang, K., Sun, Y., Li, X., Borys, N. J., Yuan, H., Fullerton-Shirey, S. K., Chernikov, A., Zhao, H., McDonnell, S., Lindenberg, A. M., Xiao, K., LeRoy, B. J., Drndić, M., Hwang, J. C. M., Park, J., Chhowalla, M., Schaak, R. E., Javey, A., Hersam, M. C., Robinson, J., & Terrones, M. (2016). 2D materials advances: From large scale synthesis and controlled heterostructures to improved characterization techniques, defects and applications. *2D Materials, 3*(4), 042001.

Liu, T., & Liu, Z. (2018). 2D MoS2 nanostructures for biomedical applications. *Advanced Healthcare Materials, 7*(8), 1701158.

Loh, T. A. J., Hu, Y., Pham, K. C., Tan, Z., & Chua, D. H. C. (2016). Multifunctional metal oxides and 2D materials utilizing carbon nanotubes as a base template for clean energy and other applications. In *2016 IEEE 16th International Conference on Nanotechnology (IEEE-NANO).*

Lv, R., Robinson, J. A., Schaak, R. E., Sun, D., Sun, Y., Mallouk, T. E., & Terrones, M. (2015). Transition metal dichalcogenides and beyond: Synthesis, properties, and applications of single- and few-layer nanosheets. *Accounts of Chemical Research, 48*(1), 56–64.

Ma, S., Zeng, L., Tao, L., Tang, C. Y., Yuan, H., Long, H., Cheng, P. K., Chai, Y., Chen, C., Fung, K. H., Zhang, X., Lau, S. P., & Tsang, Y. H. (2017). Enhanced photocatalytic activity of WS(2) film by laser drilling to produce porous WS(2)/WO(3) heterostructure. *Scientific Reports, 7*(1), 3125–3125.

Mannix, A. J., Kiraly, B., Hersam, M. C., & Guisinger, N. P. (2017). Synthesis and chemistry of elemental 2D materials. *Nature Reviews Chemistry, 1*, 0014.

Mas-Ballesté, R., Gómez-Navarro, C., Gómez-Herrero, J., & Zamora, F. (2011). 2D materials: To graphene and beyond. *Nanoscale, 3*(1), 20–30.

Mei, X., Meng, X., & Wu, F. (2015). Hydrothermal method for the production of reduced graphene oxide. *Physica E: Low-Dimensional Systems and Nanostructures, 68*, 81–86.

Mishra, A. K., Lakshmi, K. V., & Huang, L. (2015). Eco-friendly synthesis of metal dichalcogenides nanosheets and their environmental remediation potential driven by visible light. *Scientific Reports, 5*, 15718.

Mulenko, S. A., Stefan, N., Miroiu, F., Mihailescu, I. N., Gorbachuk, N. T., & Nikirin, V. A. (2016). Laser synthesis of 2D heterostructures of transitional metal oxides for photo sensors with high sensitivity. *Journal of Laser Applications, 28*(4), 042006.

Osada, M., & Sasaki, T. (2013). 2D oxide nanosheets: Controlled assembly and applications. *ECS Transactions, 50*(6), 111–116.

Osborne, I. S. (2016). The rise and rise of 2D materials. *Science, 353*(6298), 458–460.

Peng, L., Xiong, P., Ma, L., Yuan, Y., Zhu, Y., Chen, D., Luo, X., Lu, J., Amine, K., & Yu, G. (2017). Holey two-dimensional transition metal oxide nanosheets for efficient energy storage. *Nature Communications, 8*, 15139.

Peng, W., Li, Y., Zhang, F., Zhang, G., & Fan, X. (2017). Roles of two-dimensional transition metal dichalcogenides as cocatalysts in photocatalytic hydrogen evolution and environmental remediation. *Industrial & Engineering Chemistry Research, 56*(16), 4611–4626.

Qiu, B., Zhou, Y., Ma, Y., Yang, X., Sheng, W., Xing, M., & Zhang, J. (2015). Facile synthesis of the Ti 3+ self-doped TiO 2-graphene nanosheet composites with enhanced photocatalysis. *Scientific Reports, 5*, 8591.

Rasmussen, F. A., & Thygesen, K. S. (2015). Computational 2D materials database: Electronic structure of transition-metal dichalcogenides and oxides. *The Journal of Physical Chemistry C, 119*(23), 13169–13183.

Ren, X., Pang, L., Zhang, Y., Ren, X., Fan, H., & Liu, S. (2015). One-step hydrothermal synthesis of monolayer MoS2 quantum dots for highly efficient electrocatalytic hydrogen evolution. *Journal of Materials Chemistry A, 3*(20), 10693–10697.

Ren, X., Qi, X., Shen, Y., Xiao, S., Xu, G., Zhang, Z., Huang, Z., & Zhong, J. (2016). 2D co-catalytic MoS2nanosheets embedded with 1D TiO_2 nanoparticles for enhancing photocatalytic activity. *Journal of Physics D: Applied Physics, 49*(31), 315304.

Robinson, J. T., Burgess, J. S., Junkermeier, C. E., Badescu, S. C., Reinecke, T. L., Perkins, F. K., Zalalutdniov, M. K., Baldwin, J. W., Culbertson, J. C., & Sheehan, P. E. (2010). Properties of fluorinated graphene films. *Nano Letters, 10*(8), 3001–3005.

Rosman, N. N., Mohamad Yunus, R., Jeffery Minggu, L., Arifin, K., Salehmin, M. N. I., Mohamed, M. A., & Kassim, M. B. (2018). Photocatalytic properties of two-dimensional graphene and layered transition-metal dichalcogenides based photocatalyst for photoelectrochemical hydrogen generation: An overview. *International Journal of Hydrogen Energy, 43*(41), 18925–18945.

Sajedi-Moghaddam, A., Saievar-Iranizad, E., & Pumera, M. (2017). Two-dimensional transition metal dichalcogenide/conducting polymer composites: Synthesis and applications. *Nanoscale, 9*(24), 8052–8065.

Schmidt, H., Giustiniano, F., & Eda, G. (2015). Electronic transport properties of transition metal dichalcogenide field-effect devices: Surface and interface effects. *Chemical Society Reviews, 44*(21), 7715–7736.

Schriver, M., Regan, W., Gannett, W. J., Zaniewski, A. M., Crommie, M. F., & Zettl, A. (2013). Graphene as a long-term metal oxidation barrier: Worse than nothing. *ACS Nano, 7*(7), 5763–5768.

Shavanova, K., Bakakina, Y., Burkova, I., Shtepliuk, I., Viter, R., Ubelis, A., Beni, V., Starodub, N., Yakimova, R., & Khranovskyy, V. (2016). Application of 2D non-graphene materials and 2D oxide nanostructures for biosensing technology. *Sensors (basel, Switzerland), 16*(2), 223–223.

Song, J.-G., Park, K., Park, J., & Kim, H. (2015). Vapor deposition techniques for synthesis of two-dimensional transition metal dichalcogenides. *Applied Microscopy, 45*(3), 119–125.

Su, C.-Y., Lu, A.-Y., Xu, Y., Chen, F.-R., Khlobystov, A. N., & Li, L.-J. (2011). High-quality thin graphene films from fast electrochemical exfoliation. *ACS Nano, 5*(3), 2332–2339.

Tiwari, J. N., Tiwari, R. N., & Kim, K. S. (2012). Zero-dimensional, one-dimensional, two-dimensional and three-dimensional nanostructured materials for advanced electrochemical energy devices. *Progress in Materials Science, 57*(4), 724–803.

Tripathi, P., Patel, C., Prakash, R., Shaz, M., & Srivastava, O. (2013). *Synthesis of high-quality graphene through electrochemical exfoliation of graphite in alkaline electrolyte*. arXiv preprint arXiv:1310.7371.

Unarunotai, S., Murata, Y., Chialvo, C. E., Kim, H.-S., MacLaren, S., Mason, N., Petrov, I., & Rogers, J. A. (2009). Transfer of graphene layers grown on SiC wafers to other substrates and their integration into field effect transistors. *Applied Physics Letters, 95*(20), 202101.

Vattikuti, S. V. P., & Byon, C. (2015). Synthesis and structural characterization of Al_2O_3-Coated MoS2 spheres for photocatalysis applications. *Journal of Nanomaterials, 2015*, 9.

Wan, X., Chen, K., Chen, Z., Xie, F., Zeng, X., Xie, W., Chen, J., & Xu, J. (2017). Controlled electrochemical deposition of large-area MoS2 on graphene for high-responsivity photodetectors. *Advanced Functional Materials, 27*(19), 1603998.

Wang, F., Wang, Z., Wang, Q., Wang, F., Yin, L., Xu, K., Huang, Y., & He, J. (2015). Synthesis, properties and applications of 2D non-graphene materials. *Nanotechnology, 26*(29), 292001.

Wassei, J. K., & Kaner, R. B. (2010). Graphene, a promising transparent conductor. *Materials Today, 13*(3), 52–59.

Wei, Z., Li, B., Xia, C., Cui, Y., He, J., Xia, J.-B., & Li, J. (2018). Various structures of 2D transition-metal dichalcogenides and their applications. *Small Methods, 2*(11), 1800094.

Wen, W., Song, Y., Yan, X., Zhu, C., Du, D., Wang, S., Asiri, A. M., & Lin, Y. (2018). Recent advances in emerging 2D nanomaterials for biosensing and bioimaging applications. *Materials Today, 21*(2), 164–177.

Wu, J., Rodrigues, M. T. F., Vajtai, R., & Ajayan, P. M. (2016). Tuning the electrochemical reactivity of boron-and nitrogen-substituted graphene. *Advanced Materials, 28*(29), 6239–6246.

Wu, Y., Zou, X., Sun, M., Cao, Z., Wang, X., Huo, S., Zhou, J., Yang, Y., Yu, X., & Kong, Y. (2016). 200 GHz maximum oscillation frequency in CVD graphene radio frequency transistors. *ACS Applied Materials & Interfaces, 8*(39), 25645–25649.

Xia, C., & Li, J. (2016). Recent advances in optoelectronic properties and applications of two-dimensional metal chalcogenides. *Journal of Semiconductors, 37*(5), 051001.

Xie, L., & Cui, X. (2016). Manipulating spin-polarized photocurrents in 2D transition metal dichalcogenides. *Proceedings of the National Academy of Sciences, 113*(14), 3746–3750.

Xu, S., Zhan, J., Man, B., Jiang, S., Yue, W., Gao, S., Guo, C., Liu, H., Li, Z., & Wang, J. (2017). Real-time reliable determination of binding kinetics of DNA hybridization using a multi-channel graphene biosensor. *Nature Communications, 8*, 14902.

Yang, T., Song, T. T., Callsen, M., Zhou, J., Chai, J. W., Feng, Y. P., Wang, S. J., & Yang, M. (2019). Atomically thin 2D transition metal oxides: Structural reconstruction, interaction with substrates, and potential applications. *Advanced Materials Interfaces, 6*(1), 1801160.

Yin, Z., Tordjman, M., Lee, Y., Vardi, A., Kalish, R., & del Alamo, J. A. (2018). Enhanced transport in transistor by tuning transition-metal oxide electronic states interfaced with diamond. *Science Advances, 4*(9), eaau0480.

You, J., Hossain, M. D., & Luo, Z. (2018). Synthesis of 2D transition metal dichalcogenides by chemical vapor deposition with controlled layer number and morphology. *Nano Convergence, 5*(1), 26.

Yu, J., Hu, X., Li, H., Zhou, X., & Zhai, T. (2018). Large-scale synthesis of 2D metal dichalcogenides. *Journal of Materials Chemistry C, 6*(17), 4627–4640.

Yu, Y., Nam, G.-H., He, Q., Wu, X.-J., Zhang, K., Yang, Z., Chen, J., Ma, Q., Zhao, M., Liu, Z., Ran, F.-R., Wang, X., Li, H., Huang, X., Li, B., Xiong, Q., Zhang, Q., Liu, Z., Gu, L., … Zhang, H. (2018). High phase-purity 1T′-MoS2- and 1T′-MoSe2-layered crystals. *Nature Chemistry, 10*(6), 638–643.

Yuge, K. (2009). Phase stability of boron carbon nitride in a heterographene structure: A first-principles study. *Physical Review B, 79*(14), 144109.

Zeng, S., Hu, S., Xia, J., Anderson, T., Dinh, X.-Q., Meng, X.-M., Coquet, P., & Yong, K.-T. (2015). Graphene–MoS2 hybrid nanostructures enhanced surface plasmon resonance biosensors. *Sensors and Actuators B: Chemical, 207*, 801–810.

Zhang, G., & Zhang, Y.-W. (2017). Thermoelectric properties of two-dimensional transition metal dichalcogenides. *Journal of Materials Chemistry C, 5*(31), 7684–7698.

Zhang, H. (2018). Introduction: 2D materials chemistry. *Chemical Reviews, 118*(13), 6089–6090.

Zhang, K., Lin, Y. C., & Robinson, J. A. (2016). Chapter Five—Synthesis, properties, and stacking of two-dimensional transition metal dichalcogenides. In F. Iacopi, J. J. Boeckl & C. Jagadish (Eds.), *Semiconductors and semimetals* (Vol. 95, pp. 189–219). Elsevier.

Zheng, W., Jiang, Y., Hu, X., Li, H., Zeng, Z., Wang, X., & Pan, A. (2018). Light emission properties of 2D transition metal dichalcogenides: Fundamentals and applications. *Advanced Optical Materials, 6*(21), 1800420.

Zhou, J., Lin, J., Huang, X., Zhou, Y., Chen, Y., Xia, J., Wang, H., Xie, Y., Yu, H., Lei, J., Wu, D., Liu, F., Fu, Q., Zeng, Q., Hsu, C.-H., Yang, C., Lu, L., Yu, T., Shen, Z., … Liu, Z. (2018). A library of atomically thin metal chalcogenides. *Nature, 556*(7701), 355–359.

Zhou, S. Y., Gweon, G.-H., Fedorov, A., de First, P., De Heer, W., Lee, D.-H., Guinea, F., Neto, A. C., & Lanzara, A. (2007). Substrate-induced bandgap opening in epitaxial graphene. *Nature Materials, 6*(10), 770.

Zhu, Y., James, D. K., & Tour, J. M. (2012). New routes to graphene, graphene oxide and their related applications. *Advanced Materials, 24*(36), 4924–4955.

Zhu, Y., Murali, S., Cai, W., Li, X., Suk, J. W., Potts, J. R., & Ruoff, R. S. (2010). Graphene and graphene oxide: Synthesis, properties, and applications. *Advanced Materials, 22*(35), 3906–3924.

Chapter 3
Different Techniques for Designing and Fabrication of 2D Materials

Subhash Singh, Dharmendra Pratap Singh, Kartikey Verma, and Vikas Kumar

1 Introduction

The predominant aspect of technology is the materials. Human life is simplified through technology in the form of domestic goods and electronic gadgets like mobiles, laptop, high quality sensing devices, etc. (Blake et al., 2008; Choi et al., 2010; Tiwari et al., 2016). The field of research gets a boost both in the experimental as well as theoretical aspects when novel materials are discovered (Choi et al., 2010; Oraon et al., 2015; Orecchioni et al., 2015). This provides a stimulating opportunity to revise the existing problems and address new issues related to the particular field of research (Jo et al., 2012; Oraon et al., 2015; Orecchioni et al., 2015). Carbon is one of the most fascinating elements in the universe (Blake et al., 2008; Choi et al., 2010; Jo et al., 2012; Oraon et al., 2015; Tiwari et al., 2016). Its properties always had have a matter of deep consideration and critical research (Jo et al., 2012; Tiwari et al., 2016). Many allotropic forms of carbon are well known, among which carbon nanotubes, graphene, fullerenes and the graphene nanoribbon are widely premeditated allotropes. Especially in the nanocarbon fraternity (Tiwari et al., 2016). Among these nanocarbon materials (fullerenes, carbon nanotubes graphene and graphene

S. Singh (✉)
Department of Production and Industrial Engineering, National Institute of Technology Jamshedpur, Jamshedpur, Jharkhand 831014, India

D. P. Singh
Unité de Dynamique et Structure des Matériaux Moléculaires (UDSMM), Université du Littoral Côte d'Opale (ULCO), 62228 Calais, France

K. Verma
Department of Chemical Engineering, Indian Institute of Technology, Kanpur 208016, India

V. Kumar
Department of Automotive Technology, Mechanical Department Division, Federal TVET Institute, Addis Ababa, Ethiopia

S. Singh et al. (eds.), *Advanced Applications of 2D Nanostructures*,
Materials Horizons: From Nature to Nanomaterials,
https://doi.org/10.1007/978-981-16-3322-5_3

Nanoribbon), graphene is the latest discovery (Allen et al., 2010; Tiwari et al., 2016). Thus graphene is most recent allotrope of carbon discovered by Sir Andre Geim and Novoselov (2007). It is completely 2D graphitic material with single layer and thickness of an atom, which is unbelievably very strong, an excellent conductor of electricity and heat (Geim & Novoselov, 2007; Allen et al., 2010; Balandin, 2011; Tiwari et al., 2016). Such amazing electronic, thermal, magnetic characteristics with 2D structure, graphene has provided a lot toward essential research studies in the area of condensed matter physics, materials science, fundamental chemistry and physics (Geim & Novoselov, 2007; McCann, 2007; Nika et al., 2009; Ritter & Lyding, 2009; Balandin, 2011; Tiwari et al., 2016). Basically, graphene is a material of carbon with layer of single-atom. But at the time of production, two or more layers as by-products are unavoidable (Tiwari et al., 2016a, b). Hence these exceptional properties forced many researchers to treat graphene as a magical form of carbon (Tiwari et al., 2016b).

In this way, graphene has materialized as an exciting prospect for all researchers (Geim & Novoselov, 2007; McCann, 2007; Nika et al., 2009; Ritter & Lyding, 2009; Balandin, 2011; Tiwari et al., 2016b). The thermal conductance of graphene is greater compared to Cu and exhibits extremely essential carrier mobility (200,000 $cm^2/V^{-1}s^{-1}$) (Geim & Novoselov, 2007; Allen et al., 2010; Balandin, 2011; Tiwari et al., 2016b). The graphene possesses large surface area (>SWCNTs, 2630 m^2g^{-1}), outstanding mechanical, thermal and elastic characteristics (Geim & Novoselov, 2007; Allen et al., 2010; Balandin, 2011; Tiwari et al., 2016b). Initial research on graphene synthesis and that of its derivatives focused on oxidation of graphite (Allen et al., 2010; Luo et al., 2013; Tiwari et al., 2016b). Hummer's method (presently with various modifications) was employed to produce graphene in scalable amount which involves the processes of oxidation as well as reduction. Graphene oxide was obtained from graphite through oxidation and further reduced to graphene in a reluctant, sodium borohydride or hydrazine (Compton & Nguyen, 2010; Luo et al., 2013). However, at present many approaches have been progressed for direct and indirect production of graphene and derivatives (Compton & Nguyen, 2010; Tiwari et al., 2016b). It is very important to mention that application of functionalized and modified graphene is much greater than the pristine graphene (Pei et al., 2014; Tiwari et al., 2016b). Figure 1 shows the importance of modified graphene over pristine graphene.

The real-time uses of graphene and derivatives are still tested by problems of scalable synthesis, storage and suitable processing (Pei et al., 2014; Tiwari et al., 2016b). Therefore, suitable modifications are very necessary on the surface of graphene. In this line, several ground bricking work have been reported which mainly concerned with the incorporation different functional moieties on graphene surface. Among various modifications some techniques which involve modification of graphene which is also stable have drawn massive interest (Singh et al., 2012; Pei et al., 2014). However, some of the widely used modifications suffer from some serious drawbacks. For example many reduction processes from GR to GO removed function groups but not fervently, and resulted in oxygen-containing moieties like –OH, –COOH and groups of epoxy (Allen et al., 2010; Tiwari et al., 2016a). Hence, the reduction process gives reasonably –OH functional groups on graphene sheets, which

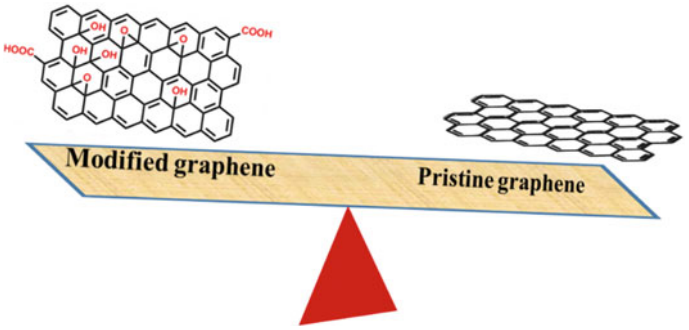

Fig. 1 Schematic illustration for the importance of modified graphene over pristine graphene

have a habit to summative irreversibly (Allen et al., 2010; Tiwari et al., 2016b). The irreversible accretion of graphene via p–p restacking will significantly encumber its fabrication, storage and distorted its uniqueness. Therefore, it is essential to have a stable, functionalized graphene through modified material. This avoids unnecessary accumulation. In this book chapter, authors have tried to recapitulate the approaches that modify graphene chemically, the effects of modification and the prospective applications across fields of science and technology. In other word for application purposes, various chemical modifications could be achieved through either covalent or non-covalent bonding.

2 Approaches for Graphene Synthesis and Its Modification

2.1 Synthesis of Graphene

For graphene production, multiple processes have been established (Allen et al., 2010; Choi et al., 2010; Tiwari et al., 2016b). However, each developed approaches has their benefits and drawbacks (Tiwari et al., 2016b). Compared to other methods, chemical exfoliation is most common and widely used. It indulges in using extremely dangerous chemicals which create severe environmental issues. It is extremely tedious and time-consuming (Allen et al., 2010; Tiwari et al., 2016a). Structural defects are an integral part of the graphene sheet, which are directly in relation to the extraordinary material properties (Allen et al., 2010; Tiwari et al., 2016a; Bhuyan et al., 2016). The micromechanical cleavage (tape method developed by A. Geim and coworker), produces graphene of excellent quality but has poor yield with a long production time (Geim & Novoselov, 2007; Tiwari et al., 2016b). Likewise, for synthesis of ultrapure graphene CVD is one among the best available techniques (Reina et al., 2009). CVD technique for graphene production is costly and requires complex instruments, hence is not widely acceptable (Reina et al., 2009). Graphene

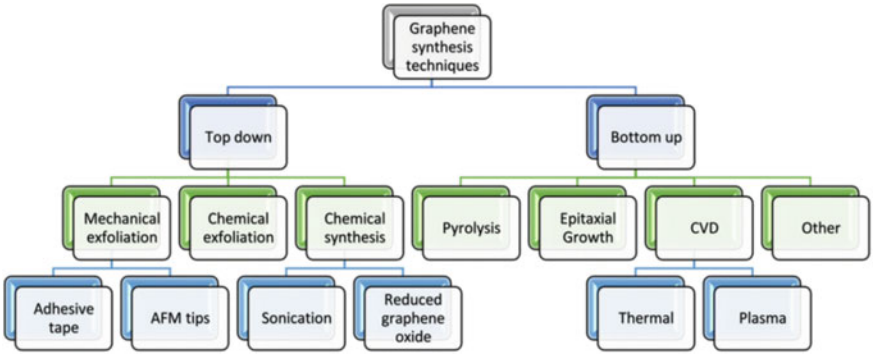

Fig. 2 Flow chart presenting the route of graphene synthesis. Reproduced with permission (Bhuyan et al., 2016)

synthesis through electrochemical expansion (ECE) is a cost and time effective which is potentially advantageous for mass production of GR. This is considered for its experimental ease and purification. In scientific community, this GR synthesis technique is widely acknowledged (Tiwari et al., 2017). Lastly, Tour and coworkers have excellently opened carbon nanotubes to produce nanoribbons (Tour & Kosynkin, 2015). However, a more enhanced technique is to be identified to effectively exfoliate graphite into graphene sheets which are solution-dispersible, which provides a better yield, without any considerable structural distortion and substance toxicity (Jiang, 2011; Bhuyan et al., 2016). Thus, for the scientists a significant challenge is to configure a facile method for pure single-layer graphene (SLGR) production at industrial scale (Reina et al., 2009). Flow chart in Fig. 2 shows the overview of GR synthesis methods. Various functional derivatives of graphene can be obtained according to the need in mass scale using various chemical regents, which generally includes an oxidation–reduction phenomenon. Oxidation of graphite sheets might help in exfoliation of GO sheets from huge graphitic layers whereas reduction technique recovers the conductivity of GO by retaining the (in-sheet conjugated) structure (Tiwari et al., 2017). However, in many modifications of graphene sheets recovery of conductivity is not possible.

2.2 Production of GO

Graphene oxide (GO) is considered as the most valuable precursors of graphene (Tiwari et al., 2016a). Graphene oxide (single or few oxidized layer of graphite) and Graphite oxide (huge aggregated oxidized graphitic layers), previously identified as graphitic acid or graphitic oxide, is an important derivative of graphite containing carbon, H_2 and O_2 in different ratios depending on extent of oxidation (Dikin et al., 2007; Chen et al., 2013; Dimiev & Tour, 2014; Tiwari et al., 2017). Strongly oxidized

bulk graphite (graphite oxide or graphene oxide) is a yellow colored solid with C to O ratio ranging from 2.1 to 2.9, which mostly restores graphite's skeletal structure but huge irregular spacing within the graphite skeleton (Dikin et al., 2007; Chen et al., 2013; Dimiev & Tour, 2014). History and discovery of graphene oxide is still a matter of debate (Brodie, 1859; Hummers & Offeman, 1958). However, it believed, that GO was initially identified by Benjamin C. Brodie (A prominent chemist of Oxford University U.K) in 1859, by nursing graphite powder with a suitable mixture of fuming potassium chlorate along with nitric acid (Brodie, 1859; Hummers, 1957; Hummers & Offeman, 1958). Benjamin reported production of "paper-like foils" with around 0.05 mm thickness (He et al., 1998). But before the Benjamin in 1957 Hummers and coworker reported a facile and safer, approach which is treated as one among the most efficient techniques for the graphene oxide production and nowadays it is commonly known as Hummers' Method (Brodie, 1859; Hummers & Offeman, 1958). In this method, they have used a mixture of H_2SO_4, $NaNO_3$, and $KMnO_4$, which is still commonly utilized, usually with certain amendments (He et al., 1998; Marcano et al., 2010). In 2012, Tang-Lau and coworkers developed a most common method (Tang-Lau method) for the production of graphene oxides using "bottom-up" approach where glucose is the only source is glucose. This method is considered safe and simple and also ecofriendly in comparison with conventional "top-down" technique, involving strong oxidizers (Tang et al., 2012). Thus characteristics of oxides of graphene are influenced by the extent of oxidation and preparation method. The Elemental composition and general specification of a good quality graphene oxide is given as

Nitrogen: 0–1%, Oxygen: 41–50%, Sulfur: 0–2%, Carbon: 49–56%, Hydrogen: 0–1%, Thickness: 80–105 μm, Porosity: 70–75%, Pore size: 0.025 μm.

2.3 Structure of Graphene Oxide

Graphene oxides reveal considerable differences in its structure and characteristics depending on extent of oxidation and preparation method (Brodie, 1859; Hummers & Offeman, 1958; Dikin et al., 2007; Tiwari et al., 2016a). Since graphene oxides contain –COOH on the edges and different oxygen functional moieties (hydroxyl groups/predominant epoxy) over the basal plane (Brodie, 1859; Hummers & Offeman, 1958; Dikin et al., 2007). FTIR spectrum of graphene oxides prepared of improved Hummers method is shown in Fig. 3b. The main peaks of graphene oxides in the FTIR spectrum very strongly support the existence of various oxygen functional groups (Reina et al., 2009; Tiwari et al., 2017). The stretching vibration of –OH peak generally rises at 3420 cm^{-1}. Here the peak is obtained at 3404 cm^{-1}. Hydrogen bonding is the reason for this lower region shift (Reina et al., 2009; Marcano et al., 2010; Tang et al., 2012; Tiwari et al., 2017). The C=O stretching vibration arises at 1743 cm^{-1}. C=C from nonoxidized sp^2 carbon bonds (1593–1620/cm), and C–O vibrations (Compton & Nguyen, 2010; Luo et al., 2013) (1250 cm^{-1}). The patterns

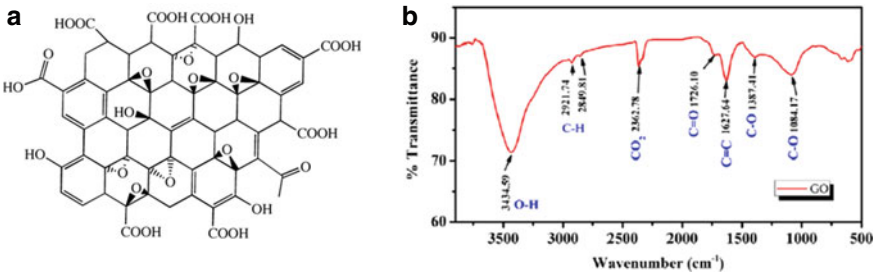

Fig. 3 Molecular structure of graphene oxide (**a**) and **b** FTIR spectrum of GO synthesized by improved Hummers methods (Taken from (Sudesh et al., 2013))

of XRD of pure graphite powder and GOSs are represented in Fig. 4b (Tiwari et al., 2017). Graphite powder exhibits a basal reflection (002) peak at $2\theta = 26.6^{o}$ (0.335 nm D-spacing) (Compton & Nguyen, 2010; Luo et al., 2013) (Fig. 4a) (Tiwari et al., 2017). However, graphene oxides show broad peaks between 9 and 12^{o} depending on the degree of oxidation (Reina et al., 2009; Marcano et al., 2010; Tang et al.,

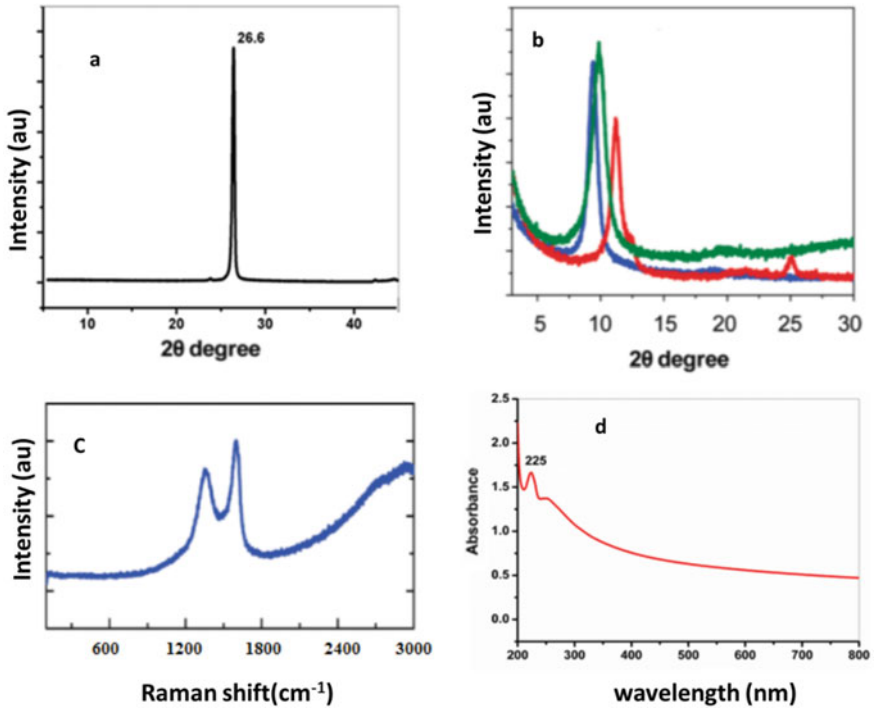

Fig. 4 XRD spectrum of graphite (**a**), GO (**b**), Raman spectrum (**c**) and Ultraviolet-visible spectrum (**d**) prepared through modified Hummers technique. Reproduced with permission (Marcano et al., 2010)

2012; Tiwari et al., 2017). Accordingly, (002) reflection peak flips to a smaller angle on oxidation (Tang et al., 2012). In present, spectrum of graphene oxides shows extremely wide peak at about 11.5°, matching to 0.77 nm inter-layer spacing (Tiwari et al., 2017). The intercalation of H_2O molecules and O_2 generation among the graphite layer enhances the D-spacing (Reina et al., 2009; Marcano et al., 2010; Tang et al., 2012; Tiwari et al., 2017). The addition, graphene oxides also have a broad and lower intense peak of $2\theta = 43^{o}$ was seen due to (001) plane of monolayers of graphene oxides (Marcano et al., 2010; Tang et al., 2012). For graphene and graphene derivatives, Raman spectroscopy corresponds to fingerprints (Marcano et al., 2010; Tiwari et al., 2016a, 2017). The fundamental characteristics in Raman spectrum of graphene oxides are the locations of band peaks (Tiwari et al., 2016a, 2017). The 1st order D and G peak, evolving through the vibrations of sp^2 hybridized carbon atoms, occur at about 1350 and 1580 cm^{-1}, respectively (Tiwari et al., 2016a, 2017). The G peak exhibits the optical phonons of E_{2g} at the Brillouin zone center. It evolves because of sp^2 stretched carbon pairs in aromatic ring and chains (Tiwari et al., 2017; Tang et al., 2012). The D peak shows the breathing manner of aromatic rings resulting due to the sample defects. Hence, D peak intensity measures the extent of disorder in graphene and derivatives (Reina et al., 2009; Tang et al., 2012; Tiwari et al., 2016a, 2017). The Raman spectrum of graphene oxides achieved at an excitation 532 nm is shown in Fig. 4c (Reina et al., 2009; Tang et al., 2012; Tiwari et al., 2017). Graphene oxides prepared by improved Hummers show intense G and D peak at 1580 and 1350 cm^{-1}, correspondingly. This uncovers prominent disorder of the structure due to functionalization of the sheets of graphite (Reina et al., 2009; Tang et al., 2012; Tiwari et al., 2017). Appearance of very wide 2D (2700/cm) along with $D + G$ or D^* (2940 cm^{-1}) peaks in graphene oxides spectrum is an indication of disorder in graphene because of oxidation (Reina et al., 2009; Tang et al., 2012). Ultraviolet-visible spectrum study provides vision into the nature and quality of GO (Tiwari et al., 2016a). Ultraviolet-visible absorbance spectrum of the graphene oxides aqueous solutions at an optimized concentration are shown in Fig. 4d (Tiwari et al., 2016a). As shown in the ultraviolet-visible spectrum, graphene oxides exhibit a $\pi - \pi^*$ absorption band around 225 nm with shoulder $n - \pi^*$ absorption band at 297 nm (Tang et al., 2012; Tiwari et al., 2016a, 2017). These two bands are treated as characteristics of graphene oxides (Tiwari et al., 2016a, 2017).

2.4 GO Characteristics and Applications

GO easily disperses in different matrices, organic solvents and water, due to the existence of O_2 functionalities (Tiwari et al., 2016a). This feature improves the electrical and mechanical characteristics of polymer or ceramic matrixes when combined with this material providing an important advantage (Tiwari et al., 2016a, b). GO has certain discrepancies within the networks of its sp^2 bonds. Hence, it behaves like an insulator when its electrical conductivity is considered (Choi et al., 2010; Tiwari et al., 2016a, b). It is essential for the GO to be reduced for its electrical conductivity

to be restored. This is possible only through the recovery of graphene's hexagonal lattice (McCann, 2007; Tiwari et al., 2016b). The dispersion of reduced GO becomes difficult upon removal of excessive groups of O_2 due to the formation of aggregates (Tang et al., 2012; Tiwari et al., 2016a). By functionalizing GO, the graphene characteristics can be altered. (Cui et al., 2011). The chemically modified graphene generated through different techniques has multiple uses (Cui et al., 2011; Sudesh et al., 2013). The GO may be functionalized through various methods based on the desired application (Zhu et al., 2010). Interestingly, GO and its almost all derivatives have dispensability in various organic solvents, H_2O, and in diverse environments, because the functional moieties of O_2 occur (Zhu et al., 2010; Sudesh et al., 2013). At the time of combining materials and ceramic/polymer mediums to enhance their properties (mechanical, magnetic and electrical), this characteristic remains extremely significant (Zhu et al., 2010; Chen et al., 2012). The physical and chemical characteristics of GO are changed by Functionalization (Chen et al., 2012). The obtained modified graphene (chemically) might have higher adaptability for a lot of applications (Zhu et al., 2010; Chen et al., 2012). The application desired determines the technique of GO functionalization (Chen et al., 2012). In biodevices/optoelectronics and drug delivery materials the modified graphene (chemically) can be more dispersible in organic solvents. The substitution of amines can enhance the dispersibility (Chen et al., 2012; Tiwari et al., 2016b). Previous studies indicate there is a possibility in the increase of nonlinear optical performance of GO nanoplatelets due to the attachment of porphyrin-modified primary amines and fullerene-modified secondary amines (Loh et al., 2010). For GO to be functional as a midway in the fabrication of multilayer or monolayer graphene nanofilms, it is crucial to form oxidization-reduction route capable of separating individual monoatomic carbon sheets and later separate them without altering their fundamental morphology (Loh et al., 2010; Tiwari et al., 2016a; b). Till date, chemical method (oxidation and reduction method) is seen as one of the most appropriate techniques for bulk production of graphene. And as mentioned above that it has been very problematic for materials chemist to conclude the assignment of synthesizing graphene sheets of bulk amount of graphene on a mass scale. Once this problem is tackled, it can be presumed that graphene will further be extensively used for industrial applications without the lag of cost. The most prominent application of GOs is diagrammatically shown in Fig. 5.

2.5 Some Very Important Surface Modification of Graphene

2.5.1 Amine-Modified Graphene

Graphene Oxide nanolayers have enormous surface area, so it can be employed as electrode material for ultra-capacitors, solar cells and for lithium and sodium batteries (De Adhikari et al., 2015; Oraon et al., 2016). It is inexpensive and easier to manufacture than graphene, and also very environmental friendly materials (De Adhikari et al., 2015; Oraon et al., 2016). It can be placed on a suitable substrate,

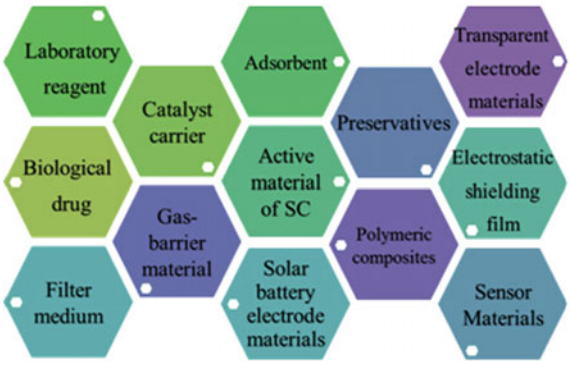

Fig. 5 Schematic representation of industrial application of graphene oxide and derivatives

and later converted as a conductor according to the need (Tiwari et al., 2016b). This is why most of the industrial research going toward the graphene oxide. In 2012 workers of BHU, University, India have produced amine-modified graphene very nicely to achieve a novel biomedical application (Singh et al., 2012; Pei et al., 2014). The method of modification and its use according to the Singh and coworkers given below;

Graphene oxide nanosheets were synthesized by refluxing commercial graphite powder of 5 g having strong acidic solution of nitric acid and sulfuric, as mentioned in the graphene oxide section (Marcano et al., 2010; Tang et al., 2012). The purified GO nanosheet solution was first dried-to-froze and then preserved in vacuum quiver at an ambient temperature until further use (Singh et al., 2012; Tang et al., 2012). The residual functional sites and vacancies are left when CO_2 is released. It is these which are the reason for the colloidal properties of reduced GO nanosheets in H_2O solutions (Singh et al., 2012). For amine functionalization, graphene oxide nanosheet (1 g) was stirred in dimethylformamide (DMF) and $SOCl_2$. This is subsequently filtered through PTFE membrane and washed repeatedly with purified methylene chloride (Singh et al., 2012). Obtained reduced graphene oxide nanosheets are now dissolved in DMF and sodium azide mixture (1.5 mM) at ambient temperature for about 40 h. The by-product was first filtered, isolated and then sonicated in concentric HCl to produce graphene amine (Singh et al., 2012). Ultimately, the by-product was cleansed multiple times with deionized H_2O till filtrate attains neutral pH (Singh et al., 2012). Similar process is explained for the carbon nanotubes functionalized through covalent amine (Fig. 6).

Such modification of graphene and derivatives possesses several applications. For intense S. K. Singh and coworkers prosperous application of amine-modified graphene as efficient drug delivery agent (Singh et al., 2012; Pei et al., 2014). They also reported the modified graphene molecules can be used in treatment of cancer (Singh et al., 2012). However, Xibo and coworkers of China reported that specific size of such modified graphene might be the important and governing parameter of biocompatibility of amine-modified graphene for the above-mentioned application. Xibo and coworkers commented on Singh's work, that when one willing to

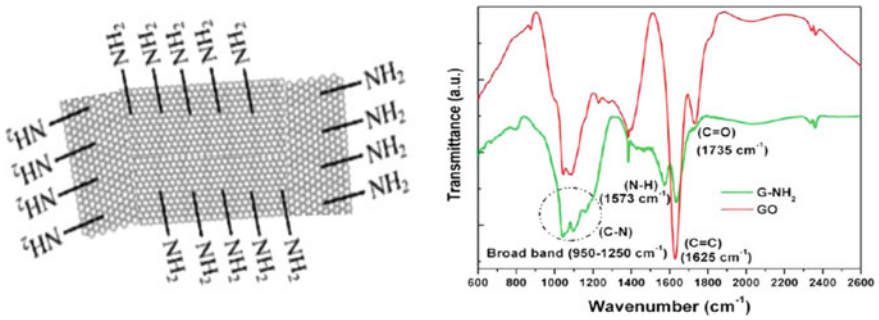

Fig. 6 Schematic structure amine-modified graphene oxide and its FTIR spectrum. Reproduced with permission (Singh et al., 2012)

examining the biocompatibility of amine-modified graphene, it is very necessary to consider nanosizing effect of used materials. According to Xibo and coworkers work carried out by Singh and coworkers "Amine-Modified Graphene: Thrombo-Protective Safer Alternative to Graphene Oxide for Biomedical Applications" is an outstanding research impute which opens a door for wider study modified graphene for the biomedical purposes. Due to the existence of huge $-NH_2$ and oxygen functional moieties of such modified graphene has extensively been used to produce various novel hybrid polymeric materials (Singh et al., 2012; Pei et al., 2014). A range of processes has been reported to produce amine-modified graphene-based hybrid nanomaterials (along with different method of functionalization and dispersion). Many authors have proved the influence of modified GO on rheological, electrical, mechanical, thermal, and barrier properties of polymer nanocomposites.

2.5.2 Carboxylic Acid-Modified Graphene

As we well know and widely accepted that single and few layer graphene is very hard to produce on at industrial scale (Tiwari et al., 2016a; b). So, that modified graphene such as GO and various reduced graphene oxides are frequently used as replacements (Azadbakht et al., 2016). Acid-modified graphene typically denotes oxygenation product of graphene sheets, produced by chemically exfoliating the graphite powder utilizing selected resilient oxidants (like $KMnO_4$,) (Azadbakht et al., 2016). However, such modifications need specific reaction condition. These modified materials not only can be produced in large scale using simple and inexpensive methods, but also are more appropriate for design high performance devices for various applications (Azadbakht et al., 2016; Tiwari et al., 2016a). Some potential applications of acid-modified graphene have been demonstrated in many areas by various research groups. For instance sensors, transparent conductors, polymer blends nanocomposites, in energy storage and conversion, and as an excellent surfactant for dispersing other insoluble carbon materials (Azadbakht et al., 2016). A typical process for the synthesis of carboxylic acid-functionalized graphene is discussed below.

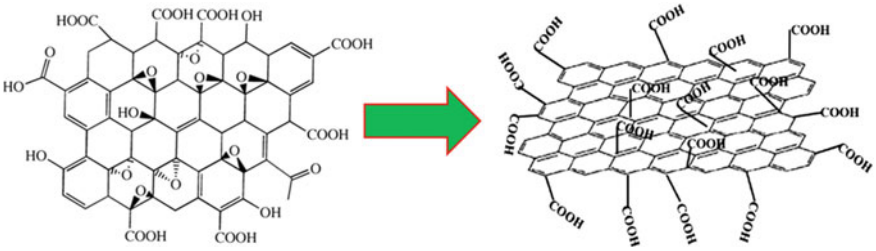

Fig. 7 Schematic representation of conversion of graphene oxide to carboxylic acid-modified graphene. Reproduced with permission (Azadbakht et al., 2016)

Azadeh and coworkers reported synthesis carboxylic acid derivative of graphene using graphene oxide as precursor. They treated graphene oxide sheet with chloroacetic acid (in a specific molar ratio) under strong basic conditions. This is to turn hydroxyl functional groups into carboxylic acid moieties. For this experiment, Azadeh and coworkers used GO and chloroacetic acid in the quantities of 50 mg and 1.2 g, respectively. Further, solid NaOH (1 g) plates were added to 100 cm^3 water. Then they sonicated whole mixture for the 3 h. The resulting mixture contains carboxylic acid-functionalized graphene and it can be defused using HCl, and cleansed with H_2O by washing again and again. The modified electrode used by Azadeh and coworkers has very high sensitivity, short response time, low limit of detection and lower potential for operation. They reported that some kinetic constraints, such as catalytic rate constant, diffusion and electron transfer coefficients, coefficient of the catalytic reaction can also be obtained easily using this modified graphene oxide. This using by carboxylic acid-functionalized graphene a sensitive amperometric method was introduced by Azadeh and coworkers for the establishment of urea with advantages of good reproducibility and fast response (Fig. 7; Table 1).

Readers who just starting his/her research in field of graphene must learn the fundamental of graphene like electronic characteristics of graphene sheets without defects, chemical processes for the graphene and HRG synthesis, its backdrop and unique characteristics of graphene without defects. For these purposes, they may consult some outstanding reviews published by Tiwari et al. (2017).

3 Conclusion

In present scenario, 2D materials are attaining significant attraction from both technological and fundamental science aspect owing to their chemical, physical, magnetic and electronic characteristic differences over conventional bulk material. In this chapter, the author critically discussed different methods for production of 2D materials. Methods are broadly classified as mechanical and chemical exfoliation methods.

Table 1 Efficiency of procedure developed by Azadeh and coworkers using carboxylic acid-functionalized graphene as electrode material (Azadbakht et al., 2016)

Modifier	Linear range/μmol dm^{-3}	Detection limit/μmol $dm-^{3}$	Sensitivity	Stability/days
PANi-Nafion	$0.98 - 9.89 \times 10^2$	0.49	10.9 μAmM^{-1} cm^{-2}	60
Functionalized H40-Au nanoparticles	$10^3 - 35.0 \times 10^3$	11.0	7.48×10^{-3} μAmM^{-1}	126
PPy	$49.4 - 1.64 \times 10^2$	49.4	–	28
Urs-GLDH/N-DNW	$1.66 \times 10^4 - 1.66 \times 10^5$	6.44×10^3	37.1 μAmM^{-1} cm^{-2}	30
Hematein/Pt electrode	10.0–200	3	0.30 μAmM^{-1} cm^{-2}	21
o-Toluidine/Pt electrode	0.00–800	20.0	0.98 μAmM^{-1} cm^{-2}	–
MIP-PEV A/Au	0.33–50.0	0.16	–	–
PAPCP	1.60–50.2	1.60	–	60
Using GO–COOH	100–18,000	40.0	–	70

PANi polyaniline, *Urs* urease, *PAPCP* poly(aminopropylpyrrole-co-pyrrole), *PPy* polypyrrole, *GLDH* glutamate dehydrogenase, incorporated diamond nanowire, *PEVA* poly(ethylene-co-vinyl alcohol)

The mechanical exfoliation provides versatility and low cost whereas chemical exfoliation provides chemical homogeneity and molecular level mixing. The synthesis and fabrication processes control the morphology and size of product which further improves the performance of 2D NSMs in different applications.

References

Allen, M. J., Tung, V. C., & Kaner, R. B. (2010) Honeycomb carbon: a review of graphene. *Chemical Reviews*. https://doi.org/10.1021/cr900070d.

Azadbakht, A., et al. (2016). Preparation of the carboxylic acid-functionalized graphene oxide/gold nanoparticles/5-amino-2-hydroxybenzoic acid as a novel electrochemical sensing platform. *Monatshefte fur Chemie*. https://doi.org/10.1007/s00706-015-1527-3.

Balandin, A. A. (2011). Thermal properties of graphene and nanostructured carbon materials. *Nature Materials*. https://doi.org/10.1038/nmat3064.

Bhuyan, M. S. A., et al. (2016). Synthesis of graphene. *International Nano Letters, 6*(2), 65–83. https://doi.org/10.1007/s40089-015-0176-1.

Blake, P., et al. (2008). Graphene-based liquid crystal device. *Nano Letters*. https://doi.org/10.1021/nl080649i.

Brodie, B. C. (1859) On the atomic weight of graphite. *Philosophical Transactions of the Royal Society of London, 149*(259). https://doi.org/10.1098/rstl.1859.0013.

Chen, D., Feng, H., & Li, J. (2012). Graphene oxide: Preparation, functionalization, and electrochemical applications. *Chemical Reviews*. https://doi.org/10.1021/cr300115g.

Chen, J., et al. (2013). An improved Hummers method for eco-friendly synthesis of graphene oxide. *Carbon*. https://doi.org/10.1016/j.carbon.2013.07.055.
Choi, W., et al. (2010). Synthesis of graphene and its applications: A review. *Critical Reviews in Solid State and Materials Sciences*. https://doi.org/10.1080/10408430903505036.
Compton, O. C., & Nguyen, S. T. (2010). Graphene oxide, highly reduced graphene oxide, and graphene: Versatile building blocks for carbon-based materials. *Small*. https://doi.org/10.1002/smll.200901934.
Cui, X., et al. (2011). Liquid-phase exfoliation, functionalization and applications of graphene. *Nanoscale*. https://doi.org/10.1039/c1nr10127g.
De Adhikari, A., et al. (2015). Effect of waste cellulose fibres on the charge storage capacity of polypyrrole and graphene/polypyrrole electrodes for supercapacitor application. *RSC Advances, 5*(35), 27347–27355. https://doi.org/10.1039/C4RA16174B.
Dikin, D. A., et al. (2007). Preparation and characterization of graphene oxide paper. *Nature*. https://doi.org/10.1038/nature06016.
Dimiev, A. M., & Tour, J. M. (2014). Mechanism of graphene oxide formation. *ACS Nano*. https://doi.org/10.1021/nn500606a.
Geim, A. K., & Novoselov, K. S. (2007). The rise of graphene. *Nature Materials*. https://doi.org/10.1038/nmat1849.
He, H., et al. (1998). A new structural model for graphite oxide. *Chemical Physics Letters*. https://doi.org/10.1016/S0009-2614(98)00144-4.
Hummers, J. W. S. (1957). Preparation of graphitic acid.
Hummers, W. S., & Offeman, R. E. (1958). Preparation of graphitic oxide. *Journal of the American Chemical Society*. https://doi.org/10.1021/ja01539a017.
Jiang, H. (2011). Chemical preparation of graphene-based nanomaterials and their applications in chemical and biological sensors. *Small*. https://doi.org/10.1002/smll.201002352.
Jo, G., et al. (2012). The application of graphene as electrodes in electrical and optical devices. *Nanotechnology*. https://doi.org/10.1088/0957-4484/23/11/112001.
Loh, K. P., et al. (2010). Graphene oxide as a chemically tunable platform for optical applications. *Nature Chemistry*. https://doi.org/10.1038/nchem.907.
Luo, J., Kim, J., & Huang, J. (2013). Material processing of chemically modified graphene: Some challenges and solutions. *Accounts of Chemical Research*. https://doi.org/10.1021/ar300180n.
Marcano, D. C., et al. (2010). Improved synthesis of graphene oxide. *ACS Nano*. https://doi.org/10.1021/nn1006368.
McCann, E. (2007). Interlayer asymmetry gap in the electronic band structure of bilayer graphene. *Physica Status Solidi (B) Basic Research*. https://doi.org/10.1002/pssb.200776105.
Nika, D. L., et al. (2009). Phonon thermal conduction in graphene: Role of Umklapp and edge roughness scattering. *Physical Review B—Condensed Matter and Materials Physics*. https://doi.org/10.1103/PhysRevB.79.155413.
Oraon, R., et al. (2015). Fabrication of nanoclay based graphene/polypyrrole nanocomposite: An efficient ternary electrode material for high performance supercapacitor. *Applied Clay Science, 118,* 231–238. https://doi.org/10.1016/J.CLAY.2015.09.019.
Oraon, R., et al. (2016). Enhanced specific capacitance of self-assembled three-dimensional carbon nanotube/layered silicate/polyaniline hybrid sandwiched nanocomposite for supercapacitor applications. *ACS Sustainable Chemistry and Engineering*. https://doi.org/10.1021/acssuschemeng.5b01389.
Orecchioni, M., et al. (2015). Graphene as cancer theranostic tool: Progress and future challenges. *Theranostics*. https://doi.org/10.7150/thno.11387.
Pei, X., Wang, J., & Wan, Q. (2014). Comment on "Amine-modified graphene: Thrombo-protective safer alternative to graphene oxide for biomedical applications". *ACS Nano, 8*(3), 1966. https://doi.org/10.1021/nn5000578.
Reina, A., et al. (2009). Large area, few-layer graphene films on arbitrary substrates by chemical vapor deposition. *Nano Letters*. https://doi.org/10.1021/nl801827v.

Ritter, K. A., & Lyding, J. W. (2009). The influence of edge structure on the electronic properties of graphene quantum dots and nanoribbons. *Nature Materials*. https://doi.org/10.1038/nmat2378.

Singh, S. K., et al. (2012). Amine-modified graphene: Thrombo-protective safer alternative to graphene oxide for biomedical applications. *ACS Nano*. https://doi.org/10.1021/nn300172t.

Sudesh, et al. (2013). Effect of graphene oxide doping on superconducting properties of bulk MgB2. *Superconductor Science and Technology*. https://doi.org/10.1088/0953-2048/26/9/095008.

Tang, L., et al. (2012). Bottom-up synthesis of large-scale graphene oxide nanosheets. *Journal of Materials Chemistry*. https://doi.org/10.1039/c2jm15944a.

Tiwari, S. K., Huczko, A., et al. (2016a). A time efficient reduction strategy for bulk production of reduced graphene oxide using selenium powder as a reducing agent. *Journal of Materials Science*. https://doi.org/10.1007/s10853-016-9903-x.

Tiwari, S. K., Kumar, V., et al. (2016b). Magical allotropes of carbon: Prospects and applications. *Critical Reviews in Solid State and Materials Sciences*. https://doi.org/10.1080/10408436.2015.1127206.

Tiwari, S. K., et al. (2017). Facile electrochemical synthesis of few layered graphene from discharged battery electrode and its application for energy storage. *Arabian Journal of Chemistry*. https://doi.org/10.1016/j.arabjc.2015.08.016.

Tour, J. M., & Kosynkin, D. (2015). Graphene nanoribbons prepared from carbon nanotubes via alkali metal exposure.

Zhu, Y., et al. (2010). Graphene and graphene oxide: Synthesis, properties, and applications. *Advanced Materials*. https://doi.org/10.1002/adma.201001068.

Chapter 4
2D Graphene Oxide-Based Composites and Their Application in Catalysis and Sensing

Karan Chaudhary and Dhanraj T. Masram

1 Introduction

In 1859, for the first time, term "Graphon" was introduced by B. C. Brodie which actually is a suspension of tiny crystals of graphene oxide, that is, a graphene sheet densely covered with hydroxyl, carboxyl, and epoxide groups that he observed at that time (Geim, 2012). Then in 2003, one ingenious physicist Andre Geim along with his colleague, Kostya Novoselov, with a lot of patience and persistence, took a graphite block and some Scotch tape and produced a wonder material which was million times thinner than paper, stronger than diamond, more conductive than copper called graphene (Randviir et al., 2014). Graphene is a carbon sheet which is one-atom-thick and carbon atoms form a two-dimensional hexagonal lattice. Each carbon atom is 1.42 Å apart, each of which four bonds, three are σ bonds with three neighboring atoms, and fourth bond is a π-bond oriented in the z-direction (out of the plane). Each atom has one of these π-bonds, hybridized together to form π-band and π*-bands. Most of the electronic properties of graphene are the result of these bands (Cooper et al., 2012). Graphene exhibits many properties such as a large theoretical specific surface area (2630 m^2g^{-1}), high values of Young's modulus (~1.1 Tpa), excellent thermal conductivity (~5000 $Wm^{-1}s^{-1}$), and amazing intrinsic mobility (200,000 $cm^2v^{-1}s^{-1}$) (Wang & Chen, 2011). Graphene sheet is building block for graphitic materials of all other dimensionalities (Fig. 1) (Bhuyan et al., 2016).

The graphitic oxide is bulk material synthesized by oxidizing graphite a multilayer allotrope of carbon with an oxidizing mixture made of strong oxidizing substances. The graphitic oxide is bright yellow colored solid having an atomic ratio between 2.1 and 2.9 of carbon to oxygen (Hummers Jr & Offeman, 1958). Depending on the oxidizing system used, the oxygen content can vary in graphitic oxide, and by this, it can be said that graphitic oxide is nonstoichiometric compound. The layered

K. Chaudhary · D. T. Masram (✉)
Department of Chemistry, University of Delhi, Delhi 110007, India

S. Singh et al. (eds.), *Advanced Applications of 2D Nanostructures*,
Materials Horizons: From Nature to Nanomaterials,
https://doi.org/10.1007/978-981-16-3322-5_4

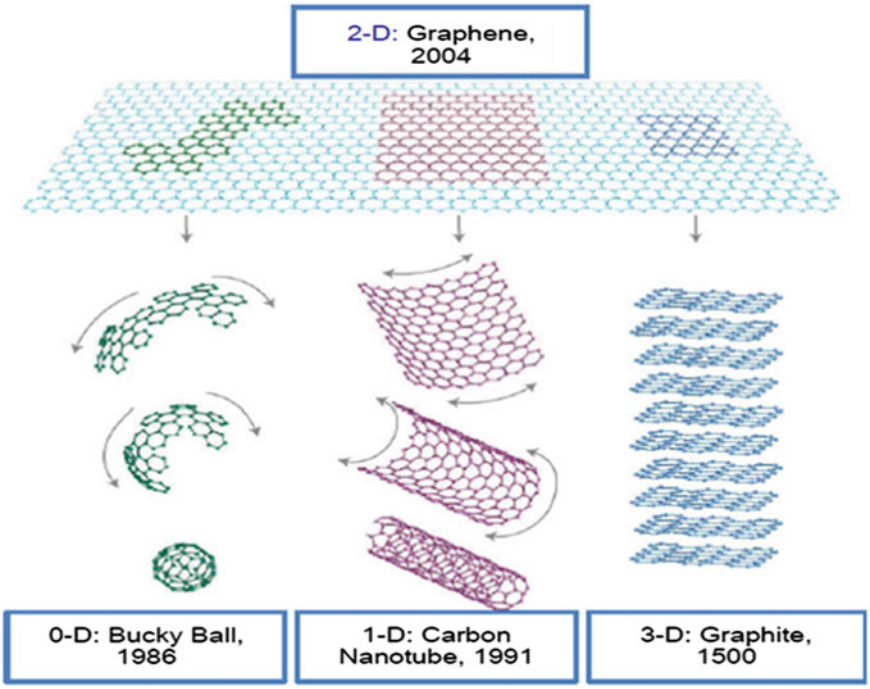

Fig. 1 Image showing 2D graphene and all other dimensional carbon materials (Bhuyan et al., 2016) (© 2016, Md. Sajibul Alam Bhuyan, Md. Nizam Uddin, Md. Maksudul Islam et al., Springer Nature. Used with permission.) (Geim & Novoselov, 2007) (© 2007, Springer Nature. Used with permission)

structure of graphite is preserved in graphitic oxide, but the interlayer spacing of graphitic oxide is asymmetrical and has variation from 6 to 12 Å (Buchsteiner et al., 2006).

In this chapter, we are concerned about graphene oxide, and till here, we have discussed graphitic oxide (stacked graphene sheet densely covered with oxygen functionalities). The reason behind discussing graphitic oxide is its chemical similarity with graphene oxide. Structure of graphene oxide is different from graphitic oxide; therefore, they are not identical to each other (Dreyer et al., 2010). Thermal or mechanical exfoliation of graphitic oxide in polar solvents results in graphene oxide. Graphene oxide is monolayer (~1.0–1.4 nm thick) or few layered structure having a large number of oxygen-containing functionalities on both sides (Fig. 2), as this monolayer structure is an important reason behind its eye-catching properties (Paredes et al., 2008).

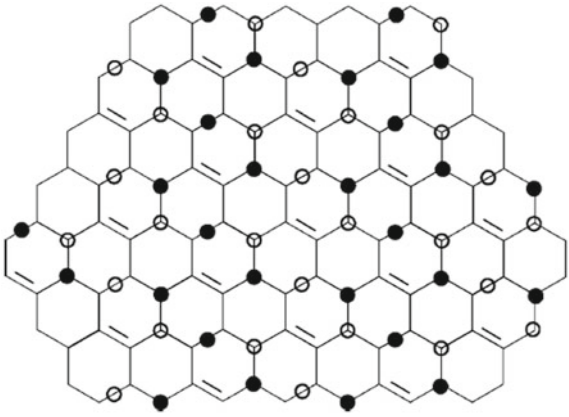

Fig. 2 Graphene oxide structure showing –OH groups (circles at hexagon corners) and epoxides groups (circles at hexagon edges) (Buchsteiner et al., 2006) (© 2006, American Chemical Society. Used with permission.)

2 Background of Graphene Oxide

The first report on graphite oxide came long back in the middle of the nineteenth century, by B. C. Brodie a British chemist. While exploring the structure of Ceylon graphite, the reaction was performed in which "potash of chlorate" was mixed with graphite to which addition of fuming nitric acid was done. He confirmed that material so formed is composed of hydrogen, carbon, and oxygen with percentage composition 1.85, 61.04, and 37.11, respectively. Graphitic oxide was found to have increased mass as compared to graphite. He also said that it was insoluble in acidic media, slightly soluble in pure water and its conversion to transparent jelly in basic media (ammonia). Then he also performed temperature treatment on graphitic oxide, results show that products were water, carbon dioxide, and black carbonaceous residue. He also stated, "*This form of carbon should be characterized by a name marking it as a distinct element. I propose to term it Graphon.*" (Brodie, 1859). Later in 1898, L. Staudenmaier came up with the improvement for oxidizing the graphite. He added $KClO_3$ during reaction course in small lots and used a mixture of graphite in concentrated sulfuric acid and fuming nitric acid, as this improvement was found to be effective as Brodie's method but in a single vessel (Staudenmaier, 1898). Then in 1957, Hummers and Offeman reported a new method for the preparation of graphitic oxide in which they treated graphite with $KMnO_4$ and $NaNO_3$ in the presence of concentrated sulfuric acid under water-free conditions. And the effectiveness of this method was clear by the proportion of the obtained graphitic oxide and carbon to oxygen ratio (~2.1–2.9 At ratio). This method was less hazardous and requires lesser time (Hummers Jr & Offeman, 1958). And this method is still used for the preparation of graphitic oxide with new modification popularly known as improved Hummer's method. These methods are well known and are called as primary methods for the preparation of graphitic oxide. Important is to know that the graphitic oxide obtained depends upon the source of graphite, reaction conditions, and also on the type of oxidant.

3 Characterization and Structural Features of Graphene Oxide

Graphite oxide has been well studied through **^{13}C NMR**, and a spectrum so obtained has been shown in Fig. 3. Studies reveal the presence of three lines at 60, 70, and 130 ppm which belongs to epoxide groups, C–OH groups, and aromatic entities along with conjugated double bonds, respectively. So it was found that graphitic oxide is composed of two regions one is aromatic unoxidized benzene rings, and another is aliphatic six-membered rings. Therefore, based on findings, it was concluded that the basic carbon grid was flat, but it is distorted where carbon is attached to –OH group which results in some wrinkling of the sheet (Lerf et al., 1998).

To measure the surface area of graphene oxide, **BET** experiment was performed and by the adsorption and desorption of N_2 on the surface revealed that 700–1500 m^2/g is the range of determined surface area of graphene oxide. However, in case of reduced graphene oxide increase in surface area was observed result of further exfoliation of sheets took place during the reduction process. Atomic force spectroscopy (**AFM**) was employed to study topological features of a single sheet (graphene oxide), the result obtained (Fig. 4a, b) clearly shows that the average height of the carbon grid is 2 nm and has bumps on the surface. Also, the presence of large wrinkles having a height up to 10 nm was witnessed (Schniepp et al., 2006).

Aksay et al. on the basis of the first-principles atomistic model having –OH and epoxy groups explained the structure of graphitic oxide sheet (Fig. 4c). The result shows that there is a 0.44 nm increase in the carbon grid height due to the addition of these groups and lead to the conversion of sp^2 hybridized planar carbon to distorted sp^3 hybridized carbon which causes bumps on the surface and increased interlayer distance between graphene sheets. Epoxy groups formed during oxidation of graphite have a tendency to form chains through cooperative reaction across the surface which leads to large wrinkles having height up to 10 nm. The release of carbon dioxide is the result of faster heating of graphitic oxide sheet which certainly results in vacancies and defects on the sheet structure of graphitic oxide (Fig. 4d) (Schniepp et al., 2006).

For characterizing the carbon products, **Raman spectroscopy** is commonly used technique due to high Raman intensities for C=C and conjugated bonds. Raman spectra are shown in Fig. 5 and reveals the presence of only two Raman active

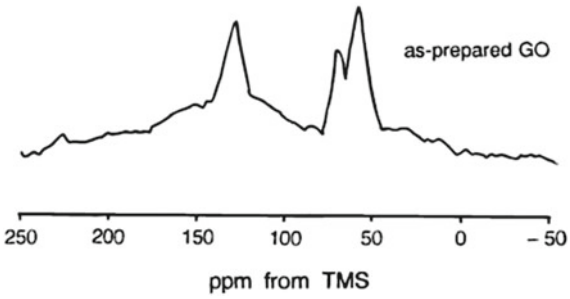

Fig. 3 Proton decoupled ^{13}C MAS NMR spectra of graphene oxide (Lerf et al., 1998) (© 1998, American Chemical Society. Used with permission.)

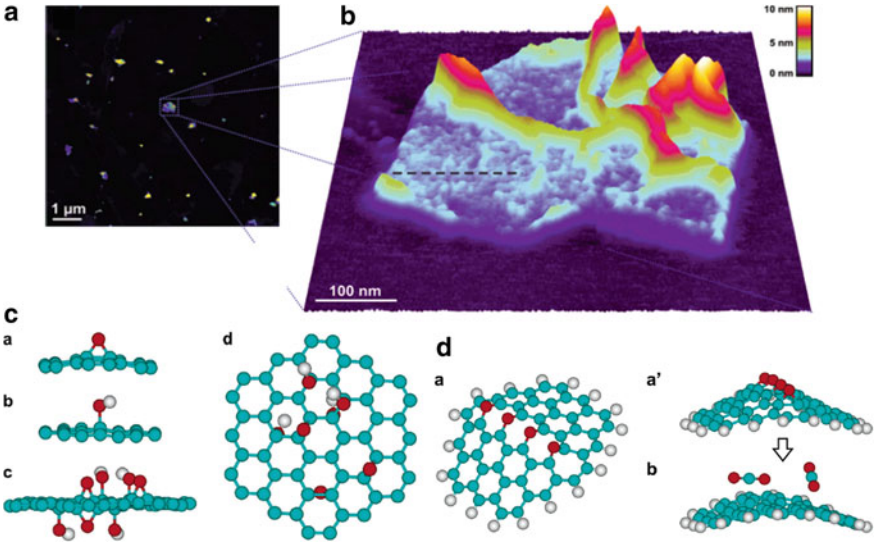

Fig. 4 **a** AFM image showing the topography of individual graphene oxide flakes which are exfoliated thermally. **b** Individual graphene oxide sheet in pseudo-3D representation obtained from AFM. **c** Atomistic model of graphene oxide showing (**a**) epoxy group, (**b**) hydroxyl group, (**c**) edge view having various hydroxyl and epoxy functional sites, and (**d**) view from the top. **d** Atomistic model for (**a and a'**) graphene oxide having linearly arranged epoxy groups. (**b**) Removal of carbon dioxide during thermal reduction of graphene oxide (Schniepp et al., 2006) (© 2006, American Chemical Society. Used with permission.)

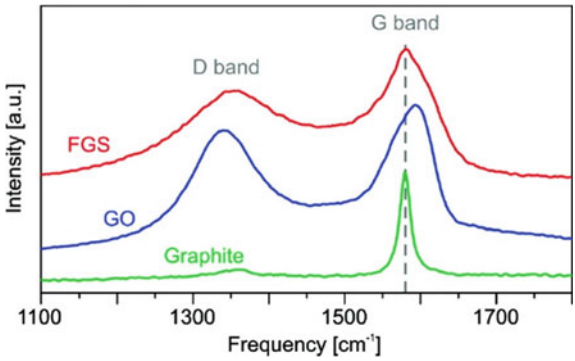

Fig. 5 Raman spectra for graphite, graphene oxide and functionalized graphene sheet (Kudin et al., 2008) (© 2008, American Chemical Society. Used with permission.)

bands in graphite which are G and D bands. Band appeared at 1575 cm^{-1} is G band result due to vibrating of graphitic lattice in-phase and band appeared at 1355 cm^{-1} corresponds to D band due to graphite edge. Raman spectra observed for graphitic oxide are different from graphite which is due to the vacancies and topological defects present in the sheet of graphitic oxide. So, the G band in case of graphitic oxide is significantly broadened and appears at a higher frequency (blue shift), whereas D

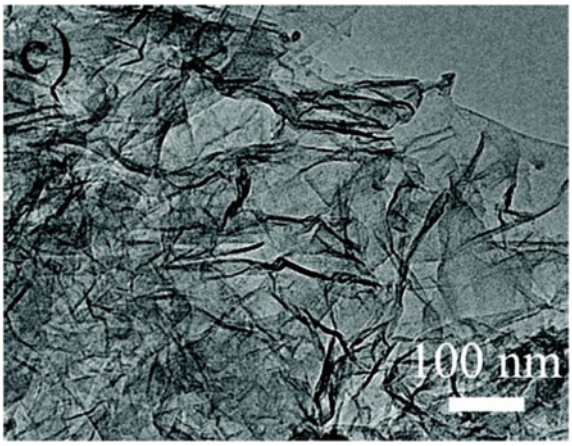

Fig. 6 TEM micrograph for graphite oxide (Xu et al., 2010) (© 2010, American Chemical Society. Used with permission.)

band has a higher intensity as compared to the D band of graphite (Kudin et al., 2008). Reduced graphene oxide obtained by reduction or exfoliation of graphene oxide has different Raman spectra as compared to graphene oxide but pattern remains similar. Broadening of D band due to increased defects/disorderness and G band which is unusual is observed in reduced graphene oxide Raman spectra (Kaniyoor & Ramaprabhu, 2012). If the ratio of intensity for D versus G band, i.e., I_D versus I_G, increases it attributes to decrease in sp^2 character of carbon and whereas if it decreases it shows increased 'graphitization' (Yang et al., 2009).

Sheet-like morphology with different transparencies was observed in transmission electron microscopy (**TEM**) studies for graphene oxide (Fig. 6) and reduced graphene oxide. Dark region appeared is the result of stacked sheets, whereas few layer thick sheets appeared much brighter. Sheets of high transparencies were more in the case of reduced graphene oxide in comparison to graphene oxide because during reduction exfoliation of sheets occurs (Stobinski et al., 2014).

When graphene oxide and reduced graphene oxide were studied by X-ray diffraction, pattern obtained is demonstrated in Fig. 7a. Diffraction obtained at $2\theta = 10.09°$ for graphene oxide is characteristic for (002) plane, whereas diffraction for reduced graphene oxide appears shifted at $2\theta = 23.77°$. These (002) peaks indicate the interlayer distance between the sheets (Li et al., 2014). Moreover, the diffraction peak for (100) plane is observed at $2\theta = 42.26°$ and 42.74° for graphene oxide and reduced graphene oxide, respectively. It was found that there were 6–7 stacked layers in graphene oxide having an interlayer distance of 0.9 nm, and in case of reduced graphene oxide, there were 2–3 stacked layers having 0.4 nm as interlayer distance (Stobinski et al., 2014).

X-ray photoelectron spectroscopy (**XPS**) was also employed to study graphene oxide, and spectra for C1s is discussed. Studies revealed that difference in binding energy of sp^2 and sp^3 bonded carbon is 0.9 eV. Binding energy for sp^2 carbon falls in the range of 284.5–284.6 eV, whereas carbon bonded to a hydroxyl (C–OH), carbonyl (C=O), and carboxyl and ester appears 1.3–2.4 eV, 2.6–3.5 eV and 4.3–5.4 eV shifted

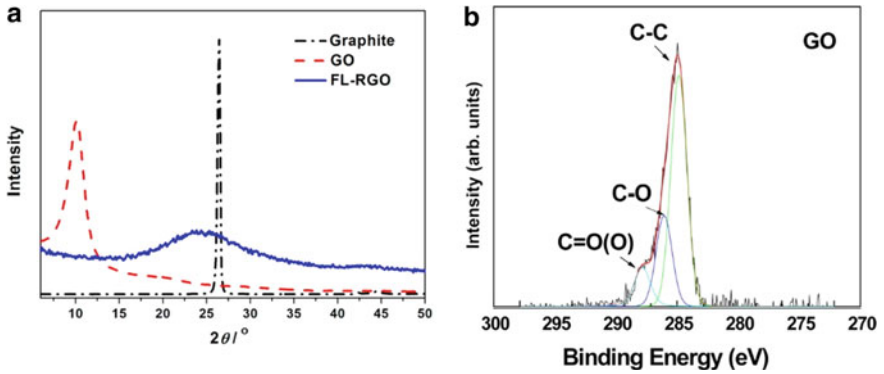

Fig. 7 **a** XRD patterns for graphite, graphene oxide, and reduced graphene oxide (Li et al., 2014) (© 2014, American Chemical Society. Used with permission.). **b** C1s fitted XPS spectrum of graphene oxide (Stathi et al., 2015) (© 2015, American Chemical Society. Used with permission.)

with respect to sp^2 carbon. In case of reduced graphene oxide C=O appears at 530–531.6 eV and C–OH appears at 532.4–533.3 eV. It was also observed that graphene oxide has a higher content of sp^3 carbon, epoxy, hydroxyl, carbonyl, carboxyl, and water. But in reduced graphene oxide content of sp^2 carbon, carboxyl, hydroxyl, and water were increased, and content of epoxy, carbonyl, and sp^3 carbon was decreased (Stobinski et al., 2014).

IR spectra (Fig. 8) of graphene oxide and its reduced form were also found to be very informative. In spectra of graphene oxide peaks obtained at 1043, 1124,, and 1732 cm^{-1} attributes for C–O (alkoxy), C–O (epoxy), and C=O (carboxylic) moieties indicating successful oxidation of graphite to graphene oxide. However, in

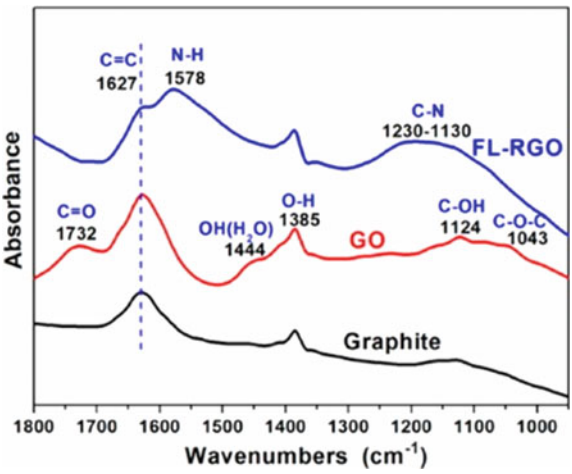

Fig. 8 IR spectra of graphite, graphene oxide, and reduced graphene oxide (Li et al., 2014) (© 2014, American Chemical Society. Used with permission.)

the case of reduced graphene, oxide peak intensities were significantly reduced for oxygen associated moieties (Li et al., 2014).

Graphitic oxide result of oxidation of graphite can be exfoliated for the preparation of graphene oxide. Presence of oxygen functionalities on the surface of graphene oxide is the reason behind its dispersion in water, but make it electrically insulating. This is a result of sp^2 to sp^3 conversion of bonded carbon in graphene oxide due to the addition of functionalities. The electrical conductivity of graphene oxide can be recovered by reduction of graphene oxide. Now reduction cases removal of oxygen functionalities from the graphene oxide surface makes its dispersion difficult and reduced graphene oxide tends to agglomerate. Moreover, this agglomeration and the problem of dispersion of reduced graphene oxide were sorted by reducing graphene oxide by chemical modification (Li et al., 2008).

4 Application in Sensor

Before using graphene oxide in the field of sensors, it is reduced by modifying the graphene oxide surface as per requirement so that the target can interact and can be sensed more specifically and selectively. Herein, we discuss the work in which graphene oxide has been used by us in the field of sensors.

Lanthanum oxide and reduced graphene oxide nanocomposite, LO/RGO was synthesized by hydrothermal treatment of an ultrasonicated mixture of $La(NO_3)_3{\cdot}6H_2O$ and poly(ethylene glycol) along with graphene oxide. This LO/RGO nanocomposite has been used in sensing of ascorbic acid. On characterization of nanocomposite, nanospheres of La_2O_3 found to be anchored over the surface of graphene oxide. When LO/RGO nanocomposite electrode used for sensing ascorbic acid, successful and efficient detection of ascorbic acid was resulted because of lanthanum oxide and graphene oxide as combined. And it is due to electrocatalytic oxidation of ascorbic acid taking place at the electrode surface by covalent linkage of ascorbic acid and the electron transfer kinetics between LO/RGO surface and ascorbic acid and was found that it possesses mass transfer controlled process. Results showed increase in anodic peak current with increase in ascorbic acid concentration. Also the detection limit of ascorbic acid found to be in the range of 14–100 μM. Moreover, vitamin C tablets, which are commercially available, were analyzed to check the acceptability of LO/RGO-based sensor and obtained recovery percentage in the range of 97.64–99.7% proving its potential as an ascorbic acid sensor (Mogha et al., 2014).

A efficient and biocompatible biosensor for acetylcholinesterase (AChE)-based chlorpyrifos detection was reported using zirconium oxide supported on reduced graphene oxide (AChE/ZrO_2/RGO). This AChE/ZrO_2/RGO nanocomposite was synthesized by hydrothermal treatment of an ultrasonicated mixture of $Zr(NO_3)_4{\cdot}5H_2O$ and poly(ethylene glycol) along with graphene oxide, as acetylthiocholine (ATCl) substrate was used to measure the AChE activity, which is hydrolyzed to thiocholine enzymatically and undergoes electrocatalytic oxidative dimerization.

Chlorpyrifos act as an AChE inhibitor and was found that inhibition of AChE activity is a function of Chlorpyrifos concentration. When AChE/ZrO_2/RGO was used for Chlorpyrifos (pesticide) detection, result demonstrated that using this nanocomposite, 10^{-13} M is the lowest concentration of chlorpyrifos that can be detected with enzyme inhibition about 28%. Furthermore, more than 70% enzyme inhibition was observed in the case of high concentration (up to 10^{-4} M) of Chlorpyrifos. It was said that material like reduced graphene oxide has high electrical conductivity and large surface area when immobilized with metal oxide NPs results in enhancement of electrocatalytic performance (Mogha et al., 2016).

An article on DNA biosensor was reported for detecting Mycobacterium tuberculosis using nanocomposite of reduced graphene oxide nanoribbons (RGONR) as support for immobilizing Au NPs. Chemistry at the edges and defects which are the reason behind electrical conductivity and catalytic performance makes graphene oxide nanoribbons as promising material to be used as support material. This Au NPs (~6 nm) were in situ immobilized on RGONR to which thiolated probe DNA was attached covalently (S–Au) to synthesize ssDNA/Au/RGONR electrode. When it was applied for the detection of Mycobacterium tuberculosis by using target DNA, the process was studied and found to be diffusion controlled process taking place at the electrode surface. Also, using this ssDNA/Au/RGONR electrode, it was found that 0.1 fM of target DNA can be detected showing its high detection efficiency. In the presence of target DNA, ssDNA got hybridized and observed that on increasing the target DNA concentration from 0.1 fM to 10^{-6} M hybridization percentage increased from 10.6 to 51.3%. While in the case of non-complementary DNA, no hybridization was observed. All this indicated high selectivity and sensitivity of ssDNA/Au/RGONR nanocomposite toward detection of Mycobacterium tuberculosis (Mogha et al., 2018).

5 Application in Catalysis

Synthesis of La_2O_3/RGO nanocomposite was reported by adding $NaBH_4$ to the ultrasonicated suspension of graphene oxide added with the mixture of $La(NO_3)_3{\cdot}6H_2O$ and poly(ethylene glycol), and solid obtained was annealed at 300 °C. On characterizing, the material found La_2O_3 nanocluster to be present over the RGO surface. This La_2O_3/RGO nanocomposite has been applied in the synthesis of bis(indolyl)methanes using indole and various aldehydes under a solvent-free condition at mild conditions. Bis(indolyl)methanes, molecules which are biologically important were synthesized with excellent yield (88–97%). Presence of La_2O_3 on the surface of RGO interacts with first indole molecule, and intermediate is formed at catalyst with iminium ion formed through aldehyde. Another indole molecule leads to the formation of another intermediate which on rearrangement gave the desired product. Green synthesis of catalyst and its reusability proved catalyst potential in bis(indolyl)methanes synthesis (Mogha et al., 2017b).

In 2017, another article reported using graphene oxide in which the hybrid of brominated graphene oxide with poly (dimethylaminoethyl methacrylate) was made to which Au NPs was immobilized. A method known as atom transfer radical polymerization was employed for making PDMAEMA brushes on graphene oxide, whereas Au NPs were immobilized by simple chemical reduction. On characterizing Au/PDMAEMA/RGO, it was found that Au NPs attached to polymer brushes surface instead of GO surface with two types of morphologies normal spherical and another was a worm. This gold immobilized graphene oxide polymer brush nanohybrid was used as a catalyst in degradation of organic dyes such as Rhodamine B (RB), Methyl Orange (MO), and Eosin Y (EY) in the presence of $NaBH_4$. The rate constant for the degradation of RB, MO, and EY dyes was found to be 21.8, 26.2, and 8.7 ($\times 10^{-3}$ s^{-1}), showing the excellent catalytic activity of Au/PDMAEMA/RGO toward dye degradation. The result showed degradation down to 82%, 74%, and 93% of RB, MO, and EY dyes, respectively, as the process of degradation starts from the electron transfer by BH_4^- to Au by PDMAEMA/RGO network which is transferred to dye connected to RGO by $\pi - \pi$ interactions result in the degradation of dyes. Au/PDMAEMA/RGO exhibited high efficiency and recyclability as a catalyst which demonstrated that this hybrid material has potential in wastewater treatment application (Mogha et al., 2017a).

Beside this, in 2018, we reported CuO NPs immobilized over Fur-Imine-Functionalized Graphene Oxide (Cu(II)-Fur-APTES/GO) nanocomposite. This nanocomposite was applied as a catalyst for synthesis of xanthene and its derivative which are industrially important under green solvent condition (EtOH-water) at mild conditions using aromatic aldehydes and dimedone or 1,3-cyclohexanedione. On characterizing this (Cu(II)-Fur-APTES/GO), high copper content (13.5 at.%) was obtained which was uniformly decorated over the graphene oxide surface which acts as an active site for catalyzing the reaction. As per mechanism, it initiates by the interaction of aldehyde with CuO and activates carbonyl group which is attacked by 5,5-dimethyl-1,3-cyclohexanedione molecule resulting in intermediate to which another molecule of 5,5-dimethyl-1,3-cyclohexanedione is added by Michael addition to form the second intermediate. The release of water due to intramolecular cyclization is resulted in the desired product. Xanthene products synthesized by using Cu(II)-Fur-APTES/GO as a catalyst were obtained in excellent yield (up to 95%) under lesser reaction time. Result demonstrated that this nanocomposite is stable, efficient, cost-effective, and reusable as nanocatalyst for pharmaceutically important xanthene derivatives (Subodh et al., 2018).

6 Conclusion

Graphene sheets, a single-layered 2D carbon material has a combination of various exceptional properties such as high conductivity, high surface area, and graphitized basal plane structure, when oxidized using oxidizing mixture results in graphene

oxide whose surface is rich in oxygen-containing functionalities. Due to these functionalities on graphene oxide, makes it more feasible for the modification which can be done in numerous ways and as per requirement which results in a reduction of graphene oxide with chemical modification. This reduced form has increased surface area, vacancies, and defects in a structure which makes it suitable as support material. A marked growth over a decade has been observed for graphene oxide and reduced graphene oxide application in various fields such as electronics, energy storage, biomedical applications, electrochemical sensors, water purification, and biosensors.

7 Future Aspects

Many challenges have been overcome, and some challenges are still a big concern. Major challenges related to graphene oxide and reduced graphene oxides are related to their synthesis and functionalization in which focus required on controlling its size, morphology, defects, and functionalization along with its toxicity and effects on cells which would help to create and develop more efficient biosensors, drug delivery system, energy storage devices, and achieve the limitations in other application fields as well.

References

Bhuyan, M. S. A., Uddin, M. N., Islam, M. M., Bipasha, F. A., & Hossain, S. S. (2016). Synthesis of graphene. *International Nano Letters, 6,* 65–83.

Brodie, B. C. (1859). XIII. On the atomic weight of graphite. *Philosophical Transactions of the Royal Society of London* 249–259.

Buchsteiner, A., Lerf, A., & Pieper, J. (2006). Water dynamics in graphite oxide investigated with neutron scattering. *The Journal of Physical Chemistry B, 110,* 22328–22338.

Cooper, D. R., D'Anjou, B., Ghattamaneni, N., Harack, B., Hilke, M., Horth, A., Majlis, N., Massicotte, M., Vandsburger, L., & Whiteway, E. (2012). Experimental review of graphene. *ISRN Condensed Matter Physics, 2012.*

Dreyer, D. R., Park, S., Bielawski, C. W., & Ruoff, R. S. (2010). The chemistry of graphene oxide. *Chemical Society Reviews, 39,* 228–240.

Geim, A. (2012). Graphene prehistory. *Physica Scripta, 2012,.*

Geim, A., & Novoselov, K. (2007). The rise of graphene. *Nature Materials*, *6*, 183–191.

Hummers Jr, W. S., & Offeman, R. E. (1958). Preparation of graphitic oxide. *Journal of the american chemical society, 80*, 1339–1339.

Kaniyoor, A., & Ramaprabhu, S. (2012). A Raman spectroscopic investigation of graphite oxide derived graphene. *AIP Advances, 2,.*

Kudin, K. N., Ozbas, B., Schniepp, H. C., Prud'Homme, R. K., Aksay, I. A., & Car, R. (2008). Raman spectra of graphite oxide and functionalized graphene sheets. *Nano Letters, 8,* 36–41.

Lerf, A., He, H., Forster, M., & Klinowski, J. (1998). Structure of graphite oxide revisited. *The Journal of Physical Chemistry B, 102,* 4477–4482.

Li, D., Müller, M. B., Gilje, S., Kaner, R. B., & Wallace, G. G. (2008). Processable aqueous dispersions of graphene nanosheets. *Nature Nanotechnology, 3,* 101.

Li, J., Li, L., Zhang, B., Yu, M., Ma, H., Zhang, J., et al. (2014). Synthesis of few-layer reduced graphene oxide for lithium-ion battery electrode materials. *Industrial and Engineering Chemistry Research, 53,* 13348–13355.

Mogha, N. K., Gosain, S., & Masram, D. T. (2017a). Gold nanoworms immobilized graphene oxide polymer brush nanohybrid for catalytic degradation studies of organic dyes. *Applied Surface Science, 396,* 1427–1434.

Mogha, N. K., Kirti, S., & Masram, D. T. (2017b). La_2O_3/reduced graphene oxide nanocomposite: a highly efficient, reusable heterogeneous catalyst for the synthesis of biologically important bis (indolyl) methanes under solvent free conditions. *Journal of Nanoscience and Nanotechnology, 17,* 2508–2514.

Mogha, N. K., Sahu, V., Sharma, M., Sharma, R. K., & Masram, D. T. (2014). Sensitive and reliable ascorbic acid sensing by lanthanum oxide/reduced graphene oxide nanocomposite. *Applied Biochemistry and Biotechnology, 174,* 1010–1020.

Mogha, N. K., Sahu, V., Sharma, M., Sharma, R. K., & Masram, D. T. (2016). Biocompatible ZrO_2-reduced graphene oxide immobilized AChE biosensor for chlorpyrifos detection. *Materials and Design, 111,* 312–320.

Mogha, N. K., Sahu, V., Sharma, R. K., & Masram, D. T. (2018). Reduced graphene oxide nanoribbon immobilized gold nanoparticle based electrochemical DNA biosensor for the detection of Mycobacterium tuberculosis. *Journal of Materials Chemistry B, 6,* 5181–5187.

Paredes, J., Villar-Rodil, S., Martínez-Alonso, A., & Tascon, J. (2008). Graphene oxide dispersions in organic solvents. *Langmuir, 24,* 10560–10564.

Randviir, E. P., Brownson, D. A., & Banks, C. E. (2014). A decade of graphene research: Production, applications and outlook. *Materials Today, 17,* 426–432.

Schniepp, H. C., Li, J.-L., McAllister, M. J., Sai, H., Herrera-Alonso, M., Adamson, D. H., et al. (2006). Functionalized single graphene sheets derived from splitting graphite oxide. *The Journal of Physical Chemistry B, 110,* 8535–8539.

Stathi, P., Gournis, D., Deligiannakis, Y., & Rudolf, P. (2015). Stabilization of phenolic radicals on graphene oxide: An XPS and EPR study. *Langmuir, 31,* 10508–10516.

Staudenmaier, L. (1898). Verfahren zur darstellung der graphitsäure. *Berichte der Deutschen Chemischen Gesellschaft, 31,* 1481–1487.

Stobinski, L., Lesiak, B., Malolepszy, A., Mazurkiewicz, M., Mierzwa, B., Zemek, J., et al. (2014). Graphene oxide and reduced graphene oxide studied by the XRD, TEM and electron spectroscopy methods. *Journal of Electron Spectroscopy and related Phenomena, 195,* 145–154.

Subodh, M. N. K., Chaudhary, K., Kumar, G., & Masram, D. T. (2018). Fur-Imine-functionalized graphene oxide-immobilized copper oxide nanoparticle catalyst for the synthesis of xanthene derivatives. *ACS Omega, 3,* 16377–16385.

Wang, X., & Chen, S. (2011). Graphene-based nanocomposites. *Physics and Applications of Graphene-Experiments.* IntechOpen.

Xu, J., Wang, K., Zu, S.-Z., Han, B.-H., & Wei, Z. (2010). Hierarchical nanocomposites of polyaniline nanowire arrays on graphene oxide sheets with synergistic effect for energy storage. *ACS Nano, 4,* 5019–5026.

Yang, D., Velamakanni, A., Bozoklu, G., Park, S., Stoller, M., Piner, R. D., et al. (2009). Chemical analysis of graphene oxide films after heat and chemical treatments by X-ray photoelectron and Micro-Raman spectroscopy. *Carbon, 47,* 145–152.

Chapter 5
Nanostructured 2D Materials as Nano Coatings and Thin Films

S. V. Satya Prasad, S. B. Prasad, and Subhash Singh

1 Introduction

The process of thin film coating is the controlled enhancement of the characteristics of a compatible surface. The coating is accomplished as the film is deposited on the surface thus making it a surface treatment process. The coating maybe applied to a surface in the state of solid, liquid, or gas. The industrial development has enforced the economic development of coatings, capable of sustaining the extreme conditions. The attention has been drawn towards nanocoatings as materials with inimitable mechanical and tribological properties can be obtained (Zhang et al., 2003). Primarily, the coating type is influenced by nature of material, process parameters, and the method of deposition (Musil et al., 2001). These impact the material properties like conductivity, structure, and adhesiveness of the nanocoatings in the final component. The discovery of 2D materials has boosted their use in nanofilms and coatings. The 2D materials are synthesized through isolation from the bulk of layered materials because of weak van der Waals forces between layers. Hence 2D materials possess sheet-like structure and negligible atomic thickness. Conventional techniques in the fabrication of 2D materials include top-down exfoliation and bottom-up growth (Ng et al., 2018). Graphene for instance is obtained from graphite by isolating it and through the process of continuous exfoliation (scotch tape technique). This technique produces extremely good quality crystals but has a very low yield and unfitting for large-scale production. The process of chemical vapour deposition (bottom-up growth technique) promotes the growth of good quality 2D materials of monolayer on a given substrate.

The distinctive properties of the 2D materials are the reason for their growth in the field of nanocoatings. The various applications of 2D materials as coatings are

S. V. Satya Prasad · S. B. Prasad · S. Singh (✉)
Department of Production and Industrial Engineering, National Institute of Technology Jamshedpur, Jamshedpur, Jharkhand 831014, India

S. Singh et al. (eds.), *Advanced Applications of 2D Nanostructures*,
Materials Horizons: From Nature to Nanomaterials,
https://doi.org/10.1007/978-981-16-3322-5_5

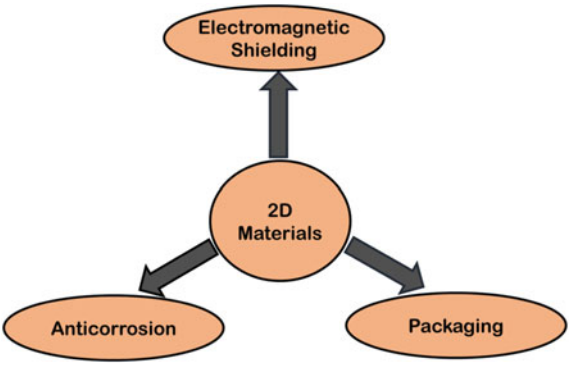

Fig. 1 Applications of 2D materials as coatings

represented in Fig. 1. The mostly used 2D material in nanocoatings, with exceptional properties is graphene. Graphene has excellent thermal and electrical conductance and therefore can be used as coatings in the applications of semiconductors. Graphene due to its high surface area can be used as protective coatings against corrosion (Böhm, 2014). Apart from graphene, the use of synthesized extended family of 2D materials (transition metal dichalcogenides (TMDCs)) has become an interesting aspect of the research for coating applications in the field of electronics. Therefore, the increasing demand of 2D materials has become the driving force behind the development of advanced fabrication and deposition techniques of these materials for coating applications.

2 The 2D Material Coatings

2.1 Graphene

Graphene with 2D sheet-like structure having sp^2 bonded atoms of carbon is a brilliant ultra-thin anticorrosion coating. This is because of its mechanical robustness, chemical inertness, flexibility and its ability to produce an impermeable shield (Krishnamurthy et al., 2015). The dimensions and functionalities (thermal or electrical conductivity) of the metal beneath the ultra-thin coating layer remains unaffected due to the application of graphene coatings. In the physical environment, the use of such anticorrosion graphene coatings for metals (alloys of copper, nickel and steel) has become pertinent (Kirkland et al., 2012; Prasai et al., 2012). But the time scales were relatively shorter (hours/minutes) for these research studies. Recent studies on the use of graphene coatings on the substrates of copper report the failed attempts. These studies were conducted in abiotic environmental conditions. The transfer of mass through nano scale defects in the graphene sheet lead to the failure of coatings. This problem of defective graphene films was easily and effectively dealt by Tiwari and Singh Raman (2017). Multiple layers were deposited on the copper surface to

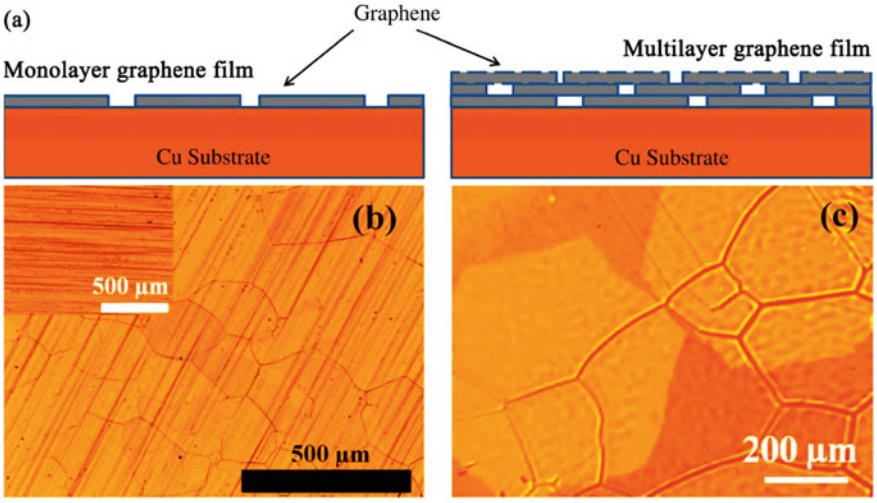

Fig. 2 **a** Schematics of multi-layered film of graphene, **b** optical image of multilayer graphene film, **c** optical image of monolayer graphene film (Wu et al., 2013; Tiwari & Singh Raman, 2017; Ding et al., 2018)

reimburse the defects in single-layered films of graphene as represented in Fig. 2. The electrochemical analysis signified enhanced resistance towards corrosion in copper. This analysis was in a medium containing chlorine and revealed the presence of corrosion resistance for 400 h duration. The optical transparency of the graphene layers (about 4–5) was detected through the optical microscopy (Fig. 2b) (Ding et al., 2018). The non-existence of isolated grains of graphene (Fig. 2c) confirms the shielding of entire surface of copper (Wu et al., 2013). Using few layers of graphene can significantly reduce the nanoscale defects (Hsieh et al., 2014).

The steel industries face a major problem of corrosion which is influenced by factors in the environment like oxygen, electrolytes, and water. The increasing demand for cost-effective and environment favourable coatings against corrosion, gained the graphene's attention since its discovery in the year 2004 (Novoselov et al., 2004). Graphene is an excellent choice for anticorrosion coatings in steels because it is impermeable to various gases and salts. The surface area and exceptional electrical conductance favor the anticorrosion mechanism of graphene. The overall anticorrosion mechanism of graphene is a combined effect of 3 activities. The first, graphene coating complicates the path of seeping water. The impermeable nature of graphene coating makes it an exceptional shield against various corrosive elements. Moreover, the higher electrical conductance of graphene over steel creates an alternative path for electrons. Due to this, there is a possibility of electrons to not reach the cathode. This prevents the steel from getting corroded. Hence it becomes inevitable to the use graphene and its hybrid nanocomposites as protective coatings for longer durations. The metal oxidation beneath the coating layers can be prevented (Böhm, 2014). The graphene may be integrated into the organic coatings through the

process of liquid exfoliation of graphite. This is an efficient technique proposed for producing graphene in industries (Prasai et al., 2012; Tong et al., 2013; Böhm, 2014). The graphene-based coatings were used on bipolar plates (made of stainless steel) within the fuel cells. The low-carbon stainless steels (SS 304L and SS 316L) have higher corrosion rates in the acidic environments of fuel cells. The use of graphene-based coatings significantly reduced the corrosion rates of the stainless steels thereby enhancing their performance in corrosive atmospheric conditions. The use of functionalized graphene is advantageous for anticorrosion applications. This is because graphene has to utilized as a single component within multicomponent distribution of coating. As functionalization can be carried out at the time of exfoliation, the entire process of preparation becomes continuous.

It is known that graphene has excellent electrical conductivity. Apart from this, the exceptional carrier mobility of graphene and its optical transmission abilities within the visible spectrum makes the materials of graphene exceptionally good transparent conductive films (TCFs). Particularly it is the graphene oxide (GO) that has found applications in the TCFs (Zhu et al., 2010). The production scale and ease in processing GO are one of the main reasons behind this. The techniques employed for deposition of GO platelet films are vacuum filtration (Eda et al., 2008), dip coating (Wang et al., 2008), and spin coating with subsequent thermal annealing or/and chemical reduction. The applications of GO TCFs include LCDs (Blake et al., 2008), organic LEDs (Wu et al., 2010) and dye sensitized solar cell electrodes (Wang et al., 2008). The process of chemical vapour deposition was employed to deposit monolayer graphene on a prepared film of indium tin oxide (ITO) to improve its electrical characteristics. The spin coating of PMMA (Poly methyl methacrylate), an indirect transfer technique was employed to transfer graphene onto ITO. The electrical conductivity of ITO was enhanced due to the enhancement in carrier mobility and concentration of surface carrier by graphene. Graphene exhibited an optical transmittance of 96.94% for 550 nm wavelength. It was also observed that by CVD of graphene, there was a reduction in the sheet resistance by 12% without affecting the smoothness of the bi-film (Hemasiri et al., 2017).

Graphene coatings are used in the prevention of microbial corrosion as it is essential to avert microbial corrosion for various biotic applications. Due to the presence of microbes, there is a development of biofilm layers on the metal surfaces in aqueous medium (Videla & Herrera, 2009). This alters the metal-solution interface leading to aggravated metal corrosion. Hence, the microbial-induced corrosion (MIC) restricts the use of metals for different biotic applications. Previous studies suggest that the conformal coatings of graphene are extremely efficient against MIC for durations up to 2700 h. In case of nickel, CVD deposited multi-layered (3–4 layers) graphene films provide corrosion resistance for durations of approximately 2400 h in microbial environments (Krishnamurthy et al., 2013). The MIC is countered by the graphene coating through the following ways: (a) restricting the microbe access onto the surface of the nickel, (b) minimizing the charge transport through a developed protective boundary across the metal (Ni) surface and anolyte, and (c) shielding the surface of Ni from the by-products (like H^+) of microbes which aggravate the dissolution process of Ni. The protective boundary is much stable in the case of graphene coating as compared

to that of the films of oxide that make the unshielded surface passive (Krishnamurthy et al., 2013).

The comparative study on the performance of graphene against polymer (parylene–C, polyurethane) coatings exhibits higher resistance of graphene against microbial corrosion in galvanic conditions. The electrochemical analysis demonstrates higher MIC resistance in graphene which is approximately 10 and 100 times higher than polyurethane and parylene–C respectively (Krishnamurthy et al., 2015). The SEM photographs in Fig. 3 a, c and e represent the coated biofilms of graphene, parylene–C, and polyurethane on nickel respectively. In-depth analysis of the polymer-coated Ni specimens reveals the green colored microbial corrosion by-products along with the specimens as seen in Fig. 3d for parylene–C coated nickel and in Fig. 3f for polyurethane coated nickel. The extensively corroded edges in parylene–C coated nickel may be due to the direct microbe-metal interface or due to the presence of intermediate metabolites (unstable fatty acids). This also indicates better performance of polyurethane coatings against microbial corrosion. However, focus needs to be shifted on the graphene-coated Ni as an unaffected Ni specimen is seen in Fig. 3b. These are the results obtained after the specimens have been continuously exposed to MIC conditions for duration of 30 days. This shows graphene coatings are extremely resistant to MIC. This is a significant discovery keeping in mind the

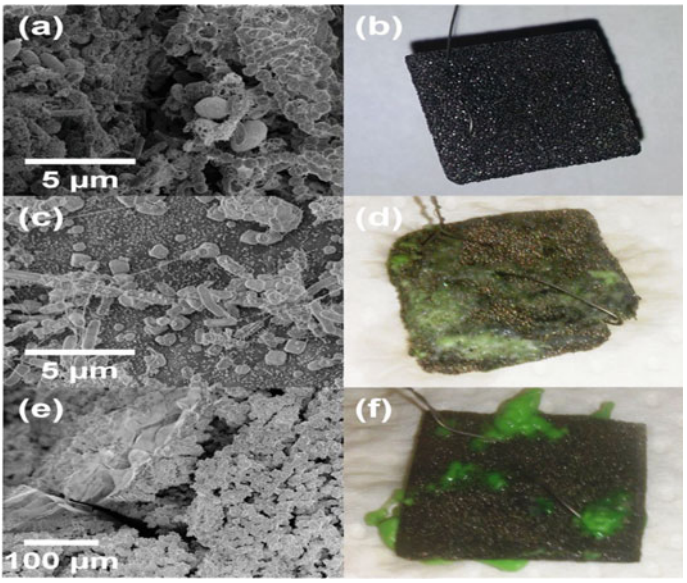

Fig. 3 **a** SEM image of graphene biofilm on nickel, **b** MIC-resistant anode of graphene coated nickel anode post 30 days of MIC tests, **c** SEM image of parylene–C biofilm on nickel, **d** Corroded anode of parylene–C coated nickel specimen post 30 days of MIC test, **e** SEM image of polyurethane-coated nickel specimen, **f** Corroded polyurethane-coated nickel anode post 30 days of MIC test (Krishnamurthy et al., 2015)

average thickness of the graphene film (1–2 nm) which is very low compared to its polymer counterparts.

Graphene, a renowned 2D material has been rigorously studied in various applications like water treatment, energy storage/conversion, optronics, catalysis, etc. (Duan et al., 2015; Kim et al., 2015). Because of its high electrical conductivity and optronic properties (R_s ~ 60 Ω/sq at T ~ 97.7% per single layer), graphene is considered as an effective replacement for tin-doped indium oxide and fluorine-doped tin oxide. The thin, transparent, and flexible graphene-derived TCEs offer high chemical stability and optronic characteristics, identical to carbon nanotube (CNT) based TCEs (De & Coleman, 2011). Essentially, transparent graphene-derived supercapacitors are best known for its longevity, great capacitance, and response rate.

2.2 Transition Metal Dichalcogenides (TMDs)

2.2.1 Molybdenum Disulphide (MoS_2)

The TMDs are a part of the 2D material family with a similar structure to graphene. The TMDs have MX_2 (M-Transition metals and X-chalcogens) general formula with semiconducting, superconducting, and metallic characteristics (Li & Zhu, 2015). As a result of this, the TMDs have interested the researchers for their wide prospects in the applications of electronic devices. Among the various TMDs, molybdenum disulphide (MoS_2) is the most unique and researched TMD. The band gap of 1.8 eV in a single layer of MoS_2 makes it an encouraging prospect for nanoelectronic applications, especially optoelectronic and switching devices. This is because the properties possessed by MoS_2 provides a possibility to regulate the layer numbers and also to select the type of dielectric materials (Yim et al., 2014). This band gap in MoS_2 overcomes the limitations in graphene which doesn't have a band gap which has become one of the prime reasons of interest (Li & Zhu, 2015). The films of MoS_2 possess excellent photodetection and optoelectronic properties. Though mechanical exfoliation is widely employed technique for fabrication MoS_2 thin films, it is challenging to control the layer thickness and enhance the lateral size. Methods like molecular beam epitaxy and CVD are expensive with low scalability (Dam et al., 2019). Hence, vapor phase techniques in which vaporised sulphur reacts with MoS_2 has been developed. Thin films for large areas and controllable thickness can be developed by this method. MoS_2 thin films with regulating thickness can be used in phototransistors, sensors, and solar cells (Dam et al., 2019).

The satellites and spacecraft function in conditions where the range of temperature variation is high, vacuum and radiation are high. These extreme conditions restrict the use of liquid lubricants. Hence, in the past decade, there has been extensive study on the solid lubricant films due to their stable nature in irradiated environments and varying temperatures. The low vapour pressure of solid film lubricants makes them an important prospect from engineering perspective. TMDs based solid lubricant coatings have the desired properties to be applied in areas of high vacuum, speeds, and

loads. The low shear planes along the direction of crystallographic direction determine the exceptional tribological characteristics. The shear strength is low due to the filled dz^2 orbital in MoS_2 (Li et al., 2016). The remaining anti-bonding orbitals of high energy present for interlayer bonding weakens the interaction between layers. Among various solid lubricants, MoS_2 is an exceptional choice as solid lubricant for space-related applications in comparison to other TMDs like WSe_2, $MoSe_2$ and WS_2. But MoS_2 reacts with water molecules in water vapor to form MoO_3 and H_2SO_4 (Zhang et al., 2019). This fascination towards water is due to the presence of unsaturated bonds within the MoS_2 crystals. These reaction compounds lead to film degradation and metal corrosion. The coefficient of friction also enhances due to the enhanced shear strength of MoO_3. This demerit of MoS_2 limits its use for technology-related applications within the earth's environment. But the rising demand for adaptable solid lubricant coatings with changing atmospheric conditions and also which are robust has forced the researchers to look for enhancements. Aircrafts for example, experience varying humid conditions with respect to the change in altitude. Similarly, at the time of launching or assembly, satellites are exposed to moisture leading to oxidation within the earth's atmosphere. Therefore, it is essential to optimize the coatings of MoS_2 to overcome the challenges. Hence MoS_2 films doped with metals are under use for such applications. Doped MoS_2 films have enhanced load capacity and adhesion (Qin et al., 2013). They reduce the porosity and restrict the penetration of water. Hence doped MoS_2 films are extremely desirable as solid lubricant films. One such research attempt is the use of the doped MoS_2–Pb–Ti film as a solid film lubricant. It possessed extraordinary tribological characteristics in vacuum as well as air tests for various levels of humidity (Zhao et al., 2018). Enhanced transfer layer, modulus of elasticity, and dominant contact interface of MoS_2 are the reason for exceptional performance of the film. Mainly, the sacrificial nature of the doped metals in shielding MoS_2 from oxygen and water appreciably influences the tribological properties. This adds to the enhanced performance of the doped film in humid conditions.

The MoS_2 slides easily in conditions of low shear stress allied with low coefficient of friction due to weak Van der Waals bonds between layers and its hexagonal shaped sheet-like structure (lamellar crystal structure). In the dry atmospheric conditions and high vacuum, the sputter MoS_2-film coating is essential prospects as solid lubricant coatings for aerospace applications. The extremely low coefficient of friction (approximately 0.001) of the coating is the main reason for this (Ye et al., 2016). It is known that pure MoS_2 film degrades in humid conditions due to reaction with oxygen, its poor adhesion, low hardness, and loose structure. Hence, adding oxides (like PbO) or metals (like Ti, W, Ag, and Cr) to MoS_2 films have been proved to improve its tribological as well as mechanical properties in humid conditions. Hence metal coatings of MoS_2 perform better over pure MoS_2 films in humid conditions in terms of hardness, adhesion, and wear resistance. The composite coatings of MoS_2–Ti among various metal-doped coatings had better resistance to wear and lower sensitivity to water vapor in terrestrial conditions in comparison to pure MoS_2 films. But Ti-doped coatings doesn't exhibit lower friction in extreme humid conditions. There were cases which reported of poor adhesion of coatings and film degradation.

Previous studies supported the presence of lower frictional characteristics and long durability of sputtered Ti–MoS_2 thin films in vacuum and air. Hence they are extensively used as solid lubricants of rolling parts in spacecraft. But the sputtered films of Ti–MoS_2 eventually degrade withstanding friction over a period of time in air. For a film of lubricant, the transfer layer influences its resistance against wear. The humidity within the air infiltrates into the film leading to its degradation (Ye et al., 2009).

Multiple layered and metal-doped films have been developed in an attempt to enhance the resistance of MoS_2 against humidity (Zhao et al., 2018). Previous research supports the enhancement in tribological characteristics due to the deposition of multi-layered MoS_2 metal films in moist environmental conditions. The multi-layered films exhibited higher resistance to wear and lower coefficient of friction in vacuum or air. The deposition of multi-layered film of MoS_2/Pb–Ti on SS 316 and silicon wafer resulted in enhanced compactness and reduced defects and surface roughness in the coatings (Shang et al., 2018). The resistance against corrosion and oxidation in moist conditions improved within the film of multiple layers due to the presence of heterogeneous interfaces. This ensures negligible effect of the corrosive mediums on the inner film layers. The exhibition of superior tribological characteristics by the multi-layered films maybe attributed to their excellent mechanical characteristics and lower sensitivity towards moisture. The multi-layered MoS_2/Pb–Ti film was extremely resistant to corrosion and oxidation. It exhibited tremendous tribological performance post the salt spray test (Shang et al., 2018).

The addition of LaF_3 inhibits the oxidation of MoS_2 solid film lubricant in humid conditions. LaF_3 is an excellent anti-oxidant for MoS_2 and combination of the two compounds possesses a hexagonal structure. Adsorption of the LaF_3 particles on the MoS_2 matrix's surface results in a strong interfacial bond This bonding between the lubricant matrix and particles enhances the resistance of the LaF_3 doped MoS_2 film against wear. Hence, LaF_3 doping was done on Ti–MoS_2 thin composite films which caused a dense MoS_2 film having columnar grains. Scratch tests exhibited excellent adhesion between film and the substrate but excessive LaF_3 doping (0.8%) resulted in excessive brittleness. Also, increase in LaF_3 led to increased film hardness (6.2–8.7 GPa). The wear tests also favored the LaF_3 doped Ti–MoS_2 films which revealed enhanced endurance at 0.3% LaF_3 content addition in comparison to the conventional Ti–MoS_2 films. Moreover, the tribological characteristics of LaF_3 doped Ti–MoS_2 films is influenced by the dense columnar microstructure (Zhang et al., 2019).

The behavior of zirconium (Zr) might be similar to that of Ti within the films of MoS_2 especially for certain definite applications like machining steel. Since Zr has lower solubility in Fe, there is a possibility of better performance (Renevier et al., 2000). Considering this, composite MoS_2/Zr coatings were deposited on polished steel through the system of unbalanced magnetron sputtering ion plating in closed field. Enhanced tribological and mechanical characteristics were observed in Zr doped MoS_2 films. The adhesion and hardness were the highest in the MoS_2/0.4 Zr coating. Apart from this, the MoS_2/Zr coated films exhibited lower coefficient of friction and had an endurance life longer than pristine MoS_2 coated films. There was a gradual decrease in the coefficient of friction in the coatings with increasing loads.

The MoS_2/0.4 Zr coating exhibited superior resistance against wear and lubricant at 20 N load. At this point, the coefficient of friction (0.04) was at a steady state. The tribology of coated films is influenced by the characteristics like excellent adhesion, hardness, and lower coefficient of friction (Ye et al., 2016). This justifies the use of the MoS_2/Zr coating as shielded coatings in the applications of solid lubricants.

Similar results were obtained in MoS_2/Pb composite coatings where there was an enhancement in the Young's modulus and hardness with increased Pb concentration till 8.9% beyond which it decreased. The anti-oxidant characteristics of MoS_2/Pb coatings were negligible under dry conditions but increased with increasing levels of humidity. In elevated humid conditions (RH 75%) the tribological characteristics of MoS_2/Pb coatings were influenced by the anti-oxidant nature of the coatings (Li et al., 2016).

The lithium (Li) is an excellent lightweight material for anode. The anodes of Li in Li–S batteries form uncontrollable dendrites when Li is deposited multiple times over certain duration. There is also an unstable solid electrolyte interphase formed between Li and electrolyte which may be attributed to the deposition of inhomogeneous Li. To negate this, a layer of 2D MoS_2 is deposited to develop a shielding film between the electrolyte and the metal Li. This facilitates the insertion of Li atoms into the sheet structured MoS_2 which leads to the constant flow of Li^+ through the metal. Also the improved conductivity of MoS_2 removes the favored sites of dendrite nucleation of lithium. There was uniform deposition of MoS_2 film by the process of sputtering followed by lithiation to the metal surface. Strong adhesion of the MoS_2 coating leads to the suppression of the dendrites due to stable electrodeposition of lithium (Cha et al., 2018).

2.2.2 Tungsten Disulphide (WS_2)

Among the 2D materials with low coefficient of friction, Tungsten disulphide (WS_2) is inherent. The most common mode of its use is as coatings. Especially in dry situations, WS_2 exhibits low friction coefficient which is abolished under humid conditions. Hence the applications of WS_2 are limited. Adding selective metals enhances the mechanical characteristics of WS_2 through structural changes which incapacitate the disadvantages of WS_2. Apart from the added metals, it is the process parameters and the method of deposition that influence the coating characteristics. The study on Cr–WS_2 coatings deposited by unbalanced sputtering process on stainless steel and silicon suggested significant enhancement of the lubricating characteristics due to the substrate bias. The power source was direct current with four cathodes. The superlative lubricating characteristics were exhibited at the voltage with zero bias having 0.07 friction coefficients up to 1300 cycles and 0.10 frictional coefficients up to 1800 cycles (Deepthi et al., 2011). All the experimental investigations were carried out in ambient conditions of the atmosphere.

It is evident that the layer structured TMDs like WS_2, have been researched for their lower frictional characteristics in mediums of extreme vacuum and using them as solid lubricant films. But the direct magnetron sputtering of these WS_2

films having porous microstructure leads to low resistance against wear. The low hardness of the films is low is also one of the reasons for low life against wear in applications that involve rubbing parts. This is especially in the case of space applications. Hence the focus has been on enhancing the tribological properties of WS_2 nano-films by introducing modifications to the microstructure or by deposition of multiple layers. But in engineering applications, the deposition process of multi-layered nano-films is complex for substrates with intricate shapes. An alternative is fabrication of nanocomposite TMD film by adding metals or non-metals to enhance resistance against wear without much change in the frictional coefficient. Previous studies on nanocomposite TMD films support properties like enhanced adhesion, reduced porosity, and enhanced tribological and mechanical characteristics.

The existing research emphasises that the surface morphology of the interlayer enhances the tribological characteristics of the lubricating films. Therefore, a self-formed textured layer can positively enhance the film's tribological characteristics (Wang et al., 2011, 2017). Hence, the WS_2 film was textured by a self-formed interlayer of Ni nanocone-array to enhance the WS_2 film's tribological characteristics. The process of one-step electrodeposition was employed to make the Ni interlayer a texture layer for WS_2 film (Wang et al., 2019). The process of deposition was monitored in the formation of rough; unvarying textured layer of Ni was formed. Further, investigations were carried out to study the effect of textured layer morphology on the bilayer WS_2/Ni nanofilm. The interlayer was seen having a structure similar to cabbage as seen in Fig. 4.

The plates of WS_2 columns around the nanocones of Ni are the reason for this structure. The enhancements in the life of wear and lubrication characteristics of the thin WS_2/Ni nanofilm were observed. The restocking of WS_2 lubricates at the time of friction are the reason behind enhanced characteristics of the tribology. This is for the cabbage structured film of WS_2. Moreover, it is the reduced contact area and diminished levels of friction coefficient in Ni nanocone that influence the wear resistance positively within the lubricant at the time of exposed nanocones of nickel. This also retains the low friction coefficient under working conditions.

In the applications related to semiconductor manufacturing at sub-10 nm system, a degradation is observed in the overall transistor functioning which happens to be the mainstay in electronic circuits. The unwarranted dispersion of power due to the tunneling effect at the potential boundary of the channel is the main cause of this diminished performance. Construction of an all optical system with various functionalities is an option to avert this issue. Coating a microfiber with 2D material coatings provides the functionality which enables tuning of light amplitude. WS_2 having exceptional characteristics like varying thickness, adjustable band gap, broadband absorption of light, good nonlinear susceptibility, and good mobility of carriers is the obvious choice for coating microfibers (Zhang et al., 2015). The all-light control actions is extremely feasible in WS_2 coated devices due to the exhibition of WS_2 band gap (direct) within the region of visible to near-infrared rays (Zhao et al., 2013). Unlike the materials like black phosphorus and graphite with narrow/zero band gap with restricted use, WS_2 coatings have multiple applications and are also economically efficient on microfibers. Black phosphorus being instable cannot meet

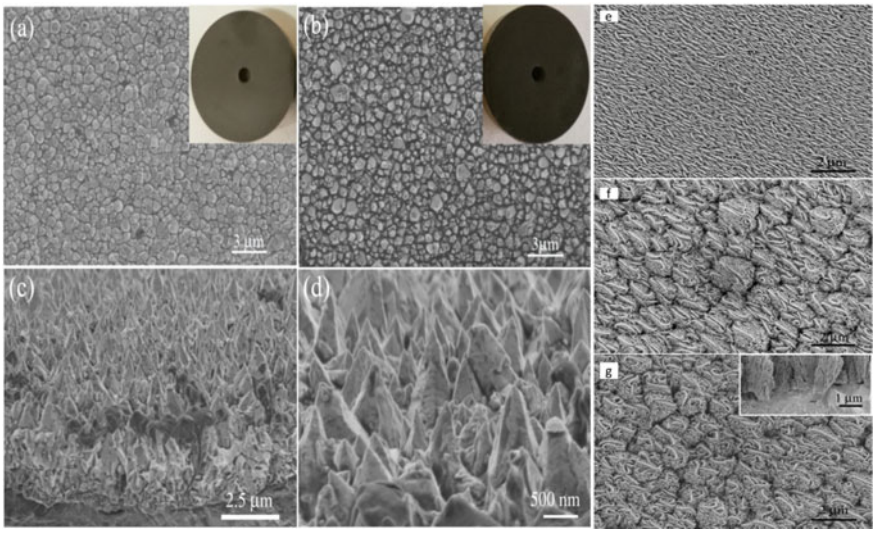

Fig. 4 **a** SEM image represents the Ni layer, **b** rough surface of the Ni layer, **c** image reveals the arrays of Ni nanocone on the surface, **d** Image at various magnifications showing the cross-section of Ni nanocone arrays. The insets in (**a**) and (**b**) represent optical images of Ni coated substrates of copper, **e** surface of pure film of WS_2, **f** Films of WS_2/Ni having rough interlayer of Ni and **g** Films of WS_2/Ni having nanocone-array of Ni interlayer. The inset image in (**g**) shows the cross-section of the Ni-WS_2 layer interface

the long-term stability demands in electronic devices. Though MXenes (2D nitrides or carbides) have a band gap that can be tuned and exceptional conductivity, their process of fabrication with microfibers is complex and expensive (Jiang et al., 2018).

Therefore, WS_2 is extremely appropriate for the analysis of photonic devices with nonlinear optical effects. WS_2 nano coatings (within 100 nm wavelength) on microfibers provide the functionality of all optical tuning. The tuning of the broadcasted amplitude of light through pump light excitations (internal/external) is possible due to the interface of momentary microfiber light-WS_2. It is possible to monitor largely varying broadcasted power due to this sound interface between the matter (WS_2) and light. The maximum limit of tenability is 0.3744 dB/mW and it is through the excitation of external 405 nm pump light (Li et al., 2019a, b). The attainment of the fabrication technique dependent moderate response time suggests modulation of transferred power in microfibers coated with WS_2. This modulation may be carried out with various pump lights with mW power capacity. Hence the applications of WS_2 coated microfibers are spread across various sensors and devices that can be optically controllable.

The nanocoatings of WS_2 having excellent wear-resistant properties are the principal choice in wear-related applications. They are also used in conjunction with other coatings to form composite coatings for various applications. One such research study on enhancing the wear characteristics of sol-gel processed coatings of zirconium

oxide (ZrO_2) utilized WS_2 films in conjunction with surface textures. The sol-gel process was employed to produce the coatings of ZrO_2 on the surfaces of cemented carbide (Li et al., 2019a, b). The lubricant film of WS_2 was fabricated by the technique of electro hydrodynamic atomization (EHDA) and combined with the laser surface textures to enhance the wear characteristics and friction. Through the EHDA technique, a uniform and defect/crack free film of WS_2 was engineered effectively and quickly. The results endorsed the exhibition of enhanced wear and frictional characteristics by ZrO_2 textured coatings post the deposition of WS_2. The interaction between microtextures and the lubricant film was attributed for these enhanced properties. The lubricating effect of WS_2 was enlarged due to the prolongation of wear life in WS_2 coatings. The textures were responsible for this prolonged life of wear in the coatings of WS_2. There was also a reduction in the coefficient of friction (16% approx.) and the rate of wear (92% approx.) observed for the textured coatings of ZrO_2. Hence, the applications of composite coatings like WS_2/ZrO_2 could have great prospects as protective coatings for surfaces with further advancements.

2.3 Hexagonal Boron Nitride (H-BN)

One of the most stable and non-reactive 2D materials is hexagonal boron nitride (h-BN). It remains stable in air at temperatures of 1500 °C with no reaction with majority of chemicals. The applications of h-BN have increased in the recent past due to its excellent dielectric characteristics which makes it appropriate for devices centred on graphene. The use of single layered h-BN in high-performance devices of graphene as substrates has become successful. The use of h-BN in vertical heterostructures as the barrier material in conjunction with TMDs and graphene is known (Britnell et al., 2012). If good quality, uniform coatings with large areas can be produced on the surfaces needing protection then h-BN may be considered as the ultimate coating material for oxidation. The outstanding characteristics like chemical or thermal stability may be attributed for such superlative performance of h-BN coatings on 2D layered materials which further can be improved. The pulsated layer deposition is a conventional technique to produce h-BN films but it is expensive and form amorphous BN. Though mechanical exfoliation is a good option for producing h-BN films of exceptional quality, the small h-BN footprints restrict the h-BN applications as coatings. Hence, h-BN may be used as oxidation-resistant coatings on Ni surfaces for high-temperature applications in conditions with high quantities of oxygen. A research on Ni surfaces with extremely thin h-BN layers under controlled conditions (number of layers and thickness) was carried out to examine the resistance of coatings in temperatures up to 1100 °C (Liu et al., 2013). The intention behind the research is to observe the coating's resistance to diffusion to oxygen. The final observations concluded that the h-BN coatings with suitable thickness and extremely good quality are capable to radically enhance the resistance against oxidation in metal under conditions rich in oxygen with elevated temperatures. The layers of graphene are also conserved when coated upon h-BN at extreme temperatures. Hence h-BN coatings

engineered by the CVD technique with 2 layers are the thinnest possible coatings providing chemical stability appropriate for conditions with elevated temperatures.

The h-BN has a 2D crystal structure with approximately 6 eV band gap. It is chemically stable having excellent thermal conductivity and mechanical strength due to the covalent bonds of sp^2 which are extremely strong. Since it is free from charge traps or dangling bonds, h-BN makes a perfect dielectric substrate in the applications related to field-effect transistors (Dean et al., 2010). The smooth surface of h-BN makes it ideal for spacer in tunnelling devices as well. The properties of h-BN allow it to be used in ballistic electronics at ambient temperatures. A study to comprehend the growth and nucleation process of h-BN, mono crystal h-BN grains of huge sizes were considered on the alloy of copper-nickel. A layer of uniform thickness and large h-BN grains using CVD process was developed on copper-nickel substrate. There was a tremendous decrease (till 60 sq. mm) in the nucleation density due to the 10–20% of Ni. The area of h-BN grains 7500 sq. mm produced was twice compared to the ones obtained in previous studies (Lu et al., 2015). The production of good quality h-BN grains is due to the presence of nickel which decomposed poly-aminoborane thereby freeing the h-BN grain from nanoparticles. The presence of uniform h-BN grains is established through various characterization techniques like TEM, AFM, etc. The superior dielectric characteristics of the layers of h-BN were revealed due to the electric transport measurements. Hence, the importance of CVD processed h-BN grains and the heterostructure of graphene/h-BN is established for applications of devices.

The use of polyacrylics in applications like adhesives, coatings, paints has increased due to their exceptional characteristics like great cohesiveness, dimensional stability (Yeh et al., 2002), good strength and film formation. In spite of such excellent properties, their inability to resist corrosion restricts their applications. The resistance against corrosion can be enhanced through surface modification techniques like electrochemical polishing, surface passivation or use of fillers with suitable characteristics. These methods reduce the phenomenon of ion liberation and develop higher resistance against corrosion in polyacrylics.

The boron nitride has distinctive characteristics such as high melting point, low coefficient of friction and density, excellent resistance to chemicals and inert nature, high resistance to wear and oxidation, exceptional thermal conductivity, and electrical resistivity. These properties make boron nitride one of the most commonly used materials for technology-related applications. The applications of boron nitride in electronics and ceramic composites are in the form of fibres, thin films or coatings. Sometimes even the bulk nature of the ceramics is also used. But the h-BN is most suitable for coating applications as it enhances the barrier characteristics and also endorses the particle alignment with the surface.

AISI 304 was studied by applying a composite coating of PMMA/h-BN to understand the influence of h-BN quantity in resistance against corrosion. Dip coating technique was adopted. Various quantities of h-BN were engineered as shown in Fig. 5 to understand its influence on enhancing the corrosion resistance properties (Coan et al., 2013). The images of SEM (Fig. 5) reveal uniform deposition of the coatings with a velocity of 0.3 m per minute. The coating layers were strongly stuck

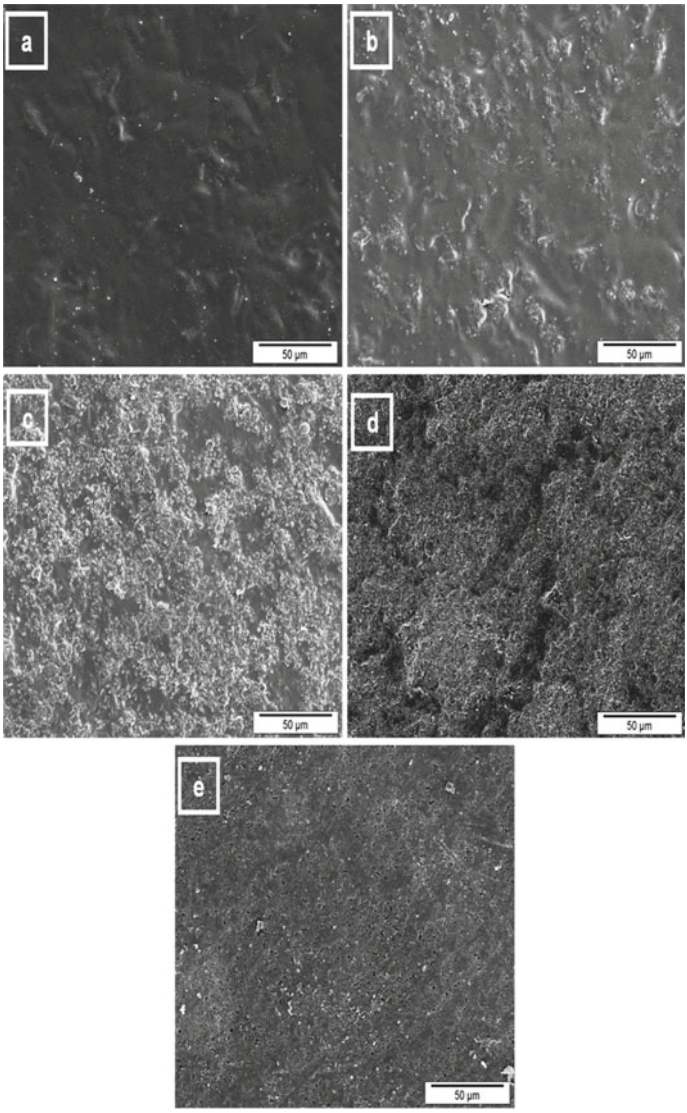

Fig. 5 SEM images showing coatings on: **a** pure PMMA; **b** 90%–10% of PMMA/h-BN; **c** 70%–30% of PMMA/h-BN; **d** 50%–50% of PMMA/h-BN; **e** 30%–70% PMMA/h-BN, on AISI 304 stainless steel (Coan et al., 2013)

to the substrate surface indicating no separation of the samples. The study revealed better performance of the PMMA/h-BN coatings as compared to the pure PMMA. Moreover, no signs of cracks were observed in any of the samples. The sample with 70% PMMA and 30% h-BN exhibited the best resistance properties against corrosion post 15 h of immersion in 1 N solution of HCl. Optimum levels of h-BN and provided

higher corrosion resistance in acid solution whereas optimum porosity restricted the seeping of HCl solution within the coating.

2.4 Black Phosphorous (BP)

The sheet structured black phosphorus offers multiple chances for thorough analysis in its applications. The band gap of BP is analogous to the TMDs from 0.3 to 1.9 eV in case of monolayer BP (phosphorene). Hence, the applications of BP having great electrical characteristics are similar to TMDs especially in transistors and optoelectronics. The BP has a tuneable bandgap depending on the electric field (vertical) and the layer number. The electromagnetic range is from mid-infrared to visible. Though visible progress have been made in the optoelectronics, not much research has been carried out related to photoluminescence (PL) of BP films. Only 1–5 layers of PL has been explored related to the region of visible- near infra-red.

It is the fields of physics and devices that gathered interest in BP due to its unique properties like great in-plane anisotropy, good mobility of carriers, wide band structure that is tuneable. An outstanding platform is created by the bandgap that is tuneable for the applications of infrared optoelectronics (Izquierdo et al., 2019). In case of thin BP films with more than 6 layers of thickness the characteristics of light emission have little findings. The issues of measuring PL in the region of mid-infrared are the reason for this. Research on 46 nm BP film revealed strong and bright PL emission with 0.308 and 0.334 eV at respective temperatures of 80 and 300 K (Chen et al., 2019). Incidentally, this intense emission is similar to the one in the active range of laser (at room-temperature). This proves BP in the region of mid-infrared emission of light has great prospects including laser applications.

The BP to be manufactured in large-scale there is a necessity of a pressure over 1 GPa. But one of the prime issues related to manufacturing of phosphorene is that there are no techniques (mechanical or liquid) of exfoliation where flakes covering vast areas with proper thickness and orientation (Chen et al., 2019). Hence, production of phosphorene is tough and is restricted to smaller devices.

3 Conclusions

The 2D materials since their discovery in the year 2004 due to their unique properties and sheet-like structure find themselves in various applications. The present chapter is related to the nano coatings and thin film applications of 2D materials. Among various 2D materials graphene and graphene oxide are the first 2D materials to be discovered and the most researched materials. The nanofilms of graphene and GO extend to wear-resistant, friction applications, electronic applications, bio applications. Further developments in research lead to the discovery of TMDs. The TMDs include materials like MoS_2, WS_2 and the coatings of TMDs or the thin

film applications are used in solid lubricants for space applications. The friction and wear-resistant applications of TMDs include composite films where 2D materials are additives. The 2D material coatings on metal surfaces are used for enhancement of mechanical properties. The optical properties of TMDs also find its applications in electronic devices. The general technique for the deposition of 2D materials is CVD where uniform layered coating without any cracks are obtained. The coatings have excellent adhesion with the substrate. This technique is extremely suitable for cost-effective large-scale production. The h-BN coatings find its applications in corrosion-resistant applications. The films of h-BN are also used in electronic applications. One of the recently rediscovered materials is BP which has its applications in electronics. There are no other applications of BP apart from electronics. Further research is needed and BP needs to be explored. Though 2D materials have wide applications it is graphene that has been studied and applied. Further research is necessary on the extended family of 2D materials for the exploitation of their unique characteristics.

References

Blake, P., et al. (2008). Graphene-based liquid crystal device. *Nano Letters*. https://doi.org/10.1021/nl080649i.

Böhm, S. (2014). Graphene against corrosion. *Nature Nanotechnology*. https://doi.org/10.1038/nnano.2014.220.

Britnell, L., et al. (2012). Field-effect tunneling transistor based on vertical graphene heterostructures. *Science*. https://doi.org/10.1126/science.1218461.

Cha, E., et al. (2018). 2D MoS 2 as an efficient protective layer for lithium metal anodes in high-performance Li-S batteries. *Nature Nanotechnology*. https://doi.org/10.1038/s41565-018-0061-y.

Chen, C., et al. (2019). Bright mid-infrared photoluminescence from thin-film black phosphorus. *Nano Letters*. https://doi.org/10.1021/acs.nanolett.8b04041.

Coan, T., et al. (2013). Preparation of PMMA/hBN composite coatings for metal surface protection. *Materials Research, 16*(6), 1366–1372. https://doi.org/10.1590/S1516-14392013005000140.

Dam, S., et al. (2019). Synthesis and characterisation of MoS_2 thin films by electron beam evaporation. *Thin Solid Films*. https://doi.org/10.1016/j.tsf.2019.04.041.

De, S., & Coleman, J. N. (2011). The effects of percolation in nanostructured transparent conductors. *MRS Bulletin*. https://doi.org/10.1557/mrs.2011.236.

Dean, C. R., et al. (2010). Boron nitride substrates for high-quality graphene electronics. *Nature nanotechnology*. https://doi.org/10.1038/nnano.2010.172.

Deepthi, B., et al. (2011). *Nanostructured Au-WS_2 solid lubricant coatings prepared by magnetron sputtering*.

Ding, R., et al. (2018). A brief review of corrosion protective films and coatings based on graphene and graphene oxide. *Journal of Alloys and Compounds, 764*, 1039–1055. https://doi.org/10.1016/j.jallcom.2018.06.133.

Duan, X., et al. (2015). Effects of nitrogen-, boron-, and phosphorus-doping or codoping on metal-free graphene catalysis. *Catalysis Today*. https://doi.org/10.1016/j.cattod.2014.10.005.

Eda, G., Fanchini, G., & Chhowalla, M. (2008). Large-area ultrathin films of reduced graphene oxide as a transparent and flexible electronic material. *Nature Nanotechnology*. https://doi.org/10.1038/nnano.2008.83.

Hemasiri, B. W. N. H., Kim, J. K., & Lee, J. M. (2017). Fabrication of highly conductive graphene/ITO transparent bi-film through CVD and organic additives-free sol-gel techniques. *Scientific Reports, 7*(1), 1–12. https://doi.org/10.1038/s41598-017-18063-w.

Hsieh, Y.-P., et al. (2014). Complete corrosion inhibition through graphene defect passivation. *ACS Nano, 8*(1), 443–448. https://doi.org/10.1021/nn404756q.

Izquierdo, N., et al. (2019). Thin-film deposition of surface passivated black phosphorus. *ACS Nano.* doi:10.1021/acsnano.9b02385.

Jiang, X., et al. (2018). Broadband nonlinear photonics in few-layer MXene $Ti_3C_2T_x$ (T=F, O, or OH). *Laser & Photonics Reviews*. https://doi.org/10.1002/lpor.201700229.

Kim, Y. H., et al. (2015). Self-activated transparent all-graphene gas sensor with endurance to humidity and mechanical bending. *ACS Nano.* https://doi.org/10.1021/acsnano.5b04680.

Kirkland, N. T., et al. (2012). Exploring graphene as a corrosion protection barrier. *Corrosion Science*. https://doi.org/10.1016/j.corsci.2011.12.003.

Krishnamurthy, A., et al. (2013). Passivation of microbial corrosion using a graphene coating. *Carbon*. https://doi.org/10.1016/j.carbon.2012.12.060.

Krishnamurthy, A., et al. (2015). Superiority of graphene over polymer coatings for prevention of microbially induced corrosion. *Scientific Reports, 5,* 1–12. https://doi.org/10.1038/srep13858.

Li, H., Zhang, G., & Wang, L. (2016). Low humidity-sensitivity of MoS_2/Pb nanocomposite coatings. *Wear, 350–351,* 1–9. https://doi.org/10.1016/J.WEAR.2015.12.008.

Li, X., & Zhu, H. (2015). Two-dimensional MoS_2: Properties, preparation, and applications. *Journal of Materiomics, 1*(1), 33–44. https://doi.org/10.1016/J.JMAT.2015.03.003.

Li, H., et al. (2019a). Broadband all-light-control with WS_2 coated microfibers. *Optics Express*. https://doi.org/10.1364/oe.27.012817.

Li, X., et al. (2019b). Effect of surface textures and electrohydrodynamically atomized WS_2 films on the friction and wear properties of ZrO_2 coatings. *Ceramics International*. https://doi.org/10.1016/j.ceramint.2018.09.281.

Liu, Z., et al. (2013). Ultrathin higherature oxidation-resistant coatings of hexagonal boron nitride. *Nature Communications, 4*(May), 1–8. https://doi.org/10.1038/ncomms3541.

Lu, G., et al. (2015). Synthesis of large single-crystal hexagonal boron nitride grains on Cu-Ni alloy. *Nature Communications*. https://doi.org/10.1038/ncomms7160.

Musil, J., Karvánková, P., & Kasl, J. (2001). Hard and superhard Zr–Ni–N nanocomposite films. *Surface and Coatings Technology, 139*(1), 101–109. https://doi.org/10.1016/S0257-8972(01)00989-6.

Ng, L. W. T., et al. (2018). Printing of graphene and related 2D materials, printing of graphene and related 2D materials. https://doi.org/10.1007/978-3-319-91572-2.

Novoselov, K. S., et al. (2004). Electric field effect in atomically thin carbon films. *Science, 306*(5696), 666–669. https://doi.org/10.1126/science.1102896.

Prasai, D., et al. (2012). Graphene: Corrosion-inhibiting coating. *ACS Nano, 6*(2), 1102–1108. https://doi.org/10.1021/nn203507y.

Qin, X., et al. (2013). Microstructure, mechanical and tribological behaviors of MoS_2-Ti composite coatings deposited by a hybrid HIPIMS method. *Surface and Coatings Technology, 228,* 275–281. https://doi.org/10.1016/J.SURFCOAT.2013.04.040.

Renevier, N., et al. (2000). Coating characteristics and tribological properties of sputter-deposited MoS_2/metal composite coatings deposited by closed field unbalanced magnetron sputter ion plating. *Surface and Coatings Technology. Elsevier, 127*(1), 24–37. https://doi.org/10.1016/S0257-8972(00)00538-7.

Shang, K., et al. (2018). Improving the tribological and corrosive properties of MoS_2-based coatings by dual-doping and multilayer construction. *Applied Surface Science*. https://doi.org/10.1016/j.apsusc.2017.12.167.

Tiwari, A., & Singh Raman, R. K. (2017). Durable corrosion resistance of copper due to multi-layer graphene. *Materials*. https://doi.org/10.3390/ma10101112.

Tong, Y., Bohm, S., & Song, M. (2013). Graphene based materials and their composites as coatings. *Austin Journal of Nanomedicine & Nanotechnology*.

Videla, H. A., & Herrera, L. K. (2009). Understanding microbial inhibition of corrosion. A comprehensive overview. *International Biodeterioration and Biodegradation*. https://doi.org/10.1016/j.ibiod.2009.02.002.

Wang, X., Zhi, L., & Müllen, K. (2008). Transparent, conductive graphene electrodes for dye-sensitized solar cells. *Nano letters*. https://doi.org/10.1021/nl072838r.

Wang, D., et al. (2011). Broadband antireflection of silicon nanorod arrays prepared by plasma enhanced chemical vapor deposition. *Applied Surface Science, 258*(3), 1058–1061. https://doi.org/10.1016/J.APSUSC.2011.08.129.

Wang, D., et al. (2017). Preparation and characterization of the CrN nanocone array textured WS2 film. *Materials Letters, 188,* 267–270. https://doi.org/10.1016/J.MATLET.2016.10.115.

Wang, D., et al. (2019). Cabbage-like WS_2/Ni bilayer thin film for improved tribological property. *Surface and Coatings Technology, 358,* 50–56. https://doi.org/10.1016/J.SURFCOAT.2018.11.026.

Wu, J., et al. (2010). Organic light-emitting diodes on solution-processed graphene transparent electrodes. *ACS Nano*. https://doi.org/10.1021/nn900728d.

Wu, T., et al. (2013). Triggering the continuous growth of graphene toward millimeter-sized grains. *Advanced Functional Materials*. https://doi.org/10.1002/adfm.201201577.

Ye, Y.-P., Chen, J.-M., & Zhou, H.-D. (2009). Influence of nanometer lanthanum fluoride on friction and wear behaviors of bonded molybdenum disulfide solid lubricating films. *Surface and Coatings Technology, 203*(9), 1121–1126. https://doi.org/10.1016/J.SURFCOAT.2008.10.001.

Ye, M., et al. (2016). Microstructure and tribological properties of MoS_2 +Zr composite coatings in high humidity environment. *Applied Surface Science*. https://doi.org/10.1016/j.apsusc.2016.01.163.

Yeh, J. M., et al. (2002). Anticorrosively enhanced PMMA-clay nanocomposite materials with quaternary alkylphosphonium salt as an intercalating agent. *Chemistry of Materials*. https://doi.org/10.1021/cm010337f.

Yim, C., et al. (2014). Investigation of the optical properties of MoS_2 thin films using spectroscopic ellipsometry. *Applied Physics Letters*. https://doi.org/10.1063/1.4868108.

Zhang, S., et al. (2003). Recent advances of superhard nanocomposite coatings: A review. *Surface & Coatings Technology*. https://doi.org/10.1016/S0257-8972(02)00903-9.

Zhang, S., et al. (2015). Direct observation of degenerate two-photon absorption and its saturation in WS_2 and MoS_2 monolayer and few-layer films. *ACS Nano*. https://doi.org/10.1021/acsnano.5b03480.

Zhang, C., et al. (2019). Microstructure and friction behavior of LaF_3 doped Ti-MoS_2 composite thin films deposited by unbalanced magnetron sputtering. *Surface & Coatings Technology*. https://doi.org/10.1016/j.surfcoat.2018.12.041.

Zhao, W., et al. (2013). Evolution of electronic structure in atomically thin sheets of WS_2 and WSe_2. *ACS Nano*. https://doi.org/10.1021/nn305275h.

Zhao, X., et al. (2018). Self-adaptive MoS_2 -Pb-Ti film for vacuum and humid air. *Surface & Coatings Technology*. https://doi.org/10.1016/j.surfcoat.2018.04.022.

Zhu, Y., et al. (2010). Graphene and graphene oxide: Synthesis, properties, and applications. *Advanced Materials*. https://doi.org/10.1002/adma.201001068.

Chapter 6
MXene: A Non-oxide Next-Generation Energy Storage Materials for Batteries and Supercapacitors

Mayank Mishra, Sanjay K. Behura, Majid Beidaghi, Kartikey Verma, and Subhash Singh

1 Introduction

The themes of sustainability, carbon neutrality and energy efficiency have spearheaded the increased focus on developing new and advanced renewable sources of energy production and conversion to lay the foundations for next-generation electrochemical and capacitive energy storage devices, an obvious shift from fossil fuel-based systems.

Batteries, a part and parcel of our daily lives, have infused life into both small and big electronics right from microcomputers to electric vehicles and are the predominant energy storage devices. Lithium-ion batteries (LIBs), common household names now because of their easy usability and portability, provide very high energy and power density. There has been a surge in research activities to further enhance performance, efficiency and life cycle of LIBs and other metal-ion batteries by studying and experimenting newer ways of electrode material design, their charge storage mechanisms and manufacturing techniques which could also help bring down the cost of energy production and storage (Mao et al., 2018). Similarly, extensive adaptation of portable electronic and microelectronic systems has hard pressed the need to develop better supercapacitors and microsupercapacitors. Constrained by size, these

M. Mishra · S. Singh (✉)
Department of Production and Industrial Engineering, National Institute of Technology Jamshedpur, Jamshedpur, Jharkhand 831014, India

S. K. Behura
The University of Arkansas at Pine Bluff, Pine Bluff, AR 71601, USA

M. Beidaghi
Department of Mechanical Engineering, Auburn University, Auburn 36849, USA

K. Verma
Department of Chemical Engineering, Indian Institute of Technology, Kanpur 208016, India

S. Singh et al. (eds.), *Advanced Applications of 2D Nanostructures*,
Materials Horizons: From Nature to Nanomaterials,
https://doi.org/10.1007/978-981-16-3322-5_6

are expected to provide higher energy density, higher temperature tolerance, and quick charge and discharge capability with extended life cycles (Fan et al., 2018).

There is one common thread that connects all these seemingly daunting tasks and is at the heart of battery technology. And that is our ability to design and integrate highly compatible materials with exceptional mix of electronic, electrochemical, mechanical and functional properties as electrode material.

In this regard, two-dimensional (2D) materials have revealed tremendous potential by far. Single layer atom thick, they exhibit quite remarkable mechanical, electrical, electronic and chemical properties owing to which they have been able to make deep headways in the fields of semiconductors, electrodes, photovoltaics, water purification, etc. One prominent material among them is graphene, which also holds the distinction of being the first discovered 2D material in 2004, which has come to singlehandedly dominate electronic industry and garnered major research interest.

The year 2011 saw the world being introduced to a new class of 2D materials in the form of MXenes when the first in the family, a non-oxide, layered Ti_3C_2 ceramic was synthesized from its three-dimensional bulk crystalline Ti_3AlC_2 phase by a chemical process known as exfoliation that included selective etching at room temperature and was soon followed by discovery and synthesis of more than a dozen other MXenes structures, an endeavour driven by worldwide skyrocketing demand of high performance energy storage materials for new generation metal-ion batteries and supercapacitors. What impressed researchers about these materials was their interesting mechanical, thermal and electrochemical properties that manifested metal-like electrical and thermal conductivity, ceramic like strength, stiffness and heat resistance together with higher volumetric capacitance and unique structural characteristics which facilitated both effective charge storage and transport (Naguib et al., 2011) (Ghidiu et al., 2014).

2 MXene: A Novel 2D Material

MXenes are novel entrants in the world of two-dimensional materials and are essentially the layered carbides, carbonitrides and very recently nitrides of early transition metals. These are denoted by $M_{n+1}X_n$ ($n = 1, 2, 3$) where 'M' represents an early transition metal (like Sc, Ti, Zr, V, Nb, Cr, Mo) and 'X' represents a carbon or a nitrogen. The 'ene' in MXene draws inspiration from graphene due to its sheet-like structure. They may have more than one 'M' in them which may be arranged as either solid solutions or ordered phases.

Alternatively, in the representation of functionalized MXenes $M_{n+1}X_nT_x$, the additional denotation 'T' refers to free active group (like –H, –F, = O and –OH) surface terminations which are leftovers from the aqueous etchants (HF, H_2O, HCl) used during selective etching of element 'A' from their parent MAX phase. These terminations add hydrophilic nature to the MXenes and strongly influence their electrochemical and dielectric properties. Also, MXene with certain specific terminations

can be achieved via controlled chemical treatment, intercalation and delamination, thermal annealing and exfoliation methods.

The MAX phases are themselves a group of layered structures given as M_nAX_{n+1} ($n = 1$–3) where '*A*' may be one of Al, P, Si, Ga, S, As, Ge, In, Sn, etc. The MAX phase consists of alternate stacked MX layer and '*A*' layer. Selective etching removes the A element, while keeping the MX arrangement unchanged as A element is bonded relatively weaker and is more reactive as compared to very strong M–X bond (Luo, 2018).

Structure wise, MXenes have hexagonal symmetry, a property derived from parent MAX phase lattice structure. MXenes can be prepared in three different forms. One with single *M* element such as Ti_2C and Mo_2C, other existing as a solid solution of one or more *M* elements arranged randomly such as $(Ti, V)_2C_2$ and $(Cr, V)_3C_2$ and finally as double-ordered *M* elements where either a single *M* element layer or two layers of a single *M* element are arranged in between layers of a second M element such as Mo_2TiC_2 and $Mo_2Ti_2C_3$. All of these MXenes can be thus represented as M_2X, M_3X_2 and M_4X3, derived from their corresponding MAX phases M_2AX, M_3AX_2 and M_4AX_3 (Khazaei et al., 2017). Figure 1 shows the structure of these MAX phases and their related MXenes.

The first MXene, titanium carbide Ti_3C_2Tx, the most widely studied MXene, was synthesized, or rather discovered in 2011. The MAX phase Ti_3AlC_2 powders were

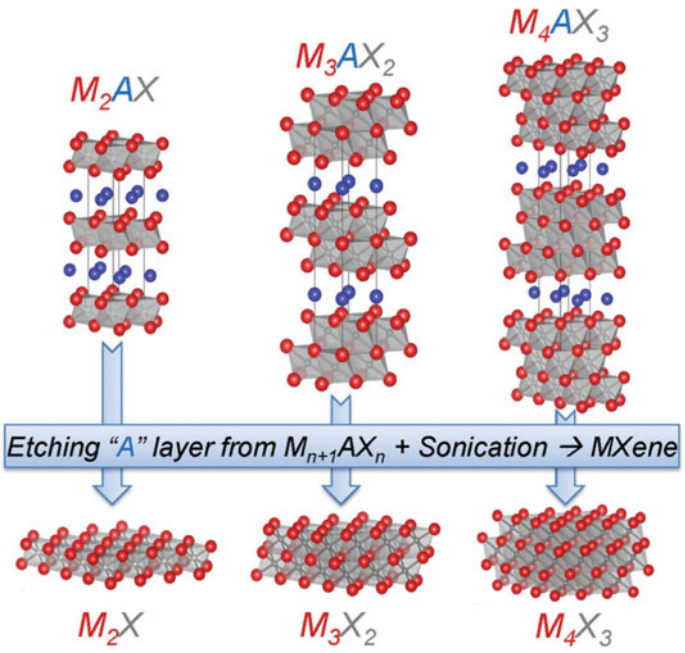

Fig. 1 Structure of different MAX phases and their respective MXenes. 2021 Reproduced with permission from ref. Iqbal et al. (2021). Copyright 2021, Elsevier

mixed with 50 wt. % hydrofluoric acid (HF) solution for 2 h at room temperature.

$$Ti_3AlC_2 + 3HF \rightarrow AlF_3 + 1.5H_2 + Ti_3C_2$$

The following suspension solution was washed with deionized water multiple times, and the powdered precipitate was allowed to settle via centrifuge action.

$$Ti_3C_2 + 2H_2O \rightarrow Ti_3C_2(OH)_2 + H_2$$

$$Ti_3C_2 + 2HF \rightarrow Ti_3C_2F_2 + H_2$$

The above two equations show the formation of MXenes with surface groups, namely OH and F. This process, termed as selective etching process, has been since applied to other precursor MAX phases with the help of other acids as well such as hydrochloric acid (HCl) and lithium fluoride salt (LiF) to synthesize various different MXenes. Upon sonication treatment, MXenes can be delaminated to produce single flake suspensions. Before delamination, MXenes are essentially multilayered structures (Tang et al., 2018). Figure 2 explicitly explains the aforementioned process.

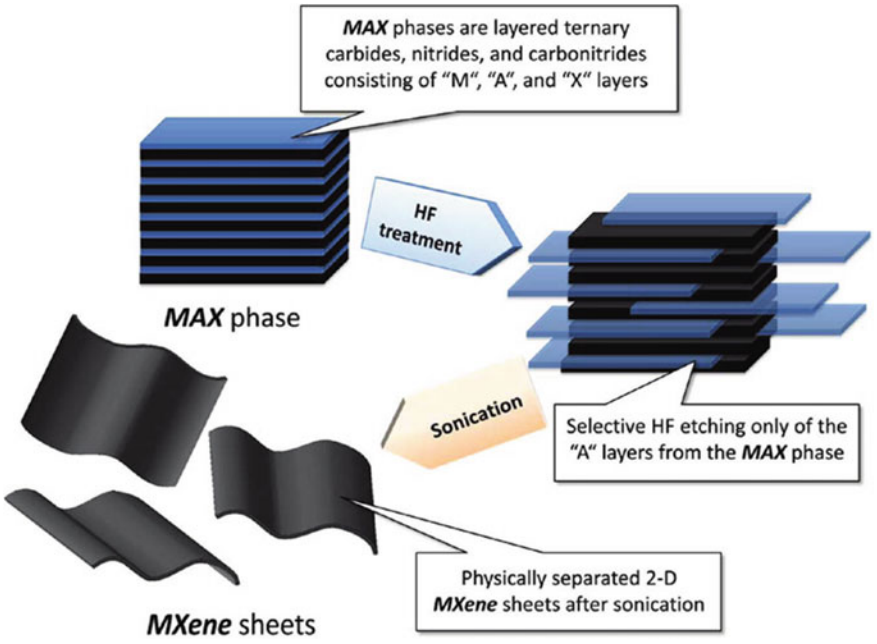

Fig. 2 Schematic for the preparation route of MXenes from the MAX phases. Reproduced with permission from ref. Naguib et al. (2011). Copyright 2012, American Chemical Society

This method was further extended to synthesize other MXenes such as Ti_2C, Ta_4C_3, $(Ti_{0.5}, Nb_{0.5})_2C$, Ti_3CN, $(V_{0.5}, Cr_{0.5})_3C_2$, Ti_2C_3, and Cr_2TiC_2. Alternatively, NH_4HF_2 and mixture of LiF and HCl were also reported to be used as etchants to prepare some MXenes. With time, various endeavours were carried out to produce different MXenes by using different etchants and etching techniques. Needless to say that etching parameters like etching time, etchant concentration, particle size of the MAX phase and temperature during the chemical reactions play crucial parts in the conversion of given MAX phase into MXene. Mo_2C, one of the early transition metal carbides, is the first MXene synthesized from Mo_2Ga_2C phase rather than its MAX phases. Also, Zr_3C_2 MXene was prepared from $Zr_3Al_3C_5$, also not its MAX phase. As of now, over 70 different types of MXenes have been identified and prepared including Ti_3C_2, Ti_2C, V_2C, Cr_3C_2, Fe_2C, Nb_4C_3, Nb_2C, $Mo_{1.33}C$, Mo_2C, Hf_3C_2, V_2C, Cr_2C, Ta_2C, Cr_2N, Ti_4N_3, etc. Many more have been predicted to exist, waiting to be discovered (Zhu et al., 2017).

3 MXene: Properties

MXenes, comparatively the newer entrants into the family of 2D materials, have posed several interesting questions to scientists across disciplines by providing interesting mix of properties. They are both chemically and mechanically stable due to their ceramic nature. Structurally, they are found in both mono-layer and multilayer forms with very large interlayer spacing, even greater than that found in graphite and this thickness of layers can be controlled. This open space between the layers is capable of ion intercalation which means the ions of a range of sizes can be inserted into this space which is very important for the material to be used as cathode in energy conversion applications. Thus, as the layered structure is partially delaminated, not only does it allow ion intercalation but also electric double layer (EDL) formation contributing to charge storage in capacitors. Hydrogen bonding and van der Waals attraction mainly contribute to the interaction between layers of MXenes. The presence of functional groups as terminations provides abundant opportunities for creating desired surface properties and helps control their electrochemical, thermoelectric and dielectric properties. Surface terminations render the otherwise metallic MXenes into semiconductors such as Sc_2CF_2, Sc_2CO_2 and Ti_2CO_2. Moreover, the transition elements (M) in MXenes are very active. Also, a range of transition metals can be used to make the same where each can be tailored for specific applications (Tang et al., 2018; Zhu et al., 2017).

With regards to their mechanical property, it has been estimated by direct functional theory that the in-plane elastic constants of some of these MXenes exceed 500 GPa, which is even more than that of commonly used structural steel which has stiffness value of 400 GPa (Kurtoglu et al., 2012). The electrode material application requires that the MXenes possess very good structural, mechanical, electrochemical, ion movement and electronic transport properties. Their electronic properties are derived from the '*M*' atoms. All the non-functionalized MXenes display metallic

nature, and surface functionalized ones generally display semiconducting nature. Density functional theory (DFT) optimized calculations have shown that Sc-based MXenes such as Sc_2CF_2, $Sc_2C(OH)_2$ and Sc_2CH_2 nanotubes and Mo_2CTx films to have semiconductor-like properties. High conductivity of Ti-based MXenes such as Ti_3C_2Tx was attributed to the Ti vacancy defects. This high conductivity characteristic has put them up for potential application as transparent conductors, electrochemical biosensors, magnetic materials, superconductors, absorbents for heavy metals and flexible electronic devices in addition to their usage in energy storage devices. MXenes have already been experimentally incorporated for potential applications such as rechargeable metal-ion batteries, supercapacitors, field effect transistors, electromagnetic interference shielding, hydrogen storage, sensing, catalysts, composites and biomedical devices among many others. The experimental results have been extremely promising and motivating (Khazaei et al., 2017).

4 MXene for Energy Storage Applications

Aided by modern industrial trends and progressive national policies, as the world transitions from fossil fuel-based energy generation to that derived from renewable sources like wind, sun etc., the need for energy storage devices like electrochemical batteries and supercapacitors is projected to soar higher by the day. They find wide range of applications from portable electronic devices, electric mobility systems to large electric grid systems. Lithium-ion batteries are the most popular form of electrochemical energy storage (EES) systems but they face plethora of challenges as well. These batteries have their own set of safety and cost concerns. They are also marred by very long charging time. It is believed that battery electrode materials have achieved their operational limitations and newer and better devices working on other metal ions like sodium, potassium, magnesium, calcium, etc., are the need of the hour due to their wider and easier availability together with multivalent character. These newer systems also call for improved electrolyte and electrode material development and selection for optimum efficiency (Er et al., 2014).

Of many hurdles facing the growth of LIBs and supercapacitors, two are of extreme significance:

1. It is quite tough to obtain high energy and power density at the same time for these devices.
2. There is an obvious resource crunch with supply chain issues leading to their higher prices (Sun et al., 2018).

Also, the challenge to utilize and store all of the energy produced at larger scales has propelled the scientists to incorporate high performance materials into these devices for optimum efficiency. Working-wise, both rechargeable batteries and supercapacitors have altogether different pros and cons. Batteries produce very high energy densities in expense of poor power densities. Supercapacitors, on other hand, have

superior power densities and fast charge–discharge rate but very low energy densities. Thus, researchers have made immense endeavours to develop electrodes capable of giving a mix of longer life cycle, high energy density and high power density outputs (Xiong et al., 2018). MXenes have been able to help achieve exactly these characteristics. Following are some of the research outputs that establish MXene and MXene-based hybrid structures as the next-generation high-efficient electrode materials for novel batteries and supercapacitors.

4.1 MXenes for Metal-Ion Batteries

Lithium-ion batteries have come to dominate the world of commercial metal-ion-based batteries. They form the backbone of modern-day portable electronic gadgets and are poised for growth in electric vehicles and standalone power storage units. Due to intermittent nature of energy generation of the new renewable energy systems like wind turbines and solar photovoltaics, it becomes increasingly necessary to have a totally reliable storage facility to compensate them in an environmentally sustainable manner devoid of carbon footprints and therein lies the applicability of these rechargeable battery systems.

Of late, they have reached operational ceiling due to lower power density output due to graphite electrodes which is used because of its easy cyclability and low cost. Thus, it was of paramount importance that novel electrode materials be explored for greater electrochemical performance. Also, due to relative scarcity of lithium metal, it is also wise to look for other possible metal based alternatives like battery technologies based on ions of sodium (Na), magnesium (Mg), potassium (K), aluminium (Al) and calcium (Ca). MXenes have come to show their high metal-ion absorption capacity with minimum ion diffusion barrier which arises owing to their high electronic conductivities, greater interlayer spacing and availability of highly active transition metals. $Ti_3C_2T_x$ MXene, the most widely studied MXene in the whole of MXene world, has shown immense promise (Meng et al., 2018a).

Following results discuss the various efforts being put into the development of highly efficient MXene-based rechargeable battery electrodes.

Wang et al. investigated the current collecting capacity of free-standing $Ti_3C_2T_x$ film to replace the conventionally used Al- and Cu-based anode and cathode materials in rechargeable Li-based batteries. For the purpose of the experiment, anode made of multilayer $Ti_3C_2T_x$ and cathode of $LiFePO_4$ was used. The MXene film, in comparison with Cu metal, offered reduction in weight of the battery by about three times. The cyclic voltammograms showed improved Li-ion insertion and extraction in $LiFePO_4$ structure. The high flexibility of the electrode also positioned itself for its applications in flexible electronics (Wang).

Lu et al. studied the effect of reduction in fluorine (−F) surface terminations on the energy storage efficiency of Ti_3C_2 MXene for anode material in lithium-ion batteries. These terminations in large amount significantly brought down Li-ion storage capacity by providing higher diffusion barrier. Thus, hydrogen annealing was

employed to remove excess –F terminations, and the resulting MXene was used as anode in Li-ion battery, it displayed improved volumetric specific capacity of about 123.7 mAh/cm^3 and quite high cycling stability after 100 cycles (Lu et al., 2018).

Du et al. fabricated Ti_2CX_2/graphene hybrid flexible electrode for applications in electrochemically efficient lithium-ion batteries and used first principle method to study its behaviour. It was found that graphene helps avoid restacking of delaminated MXene layers in turn raising its electrical conductivity. The Li-ion mobility was greatly increased which is important for quick ion transport, with high adsorption of Li ions as well. Also, the improved structural stability characterized better structural stiffness (Du et al., 2019).

Zheng et al. employed a microwave irradiation method to uniformly grow carbon nanotubes (CNTs) in situ over Ti_3C_2, Ti_2C and V_2C MXenes to form a hybrid composite structure for potential applications in anode material in Li-ion batteries. The CNT/Ti_3C_2 system showed high reversible capacities of 430 and 175 mAhg^{-1} at current densities of 1 Ag^{-1} and 10 Ag^{-1}, respectively, which is much better than the values for pristine Ti_3C_2. This proved their great potential in energy conversion applications (Zheng et al., 2018).

Kong et al. prepared a nanocomposite mixture of Silicon and Ti_3C_2 MXene with a 1:5 weight ratio via simple ultrasonic mixing to replace traditional Si-based anode in Li-ion batteries. The electrochemical measurements clearly showed the rise in reversible capacity of the composite with 188 mAhg^{-1} at 0.2 Ag^{-1} at the end of 150 cycles as compared to 17 mAhg^{-1} of pure Si. This phenomenon was because of Si-filled interlayer of the Ti_3C_2 MXene (Kong et al., 2018).

Zhao et al. developed an altogether new hybrid composite with MXene/MXene combination of transition metal carbide ($Ti_3C_2T_x$) and transition metal oxides (Co_3O_4 and $NiCo_2O_4$). These were used as anodes in Li ion battery and their electrochemical performance was studied. The $Ti_3C_2Tx/NiCo_2O_4$ electrode fabricated by spray coating showed particularly high rate capacitance of about 1330 mAh/g. Generally speaking, all MXenes composites had improved discharge–charge cycle performance and impressive rate capabilities over standalone parent MXenes (Zhao et al., 2016).

Ali et al. developed two-dimensional nanocomposite heterostructures of iron oxide (Fe_2O_3) and $Ti_3C_2T_x$ MXene for anode material in Li-ion batteries. Composites of varying ratios, i.e. $Ti_3C_2T_x$/25 wt. % Fe_2O_3 and $Ti_3C_2T_x$/50 wt. % Fe_2O_3, were prepared via ball milling, hydrothermal process and wet sonication process; and effect of all these processes was studied. Hydrothermal and wet sonication processes resulted in high oxidation of MXene surface, whereas ball milling produced low surface oxidation and high specific surface area. It was seen that nanocomposite with 50 wt. % Fe_2O_3 prepared via ball milling presented the highest specific energy capacity of about 270 mAhg^{-1} and charge–discharge performance reached 100 mAh/g. Thus, this result showed good promise for their utility in energy storage applications (Ali et al., 2018).

Wang et al. synthesized layered $Li_4Ti_5O_{12}/Ti_3C_2T_x$ MXene composite via in situ method. It provided exemplary Li-ion storage capability and rapid ionic diffusion by reducing the travel path of ions and electrons. Moreover, it manifested high discharge

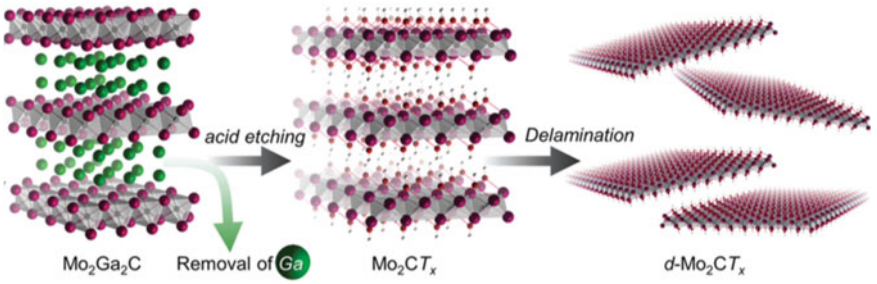

Fig. 3 Schematic of synthesis and delamination process of Mo_2CT_x. Reproduced with permission from ref. Gao, et al. (2020) Copyright 2020, American Chemical Society

capacity with 116 $mAhg^{-1}$ at a rate of 10 Ag^{-1} and high cyclic stability after 500 cycles at 178 $mAhg^{-1}$ (Wang, 2018).

Halim et al. investigated the electrochemical properties of delaminated molybdenum carbide (Mo_2CT_x) MXene prepared from its MAX phase Mo_2Ga_2C by selectively etching out gallium followed by delamination and intercalation with tetrabutylammonium hydroxide (TBAOH) in water, as shown in Fig. 3. The MXene showed semiconductor-like characteristics. It also showed very high capacitance retention upon 10,000 cycles at 10 A/g when tests were carried out on thick Mo_2CT_x film for supercapacitor application. When 8% carbon nanotubes were added into these MXene films to test Li-ion storage capability, over 1000 cycles, it displayed very good cycle performance with reversible capacity of 250 mAh/g (Halim et al., 2016).

Lv et al. have studied the application of delaminated $Ti_3C_2T_x$ MXene in Na-ion batteries. Intercalation and delamination were achieved by ultrasonic treatment in alcohol and dimethyl sulfoxide (DMSO), and a well-developed layered structure was obtained. It was confirmed that delamination led to layer space increase. A relatively higher sodium storage capability was observed in the charge–discharge process while Na-ion insertion into interlayer space concluded the very high rate performance. Cycle performance also confirmed the high stability of the structure of electrodes (Lv et al., 2018).

Meng et al. designed an S-functionalized Ti_3C_2 MXene and investigated the Na-ion storage capacity of Ti_3C_2, $Ti_3C_2O_2$ and $Ti_3C_2S_2$ MXenes to study the changes in storage capabilities with changes in the surface terminations. It was found that $Ti_3C_2S_2$ shows substantially reduced ion diffusion barrier, fast discharge/charge rate and higher Na specific capacity compared to $Ti_3C_2O_2$ mono-layer and thus has an upper hand in terms of electrical conductivity for more efficient electrode material. This was due to large non-positive Na adsorption energies for individual $Ti_3C_2S_2$ layers (Meng, 2018a, 2018b).

Xie et al. developed porous $Ti_3C_2T_x$ MXene electrode via sulphur loading and removal method and analysed its performance for Na-ion storage for practical applications in large-scale Na-ion batteries. It was observed that the ultrathin MXene nanosheets and its open framework due to porous nature facilitated Na-ion storage on its surface. Its volumetric efficiency (216 $mAhcm^{-3}$) was greater than that of

non-porous $Ti_3C_2T_x$ film (64 $mAhcm^{-3}$) at a current density of 100 mAg^{-1}. Thermal annealing helped raise its columbic efficiency to 99% from 96.5% for multilayered $Ti_3C_2T_x$. The rate performance achieved was judged to be the best by far of all previous investigations (Xie et al., 2018).

Tao et al. employed a combination of facile hydrothermal and annealing methods to synthesize $CoNiO_2$ nanoparticles chemically bonded to $Ti_3C_2T_x$ forming a multilayer composite structure. It showed excellent rate capability, electrical conductivity and electrochemical performance which was attributed to the fact that nano size of $CoNiO_2$ helps increase the number of electrochemically active sites and reduces distance for sodium-ion diffusion during discharge–charge cycles (Tao et al., 2018).

Xu et al. synthesized layered composite made of a few nanosheets of MoS_2 on highly conductive $Ti_3C_2T_x$ MXene substrate by one step hydrothermal process for applications in magnesium metal batteries. When used as cathode material, composite showed an increased capacity with 165 mAh/g at 50 mA/g and rate performance was found to be 93 mAh/g at 200 mA/g. It was also evident that Mg-ion charge storage had significantly increased (Xu et al., 2018).

Zhao et al. studied the magnesium-ion storage capacity of porous Ti_3C_2Tx anode films in magnesium-ion storage batteries in Mg-ion-containing electrolyte condition. The cathode performed extremely well in the context of rate performance and cycle consistency. The specific capacitance stood at 210, 140 and 55 $mAhg^{-1}$ at 0.5, 1, and 5 C, making them promising candidates for Mg-ion batteries (Zhao et al., 2019).

Liu et al. demonstrated growth of nickel sulphide (Ni_3S_2) nanofibres on nickel foam by hydrothermal process for the development of binder-less electrode for higher efficiency Na-ion battery. These interconnected nanofibres were able to reduce the diffusion paths of Na ions, thus enhancing the conductivity, specific capacitance, capacity retention and discharge–charge cycle stability. They have proved their suitability to be used as anode material with cathode made of activated carbon due to generation of high energy and power density (Liu et al., 2019).

Mashtalir et al. picked Nb_2CT_x MXene, delaminated it using iso-propylamine and later produced carbon nanotube/MXene composite thin film electrodes and tested it for its lithium storage ability. The CNT/Nb_2CT_x anode exhibited specific capacity of greater than 400 mAh/g at 0.5 C and very high volumetric capacitance of about 325 F/cm^3 (Mashtalir et al., 2015).

Zhu et al. synthesized Ti_3CN nanosheets from the MAX phase Ti_3AlCN for potential application in Na-ion batteries. Its properties were compared with those of Ti_3AlC_2 and Ti_3C_2 nanosheets prepared from the same MAX phase. The electrochemical tests indicated that Na-ion battery based on nanosheets of Ti_3CN had higher specific capacity (507 $mAhg^{-1}$) as compared to that based on Ti_3C_2. Its columbic efficiency reached almost 100% at the end of seven cycles and remained 100% at specific capacity of 139 $mAhg^{-1}$ after 50 cycles while operating at current density of 20 mAg^{-1}. For a test condition of 500 mAg^{-1}, the discharge capacity fared at 98.9 $mAhg^{-1}$ for the electrode made of nanosheets of Ti_3CN, a 1.65 times rise over the value of 59.7 $mAhg^{-1}$ for Ti_3C_2 electrode. This was a clear representation of

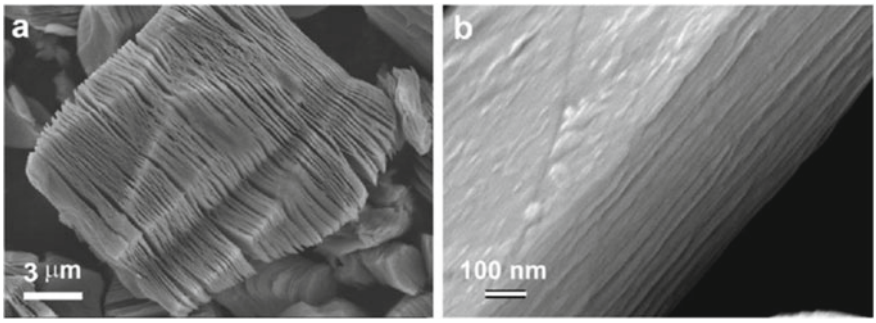

Fig. 4 **a** SEM images of Ti_3CN nanosheets, **b** High magnification SEM images of Ti_3CN nanosheets. Reproduced with permission from ref. Zhu et al. 2018a. Copyright 2018, American Chemical Society

its superior electrochemical efficiency for its use in sodium-ion batteries (Zhu et al., 2018a). Figure 4 shows scanning electron microscopy (SEM) images for Ti_3CN nanosheets at different magnifications.

Meng et al. performed DFT method to quantify the adsorption of Na ions on MXenes of zirconium carbide family, i.e. Zr_2C, Zr_3C_2, Zr_2CO_2, and $Zr_3C_2O_2$. Zr_2C and Zr_3C_2, displayed magnetic nature while Zr_2CO_2 was semiconductor. All of these MXenes displayed metallic behaviour after Na adsorption which is reflective of the rapid electron movement within the electrode in sodium-ion batteries which in turn enhanced the rate capability of the MXene. The combined properties of $Zr_2CO_2/Zr_3C_2O_2$ MXenes like low diffusion barrier, high electrical conductivity, high theoretical values of sodium-ion storage capacity greatly consolidated the confidence that it would make a promising electrode material for Na-ion battery (Meng, 2018).

Du et al. brought about a new method of preparing sulphur cathode in the lithium–sulphur (Li–S) batteries wherein hollow nanospheres of TiO_2 with sulphur additions were embedded into the interlayers of Ti_2C MXene to form a composite cathode. It effectively improved the cathode's cycle performance. With initial discharge specific capacity of 1408.6 $mAhg^{-1}$ at 78.4 wt. % sulphur, after 200 cycles, it was maintained at an impressive 464.0 $mAhg^{-1}$. This was mainly attributed to high conductivity and enhanced volumetric expansion of Ti_2C (Du et al., 2019).

Demiroglu et al. investigated the electrochemical behaviour of hybrid heterostructures of $Sc_2C(OH)_2$/graphene, Ti_2CO_2/graphene and V_2CO_2/graphene and studied the diffusion and adsorption of alkaline sodium, potassium and calcium atoms. The latter two systems showed better metal-ion intercalation and thermal stability. The energy barriers were reduced by half and rate capacities increased as compared to those of only MXene-based structures. These heterostructures systems were thus found suitable for certain low and high voltage applications (Demiroglu et al., 2019).

Yang et al. prepared a flexible composite cathode material made of carbon nanofibres with MoS_2 MXene via electrospinning followed by annealing method for

applications in rechargeable aluminium metal-ion batteries. The composite electrode displayed very good aluminium storage capabilities together with excellent discharge–charge capacity with 293 $mAhg^{-1}$ at current density of 100 mAg^{-1} which was retained up to 126.6 $mAhg^{-1}$ at the end of 200 cycles (Yang et al., 2019). Table 1 summarizes the electrochemical performance of various MXene-based systems for applications in metal-ion batteries.

4.2 MXenes for Supercapacitors

Supercapacitors are capacitors with quite high capacitance lying between those of rechargeable batteries and electrolytic batteries. They have faster charge delivery rate and longer charge–discharge cycle than a typical rechargeable battery. They are famed for their temperature tolerance and the ability to be integrally assembled in tandem with solar cells and batteries.

Broadly speaking, there can be two kinds of supercapacitors, both with different processes of charge storage and transfer. Some supercapacitors do not undergo phase change during operation and instead employ redox reactions, intercalations and electrosorption which are quite fast thus providing greater energy densities. These are called pseudocapacitors and are quite different from electrical double layer capacitors (EDLCs), which primarily operate by forming electrical double layer at the interface of the electrode and electrolyte solution. The more the specific surface area of this interface, the more is its capacitance. EDLCs mainly employ electrodes made from carbon or its derivatives like activated carbon and graphite. Regarding pseudocapacitors, traditional materials like MnO_2, MoO_3, Nb_2O_5, RuO_2, etc., do provide high capacitance, but they lack behind owing to their low electrical conductivity. On this front, MXenes have shown tremendous improvement. Their unique structure and electronic properties make them highly suitable for supercapacitor applications. The interlayer provides large space for unhindered and fast electron movement, and in-depth researches have shown that these materials both on their own and with combination of other heteroatoms have achieved very high volumetric capacitance, structural stability, flexibility and rate performance due to lower ion diffusion barrier and ultrahigh ion storage and delivery (Lukatskaya et al., 2017). Some of these results have been discussed ahead.

Zhang et al. used alkalinizing and annealing to strike out excess surface group terminations from the self-assembled layers of $Ti_3C_2T_x$ MXene film to form the supercapacitor electrode. Upon electrochemical tests, it was evident that the electrode film showed very high volumetric capacitance having value of 1805 Fcm^{-3} at current density of 1 Ag^{-1} and capacitance containment of 98% after 8000 cycles. This was contributed mainly by improvement in number of active sites in the MXene (Zhang et al., 2018).

Li et al. prepared $Ti_3C_2T_x$ MXene film electrode decorated with silver (Ag) nanoparticles aqueous dispersion method. The hybrid material displayed high areal capacitance of 332.2 mF cm^{-2}, good rate performance and cycle stability with 87% after 10,000 cycles (Li et al., 2018).

Table 1 Preparation method, rate performance, specific capacity and retention percentage of various MXene-based electrodes for potential applications in rechargeable batteries

S. no	Author	Materials	Preparation method	Parameters					
				Rate performance		Discharge/charge capability			Retention (%)/cycles
				Discharge capacity ($mAhg^{-1}$)	Current density (Ag^{-1})	Specific capacity ($mAhg^{-1}$)	Current density (Ag^{-1})	Cycles	
1	Lv et al.	$Ti_3C_2T_x$	HF etching, ultrasonication in DMHO	140 70	0.02 1	–	–	–	85.8% / 500 cycles
2	Yang et al.	MoS_2/carbon nanofibres	Electrospinning and annealing	293.2 111.9	0.10 0.25	–	–	–	95% / 200 cycles
3	Liu et al.	Ni_3S_2 nanofibers	Hydrothermal method	584.2 355	0.2 1	–	–	–	91.9% / 100 cycles
4	Lu et al.	Ti_3C_2 films	HF etching, sonication, filtration	–	–	123.7 mAh/cm^3	100 mA/cm^3	100	75% /100 cycles
5	Ali et al.	$Ti_3C_2T_x$/25 wt. % Fe_2O_3	LiF and HCl etching, composite by ball milling	100	2	595 372 348	0.3	1 10 50	–
6	Tao et al.	$CoNiO_2/Ti_3C_2T_x$	HF etching, ultrasonication, hydrothermal reaction	413.4 317.6 248.1 211 188.4	20 50 100 200 300	287 239 222	0.1	2 50 140	–

(continued)

Table 1 (continued)

S. no	Author	Materials	Preparation method	Parameters					
				Rate performance		Discharge/charge capability			Retention (%)/cycles
				Discharge capacity ($mAhg^{-1}$)	Current density (Ag^{-1})	Specific capacity ($mAhg^{-1}$)	Current density (Ag^{-1})	Cycles	
7	Er et al.	Ti_3C_2	HF etching	–	–	447.8 (Li) 351.8 (Na) 191.8 (K) 319.8 (Ca)	–	–	–
8	Xie et al.	Porous $Ti_3C_2T_x$	Sulphur loading and removal method	180 166 124 24	0.1 1 10 100	–	–	–	–
9	Zhao et al.	$Ti_3C_2T_x/NiCo_2O_4$ film	Spray coating	1330 650 350	0.03 1.5 3	–	–	–	–
10	Zhu et al.	Ti_3CN	HF etching	–	–	507 217 133	0.02	1 2 100	–

(continued)

Table 1 (continued)

S. no	Author	Materials	Preparation method	Parameters					
				Rate performance		Discharge/charge capability			Retention (%)/cycles
				Discharge capacity ($mAhg^{-1}$)	Current density (Ag^{-1})	Specific capacity ($mAhg^{-1}$)	Current density (Ag^{-1})	Cycles	
11	Zheng et al.	$CNTs/Ti_3C_2$	HF etching and microwave irradiation	430 175	1 10	–	–	–	–
12	Zhao et al.	Porous $Ti_3C_2T_x$ films	LiF + HCl etching, annealing and magnesium-ion intercalation	210 140 70 55	0.05 0.1 0.3 0.5	–	–	1 2 8 15	–
13	Halim et al.	CNT/Mo_2CT_x	Vacuum–assisted filtration method	250 76	5 10	–	–	–	–
14	Du et al.	$S@TiO_2/Ti_2C$	HF etching of MXene, hydrolysis and calcination for TiO_2 synthesis	879.2 722.0 625.8 576.6 317.7	0.34 0.84 1.67 3.35 8.37	1408.6 741.5 501.1 464	0.34	1 50 100 200	–

(continued)

Table 1 (continued)

S. no	Author	Materials	Preparation method	Parameters					
				Rate performance		Discharge/charge capability			Retention (%)/cycles
				Discharge capacity ($mAhg^{-1}$)	Current density (Ag^{-1})	Specific capacity ($mAhg^{-1}$)	Current density (Ag^{-1})	Cycles	
15	Mashtalir et al.	CNT/Nb_2CT_x	HF etching, amine-assisted delamination	600 270 160	0.1 1 2	–	–	–	–
16	Kong et al.	$Si@Ti_3C_2$	MXene by wet chemical method, composite by mixing, filtration and vacuum drying	–	–	188	0.2	150	–
17	Xu et al.	$MoS_2/Ti_3C_2T_x$	MXene by LiF + HCl etching, composite by hydrothermal process	140 93 53	0.1 0.2 0.5	165 108	0.05	1 50	–

(continued)

Table 1 (continued)

S. no	Author	Materials	Preparation method	Parameters					
				Rate performance		Discharge/charge capability			Retention (%)/cycles
				Discharge capacity ($mAhg^{-1}$)	Current density (Ag^{-1})	Specific capacity ($mAhg^{-1}$)	Current density (Ag^{-1})	Cycles	
18	Wang et al.	$Li_4Ti_5O_{12}/Ti_3C_2T_x$	MXene by HF etching, composite by combination of mixing, stirring, drying and calcination	331 230 175 132 116	0.1 0.5 3 7 10	178	5	500	–

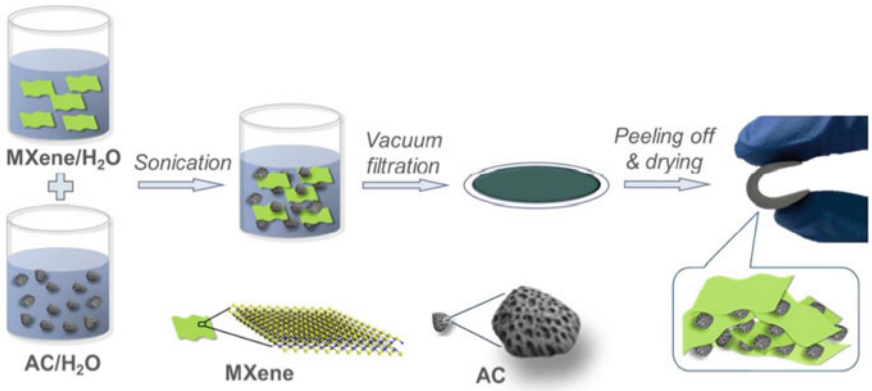

Fig. 5 Schematic representation of fabrication process of MXene-bonded activated carbon films involving sonication of MXene-AC water solution, vacuum filtration, peeling off and drying. Reproduced with permission from ref. Yu et al. Copyright 2018, American Chemical Society

Yu et al. devised a unique fabrication process, as shown in Fig. 5, which involved encapsulating activated carbon in between $Ti_3C_2T_x$ MXene layers via sonication and vacuum filtration followed by peeling off and drying the filtered layers. The MXene layers not only act as flexible backbone but also as binders. The resulting electrode displays very high capacitance of 126 F/g with improved rate performance of 57.9% at 100 A/g. These properties are ideal for its application in flexible supercapacitors (Yu, 2018).

Hu et al. prepared binder-free thick film electrode with pseudocapacitive delaminated $Ti_3C_2T_x$ MXene which were then laser cut to fabricate on-chip microsupercapacitors (MSC) which exhibited areal capacitance of about 71.16 $mFcm^{-2}$ which was a staggering seven times more than the currently used carbon-based on-chip MSCs which measure around 0.1–10 $mFcm^{-2}$ and even greater than previously studied on-chip MSCs pertaining to similar MXene (4.2–61.0 $mFcm^{-2}$), thus making its case formidable for microelectronics applications (Hu et al., 2018).

Chang et al. tried to overcome the stiffness of nano-scale MXene sheets for their application in stretchable and bendable supercapacitors by coming up with alternative electrode design in which certain $Ti_3C_2T_x$ MXene nanocoatings with programmable crumpling and folding were developed. These were then loaded and unloaded at elevated temperatures to embed memory-based deformation characteristics. When these were employed as supercapacitor electrodes, they demonstrated high mechanical stability, high volumetric capacitance and a 27 times increase in areal capacitance when compared to flat MXene electrode. This was in addition to increase in stretchability of 80% in 1D and 225% in 2D (Chang et al., 2018).

Yu et al. assembled lithium-ion capacitor (LIC) with carbon nanotubes (CNTs) filled $Ti_3C_2T_x$ MXene film as anode and activated carbon-made cathode. This composite film displayed excellent reversible capacity (489 $mAhg^{-1}$), cycle stability and performance. The capacity retention of the electrode stood at 83% after 5000 cycles together with high energy density of 67 $Whkg^{-1}$, proving its effectiveness as anode in LICs (Yu et al., 2018a, 2018b).

Zou et al. prepared a composite material for cathodes in supercapacitors by electrostatically assembling α-Fe_2O_3 and $Ti_3C_2T_x$ MXene at room temperature. The resulting composite displayed a range of working potential of 1.2 V with a high specific capacitance of 405.4 and 197.6 Fg^{-1} at current densities of 2 and 20 Ag^{-1}, respectively. Even more significant was its capacitance retention capacity of 97.7% at the end of 2000 cycles which definitely shows immense promise for supercapacitor cathode material (Zou et al., 2018).

Zhu et al. synthesized symmetric $Ti_2CT_x - Ti_2CT_x$ supercapacitor which presented considerable cyclic performance with great power and energy densities. Also, 100% capacitance was retained after 3000 cycles at 20 A/g current density (Zhu et al., 2018b).

Yang et al. reported excellent results from composite electrode made by electrophoretic deposition of carbon nanotubes (CNTs) filled Ti_3C_2 MXene film over graphite paper. The specific capacitance of the electrode was improved by over 1.5 times and 2.6 times with respect to those of pure Ti_3C_2 MXene and CNTs. After 10,000 cycles, the electrode film retained an impressive 100% capacitance. Thus, it helped prove the effectiveness of electrophoretic deposition method of cathode preparation for supercapacitors (Yang et al., 2018).

Yue et al. developed a three-dimensional aerogel structure by ice-template method for microsupercapacitor having $Ti_3C_2T_x$ and reduced graphene oxide as its components. The electrode was covered on its outside with polyurethane which provided excellent self-healing property to the material which was evident from the fact that the device possessed very high capacitance retention of about 81.7% at the end of fifth healing. At the end of 15,000 cycles, 91% charge retention was observed with very high specific capacitance of 34.6 $mFcm^{-2}$ (Yue et al., 2018).

Wen et al. prepared novel $Ti_3C_2T_x$ MXene-based electrodes which were doped with heteroatoms of nitrogen. The electrode showed significantly high capacitances of 192 F/g and 82 F/g in the electrolytic solutions of 1 M H_2SO_4 and 1 M $MgSO_4$, respectively, which were much higher in comparison with undoped MXene which stood at 34 F/g and 52 F/g, respectively (Wen et al., 2017).

Peng et al. investigated the electrochemical performance of an MXene-based solid-state microsupercapacitors where larger and smaller flakes of Mxene $Ti_3C_2T_x$ were made to act as current collector and active material, respectively. The device so fabricated manifested very high areal capacitance peaking at 27.3 $mFcm^{-2}$ and capacitance of 356.8 Fcm^{-2} with retention of capacitance after 10,000 cycles of 100% (Peng et al., 2016).

Jiang et al. fabricated MnO_2 and $Ti_3C_2T_x$ MXene-based hybrid composite electrode which showed tremendous increase in conductivity, specific capacitance, cycle and structural stability. The transfer of electron and diffusion of ions were facilitated by the chemical reaction occurring between the nanoneedles of MnO_2 and layers of $Ti_3C_2T_x$. The energy density peaked very high coupled with amazing 100% retention of capacitance upon 1000 cycles at 0.2 $mAcm^{-2}$ (Jiang et al., 2018).

Shan et al. investigated the electrochemical characteristics of vanadium carbide (V_2C) for supercapacitor application in aqueous condition. The MXene was prepared by HF etching and delaminated using tetramethylammonium hydroxide (TMAOH)

base. Measurements were taken in different electrolyte solutions, namely H_2SO_4, $MgSO_4$ and KOH to garner data on the dependence of its performance on electrolyte medium. The maximum specific capacitance obtained were 487, 184 and 225 F/g in 1 M H_2SO_4, 1 M KOH, and 1 M $MgSO_4$, respectively. That these values were much greater than what had been previously reported gave strong boost to their candidature for supercapacitor electrode application (Shan et al., 2018).

Dall'Agnese et al. sought manufacturing of a Li-ion capacitor based on vanadium carbide (V_2C) Mxene which produced capacitance of about 100 F/g at 0.2 mVs^{-1}. When assembled as a cell with carbon-based cathode and MXene anode, a cell voltage of 3.5 V was obtained (Dall'Agnese et al., 2015). Table 2 summarizes the electrochemical performance of various MXene-based systems for applications in supercapacitors.

5 Conclusion

There is a new buzz in the scientific community about a novel two-dimensional material called Mxene, which after graphene, has attracted many a minds due to its unique mechanical, electrical and primarily electrochemical properties, thus predicting its widespread utility in next-generation highly efficient electrochemical devices for energy storage and delivery which are the need of the hour due to our increasing dependence on small-scale portable electronic devices, medium-scale utility in electric vehicles and large-scale standalone or grid-connected power storage units. Mxene and Mxene-based hybrid structures are being tested for potential electrode materials in both rechargeable battery systems and supercapacitors under variety of aqueous electrolytic solutions on parameters such as power density, energy density, life cycle, charge–discharge cycles, structural stability, volumetric capacitance, areal capacitance, flexibility and deformability, rate performance, ion diffusion barrier, electron mobility, electrical and thermal conductivities. New and improved techniques of etching and post-etching treatments like sonication, annealing, etc., have been developed for optimum intercalation and exfoliation, desired interlayer spacing, removal of excess surface terminations, designed inclusion of dopants and thin and flexible Mxene-based composite films.

As the saying goes, the best way to prepare for the future is to envision and create it. The era of sustainable and carbon neutral energy generation and storage is upon us already, and it requires development of new age materials with unprecedented performance, efficiency and versatility. It demands focussed and coordinated research efforts and planned product development, so that the technology reaches wide spread application at affordable costs to public and at no cost to the nature. And that future is ours to make and is up for grabs!

Table 2 Preparation method, gravimetric/volumetric capacitance, specific capacitance and retention percentage of various MXene-based electrodes for potential applications in supercapacitors

S. no.	Author	Materials	Method	Parameters					
				Gravimetric/volumetric capacitance (Fg^{-1}/Fcm^{-3})	Current density (Ag^{-1})/scan rate (mVs^{-1})	Specific capacitance ($mFcm^{-2}$)	Scan rate (mVs^{-1})	Retention (%)	Cycles
1	Yue et al.	$Ti_3C_2T_x$/graphene aerogel	Freeze drying, reduction and laser cutting	196 120	2 mVs^{-1} 100 mVs^{-1}	34.6	1	91	15,000
2	Dall'Agnese et al.	V_2CT_x	HF etching	–	–	100 F/g	0.2	70	300
3	Halim et al.	Mo_2CT_x	HF etching, TBAOH intercalation	700 F cm^{-3}	2 mVs^{-1}	–	–	100	10,000
4	Lukatskaya et al.	porous $Ti_3C_2T_x$ film	LiF + HCl etching, vacuum filtration	310 210 100	10 mVs^{-1} 10,000 mVs^{-1} 40,000 mVs^{-1}	–	–	–	–
5	Li et al.	Ag/$Ti_3C_2T_x$	Colloidal dispersion, ultrasonication, vacuum filtration	246.2 mF cm^{-2}	2 mVs^{-1}	332.2 209.3	2 100	87	10,000
6	Yu et al.	Activated carbon/$Ti_3C_2T_x$	Minimally intensive layer delamination (MILD) method	126 F g^{-1}	10 mVs^{-1}	138 73	10 4000	92.4	100,000

(continued)

Table 2 (continued)

S. no.	Author	Materials	Method	Parameters					
				Gravimetric/volumetric capacitance (Fg^{-1}/Fcm^{-3})	Current density (Ag^{-1})/scan rate (mVs^{-1})	Specific capacitance ($mFcm^{-2}$)	Scan rate (mVs^{-1})	Retention (%)	Cycles
7	Yu et al.	CNT/$Ti_3C_2T_x$ film	HF etching, delamination by TBAOH, composite by colloidal sonication and filtration	192.6 132.6 54.6	0.1 Ag^{-1} 0.5 Ag^{-1} 2 Ag^{-1}	–	–	81.3	5000
8	Zou et al.	Fe_2O_3/ $Ti_3C_2T_x$	LiF + HCl etching	405.4 197.6	2 Ag^{-1} 20 Ag^{-1}	–	–	97.7	2000
9	Zhang et al.	$Ti_3C_2T_x$	LiF + HCl etching	1805 F cm^{-3}	1 Ag^{-1}	–	–	98	8000
10	Zhu et al.	Ti_2CT_x	HF etching	245 F cm^{-3}	20 Ag^{-1}	517 307	2 100	100	3000
11	Shan et al.	V_2C	HF etching, delamination by TMAOH	487 170	2 mVs^{-1} 100 mVs^{-1}	–	–	83	10,000

(continued)

Table 2 (continued)

S. no.	Author	Materials	Method	Parameters					
				Gravimetric/volumetric capacitance (Fg^{-1}/Fcm^{-3})	Current density (Ag^{-1})/scan rate (mVs^{-1})	Specific capacitance ($mFcm^{-2}$)	Scan rate (mVs^{-1})	Retention (%)	Cycles
12	Yang et al.	CNTs/ Ti_3C_2	LiF + HCl etching, electrophoretic deposition	134	1 Ag^{-1}	–	–	100	10,000
13	Jiang et al.	$MnO_2/Ti_3C_2T_x$	LiF + HCl etching, composite by mild chemical deposition method	130.5	0.2 Ag^{-1}	–	–	90	1000
14	Wen et al.	$N/Ti_3C_2T_x$	HF etching, annealing	128	200 mVs^{-1}	–	–	–	–

Acknowledgements This book chapter was financially supported by Empowerment and Equity Opportunities for Excellence in Science (EEQ/2018/000873), Science & Engineering Research Board (SERB), Department of Science and Technology, Government of India and Ministry of Human Resource and Development (MHRD), Government of India.

References

Ali, A., Hantanasirisakul, K., Abdala, A., Urbankowski, P., Zhao, M.-Q., Anasori, B., Gogotsy, Y., Aissa, B., & Mahmoud, K. A. (2018). Effect of synthesis on performance of MXene/Iron oxide anode material for Lithium-Ion batteries. *Langmuir*.

Chang, T.-H., Zhang, T., Yang, H., Li, K., Tian, Y., Lee, J. Y., & Chen, P.-Y. (2018). Controlled crumpling of two-dimensional titanium carbide (MXene) for highly stretchable, bendable, efficient supercapacitors. *ACS Nano.*

Dall'Agnese, Y., Taberna, P.-L., Gogotsi, Y., & Simon, P. (2015). Two-dimensional vanadium carbide (MXene) as positive electrode for sodium-ion capacitors. *The Journal of Physical Chemistry Letters, 6*(12), 2305–2309.

Demiroglu, I., Peeters, F. M., Gulseren, O., Cakir, D., & Sevik, C. (2019). Alkali metal intercalation in MXene/graphene heterostructures, a new platform for ion battery applications. *The Journal of Physical Chemistry Letters.*

Du, C., Wu, J., Yang, P., Li, S., Xu, J., & Song, K. (2019). Embedding S@TiO_2 nanospheres into MXene layers as high rate cyclability cathodes for lithium-sulphur batteries. *Electrochimica Acta, 295*, 1067–1074.

Er, D., Li, J., Naguib, M., Gogotsi, Y., & Shenoy, V. B. (2014). Ti_3C_2 MXene as a high capacity electrode material for metal (Li, Na, K, Ca) ion batteries. *ACS Applied Materials & Interfaces, 6*(14), 11173–11179.

Fan, Z., Wang, Y., Xie, Z., Xu, X., Yuan, Y., Cheng, Z., & Liu, Y. (2018). A nanoporous MXene film enables flexible supercapacitors with high energy storage. *Nanoscale, 10*(20), 9642–9652.

Gao, L., Li, C., Huang, W., Mei, S., Lin, H., Ou, Q., Zhang, Y., Guo, J., Zhang, F., Xu, S., & Zhang, H. (2020). MXene/polymer membranes: Synthesis, properties, and emerging applications. *Chemistry of Materials 32*(5), 1703–1747.

Ghidiu, M., Lukatskaya, M. R., Zhao, M.-Q., Gogotsi, Y., & Barsoum, M. W. (2014). Conductive two-dimensional titanium carbide 'clay' with high volumetric capacitance. *Nature, 516*, 78–81.

Halim, J., Kota, S., Lukatskaya, M. R., Naguib, M., Zhao, M.-Q., Moon, E. J., Pitock, J., Nanda, J., May, S. J., Gogotsi, Y., & Barsoum, M. W. (2016). Synthesis and characterization of 2D molybdenum carbide (MXene). *Advanced Functional Materials, 26*(18), 3118–3127.

Hu, H., Bai, Z., Niu, B., Wu, M., & Hua, T. (2018). Binder-free bonding of modularized MXene thin films into thick film electrodes for on-chip micro-supercapacitors with enhanced areal performance metrics. *Journal of Materials Chemistry A, 6*(30), 14876–14884.

Iqbal, A., Kwon, J., Kim, M. K., & Koo, C. M. (2021). MXenes for electromagnetic interference shielding: Experimental and theoretical perspectives. *Materials Today Advances, 9*, 100–124.

Jiang, H., Wang, Z., Yang, Q., Hanif, M., Wang, Z., Dong, L., & Dong, M. (2018). A novel $MnO_2/Ti_3C_2T_x$ MXene nanocomposite as high performance electrode materials for flexible supercapacitors. *Electrochimica Acta.*

Khazaei, M., Ranjbar, A., Arai, M., Sasaki, T., & Yunoki, S. (2017). Electronic properties and applications of MXenes: A theoretical review. *Journal of Material Chemistry C, 5*, 2488–2503.

Kong, F., He, X., Liu, Q., Qi, X., Sun, D., Zheng, Y., Wang, R., & Bai, Y. (2018). Enhanced reversible Li-ion storage in Si@Ti_3C_2 MXene nanocomposite. *Electrochemistry Communications, 97*, 16–21.

Kurtoglu, M., Naguib, M., Gogotsi, Y., & Barsoum, M. W. (2012). First principles study of two-dimensional early transition metal carbides. *MRS Communications, 2*(04), 133–137.

Li, L., Zhang, N., Zhang, M., Wu, L., Zhang, X., & Zhang, Z. (2018). Ag-Nanoparticle-decorated 2D titanium carbide (MXene) with superior electrochemical performance for supercapacitors. *ACS Sustainable Chemistry & Engineering, 6*(6), 7442–7450.

Liu, M. C., Li, J., Yang, Q.-Q., Xu, Y., Kong, L.-B., Bai, R.-J., Liu, W., Niu, W., & Chueh, Y.-L. (2019). Hierarchically Interconnected Ni_3S_2 nanofibers as binder-free electrodes for high-performance sodium-ion energy storage devices. *ACS Applied Nano Materials.*

Lu, M., Li, H., Han, W., Chen, J., Shi, W., Wang, J., Meng, X.-M., Qi, J., Li, H., Zhang, W., & Zheng, W. (2018). 2D titanium carbide (MXene) electrodes with lower-F surface for high performance lithium-ion batteries. *Journal of Energy Chemistry.*

Lukatskaya, M. R., Kota, S., Lin, Z., Zhao, M.-Q., Shpigel, N., Levi, M. D., Halim, J., Taberna, P.-L., Barsoum, M. W., Simon, P., & Gogotsi, Y. (2017). Ultra-high-rate pseudocapacitive energy storage in two-dimensional transition metal carbides. *Nature Energy, 2*(8), 17105.

Luo, K., Zha, X.-H., Zhou, Y., Guo, Z., Lin, C.-T., Huang, Q., Zhou, S., Zhang, R., & Du, S. (2018). First-principles study on the electrical and thermal properties of the semiconducting $Sc_3(CN)F_2$ MXene. *RSC Advances, 8*(40), 22452–22459.

Lv, G., Wang, J., Shi, Z., & Fan, L. (2018). Intercalation and delamination of two-dimensional MXene ($Ti_3C_2T_x$) and application in sodium-ion batteries. *Materials Letters, 219*, 45–50.

Mao, J., Zhou, T., Zheng, Y., Gao, H., Liu, H., & Guo, Z. (2018). Two-dimensional nanostructures for sodium-ion battery anodes. *Journal of Materials Chemistry A, 6*(8), 3284–3303.

Mashtalir, O., Lukatskaya, M. R., Zhao, M.-Q., Barsoum, M. W., & Gogotsi, Y. (2015). Amine-assisted delamination of Nb_2C MXene for Li-Ion energy storage devices. *Advanced Materials, 27*(23), 3501–3506.

Meng, Q., Ma, J., Zhang, Y., Li, Z., Hu, A., Kai, J.-J., & Fan, J. (2018a). Theoretical investigation of zirconium carbide MXenes as prospective high capacity anode materials for Na-ion batteries. *Journal of Materials Chemistry A, 6*(28), 13652–13660.

Meng, Q., Ma, J., Zhang, Y., Li, Z., Zhi, C., Hu, A., & Fan, J. (2018b). The S-functionalized Ti_3C_2 Mxene as a high capacity electrode material for Na-ion batteries: a DFT study. *Nanoscale, 10*(7), 3385–3392.

Naguib, M., Kurtoglu, M., Presser, V., Lu, J., Niu, J., Heon, M., Hultman, L., Gogotsi, Y., & Barsoum, M. W. (2011). Two-dimensional nanocrystals produced by exfoliation of Ti_3AlC_2. *Advanced Materials, 23*(37), 4248–4253.

Naguib, M., Mochalin, V. N., Barsoum, M. W., & Gogotsi, Y. (2013). 25th Anniversary article: MXenes: a new family of two-dimensional materials. *Advanced Materials, 26*(7), 992–1005.

Peng, Y.-Y., Akuzum, B., Kurra, N., Zhao, M.-Q., Alhabeb, M., Anasori, B., Kumbur, E. C., Alshareef, H. N., Ger, M.-D., & Gogotsi, Y. (2016). All-MXene (2D titanium carbide) solid-state microsupercapacitors for on-chip energy storage. *Energy & Environmental Science, 9*(9), 2847–2854.

Shan, Q., Mu, X., Alhabeb, M., Shuck, C. E., Pang, D., Zhao, X., Chu, X.-F., Wei, Y., Du, F., Chen, G., Gogotsi, Y., Gao, Y., & Dall'Agnese, Y. (2018). Two-dimensional vanadium carbide (V_2C) MXene as electrode for supercapacitors with aqueous electrolytes. *Electrochemistry Communications.*

Sun, S., Liao, C., Hafez, A. M., Zhu, H., & Wu, S. (2018). Two-dimensional MXenes for energy storage. *Chemical Engineering Journal, 338*, 27–45.

Tang, H., Hu, Q., Zheng, M., Chi, Y., Qin, X., Pang, H., & Xu, Q. (2018). Mxene–2D layered electrode materials for energy storage. *Progress in Natural Science: Materials International, 28*(2), 133–147.

Tao, M., Zhang, Y., Zhan, R., Guo, B., Xu, Q., & Xu, M. (2018). A chemically bonded $CoNiO_2$ nanoparticles/MXene composite as anode for sodium-ion batteries. *Materials Letters, 230*, 173–176.

Wang, C.-H., Kurra, N., Alhabeb, M., Chang, J.-K., Alshareef, H. N., & Gogotsi, Y. (2018a). Titanium carbide (MXene) as a current collector for Lithium-Ion batteries. *ACS Omega, 3*(10), 12489–12494.

Wang, J., Dong, S., Li, H., Chen, Z., Jiang, S., Wu, L., & Zhang, X. (2018b). Facile synthesis of layered $Li_4Ti_5O_{12}$-$Ti_3C_2T_x$ (MXene) composite for high-performance lithium ion battery. *Journal of Electroanalytical Chemistry, 810*, 27–33.

Wen, Y., Rufford, T. E., Chen, X., Li, N., Lyu, M., Dai, L., & Wang, L. (2017). Nitrogen-doped $Ti_3C_2T_x$ MXene electrodes for high-performance supercapacitors. *Nano Energy, 38*, 368–376.

Xie, X., Kretschmer, K., Anasori, B., Sun, B., Wang, G., & Gogotsi, Y. (2018). Porous $Ti_3C_2T_x$ MXene for ultrahigh-rate sodium-ion storage with long cycle life. *ACS Applied Nano Materials, 1*(2), 505–511.

Xiong, D., Li, X., Bai, Z., & Lu, S. (2018). Recent advances in layered $Ti_3C_2T_x$ MXene for electrochemical energy storage. *Small (weinheim an Der Bergstrasse, Germany), 14*(17), 1703419.

Xu, M., Bai, N., Li, H.-X., Hu, C., Qi, J., & Yan, X.-B. (2018). Synthesis of MXene-supported layered MoS_2 with enhanced electrochemical performance for Mg batteries. *Chinese Chemical Letters, 29*(8), 1313–1316.

Yang, L., Zheng, W., Zhang, P., Chen, J., Tian, W. B., Zhang, Y. M., & Sun, Z. M. (2018). MXene/CNTs films prepared by electrophoretic deposition for supercapacitor electrodes. *Journal of Electroanalytical Chemistry.*

Yang, W., Lu, H., Cao, Y., Xu, B., Deng, Y., & Cai, W. (2019). A Flexible Free-standing MoS_2/Carbon Nanofibers Composite Cathode for Rechargeable Aluminum-Ion Batteries. *ACS Sustainable Chemistry & Engineering.*

Yue, Y., Liu, N., Ma, Y., Wang, S., Liu, W., Luo, C., Zhang, H., Cheng, F., Rao, J., Hu, X., Su, J., & Gao, Y. (2018). Highly self-healable 3d microsupercapacitor with MXene–graphene composite aerogel. *ACS Nano, 12*(5), 4224–4232.

Yu, L., Hu, L., Anasori, B., Liu, Y.-T., Zhu, Q., Zhang, P., Gogotsi, Y., & Xu, B. (2018a). MXene-bonded activated carbon as a flexible electrode for high-performance supercapacitors. *ACS Energy Letters, 3*(7), 1597–1603.

Yu, P., Cao, G., Yi, S., Zhang, X., Li, C., Sun, X., Wang, K., & Ma, Y. (2018b). Binder-free 2D titanium carbide (MXene)/carbon nanotube composites for high-performance lithium-ion capacitors. *Nanoscale, 10*(13), 5906–5913.

Zhang, X., Liu, Y., Dong, S., Yang, J., & Liu, X. (2018). Surface modified MXene film as flexible electrode with ultrahigh volumetric capacitance. *Electrochimica Acta, 294*, 233–239.

Zhao, M.-Q., Ren, C. E., Alhabeb, M., Anasori, B., Barsoum, M. W., Gogotsi, Y. (2019). Magnesium-ion storage capability of MXenes. *ACS Applied Energy Materials.*

Zhao, M.-Q., Torelli, M., Ren, C. E., Ghidiu, M., Ling, Z., Anasori, B., Barsoum, M.-W., & Gogotsi, Y. (2016). 2D titanium carbide and transition metal oxides hybrid electrodes for Li-ion storage. *Nano Energy, 30*, 603–613.

Zheng, W., Zhang, P., Chen, J., Tian, W. B., Zhang, Y. M., & Sun, Z. M. (2018). In situ synthesis of CNTs@Ti_3C_2 hybrid structures by microwave irradiation for high-performance anodes in lithium ion batteries. *Journal of Materials Chemistry A, 6*(8), 3543–3551.

Zhu, J., Ha, E., Zhao, G., Zhou, Y., Huang, D., Yue, G., Hu, L., Sun, N., Wang, Y., Lee, L. Y. S., Xu, C., Wong, K., Astruc, D., & Zhao, P. (2017). Recent advance in MXenes: A promising 2D material for catalysis, sensor and chemical adsorption. *Coordination Chemistry Reviews, 352*, 306–327.

Zhu, J., Wang, M., Lyu, M., Jiao, Y., Du, A., Luo, B., Gentle, I., R., & Wang, L. (2018a). Two-dimensional titanium carbonitride MXene for high-performance sodium-ion batteries. *ACS Applied Nano Materials.*

Zhu, K., Jin, Y., Du, F., Gao, S., Gao, Z., Meng, X., Chen, G., Wei, Y., & Gao, Y. (2018b). Synthesis of Ti_2CT_x MXene as electrode materials for symmetric supercapacitor with capable volumetric capacitance. *Journal of Energy Chemistry.*

Zou, R., Quan, H., Pan, M., Zhou, S., Chen, D., & Luo, X. (2018). Self-assembled Mxene ($Ti_3C_2T_x$)/α-Fe_2O_3 nanocomposite as negative electrode material for supercapacitors. *Electrochimica Acta.*

Chapter 7
Nano Coatings and Thin Films of 2D Nanomaterials (MXenes) as Transparent Conductivity Electrodes and Supercapacitors

A. V. Pradeep

1 Introduction

In recent years, the whole world is keen on concentrating ecological and energy issues. Heavy duty purposes such as batteries and vehicles require efficient energy storage/conversion appliances (Hoque et al., 2017). As the present energy storage/conversion techniques have limitations like restricted and expensive use of rechargeable gadgets, complicated high energy transformation, etc., the research for energy-efficient techniques is essential (Sun et al., 2018). Due to the exceptional physico-chemical characteristics of two dimensional (2D) materials like MXenes and graphene, they have drawn attention of researchers, globally (Li et al., 2009; Zhu et al., 2011a, 2011b). Though graphene is considered the future-generation materials, MXenes also possess great abilities like high interlayer spacing, excellent biocompatibility, functionally safe, and eco-friendly. Moreover, these 2D materials have great ability to store huge amount of charge/unit volume at speeder rates (Levi et al., 2015).

The progress in nano-technology made MXenes be helpful in various environmental, waste water handling, and energy applications (Heo et al., 2012; Song et al., 2018; Wang et al., 2011; Zhu et al., 2018). Besides, MXenes effectively adsorb biological pollutants (Apul et al., 2013; Raad et al., 2016) and dense matter (Leng et al., 2012) from waste water. This is attributed to its distinctive characteristics, such as high oxidation resistance and stability, magnificent thermal/electrical conductivity, great melting point, and eminent hydrophilic nature (Lukatskaya et al., 2013). Therefore, MXenes are extensively used as pioneering membrane and adsorbents, exterminating organic toxins (Ding et al., 2017).

A. V. Pradeep (✉)
Department of Mechanical Engineering, Vignan's Institute of Engineering for Women, Visakhapatnam, India

S. Singh et al. (eds.), *Advanced Applications of 2D Nanostructures*,
Materials Horizons: From Nature to Nanomaterials,
https://doi.org/10.1007/978-981-16-3322-5_7

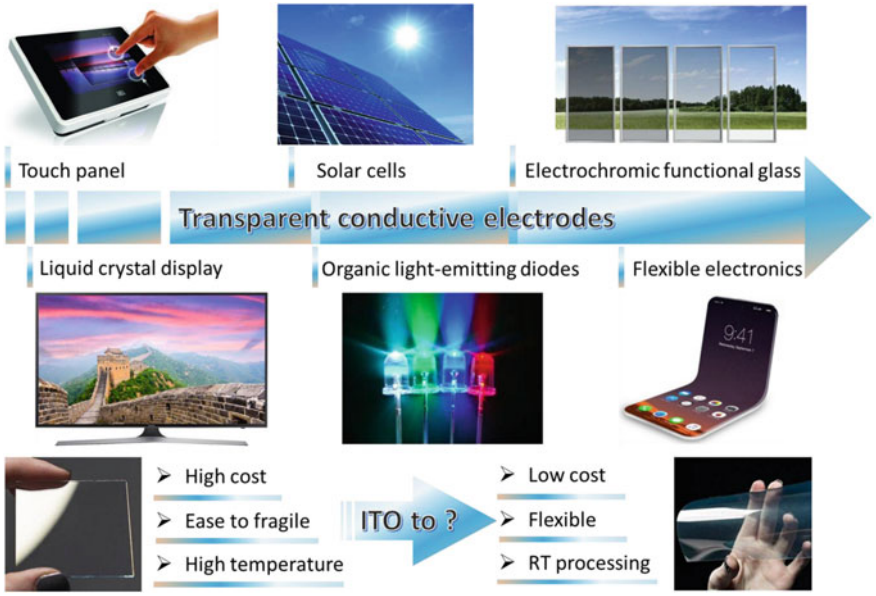

Fig. 1 Different applications of TCEs (Zhang & Nicolosi, 2019)

The exponential rise in the advent of smart optronic components like light-emitting diodes (LEDs), liquid crystal displays (LCDs), touch screens, and photovoltaics has highly influenced human lifestyle (Hecht et al., 2011). These optronic gadgets essentially constitute highly electrically conductive and transparent device, transparent conductive electrodes (TCEs), which aredisplayed in Fig. 1 (Zhang & Nicolosi, 2019). The worldwide economy for TCEs in 2013 was 4.8 billion dollars, which escalated to around 7.1 billion dollars in 2018. Presently, TCEs are primarily used in touch screens and LCDs (Chang & Lai, 2015; Yu et al., 2016).

Besides, encompassing TCEs with energy storage/conversion components, such as supercapacitors and batteries (Yu et al., 2017), can be elemental in next-generation technology, intended for smart, wearable, and compact optronic devices (Bae et al., 2010). Therefore, the functional material must retain great optronic characteristics high with storage/conversion ability. In addition, these transparent energy storage materials should own high conductivity.

MXenes, transition metal carbide, and nitrides, the emerging 2D material have swiftly gained interest of the present researchers. Of all MXene kinds, TiC ($Ti_3C_2T_x$) has been extensively examined, because of its high capacitive storage and conductivity (Lukatskaya et al., 2017; Naguib et al., 2012). Hence, $Ti_3C_2T_x$ MXenes can be effectively employed in producing flexible and transparent supercapacitors, and efficient TCEs.

The recent years have observed the exponential rise in research of 2D materials. In this regard, numerous synthesis techniques, and applications of MXenes and graphene have been exploited (Anasori et al., 2017; Cao et al., 2014). Besides,

the study of MXene and graphene-based transparent supercapacitors and TCEs have been on rise. Surprisingly, the review on MXene-derived TCEs has been very limited. Consequently, an extensive review encapsulating the modern advances in MXene-derived transparent supercapacitors and TCEs is imperative.

In this review, first the properties of MXenes and a concise outline of its synthesis techniques are elucidated. Moreover, the thin-film synthesis processes and the limitations of MXenes are discussed. Further, a detail explanation of the advancements in MXene-based TCEs is presented. In addition, the applications in transparent supercapacitors and energy storage/conversion are described. The illustrations help in comparing the optronic attributes of numerous TCEs and supercapacitors. Eventually, the prospective, challenges, and future scope of the material and the areas are discussed. Ultimately, it can be ascertained that the MXenes will progressively emerge as crucial materials for TCEs, supercapacitors, and transparent and flexible optronics.

2 MXenes Thin-Film Synthesis

The comprehensive review of synthesis techniques of MXenes has been presented by various recent investigations. At first, in 2011, researchers of Drexel University found 2D multi-layered MXenes ($Ti_3C_2T_x$) (Naguib et al., 2011). They were revealed when Ti_3AlC_2 is exploited and an A-layer from its MAX phase is etched. MAX phase belongs to the group of ternary carbide and nitride elements, which are testified to be above 70 in number (Eklund et al., 2010). These phases are composed of nitride or carbide layers (Mn + 1Xn) interweaved by layers composed of 13th and 14th group elements. In order to differentiate the MXenes from graphene, both being 2D materials originated from MAX phases, it was given a name "MXene" (Alhabeb et al., 2017). Etching using hydrofluoric etchants like HF, HCl-NaF, or HCl-LiF generate several Multi-layered MXenes as $(V_{0.5}Cr_{0.5})_3C_2$, Mo_2ScC_2, $(Nb_{0.8}Ti_{0.2})_4C_3$, Mo_2C, V_2C, Mo_2TiC_2, $(Nb_{0.8}Zr_{0.2})_4C_3$, Zr_3C_2, TiNbC, Cr_2TiC_2, $(Ti_{0.5}Nb_{0.5})_2C$, Nb_4C_3, Nb_2C, $Mo_2Ti_2C_3$, Ti_3CN, Ta_4C_3, Ti_2C, Ti_4N_3 and Ti_3C_2.

The historical evolution of MXenes is presented in Fig. 2a. Initially, in 2011, $Ti_3C_2T_x$, multi-layer MXene was originated. In the adjacent year, 2012, there evolved several MXenes comprising Ti_3CNT_x, $(TiNb)_2CT_x$, $(V,Cr)_3C_2T_x$ and $Ta_4C_3T_x$ (Halim et al., 2014). Later in 2013, with the progress of delamination and intercalation techniques, single layer MXenes were extracted. Further, in 2015, extensive delamination of MXenes was successfully achieved adopting tetrabutylammonium hydroxide (Mashtalir et al., 2015). In addition, alteration of HCl-LiF etching technique de-laminated $Ti_3C_2T_x$ into single flakes less than 2 μm (Anasori et al., 2015). Furthermore, $Mo_{1.3}CT_x$ was fabricated in 2017 from crystal vacancy defects through $(Mo_{2/3}Sc_{1/3})_2Al$ (Tao et al., 2017). Though large range of MXenes (above 70 in numbers) is synthesized by various etching practices at diverse MAX phases, $Ti_3C_2T_x$ gets utmost interest from researchers. Fabrication of $Ti_3C_2T_x$ by several hydrofluoric acid (HF) etching processes is presented in Fig. 2b (Alhabeb et al., 2017).

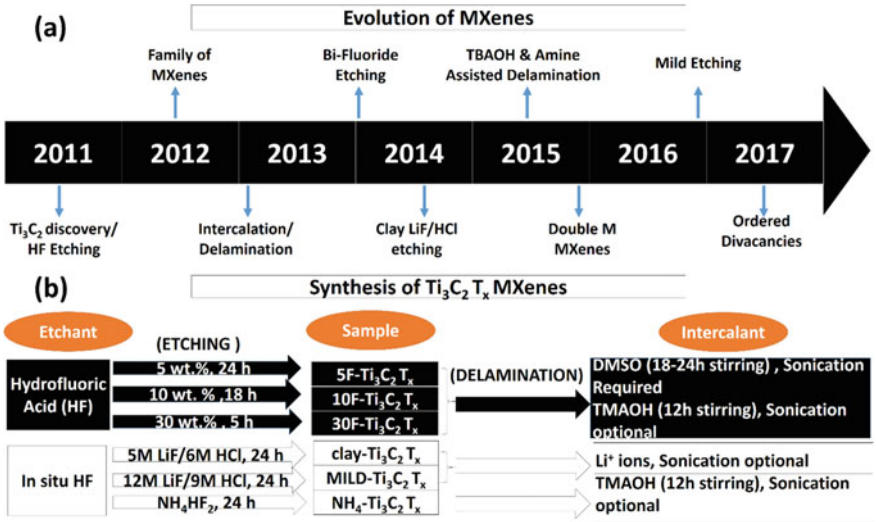

Fig. 2 **a** Historical evolution of MXenes and **b** outline of Ti_3C_2Tx synthesis through $Ti3AlC_2$ (Jun et al., 2019)

HF was applied with 3 distinctive combinations (5, 10, and 30 weight percentage) for 3 different time period (5, 18, and 24 h), where each combination successfully produced $Ti_3C_2T_x$. During the above process, tetramethylammonium hydroxide or dimethyl sulfoxide dissolved huge organic fragments into them, which after sonication resulted in delamination. In addition, clay-like structured $Ti_3C_2T_x$ interwoven with Li^+ can be delaminated using HCl-LiF etchant. Even sonication process can be eliminated by selecting appropriate concentration of LiF and HCl (Alhabeb et al., 2017).

3 Properties of MXenes

3.1 Structural

The precursor, sonication frequency, etchant, and intercalation process play instrumental roles in determining the mechanical, optical, electrical, electronic, magnetic, and structural properties of MXenes. The side and plan views of M_2X Pristine MXene is shown in Fig. 3a. Figure 3b shows 2-functional units over hollow position A of M_2X-1. Figure 3c shows 2-functional units over hollow position B of M_2X-2 (Khazaei et al., 2017). Because of six as co-ordination number in transition metals, MXenes chemically structure itself with six bonds. This produces MXenes in the form of $M_2X(OH)_2$, M_2XO_2 and M_2XF_2 (Khazaei et al., 2013).

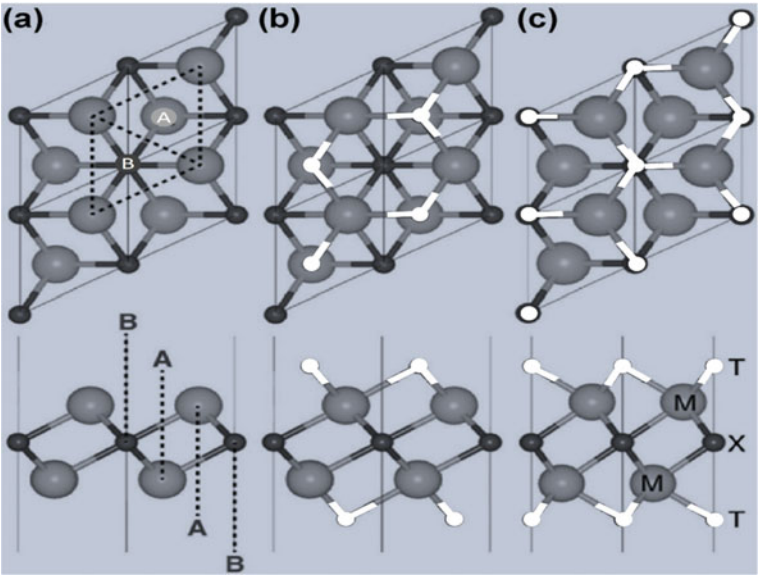

Fig. 3 Sight from top and side of **a** pristine MXene M_2X, **b** M_2X-1 and **c** M_2X-2 MXene (Jun et al., 2019)

Theoretically, functionalization of F, O, and OH in Tin+1Cn influences system tensile stresses. Moreover, because of decreased fissure of the atomic layer due to surface functionalization, the elastic property of Ti_2CO_2 enhances, which makes it endure higher uniaxial and biaxial stresses than graphene. For instance, during oxygen functionalization, the extensive charge transmission from inward Ti−C to outward Ti−C atoms results in excellent solidification. Usually, during fabrication of MXenes, the MAX phases are subjected to chemical exfoliation. This can be viably extended to mechanical exfoliation. Owing to stronger bonding of a-b plane in MAX phase, the elastic constants in c-direction will be comparatively weaker ($C_{33} < C_{11}$) (Khazaei et al., 2014). Though both pristine MXenes and MAX phases subsist metallic in nature, the semiconductive characteristics of few MXenes can be stimulated through surface functionalization (Khazaei et al., 2013). According to previous works, MXenes based on the tractability of their spin orbit pairing; insignificantly exist as semimetals/ semiconductors and metals/semiconductors (Weng et al., 2015).

Very less experimentation has been reported evaluating the optical properties of MXene through $Ti_3C_2T_x$ films. Ti_3AlC_2, a MAX phase film ensued very less transmittance of 30%. Conversely, $Ti_3C_2T_x$ presented nearly 80% rise in light transmittance (550 nm). Similarly, intercalated $Ti_3C_2T_x/NH_4HF_2$ exhibited 90% increase, using different thickness ranges of $Ti_3C_2T_x$. Because of the strong covalent bonding of the transition metal to functional groups, both functionalized and pristine MXenes exhibit non-magnetic properties (Hu et al., 2014). Nevertheless, external stains can alter the covalent bonding by discharging the electrons, invoking magnetism in them.

Most commonly, the magnetic property invokes naturally in pristine MXenes. For instance, pristine Ti_2C and Ti_2N present semi-metallic ferromagnetism with units 1.0 and 1.9 (Gao et al., 2016). While evaluating functionalized and pristine Ti_3C_2 MXene, it is revealed that the electronic transport is significantly influenced by the surface functionalization process. For example, pristine Ti_3C_2 when compared to $Ti_3C_2F_2$ exhibited four times increase in current at any particular voltage (Berdiyorov, 2015).

Under the water and oxygen atmosphere, single MXenes are indeterminately unstable (Mashtalir et al., 2014). Yet, in dry air or oxygen-less water (degassed), they remain comparatively stable. Moreover, oxidation can be progressed when light is exposed colloidal MXene suspensions. Hence, it is always suggested to store MXene colloids under chilled, dark, and oxygen-free atmosphere. As reported, MXenes of superior quality have more stability, though the synthesis technique determines their stability to oxidation (Lipatov et al., 2016). Usually, nanocrystals of metal oxides are formed by oxidizing the MXene flakes, which instigates through the edges. For instance, the oxidation of TiO_2 starts at the edge of the crystal, and by nucleation propagates to the complete area.

3.2 Stability

The stability of MXenes under elevated temperature is under research stage. The phase stability can be evaluated by analyzing phase-diagrams of transition metal oxides and carbides. The environmental condition and the composition of MXenes define its high-heat stability. Distinctive high-heat behavior was observed by various studies. In a recent study, $Ti_3C_2T_x$ is found to be stable under argon environment, even at 500 °C. In addition, oxidation was formed by generating TiO_2 crystals (Wang et al., 2016). Furthermore, though faulty annealing was ensued, the Ti_3C_2 was well-maintained under argon atmosphere, at severe temperature of 1200 °C. Moreover, the cubic TiC_x appearing in the form XRD peaks is an indication of MXene phase transition (Wang et al., 2016). As indicated by the TiC phase chart (non-stoichiometric), at 1200 °C, it is considered as the greatest steady phase. When observed under temperature-based mass spectroscopy, $Ti_3C_2T_x$ under helium environment at temperatures greater than 800 °C, substantially started losing weight. This reveals phase transformation, which is also observable during vacuum calcination at common temperature. It is also verified that under inert environment, at 250 °C, Ti_2CT_x is stable (Rakhi et al., 2015). Another study reported that, Ti_2CT_x is stable even over the phase stability temperature (1100 °C) in hydrogen and argon atmosphere (Lai et al., 2015). Though the characterization reveals positive results, still Raman or XRD analyses are required to ascertain any newly formed phases. Converse to $Ti_3C_2T_x$ which transits to cubic carbide, under vacuum condition, $Zr_3C_2T_x$ exhibited high thermal stability even at 1000 °C. This can be attributed to its energetically promising structure, unlike Ti_3C_2, having bulk cubic TiC structure, which is metastable in nature. Therefore, $Zr_3C_2T_x$ being high-temperature stable material, is utilized in high-heat applications.

3.3 Mechanical and Physical

According to molecular dynamics, M_2X MXenes possess higher strength and stiffness compared to their counterparts, M_4X_3 and M_3X_2. But, the mechanical inspection was performed only on MXene sheets rather than single layers (Anasori et al., 2017). Interestingly, a $Ti_3C_2T_x$ tube of wall thickness 5 μm can sustain a load of approximately 4000 times greater than its weight. The strength of the sheet can be further improved to 15,000 times its weight by amalgamating $Ti_3C_2T_x$ to 10 weight percent polyvinyl alcohol.

In order to enhance the wear and corrosion resistance, mechanical, electrical, and thermal properties, several MXenen-polymer composites (polydimethylsiloxane (PDMS), polyvinyl alcohol, polypyrrole, and polyethylene) were evolved. In addition, MXenes have been reinforced with carbon-nanotubes (CNTs) for its excellent electrochemical properties (Liu et al., 2015; Mashtalir et al., 2015). Afresh, self-assembled sheets have been fabricated employing the principle of electrostatic forces. In this regard, surfactant coated or oxidized CNTs were held positively charged, while MXenes were kept negatively charged, maintained under -30 to -80 mV zeta potential (Xie et al., 2016).

The MXene sheets and the hybrid composites are usually transparent in nature. Significantly, greater than 97% of light/nm thickness can be transmitted by Ti_3C_2 (Anasori et al., 2017). Moreover, the cation intercalation by electrochemical process can modify its optronic properties.

It is a well-established fact that surface termination determines the electronic properties of all the semiconducting and metallic MXenes. Few MXenes amalgamated with heftier transition metals such as molybdenum, tungsten, and chromium are considered as topographical insulators (Khazaei et al., 2016). Only few MXenes like Mo_2C, $Mo_2Ti_2C_3$, Ti_3C_2, Ti_2C, Mo_2TiC_2, etc. have been experimentally validated for electronic properties. Few studies reported that the electronic properties can be altered by varying the surface M layers (Cambaz et al., 2006). For instance, $Ti_3C_2T_x$ is metallic in nature (Anasori et al., 2017). But, semiconductor properties of MXenes are seen with Mo constituents. Moreover, at 10 K, they exhibit positive magneto resistance, (Cambaz et al., 2006). The transport characteristics can also be varied by post-treatment which modifies superficial terminations. Say, when Ti_2CT_x is subjected to annealing process under hydrogen and argon atmosphere at 1100 °C, it behaves as Ti_2CO_2, owning semiconductor features (Lai et al., 2015). Though the observations are in agreement with theoretical approximations, at particular temperature, there are chances of Ti_2CT_x for partially transforming to different phases. Therefore, it is imperative to understand the thermal behavior of MXenes.

Besides, the synthesis technique of MXenes determines its electrical conductivity. Generally, greater conductivity occurs with big flake size and less defects. High electrical conductivity can be obtained by slight etching and delamination in sonication-less environment. Also, the conductivity can be increased by improving the coplanar contact area. Consequently, the films made up of $Ti_3C_2T_x$ have conductivity varying from 1000 to 4600 S/cm for HF etchant and slighter-etched, respectively.

Few MXenes are found with ferromagnetic and anti-ferromagnetic features, but the surface termination vanishes the magnetism. Irrespective of surface terminations, Cr_2NT_x and Cr_2CT_x are expected to have magnetic properties. Yet, there is no clear understanding of their nature. A study revealed that terminated Cr-MXenes are of ferromagnetic in nature. Conversely, while concentrating anti-ferromagnetic nature, terminated Cr_2NT_x and Cr_2CT_x have found to be anti-ferromagnetic, which is exceptional for Cr_2NO_2. However, there is a need to study the magnetic behavior of MXenes.

4 MXene-DERIVED TCEs

4.1 Introduction

The transitional metal nitrides, carbonitrides, and nitrides are jointly termed as MXenes. Right from the inception of Ti_3C_2 (2011), the applications of these materials have widespread globally. Multilayer MXenes (m-) are acquired when A-elements are etched from MAX layer using fluoride constituent acids like HF, ammonium hydrogen bifluoride, NH_4HF_2 (Alhabeb et al., 2017), and hydrochloric acid along with lithium fluoride (LiF + HCl) (Ghidiu et al., 2014). The MXenes are hydrophilic in nature because of its surface functional groups. As the electrostatic force acts on the nano-films which are subjected to negative charge, an aqueous solution is thus released when MXenes are delaminated (Anasori et al., 2017). When the delamination occurs as single layer, they are termed as m-MXenes, and when happens in multi layers, they are named d-MXenes. This being eco-friendly solution, MXenes can be safely applied for coatings, devices, and composites. The titanium carbide MXene ($Ti_3C_2T_x$) exhibits high metallic conductivity of 9880 S/cm (Zhang and Nicolosi, 2019). The MXenes are also termed pseudocapacitance, because of its high faradic response along with extensive electronic conductivity (Zhang et al., 2016). Additionally, single-layer MXene nano-film is optically transparent. Conclusively, MXenes can be effectively employed for great-functioning transparent supercapacitors and conductive films. The energy-storage gadgets like batteries and supercapacitors extensively use MXenes.

4.2 $Ti_3C_2T_x$ TCEs

As reported earlier, the synthesis technique of transparent sheets is greatly restricted by the separation process. Emerging materials with great DC conductivity and contemporary thin-film synthesizing methods can help in overcoming the above problem. As MXenes possess excellent hydrophilicity and metallic conductivity, they are best suited for TCEs.

The effort of producing $Ti_3C_2T_x$ transparent sheets were first initiated by Halim et al.. Initially, the Ti_3AlC_2 sheets were deposited using sputtering, and later, the Al elements were etched. The films obtained were of thickness 19 nm with T = 90%. Moreover, this process essentially needs high deposition temperature (780 °C) and the etching of Al is tedious, limiting the production. Therefore, a fast, efficient, economical and environmental-friendly synthesis technique has to be developed.

The intercalation of m-$Ti_3C_2T_x$ with water or biological particles expands the interlayer arrangement, reducing the Vanderwaal's force amongst the nano-films. Further, when the m-$Ti_3C_2T_x$ is subjected to sonication under inert gas environment, it delaminates into single-layer nano-films (Alhabeb et al., 2017; Zhang & Nicolosi, 2019). Hence, employing the processes such as spin-coating or spray-coating, $Ti_3C_2T_x$-based TCEs can be effectively produced with controlled transparency and thickness. Further, these ultrathin nano-films interlace into uninterrupted conductive grid, providing greater flexibility of TCEs. This also reduces the limitations such as lump junctions and channeling barriers.

In a study by Gogotsi et al., the homogeneous sheets of $Ti_3C_2T_x$ were produced with thickness varying between 5 and 70 nm by spraying aqueous suspension against a substrate. This is shown in Fig. 4a–c. The transmittance of these films will be 40–91%, which is presented in Fig. 4d. At high thickness of 70 nm, T = 40%, Rs is found to be 500 Ω/sq, as shown in Fig. 4e. There is a considerable increase in transmittance, T = 91%, when the thickness is reduced to 5 nm. Adversely, the film resistance augmented to 8 kΩ/sq. In spray coating, when the drops are impinged against the heated substrate, it rapidly gets evaporated, generating bubbles on the film.

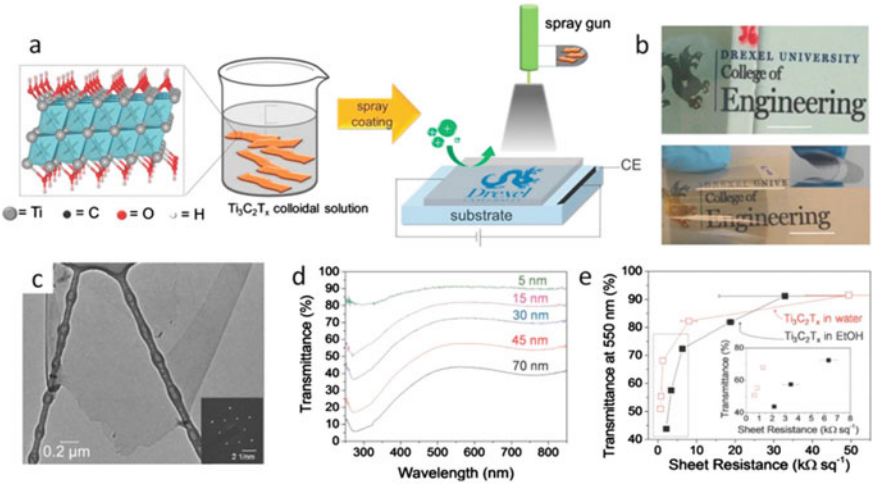

Fig. 4 **a** Preparation of $Ti_3C_2T_x$ TCEs through spray coating, **b** $Ti_3C_2T_x$ TCEs synthesized on flexible PET (bottom) and glass (top) substrate, **c** $Ti_3C_2T_x$ film observation under TEM, **d** UV bands of $Ti_3C_2T_x$ TCEs at various thickness, and **e** Sheet resistance (vs.) Transmittance of ethanol and water sprayed $Ti_3C_2T_x$ TCEs (Zhang & Nicolosi, 2019)

This forms undesirable voids inside the stack, obstructing the charge transport. As a result, the electronic conductivity of $Ti_3C_2T_x$ TCEs will be drastically reduced. A study of spraying $Ti_3C_2T_x$ reported that the sensitivity climbed up to 3.4 × 104 Ω/cm, exuding transmittance of 86.7% (Ali et al., 2016).

In a study by Taylor et al., spin-casting technique was used to disperse solution-treated $Ti_3C_2T_x$ onto TCEs (Mariano et al., 2016). The film thickness was successfully regulated by governing the spinning speed. When measured by field-effect transistor, the electronic conductivity of $Ti_3C_2T_x$ was verified, which is predicted to be 3092 S/cm. Exhibiting resistance of 437 Ω/sq at transmittance of 77% confirmed that $Ti_3C_2T_x$ sheets possess superior optronic properties (Mariano et al., 2016). The moisture content and residual adsorbents from wet MXene sheets can be eliminated by vacuum annealing at 175 °C. Consequently, there is severe reduction of resistance from 630 to 191 Ω/sq (Mariano et al., 2016). Another study witnessed higher optronic conductivity of 6500 S/cm, transmitting 97% of light/nm thickness in tandem (Dillon et al., 2016). Hence, it is important to note that every single layer (~1.2 nm) contributes to a loss of approximately 3% transmittance. Therefore, in order to enhance the conductivity of $Ti_3C_2T_x$ TCEs, the $Ti_3C_2T_x$ nano-films, should be densely interwoven, which is shown in Fig. 5b–d (Dillon et al., 2016). Therefore, the rearrangement of $Ti_3C_2T_x$ layers resulted in best performance TCEs having resistance 330 Ω/sq with 86% transmittance, as shown in Fig. 5e (Dillon et al., 2016).

In recent years, best-performance TCEs were obtained through various alignments of $Ti_3C_2T_x$ flakes (Zhang et al.,). The sheets of different transmittance can be generated by regulating the spin-velocity, which is displayed in Fig. 6a, b. These sheets display interwoven grids without extended flake edges, as displayed in Fig. 6c, d. As the flake sizes are much lower (μm), they cannot hold moisture, resulting in great capacitive characteristics (transmittance 29%, thickness 88 nm, and conductivity 9880 S/cm) (Zhang et al., 2017a, 2017b).

Surprisingly, the resistance of $Ti_3C_2T_x$ TCEs behave inversely with the film-thickness, which is presented in Fig. 6e. In general, bulk materials exhibit such properties. Simply, $Ti_3C_2T_x$ TCEs did not confront any filtration problems. The transmittance vs resistance (T vsn R_s) plot is used to confirm it, which is given in Fig. 6f. The plot displays that the evaluated values of both T and R_s falls close to the curve without deviating much. Additionally, Fig. 6f presents the values of figure of merit (electrical), FoM_e, which were nearly constant throughout the series of thickness. Moreover, the experimental and theoretical values of FoM_e are very close to each other, 19 and 16 respectively. Hence, the performance of $Ti_3C_2T_x$ MXene based TCEs can outperform that of CNT-derived and solution-treated graphene TCEs, which is shown in Fig. 6h (Becerril et al., 2008). By this, for the same conductivity, much more transparent TCEs can be generated. To be more precise, $Ti_3C_2T_x$ thin sheets can provide reliable DC conductivity irrespective of its transmittance (Zhang et al., 2017a, 2017b). This distinctive property helps $Ti_3C_2T_x$ sheets to act as effective current collectors, simultaneously being active material. Therefore, $Ti_3C_2T_x$ TCEs help in developing transparent supercapacitors, eliminating additional metals for current collecting.

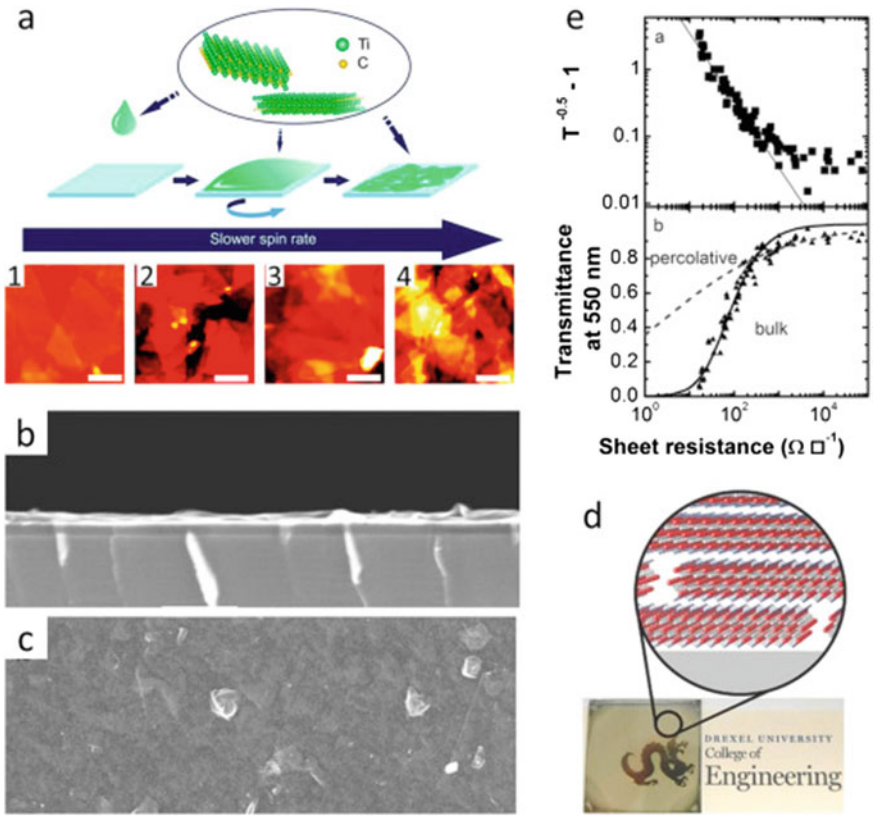

Fig. 5 **a** Fabrication of $Ti_3C_2T_x$ TCEs through spin-casting technique. **b** SEM image of Cross-section of $Ti_3C_2T_x$ TCE, **c** SEM images of $Ti_3C_2T_x$ TCE from top, **d** Optical vision of $Ti_3C_2T_x$ TCEs, **e** Sheet resistance (vs.) Transmittance of $Ti_3C_2T_x$ TCEs (Zhang & Nicolosi, 2019)

4.3 More MXene-Derived TCEs

Since form the inception of MXenes, there have been 20 different compositions developed; mostly all expected to have metallic nature. Though, the other MXenes too can be potentially employed for transparent conductive sheets. The conductivity of Vanadium carbide (V_2CT_x) sheets were measured as 1560 S/cm (Champagne et al., 2018). The difficult task is to form d-V_2CT_x by delaminating m-V_2CT_x. This was successfully accomplished by performing delamination using tetrabutylammonium hydroxide (TBAOH) suspension at a composition of 10 wt% (Ying et al., 2018). Interestingly, the FoM_e of V_2CT_x TCEs (6.5) is measured to be greater than that of $Ti_3C_2T_x$ TCEs (Ying et al., 2018). As reported earlier, conductivity mainly depends on the annealing temperature. For example, the annealing substantially enhanced the conductivity of V_2CT_x TCEs 300 times, from 10 to 3300 S/cm (Ying et al., 2018). In addition, the conductivity can be enhanced by employing optimized synthesis

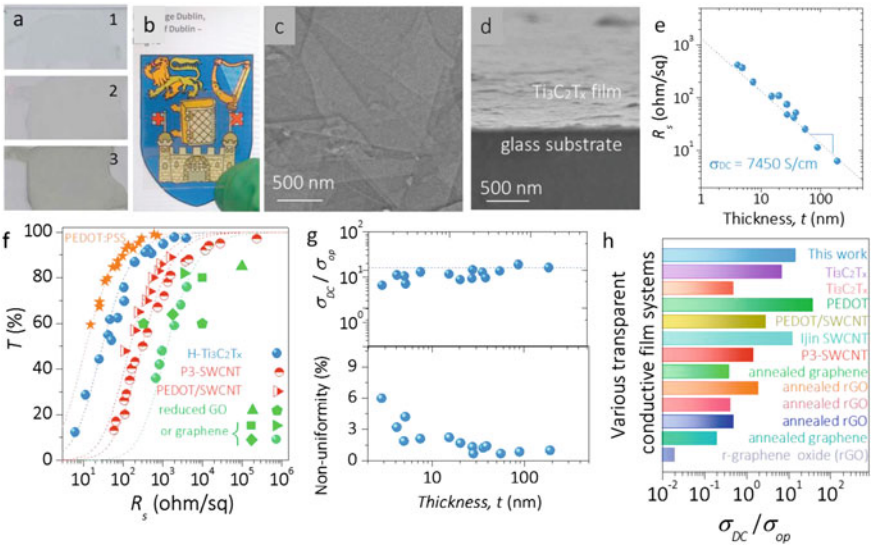

Fig. 6 **a**, **b** Vacuum-annealing (200 °C) images of Ti3C2Tx TCEs, **c** SEM image of plan-view of glass substrate, **d** cross-sectional SEM image of glass substrate, **e** Plot for Sheet resistance vs. thickness, **f** T vs. R_s graph along with comparison of various TCEs, **g** FoM_e (top) and non-uniformity (bottom) vs. thickness, and **h** FoM_e compared to other studies (Zhang & Nicolosi, 2019)

parameters like cleaner and larger films, more efficient and safe etchant. By this, higher DC conductivity can be generated due to reduced fabrication defects. As and outcome, the V_2CT_x TCEs can showcase higher FoM_e.

In another work by Ying et al., chain of Ti_2CT_x TCEs are fabricated by using 25 mg/ml colloidal solution made of Ti_2CT_x. As the charge carriers retain high density, the sheet conductivity is generated as high as 5250 S/cm, being first of its kind (Cao et al., 2014; Miranda et al., 2016). In addition, this TCE generated great FoM_e of 5. Owing to advantages like enhanced optronic characteristics, economical and non-hazardous, Ti_2CT_x TCEs can outperform $Ti_3C_2T_x$ TCEs (Cao et al., 2014). Moreover, the stability of these MXene TCEs is yet to be ascertained.

4.4 Drawbacks of MXene-Based TCEs

Despite the enhanced properties in MXene- built TCEs, still they suffer few setbacks. Basically, the MXene colloid has very low shelf life compared to graphene oxide (GO) (Zhang et al., 2017a, 2017b). However, the shelf life of $Ti_3C_2T_x$ can be improved by storing MXene colloid in Ar-filled airtight container. Surprisingly, this process decreases the shelf life of Ti_2CT_x colloid (Zhang et al., 2017a, 2017b). Moreover, compared to GO, the cost incurred in fabricating MXene TCEs is far more. This is due to non-familiarization of the MXene synthesis techniques. The MXene TCEs can be

largely manufactured when their price comes low. Few studies reported an improvement in optronic properties of graphene-TCEs when chemically doped, whereas no studies exist over MXene-based TCEs, as of now. Also, $Ti_3C_2T_x$ exhibits very low charge carrying capability of 0.9 cm^2/Vs (Dillon et al., 2016; Miranda et al., 2016).

5 MXene-Derived Energy Storage Devices

5.1 MXene Films in Transparent Supercapacitors (SCs)

In general, the metal ions and natural molecules can be instantly intercalated to MXenes. When the MXenes are intercalated with cations, they inhabit the electrochemically dynamic areas on the surface, contributing to energy storage (Lukatsakaya et al., 2013). The $Ti_3C_2T_x$ MXenes are well-inspected electrochemical capacitors. The $Ti_3C_2T_x$ sheet electrodes exhibit a volumetric capacitance of 300–400 F/cm^3 in base and neutral electrolytes. Though the influence of cations (K^+, Li^+, Na^+, Mg_2^+, and NH_4^+) moderately fluctuate the desired profile of the cyclic voltammetry contours, there exist no crests and the 'capacitor-pro' shape apparently appears (Lukatsakaya et al., 2013). The volumetric capacitance of clay-structured $Ti_3C_2T_x$ electrode in 1 M H_2SO_4 was measured over 900 F/cm^3. This can be attributed to active inhibition of protons into the electrochemically dynamic spots. This avoids inter-mounting of MXenes films during fabrication, particularly when Li^+ ions are intercalated with water particles. Moreover, even during great charge/discharge rates, $Ti_3C_2T_x$ is observed to retain excellent capacitive conduct (Ghidiu et al., 2014). The high-rate performance can be obtained when thin transparent MXene electrodes are deposited on flexible substrate (Peng et al., 2016). Moreover, $Ti_3C_2T_x$ MXene electrodes display outstanding life over 10,000 cycles with consistent capacitance (Ghidiu et al., 2014).

Yet, there was no apparent understanding of the capacitance mechanism. MXenes revealed no sharp peaks in cyclic voltammetry curves, similar to that of CNT-based capacitors. But, the surface is insufficient to determine its performance (Ghidiu et al., 2014; Lukatskaya et al., 2013). $Ti_3C_2T_x$ (1 M H_2SO_4), was subjected to in situ XAS analysis (electrochemical) in order to find out whether the capacitance mechanism is pseudocapacitive. It is revealed that the mechanism is essentially pseudocapacitive at the probe rate of 20 mV/s (Ghidiu et al., 2014).

The electrochemical capacitance of MXenes is significantly influenced by many factors. Primarily, the electrode density influences the performance of MXenes by acting as gravimetric-to-volumetric conversion element. In general, freestanding MXene electrodes (3–4 g/cm^3) are much denser than MXene-derived polymer composite ones (1–2.5 g/cm^3). This is because of higher density of carbides than carbon.

Moreover, the surface chemistry of MXene influences both volumetric and gravimetric capacitance. For instance, when oxygen functional groups replace the fluorine

elements, there will be a significant enhancement in its capacitance. Similarly, the gravimetric capacitance can be enhanced to 2–7 times when $Ti_3C_2T_x$ is synthesized with N_2H_4, DMSO or KOH colloids instead of HF solution (Dall'Agnese et al., 2014). This also depends on the type of electrolyte employed, best being with acidic electrolytes. Excellent oxygen-comprising functionalities are observed in HCl–LiF-synthesized $Ti_3C_2T_x$, compared to HF-synthesized ones (Hope et al., 2016). Because of these advantages, high capacitance of 900 F/cm^3 was reported. The electrodes (~75 μm thickness) can be instantly fabricated when HCl–LiF etched $Ti_3C_2T_x$ is subjected to rolling process. This can exhibit a capacitance of 350 F/cm^3 (Ghidiu et al., 2014). Not only $Ti_3C_2T_x$ MXenes, but other MXenes can also be effectively devoted to supercapacitors. For instance, the cyclic voltammetry profiles (rectangular) of $Mo_2TiC_2T_x$ and Mo_2CT_x revealed great volumetric capacitance.

The hybrid materials of MXene base exhibit improved mechanical and electrochemical properties. A study reported that the performance of MXenes was enhanced when it was reinforced with 5–10 weight percent of graphene or CNTs. This can be attributed to improved ion-mobility in organic and aqueous solutions. The advent of composite polymers paved a crucial way for the development in electrode technology. The polymers when intercalated within the $Ti_3C_2T_x$ MXene sheets, prevent interweaving and restacking, thereby enhancing the mechanical characteristics. This happens without affecting its electro-chemical properties (Ling et al., 2014). Moreover, the electrochemical characteristics can be improved by replacing the electrochemical-inert polymers with redox-active polymers. For instance, the gravimetric capacitance of $Ti_3C_2T_x$ –polypyrrole composite (thickness 13 μm) (420 F/g) was enhanced twice that of basic $Ti_3C_2T_x$ (240 F/g), at 2 mV/s. Besides, the improvement in volumetric capacitance (approximately 1000 F/cm^3) was not much remarkable as the composites (2.4 g/cm^3) have low density compared to pure $Ti_3C_2T_x$ (3.8 g/cm^3) (Ghidiu et al., 2014).

It is worth noting that the performance of MXenes will be excellent under cathodic (negative) charge. In addition, the capacitance will be drastically reduced when the MXenes are placed in positively charged electrolytic solution (approx. 0.2–0.4 V). This is because of the instigation of irreversible oxidation which substantially upsurges the resistance (Lukatskaya et al., 2013). Therefore, in order to develop resilient MXene-built supercapacitors, another high capacitance, electro-chemically steady substance should be placed as positive potential in an asymmetrical cell. For instance, doping of MnO_2 in neutral or base electrolyte, or graphene doped with nitrogen under acidic electrolyte can function as positive potential.

Organic electrolytes can substitute the above aqueous solution. In comparison to aqueous electrolyte, the energy density ($E = 0.5CV^2$, for V-voltage window, E-energy density, and C-capacitance) for particular capacitance of organic solution will be greater owing to broadened voltage window. Moreover, it is worth mentioning that there will be variance in the performance of MXenes in aqueous and organic suspension. In addition, organic electrolytes exhibit high organic ions (tetrabutylammonium cation) which need to be infused with active conducting materials like CNTs, in order to enhance the performance rate and capacitance, owing to increased ion accessibility. For instance, great volumetric capacitance (325 F/cm^3) was demonstrated by

Nb_2CT_x–CNT film under lithium-ion capacitor arrangement (Anasori et al., 2017). Similarly, $Ti_3C_2T_x$–CNT film presented high capacitance (245 F/cm^3) under organic solution (Dall'Agnese, et al., 2016). Very recent, MXenes are found to exhibit superior performance under ionic-liquid gel solution in an electrochemical window of 3 V (Lin et al., 2016).

In a study examining mechanical behavior of MXenes under atomic force microscopy (AFM), it is revealed that the selection of cations define the response of MXenes (Come et al., 2015). Moreover, the nature of cation, exclusively ratio of charge to size, highly influences the film deformations. The interlayer arrangement of 2D $Ti_3C_2T_x$ films is not much affected by small cations with high charge. Conversely, their interlayer positioning will be significantly deformed by large cations with low charge. This can be instrumental in developing no-volume-change energy storage components during charging/discharging. Indeed, in order to achieve reduced energy dissipation with improved lifetime, it is highly desirable to have no-volume-change property of the material.

5.2 Challenges and Future Scope of Transparent SCs

The stability of MXene devices should be given much attention as the transparent SCs have outstanding charge storage and optronic characteristics. Also, appropriate storage of MXene films can improve their shelf life (Zhang et al., 2017a, 2017b). Besides, the MXenes performance rapidly falls down when exposed to ambient temperature as the MXene nanosheets are thermally unstable, causing their flakes to immediately oxidize. However, several issues like MXene shelf-life, metal contamination and degradation, and surface characteristics have to be further examined. The performance of MXene-derived SCs and TCEs can be enhanced by implementing efficient strategies like surrendering the outermost layer in order to protect the inner films, and/or infusing foreign elements onto the surface.

Moreover, as the MXenes fabrication process uses HF solution which is toxic, environmental-hazard and expensive, serious human and environmental safety concerns need to be taken care of. Presently, Ti_3AlC_2 in MAX phase is available at a whopping cost of approximately 550 USD/150 g powder (Zhang & Nicolosi, 2019). Further processing it into *m*- and *d*-MXene films and storage/maintenance would add additional cost to the production. This is the prime concern thwarting any MXene products to enter into the manufacturing field. The synthesis technique of delaminating MAX phase to MXene sheets is highly inevitable. Therefore, the HF or additional toxic etchants should be eliminated from the MXene fabrication, along with being economical. It is only possible to manufacture MXene-built transparent SCs or TCEs when the superior-class MXene sheets are available.

In addition to the economical and stability concerns, MXene-derived transparent SCs suffer performance challenges. Compared to C/A of transparent SC built of graphene/metal hydroxide (18 mF/cm^2 with $T = 40\%$), the C/A of MXene-built transparent SCs (1.2 mF/cm^2 with $T = 73\%$) was very lesser (Li et al., 2017). The

capacitance improvement techniques should be further developed. The charge storage features of MXenes can be enhanced by reinforcing it with additional pseudocapacitive nanomaterial like conducting polymers or metal oxides (Zhang et al., 2016). The FoM_e of $Ti_3C_2T_x$ MXene TCE is much lower (16) than that of CVD-built chemically-doped graphene TCE (195), which is extremely higher (Zhu et al., 2011). The MXene TCEs can replace graphene TCEs only when its FoM_e is highly enhanced. This can be feasibly obtained in two ways. Firstly, the junction resistance can be reduced by regulating the alignment of dispersions. Secondly, the charge mobility can be drastically improved by chemically doping the MXene nanoflakes. Overcoming the above issues like economical and stability concerns, and to-be enhanced electrochemical and optronic characteristics, MXenes can bring a revolutionary change in the modern technology.

5.3 Other Energy Applications

Batteries have been one of the most indispensible energy storage appliances. Because of their increased usage in electric automobiles and consumer goods, there should be continuous improvements. In general, Li batteries are highly stable with great energy density, possess high electronic conductivity and life cycle, and inexpensive (Goodenough & Park, 2013). Graphite has been one of the most preferred anodic materials in Li batteries since its inception, 1960. The graphite usually demonstrates high specific capacity (372 mAh/g) (Xiao et al., 2016). Though the performance of Mg, Al, K, Ni, and Ca batteries have been investigated so far, there is still a need for new materials to be developed for Li batteries. As MXenes possess high electrical conductivity, great storage capability, swift ion and molecule mobility, and less functional voltage, they are considered to be a viable associate to Li batteries. In a pioneering study, delaminated 2D Ti_2C MXene was synthesized through Ti_2AlC etchant and employed as an anode for Li batteries (Naguib et al., 2012). The newly fabricated material presented 10 times larger surface area in comparison with Ti_2AlC (MAX phase). Moreover, higher spacing between Ti_2C layers, weak bonding within the MX layers, and greater surface area can be the reasons for the five-fold increase in specific capacity (225 mAh/g) (Naguib et al., 2012).

For the energy storage purpose, MoS_2 2D heterostructures including conductive properties are used. A work computationally revealed that 2D MoS_2-MXenes have exhibited metallic features. Moreover, the specific capacity of the heterostructures is found to be very high (550 mAh/g at 50 mA/g current density). This phenomenon is because of the increased adsorption of Li_2S and Li during intercalation, which stabilizes the hetrostructures (Chao et al., 2017). In general, the layer restacking is prevented by organic molecules, which maintain the interlayer spacing. This spacing can be enhanced by infusing Glycine-MXene composites allowing Ti−N bond to form, increasing cycle life and charge storage capability. Besides, the capacitance of Glycine-$Ti_3C_2T_x$ hybrids (325 F/g at 10 mV/s) is measured to be double the

capacitance of pristine electrodes ($Ti_3C_2T_x$). This is because of reduced ion diffusion-resistance which is an outcome of improved interlayer spacing. Also, because of the broadened interlayer spacing, the electrodes were able to remain stable and exhibit consistent capacitance even after 20,000 cycles.

6 Summary and Outlook

In recent years, electronic commodities have been an integral part of our life. Moreover, the research and development of compact electronics have been exponentially increased. Development of high-performance TCEs has been instrumental in advanced technology. Though Indium tin oxide (ITO) has few setbacks like complicated synthesis processes, expensive and brittleness, it ruled the technical market over a period of time. It is very essential to probe the materials which could replace ITOs, treading in technical advances such as wearable, flexible, and portable electronic devices. Although conductive polymers probably serve the purpose, still they suffer limitations like translucent and environmentally unstable nature. In the area of TCEs, 1D silver nanowires or CNTs have proved to exhibit outstanding optronic features with great FoM_e. Nevertheless, the haze effect produced by high surface roughness in these TCEs is a prime concern.

Because of their distinctive characteristics of 2D materials, the worldwide research is attracted towards them. Mxenes, a new group of 2D materials find attractive in numerous global applications because of its unique features such as excellent electrical conductivity and copious surface groups. Owing to their marvelous charge-storage capability and excellent DC conductivity (approximately 9880 S/cm), $Ti_3C_2T_x$ Mxenes have been the most examined 2D material. Though the $Ti_3C_2T_x$ MXenes outperformed electrolyte-processed graphene in optronic features, still MXenes are distant to ITO performance. Lot of research work is conducted to develop $Ti_3C_2T_x$ as effective TCEs. Initially, the optronic properties of MXene nanolayers have been enhanced by raising the charge carrier transport. This can be successfully achieved by reinforcing psuedocapacitive materials to Mxene nanolayers or by chemical doping. Moreover, it is essential to understand the charge carrier mobility across the tunneling barriers. Furthermore, the effect of surface functionalities over the conductive features of MXenes should be assessed, along with optimization of the synthesis parameters. Eventually, the $Ti_3C_2T_x$ TCEs transmittance can be enhanced by rearranging the MXene nanosheet network. This essentially needs a lot of research on thin film fabrication techniques.

Conclusively, owing to excellent conductive properties like high lifetime, great power density, and extensive volumetric capacitance, MXene TCEs can be the best material for high-performance supercapacitors. Moreover, despite of the setbacks, due to the distinctive properties and the experimental results being encouraging, MXene TCEs would have potential opportunities in future.

References

Alhabeb, M., Maleski, K., Anasori, B., Lelyukh, P., Clark, L., Sin, S., & Gogotsi, Y. (2017). Guidelines for synthesis and processing of two-dimensional titanium carbide ($Ti_3C_2T_x$ MXene). *Chem of Materials, 29*(18), 7633–7644.

Ali, A., Belaidi, A., Ali, S., Helal, M. I., & Mahmoud, K. A. (2016). Transparent and conductive $Ti_3 C_2 T_x$ (MXene) thin film fabrication by electrohydrodynamic atomization technique. *Journal of Materials Science: Materials in Electronics, 27*(5), 5440–5445.

Anasori, B., Lukatskaya, M. R., & Gogotsi, Y. (2017). 2D metal carbides and nitrides (MXenes) for energy storage. *Nature Reviews Materials, 2*(2), 16098.

Anasori, B., Xie, Y., Beidaghi, M., Lu, J., Hosler, B. C., Hultman, L., Kent, P. R., Gogotsi, Y., & Barsoum, M. W. (2015). Two-dimensional, ordered, double transition metals carbides (MXenes). *ACS Nano, 9*(10), 9507–9516.

Apul, O. G., Wang, Q., Zhou, Y., & Karanfil, T. (2013). Adsorption of aromatic organic contaminants by graphene nanosheets: Comparison with carbon nanotubes and activated carbon. *Water Research, 47*(4), 1648–1654.

Bae, S., Kim, H., Lee, Y., Xu, X., Park, J. S., Zheng, Y., Balakrishnan, J., Lei, T., Kim, H. R., Song, Y. I., & Kim, Y. J. (2010). Roll-to-roll production of 30-inch graphene films for transparent electrodes. *Nature Nanotechnology, 5*(8), 574.

Becerril, H. A., Mao, J., Liu, Z., Stoltenberg, R. M., Bao, Z., & Chen, Y. (2008). Evaluation of solution-processed reduced graphene oxide films as transparent conductors. *ACS Nano, 2*(3), 463–470.

Berdiyorov, G. R. (2015). Effect of surface functionalization on the electronic transport properties of Ti3C2 MXene. *EPL (europhysics Letters), 111*(6), 67002.

Cambaz, G. Z., Yushin, G. N., Gogotsi, Y., & Lutsenko, V. G. (2006). Anisotropic etching of SiC whiskers. *Nano Letters, 6*(3), 548–551.

Cao, X., Yin, Z., & Zhang, H. (2014). Three-dimensional graphene materials: Preparation, structures and application in supercapacitors. *Energy and Environmental Science, 7*(6), 1850–1865.

Champagne, A., Shi, L., Ouisse, T., Hackens, B., & Charlier, J. C., (2018). Electronic and vibrational properties of V 2 C-based MXenes: From experiments to first-principles modeling. *Physical Review B*, *97*(11), 115439.

Chang, D. S., & Te Lai, S. (2015). Implementation of cross-generation automation transportation system in the TFT-LCD industry. *The International JouRnal of Advanced Manufacturing Technology, 78*(5–8), 753–763.

Chao, Y., Jalili, R., Ge, Y., Wang, C., Zheng, T., Shu, K., & Wallace, G. G. (2017). Self-assembly of flexible free-standing 3D porous MoS_2-Reduced graphene oxide structure for high-performance lithium-ion batteries. *Advanced Functional Materials, 27*(22), 1700234.

Come, J., Black, J. M., Lukatskaya, M. R., Naguib, M., Beidaghi, M., Rondinone, A. J., Kalinin, S. V., Wesolowski, D. J., Gogotsi, Y., & Balke, N. (2015). Controlling the actuation properties of MXene paper electrodes upon cation intercalation. *Nano Energy, 17*, 27–35.

Dall'Agnese, Y., Rozier, P., Taberna, P.L., Gogotsi, Y., & Simon, P. (2016). Capacitance of two-dimensional titanium carbide (MXene) and MXene/carbon nanotube composites in organic electrolytes. *Journal of Power Sources*, *306*, 510–515.

Dall'Agnese, Y., Lukatskaya, M. R., Cook, K. M., Taberna, P. L., Gogotsi, Y., & Simon, P. (2014). High capacitance of surface-modified 2D titanium carbide in acidic electrolyte. *Electrochemistry Communications, 48*, 118–122.

Dillon, A. D., Ghidiu, M. J., Krick, A. L., Griggs, J., May, S. J., Gogotsi, Y., Barsoum, M. W., & Fafarman, A. T. (2016). Highly conductive optical quality solution-processed films of 2D titanium carbide. *Advanced Functional Materials, 26*(23), 4162–4168.

Ding, L., Wei, Y., Wang, Y., Chen, H., Caro, J., & Wang, H. (2017). A two-dimensional lamellar membrane: MXene nanosheet stacks. *Angewandte Chemie International Edition, 56*(7), 1825–1829.

Eklund, P., Beckers, M., Jansson, U., Högberg, H., & Hultman, L. (2010). The Mn+ 1AXn phases: Materials science and thin-film processing. *Thin Solid Films, 518*(8), 1851–1878.

Gao, G., Ding, G., Li, J., Yao, K., Wu, M., & Qian, M. (2016). Monolayer MXenes: Promising half-metals and spin gapless semiconductors. *Nanoscale, 8*(16), 8986–8994.

Ghidiu, M., Lukatskaya, M. R., Zhao, M. Q., Gogotsi, Y., & Barsoum, M. W. (2014). Conductive two-dimensional titanium carbide 'clay' with high volumetric capacitance. *Nature, 516*(7529), 78.

Goodenough, J. B., & Park, K. S. (2013). The Li-ion rechargeable battery: A perspective. *Journal of the American Chemical Society, 135*(4), 1167–1176.

Halim, J., Lukatskaya, M. R., Cook, K. M., Lu, J., Smith, C. R., Näslund, L. Å., May, S. J., Hultman, L., Gogotsi, Y., Eklund, P., & Barsoum, M. W. (2014). Transparent conductive two-dimensional titanium carbide epitaxial thin films. *Chemistry of Materials, 26*(7), 2374–2381.

Hecht, D. S., Hu, L., & Irvin, G. (2011). Emerging transparent electrodes based on thin films of carbon nanotubes, graphene, and metallic nanostructures. *Advanced Materials, 23*(13), 1482–1513.

Heo, J., Kim, H., Her, N., Lee, S., Park, Y. G., & Yoon, Y. (2012). Natural organic matter removal in single-walled carbon nanotubes–ultrafiltration membrane systems. *Desalination, 298*, 75–84.

Hope, M. A., Forse, A. C., Griffith, K. J., Lukatskaya, M. R., Ghidiu, M., Gogotsi, Y., & Grey, C. P. (2016). NMR reveals the surface functionalisation of Ti_3 C_2 MXene. *Physical Chemistry Chemical Physics, 18*(7), 5099–5102.

Hoque, M. M., Hannan, M. A., Mohamed, A., & Ayob, A. (2017). Battery charge equalization controller in electric vehicle applications: A review. *Renewable and Sustainable Energy Reviews, 75*, 1363–1385.

Hu, J., Xu, B., Ouyang, C., Yang, S. A., & Yao, Y. (2014). Investigations on V_2C and V_2CX_2 (X = F, OH) monolayer as a promising anode material for Li ion batteries from first-principles calculations. *The Journal of Physical Chemistry C, 118*(42), 24274–24281.

Jun, B. M., Kim, S., Heo, J., Park, C. M., Her, N., Jang, M., Huang, Y., Han, J., & Yoon, Y. (2019). Review of MXenes as new nanomaterials for energy storage/delivery and selected environmental applications. *Nano Research, 12*(3), 471–487.

Khazaei, M., Arai, M., Sasaki, T., Chung, C. Y., Venkataramanan, N. S., Estili, M., Sakka, Y., & Kawazoe, Y. (2013). Novel electronic and magnetic properties of two-dimensional transition metal carbides and nitrides. *Advanced Functional Materials, 23*(17), 2185–2192.

Khazaei, M., Arai, M., Sasaki, T., Estili, M. and Sakka, Y., (2014). Trends in electronic structures and structural properties of MAX phases: A first-principles study on M_2AlC (M= Sc, Ti, Cr, Zr, Nb, Mo, Hf, or Ta), M_2AlN, and hypothetical M_2AlB phases. *Journal of Physics: Condensed Matter*, *26*(50), 505503.

Khazaei, M., Ranjbar, A., Arai, M. & Yunoki, S., (2016). Topological insulators in the ordered double transition metals M_2' M $''C_2$ MXenes (M′= Mo, W; M $''$= Ti, Zr, Hf). *Physical Review B*, *94*(12), 125152.

Khazaei, M., Ranjbar, A., Arai, M., Sasaki, T., & Yunoki, S. (2017). Electronic properties and applications of MXenes: A theoretical review. *Journal of Materials Chemistry C, 5*(10), 2488–2503.

Lai, S., Jeon, J., Jang, S. K., Xu, J., Choi, Y. J., Park, J. H., Hwang, E., & Lee, S. (2015). Surface group modification and carrier transport properties of layered transition metal carbides (Ti_2CT_x, T:–OH,–F and–O). *Nanoscale, 7*(46), 19390–19396.

Leng, Y., Guo, W., Su, S., Yi, C., & Xing, L. (2012). Removal of antimony (III) from aqueous solution by graphene as an adsorbent. *Chemical Engineering Journal, 211*, 406–411.

Levi, M. D., Lukatskaya, M. R., Sigalov, S., Beidaghi, M., Shpigel, N., Daikhin, L., Aurbach, D., Barsoum, M. W., & Gogotsi, Y. (2015). Solving the capacitive paradox of 2D MXene using electrochemical quartz-crystal admittance and in situ electronic conductance measurements. *Advanced Energy Materials, 5*(1), 1400815.

Li, J. R., Kuppler, R. J., & Zhou, H. C. (2009). Selective gas adsorption and separation in metal–organic frameworks. *Chemical Society Reviews, 38*(5), 1477–1504.

Li, N., Huang, X., Zhang, H., Shi, Z., & Wang, C. (2017). Graphene-hollow-cubes with network-faces assembled a 3D micro-structured transparent and free-standing film for high performance supercapacitors. *Journal of Materials Chemistry A, 5*(32), 16803–16811.

Lin, Z., Barbara, D., Taberna, P. L., Van Aken, K. L., Anasori, B., Gogotsi, Y., & Simon, P. (2016). Capacitance of Ti_3C_2Tx MXene in ionic liquid electrolyte. *Journal of Power Sources, 326*, 575–579.

Ling, Z., Ren, C. E., Zhao, M. Q., Yang, J., Giammarco, J. M., Qiu, J., Barsoum, M. W., & Gogotsi, Y. (2014). Flexible and conductive MXene films and nanocomposites with high capacitance. *Proceedings of the National Academy of Sciences, 111*(47), 16676–16681.

Lipatov, A., Alhabeb, M., Lukatskaya, M. R., Boson, A., Gogotsi, Y., & Sinitskii, A. (2016). Effect of synthesis on quality, electronic properties and environmental stability of individual monolayer Ti_3C_2 MXene flakes. *Advanced Electronic Materials, 2*(12), 1600255.

Liu, Y., Wang, W., Ying, Y., Wang, Y., & Peng, X. (2015). Binder-free layered Ti_3C_2/CNTs nanocomposite anodes with enhanced capacity and long-cycle life for lithium-ion batteries. *Dalton Transactions, 44*(16), 7123–7126.

Lukatskaya, M. R., Kota, S., Lin, Z., Zhao, M. Q., Shpigel, N., Levi, M. D., Halim, J., Taberna, P. L., Barsoum, M. W., Simon, P., & Gogotsi, Y. (2017). Ultra-high-rate pseudocapacitive energy storage in two-dimensional transition metal carbides. *Nature Energy, 2*(8), 17105.

Lukatskaya, M.R., Mashtalir, O., Ren, C.E., Dall'Agnese, Y., Rozier, P., Taberna, P.L., Naguib, M., Simon, P., Barsoum, M.W., & Gogotsi, Y. (2013). Cation intercalation and high volumetric capacitance of two-dimensional titanium carbide. *Science*, *341*(6153), 1502–1505

Mariano, M., Mashtalir, O., Antonio, F. Q., Ryu, W. H., Deng, B., Xia, F., Gogotsi, Y., & Taylor, A. D. (2016). Solution-processed titanium carbide MXene films examined as highly transparent conductors. *Nanoscale, 8*(36), 16371–16378.

Mashtalir, O., Cook, K. M., Mochalin, V. N., Crowe, M., Barsoum, M. W., & Gogotsi, Y. (2014). Dye adsorption and decomposition on two-dimensional titanium carbide in aqueous media. *Journal of Materials Chemistry A, 2*(35), 14334–14338.

Mashtalir, O., Lukatskaya, M. R., Zhao, M. Q., Barsoum, M. W., & Gogotsi, Y. (2015). Amine-assisted delamination of Nb_2C MXene for Li-ion energy storage devices. *Advanced Materials, 27*(23), 3501–3506.

Miranda, A., Halim, J., Barsoum, M.W., & Lorke, A., (2016). Electronic properties of freestanding Ti_3C_2Tx MXene monolayers. *Applied Physics Letters*, *108*(3), 033102.

Naguib, M., Come, J., Dyatkin, B., Presser, V., Taberna, P. L., Simon, P., Barsoum, M. W., & Gogotsi, Y. (2012). MXene: A promising transition metal carbide anode for lithium-ion batteries. *Electrochemistry Communications, 16*(1), 61–64.

Naguib, M., Kurtoglu, M., Presser, V., Lu, J., Niu, J., Heon, M., Hultman, L., Gogotsi, Y., & Barsoum, M. W. (2011). Two-dimensional nanocrystals produced by exfoliation of Ti_3AlC_2. *Advanced Materials, 23*(37), 4248–4253.

Peng, Y. Y., Akuzum, B., Kurra, N., Zhao, M. Q., Alhabeb, M., Anasori, B., Kumbur, E. C., Alshareef, H. N., Ger, M. D., & Gogotsi, Y. (2016). All-MXene (2D titanium carbide) solid-state microsupercapacitors for on-chip energy storage. *Energy and Environmental Science, 9*(9), 2847–2854.

Raad, M. T., Behnejad, H., & Jamal, M. E. (2016). Equilibrium and kinetic studies for the adsorption of benzene and toluene by graphene nanosheets: A comparison with carbon nanotubes. *Surface and Interface Analysis, 48*(3), 117–125.

Rakhi, R. B., Ahmed, B., Hedhili, M. N., Anjum, D. H., & Alshareef, H. N. (2015). Effect of postetch annealing gas composition on the structural and electrochemical properties of Ti_2CT_x MXene electrodes for supercapacitor applications. *Chemistry of Materials, 27*(15), 5314–5323.

Song, B., Xu, P., Zeng, G., Gong, J., Zhang, P., Feng, H., Liu, Y., & Ren, X. (2018). Carbon nanotube-based environmental technologies: The adopted properties, primary mechanisms, and challenges. *Reviews in Environmental Science and Bio/technology, 17*(3), 571–590.

Sun, S., Liao, C., Hafez, A. M., Zhu, H., & Wu, S. (2018). Two-dimensional MXenes for energy storage. *Chemical Engineering Journal, 338*, 27–45.

Tao, Q., Dahlqvist, M., Lu, J., Kota, S., Meshkian, R., Halim, J., Palisaitis, J., Hultman, L., Barsoum, M.W., Persson, P.O., & Rosen, J., (2017). Two-dimensional Mo 1.33 C MXene with divacancy ordering prepared from parent 3D laminate with in-plane chemical ordering. *Nature communications*, *8*, 14949.

Wang, K., Zhou, Y., Xu, W., Huang, D., Wang, Z., & Hong, M. (2016). Fabrication and thermal stability of two-dimensional carbide Ti_3C_2 nanosheets. *Ceramics International, 42*(7), 8419–8424.

Wang, Q., Guo, X., Cai, L., Cao, Y., Gan, L., Liu, S., Wang, Z., Zhang, H., & Li, L. (2011). TiO_2-decorated graphenes as efficient photoswitches with high oxygen sensitivity. *Chemical Science, 2*(9), 1860–1864.

Weng, H., Ranjbar, A., Liang, Y., Song, Z., Khazaei, M., Yunoki, S., Arai, M., Kawazoe, Y., Fang, Z., & Dai, X., 2015. Large-gap two-dimensional topological insulator in oxygen functionalized MXene. *Physical Review B*, *92*(7), 075436.

Xiao, Y., Hwang, J. Y., & Sun, Y. K. (2016). Transition metal carbide-based materials: Synthesis and applications in electrochemical energy storage. *Journal of Materials Chemistry A, 4*(27), 10379–10393.

Xie, X., Zhao, M. Q., Anasori, B., Maleski, K., Ren, C. E., Li, J., Byles, B. W., Pomerantseva, E., Wang, G., & Gogotsi, Y. (2016). Porous heterostructured MXene/carbon nanotube composite paper with high volumetric capacity for sodium-based energy storage devices. *Nano Energy, 26*, 513–523.

Ying, G., Kota, S., Dillon, A. D., Fafarman, A. T., & Barsoum, M. W. (2018). Conductive transparent V2CTx (MXene) films. *FlatChem, 8*, 25–30.

Yu, L., Shearer, C., & Shapter, J. (2016). Recent development of carbon nanotube transparent conductive films. *Chemical Reviews, 116*(22), 13413–13453.

Yu, M., Lin, D., Feng, H., Zeng, Y., Tong, Y., & Lu, X. (2017). Boosting the energy density of carbon-based aqueous supercapacitors by optimizing the surface charge. *Angewandte Chemie International Edition, 56*(20), 5454–5459.

Zhang, C., Anasori, B., Seral-Ascaso, A., Park, S. H., McEvoy, N., Shmeliov, A., Duesberg, G. S., Coleman, J. N., Gogotsi, Y., & Nicolosi, V. (2017a). Transparent, flexible, and conductive 2D titanium carbide (MXene) films with high volumetric capacitance. *Advanced Materials, 29*(36), 1702678.

Zhang, C., Beidaghi, M., Naguib, M., Lukatskaya, M. R., Zhao, M. Q., Dyatkin, B., Cook, K. M., Kim, S. J., Eng, B., Xiao, X., & Long, D. (2016). Synthesis and charge storage properties of hierarchical niobium pentoxide/carbon/niobium carbide (MXene) hybrid materials. *Chemistry of Materials, 28*(11), 3937–3943.

Zhang, C. J., & Nicolosi, V. (2019). Graphene and MXene-based transparent conductive electrodes and supercapacitors. *Energy Storage Materials, 16*, 102–125.

Zhang, C. J., Pinilla, S., McEvoy, N., Cullen, C. P., Anasori, B., Long, E., Park, S. H., Seral-Ascaso, A., Shmeliov, A., Krishnan, D., & Morant, C. (2017b). Oxidation stability of colloidal two-dimensional titanium carbides (MXenes). *Chemistry of Materials, 29*(11), 4848–4856.

Zhu, Y., Cao, T., Li, Z., Chen, C., Peng, Q., Wang, D., & Li, Y. (2018). Two-dimensional SnO_2/graphene heterostructures for highly reversible electrochemical lithium storage. *Science China Materials, 61*(12), 1527–1535.

Zhu, Y., Murali, S., Stoller, M.D., Ganesh, K.J., Cai, W., Ferreira, P.J., Pirkle, A., Wallace, R.M., Cychosz, K.A., Thommes, M., & Su, D., (2011). Carbon-based supercapacitors produced by activation of graphene. *Science*, *332*(6037), 1537–1541.

Zhu, Y., Sun, Z., Yan, Z., Jin, Z., & Tour, J. M. (2011b). Rational design of hybrid graphene films for high-performance transparent electrodes. *ACS Nano, 5*(8), 6472–6479.

Chapter 8
2D Metal Oxide Nanosheets—Electronic Applications Recent Developments and Future Prospects

Faisal Ahmad and Shamim Ahmad

1 Introduction

The feasibility of altering the physical, chemical, and biological properties of the nanostructured materials has already been established during the ongoing developments in nanoscience and technology in the recent past. The theoretical and experimental investigations carried out in this context, particularly, considered the quantum mechanical interactions at the molecular and atomic levels arising out of the modifications introduced in their internal structures, external surfaces, and topologies. Detailed theoretical predictions made using density functional theory (DFT)-based simulations have continuously been providing fairly reasonable assessment of their measurable properties. The recent theoretical investigations have been reasonably successful in analyzing the behavior of these nanospecies by taking into account a range of their crystal structures, chemical (stoichiometric), and topological features for estimating their associated optical, spectroscopic, mechanical, elastic, vibrational, and thermodynamic properties required in determining their 'structure–property relationship.' Having reached to this level of success, the proposed concept of synthesizing new materials under the category of 'materials by design' was naturally anticipated closer to their practical realizations, especially, with the help of current computational experiments predicting the associated crystal structures (Hasnip et al., 2014, p. 20130270; Erba et al., 2017, p. 5019). The simultaneous developments going on for improving the measurement capabilities of the required nanocharacterization tools have also been providing adequate support in probing the above-mentioned changes reflected in their properties with better precisions (Powers et al., 2006, p. 296; Lkhmayies, 2014, p. 28; Kumar & Kumbhat, 2016). Having characterized the

F. Ahmad
Iris Worldwide, Gurugram, Haryana, India

S. Ahmad (✉)
JCB University of Science and Technology, YMCA, Faridabad, Haryana, India

S. Singh et al. (eds.), *Advanced Applications of 2D Nanostructures*,
Materials Horizons: From Nature to Nanomaterials,
https://doi.org/10.1007/978-981-16-3322-5_8

physicochemicobiological properties of a large variety of low-dimensional nanomaterials (i.e., 0, 1, and 2D) supported by their theoretical analyses in detail, efforts are now continuing to synthesize materials using these nanostructured building blocks to inculcate the predetermined set of material characteristics under 'materials by design' approach mentioned above. After rigorous experimental validations of the physicochemicobiological properties of such synthetic materials with predictable functionalities through high precision measurement techniques available, the next step would be to translate the resultant technologies into a number of viable products by doing further refinements before moving on to their commercial exploitations (Kumar & Ahmed, 2017).

Despite the availability of a number of useful solutions of the outstanding problems of developing low-dimensional nanomaterials in the recent past, the syntheses protocols available still fall short of producing a predetermined type of nanoparticles, quantum dots, nanowires, and nanosheets of a particular morphology in a precisely controlled manner. Instead, some statistical fluctuations have invariably been observed there in most of these synthesis experiments conducted in this direction globally. The polydispersive nature of these nanostructured materials synthesized could possibly be one of the reasons of not having the desired type of new materials using these nano-entities as building blocks in a true sense. Thus, the ultimate objective of synthesizing 'materials by design' could not yet be realized properly excepting some preliminary attempts made in template-based self-assembly in a limited sense. Biomimetically motivated attempts also met some partial success, but all such methods are not yet ready for large-scale production in a practical sense (Ahmad, 2016, p. 1; Ahmad, 2017, p. 24).

In a parallel development of synthesizing mono-/multiple-layered nanosheets of newer materials from the layered/non-layered bulk crystals has rather been found more promisingly useful in producing pristine quality of atomic/molecularly thin sheets (i.e., of atomic and molecular sizes) of a large variety of technologically useful materials. These 2D nanomaterials, with regular planar/quasi-planar lattice structures involving in-plane covalent bonds, are noted to be very stable and rigid monolayers with the possibility of quantum confinement in the transverse directions due overlap of the atomic orbitals. However, the hybridization of these atomic orbitals directed away from the lattice plane often results in a 2D electron sheet-like arrangement offering unusually very high charge carrier mobilities. These 2D nanosheets with controllable energy band gaps were, thus, enabled offering a variety of nanomaterials ranging from semi-metals, to semiconductors, and to insulators. The possibility of changing the band structure and charge carrier transport properties in these single-layered and multilayered nanosheets offered unique opportunity of preparing chemically conjugated combinations involving a number of organic and inorganic compounds culminating into a large group of nanocomposites for their diverse applications accordingly as discussed by several authors cited in the enclosed references (Sun et al., 2015, p. 1250; Khun, 2015; Ahmad et al., 2018, p. 1).

2D metal oxide nanosheets are examined in this chapter for their possible applications in various sectors of electronics. Out of several such applications that are fast

emerging in this category, only few are discussed here, especially, for their technological applications as per the objective of this chapter. Various aspects of metal oxide nanosheets that make them unique in the field of electronic applications are discussed here with reference to their detailed analyses already covered in detail in various reviews published recently. Some of the recent developments are included later to support the emerging trends of these unique nanomaterials highlighting the current R&D status in this significantly important area. Citations of the large number of references are purposely reduced in number by using only those review papers/theses that cover more number of material aspects assuming that the interested readers would look into the cross-references therefrom. This, in no way, amounts to attaching any lesser importance to those not mentioned in the text explicitly.

2 General Features

The 2D nanomaterials, in general, are formed out of the identical layers of the atomic and/or molecular species organized in a 2D planar/quasi-planar lattice held together by weaker type of van der Waal's or ionic bonds. Comparatively much stronger in-plane chemical bonds that hold the constituent elements in the planar/quasi-planar individual layers, consequently, offer significantly higher mechanical strength compared to inter-layer interactions arising due to van der Waal's forces or ionic bonds resulting in the formation of the corresponding layered bulk materials. The constituent layers of either the neutral atoms or the polyhedral units are held together with weak binding forces in a van der Waal's crystalline solid. The numerous examples of such 2D nanomaterials include graphene and its derivatives, hexagonal boron nitride (h-BN), layered transition metal dichalcogenides (e.g., with general chemical composition of MX_2 where M = Mo, W, Ti, Zr, Hf, V, Nb, Ta, and Re; and X = S, Se, and Te) besides other chalcogenides such as telluride of Bi, and Sb and β-FeSe out of a much larger list of other emerging materials. The weak inter-layer binding energies of the van der Waal's solids facilitate their delayering by using mechanical or liquid exfoliation in a solvent (i.e., having appropriate surface tension or intercalation of molecules/atoms) followed by shear or ultrasonic agitations of the intercalated materials (Choi et al., 2016, p. 1445). In contrast, the layered ionic solids are the crystalline materials with charged polyhedral units interleaved with cationic or anionic species as seen in the negatively charged nanosheets of layered transition metal oxides. Their precursor compounds have negatively charged layers of corner and/or edge-shared BO_6 octahedral units (i.e., where B = Ti, Nb, Mn, Ta, W, or others) that are separated by the positively charged covalent networks. The precursor compounds like $Cs_{0.7}Ti_{1.825}O_4$, $KTiNbO_5$, $K_4Nb_6O_{17}$, $K_{0.45}MnO_2$, or $Cs_{6+x}W_{11}O_{36}$ are well-known material for their easier exfoliation properties (1C, 2018).

A technologically important family of perovskite compounds, chemically expressed as ABX_3, has been identified from the layered transition metal oxides in which X is an anionic member; A, and B are the larger, and smaller cationic species, respectively, and X is represented by O. It has been observed that almost

every element of the periodic table, except the noble gases, could be incorporated into some perovskite stoichiometry with an unit cell comprising of a 3*d* network of corner-sharing octahedral BX_6 type of units with A sitting in a cube of 8 units of BX_6 where A and B as 12 and sixfold X-coordinated members. A layered perovskite material is generally expressed as $M_m\,[A_{n-1}B_nO_{3n+1}]$, where $A_{n-1}B_nO_{3n+1}$ represents the basic layer and M belongs to the inter-layer cationic structure. The thickness of such a perovskite layer is determined by the n units of corner-sharing BO_6 octahedron (LP, 2018). These layered perovskites are of great technological interest with a wide variety of properties that are directly influenced by the structural changes that alter their crystalline symmetry, bond overlap, and energy levels. These perovskites possess another useful property of cation exchange of the inter-layer ions/structures. In this process of ion exchange, the chemical modifications introduce inside the inter-layer gallery at ambient temperature, without adding any changes in the host unit, imparts unique feature of facilitating easy exfoliation of the perovskite layers in the form of unilamellar nanosheets. Here, for instance, the protonation of the complex with inter-layer situated K^+ ions during acid treatment results into a composition of $HCa_2Nb_3O_{10}.xH_20$. These protons could, subsequently, be further exchanged with the bulky organic cationic species like tetra-*n*-butyl ammonium (TBA^+) in an aqueous solution to form $TBA_{1-y}H_yCa_2Nb_3O_{10}$. Such organic cations, being too large to compensate the negative charge from one oxide unit cell, do allow only part of the protons to exchange as can be seen from the stoichiometry mentioned earlier. Such exchange reactions being accompanied by a large volume of water cause further reductions in the interaction between two successive oxide layers. The resultant swollen phase easily separates into individual perovskite layers after a weak agitation involving mechanical stirring, shaking or ultrasonication. The process of proton neutralization by hydroxide counterions of TBA^+ being the main driving force behind this reaction, the degree as well as the quality of nanosheets, so produced, is mainly governed by the factors like composition, charge density, concentration, and the nature of the exfoliating agent or solvent.

These nanosheets of layered ionic solids are noted as excellent 2D building blocks for synthesizing tailored 3*d* assemblies involving different types of superlattices synthesized at molecular levels with designable functionalities. Another basic concept of low-temperature assembly of 'molecular beaker epitaxy' was introduced way back in 1990s by discovering the solution-based counterpart of gas-phase molecular beam epitaxy. These designed solids were, however, not possible to realize by thermodynamically driven, high-temperature solid-state syntheses. Continuing progress made, in this direction, by different groups till date could, thus, provide well-established protocols for synthesizing 2D crystalline multifunctional heterostructures deploying processes like flocculation, layer-by-layer (LbL) assembly using electrostatic sequential deposition and the Langmuir–Blodgett (LB) method. In addition, other wet-processing film fabrication techniques like spin coating or evaporation-induced self-assembly (EISA) could also be deployed successfully to create nanosheets and their heterostructures. Flocculation seems to be the simplest one to combine different types of nanosheets in which adding either oppositely charged nanosheets or the electrolyte like NaCl, was found destabilizing the colloidal

suspensions of these nanosheets. The inherent advantage of this particular approach of material synthesis not only included the fast speed but also the amount of the material synthesized. The heterostructures, so prepared, however, were found lacking the precise control over the layer structures, registry, and interfacial quality (Ziegler, 2015).

Having characterized the unique physicochemical properties of graphene- and graphene-related materials, it was natural to examine the other 2D nanosheets of inorganic materials, including transition metal dichalcogenides (TMDCs), metal oxides (MO), and hydroxides (MOH) in terms of their 'structure–properties relationships' for designing newer functional materials. Out of various types of inorganic nanosheets, those of the metal oxides were found technologically very important because of their unique functional behaviors including high k ferroelectricity, superconductivity, and magnetism. Delaminated oxide nanosheets (i.e., monolayers of molecular thickness) of $Ti_{1-\delta}O_2$, $Ti_{1-x}Co_xO_2$, MnO_2, and the perovskites were obtained from their layered precursors. These oxide nanosheets were found possessing the distinct advantages including their insulating, semiconducting, conducting, as well as ferromagnetic properties decided by their compositions and structures. For example, transition metal oxides of $Ti^{\delta+}$, Nb^{5+}, Ta^{5+}, and W^{6+} were all wide-gap semiconductors or insulators (Kim et al., 2016).

The theoretical and experimental investigations involving 2D nanosheets could open up the unique opportunity of using their mechanically strong microstructures combined with their improved electronic, optoelectronic, and piezoelectric properties for designing newer materials by stacking them together either vertically or by in-plane stitching/tiling based on their higher in-plane stiffness and bending flexibility. The weak inter-layer van der Waal's forces acting on the vertically stacked crystalline nanosheets could be used for its additional feature of layer number-dependent friction, super-lubricity, creasing, and spatial modulation of the elastic properties to name a few. Such novel properties of these nanosheets would certainly be important in manufacturing and integrating them in more complex multifunctional systems in future. The strong inter-dependences among their mechanical, thermal, electronic, and optical properties would certainly be deployed in finding more novel applications arising out of mechanics joining hands with the condensed matter physics in different ways. Moreover, the mechanical interactions between 2D materials and various substrates are equally important to take into consideration for their integrated device applications as observed by several authors of the enclosed references (Akinwande et al., 2017, p. 42; Androulidakis et al., 2018, p. 032005).

Based on these unique properties of transition metal oxide nanosheets, an effort has been made here to examine fast rising number of their electronic applications, especially by considering their mechanical stability along with improved charge carrier transport in single-/multiple-layered configurations along with their equally important optoelectronic interactions resulting into several novel features to be used in device fabrications.

2.1 Syntheses

A number of single-/multiple-layered nanosheets (i.e., individually atomically thin) with relatively larger lateral dimensions are currently being prepared in the form of sheets, plates, flakes, and platelets for their growing applications as available readily. The successful preparation of scotch tape-cleaved graphene nanosheets that were first isolated from the bulk graphite piece followed by other easier exfoliation processes developed later were found extremely helpful in characterizing their associated electronic, mechanical, and optical properties in detail. Simultaneously, a number of other 2D inorganic nanosheets were also studied side by side, including transition metal dichalcogenides, hexagonal boron nitride, metal oxides, layered double hydroxides as well as metals in addition to the extensive study of the graphene and its derivatives. A brief description of 'how these nanosheets are synthesized' is included here in the following.

Liquid exfoliation has been used quite often in producing metal oxide nanosheets from their respective layered precursors comprising of the layers those are internally covalent bonded chemically (in-plane) but interact only weakly with each other through van der Waal's or electrostatic forces as mentioned already. These weak inter-layer interactions were reduced further by ultrasonic treatment in a solvent that ultimately disintegrates them into the individual nanosheets. The solvent molecules, intercalated into the inter-layer spaces, were also found initiating expansion of the bulk crystal without restacking of them together. This method has been applicable in neutral-layered metal oxides precursors such as oxides of V, Mn, and Mo. For instance, V_2O_5-nanosheets were exfoliated by sonication of the bulk powder in formamide, whereas MoO_3 was delaminated ultrasonically from the MoO_3 powder in a number of solvents as well as treating MnO_2 in an aqueous surfactant solution (Cheng, 2016).

The process of osmotic swelling due to ion exchange was found causing delamination of the layered metal oxide precursors containing negatively charged layers, such as in $KCa_2Nb_3O_{10}$, $K_4Nb_6O_{17}$, and $KTiNbO_5$. For instance, $KCa_2Nb_3O_{10}$ was first protonated into $HCa_2Nb_3O_{10}{}^{-}1.5H_2O$ in an acidic solution followed by embedding of still larger size tetrabutylammonium (TBA^+) cations, which widened the inter-layer gallery further by weakening the inter-layer electrostatic attraction and facilitating the separations of the layers during sonication or mechanical agitation. Liquid exfoliation method has been a facile, low-cost, efficient, and scalable method for producing nanosheets although limited to only the layered inorganic compounds. In case of non-layered metal oxides, such as those of Ti, Zn, Ce, W, In, Sn, Fe, and many others, several other methods were developed and reported for producing their nanosheets as mentioned elsewhere (Cheng, 2016).

The target material is deposited on a template followed by its removal to produce the target material with the morphology of the template in a template-assisted preparation of nanosheets. Although, this method was initially developed for synthesizing one-dimensional metal oxide nanostructures, it was also extended to prepare 2D nanosheets with a 2D template in case of the non-layered metal oxides as

reported in the 'template-assisted oriented growth' of free standing half-unit-cell α-Fe_2O_3 nanosheets by depositing layered iron hydroxide on CuO nano-plates as template through slow Fe^{3+} hydrolysis. Freestanding iron hydroxide nanosheets were produced successfully after dissolving the template. Subsequent heat treatment of these nanosheets produced α-Fe_2O_3 nanosheets successfully (Cheng et al., 2014, p. 10,393). Alternately, the hydrothermal and/or solvothermal methods were used for preparing non-layered metal oxide nanosheets. Recently, an efficient method of preparing the transition metal oxide nanosheets of Ti, Zn, Co, W, Fe, and Mn, was demonstrated by autoclaving the mixture of polyethylene oxide-polypropylene oxide-polyethylene oxide (P123), ethanol, ethylene glycol and inorganic metal salts/alkoxides in which the P123 surfactant molecules could confine the growth of metal oxides along specific directions. These as-prepared metal oxide nanosheets were 1.6–5.2 nm thin with 2–7 monolayers stacked together with lateral dimensions in 100s of nm to several micrometers. Another example of synthesizing ultrathin sheets of $CeCO_3OH$ was reported by hydrothermal treatment of cerium chloride in the presence of sodium oleate as surfactant. Subsequent thermal treatment of freestanding $CeCO_3OH$ samples transformed them into CeO_2 nanosheets. The same method was also used in making porous ln_2O_3 nanosheets and atomically thin cuprous oxide nanosheets followed by CoO nanosheets by solvothermal treatment of Co $(acac)_3$ in ethylene glycol + water. The resultant CoO ultrathin nanosheets were converted into porous Co_3O_4 nanosheets after annealing them in air as discussed in the enclosed references (Sun et al., 2013, p. 2899; Gao et al., 2014, p. 205; Lei et al., 2014, p. 6826; Sun et al., 2014, p. 3313).

The oriented attachment followed by fusion of the nanocrystals was studied by placing the metal oxide nanocrystals to form monocrystalline metal oxide nanowires and layered nanosheets using nanocrystalline precursors. For instance, aging the aqueous dispersion of 4–5 nm thin WO_3 nanocrystals could produce 4–5-nm-thick single crystal WO_3 nanosheets of lateral dimensions in micrometers. In addition to nanocrystals, 1D nanowires were also fused together to form monocrystalline 2D nanosheets by the oriented attachment mechanism, as noted in producing monocrystalline nanosheets after soaking the pre-synthesized Eu_2O_3 nanowire bundles in water for long duration (Chen et al., 2012, p. 3372; Zhong et al., 2013, p. 10,355).

The natural tendency of the nanosheets to align parallel to the substrate during drying of the nanosheet dispersions was exploited in preparing various kinds of thin films involving drop-casting, dip-coating, and spin coating for achieving highly oriented nanosheets. Precise control of the resultant assembly was evolved through Langmuir–Blodgett (LB) and layer-by-layer assembly methods (Ma & Sasaki, 2010, p. 5082; Ma & Sasaki, 2015a, 2015b, p. 136). It became easier to have homogeneous and dense monolayer nanosheets thin films in LB depositions. These nanosheet thin films of varying thicknesses were produced via repeated depositions. This technique was widely deployed accordingly for the assembly of charge-bearing nanosheets prepared by liquid exfoliation. For example, highly ordered lamellar films with tunable thicknesses were prepared by LB deposition of exfoliated titania nanosheets of 10–30 μm lateral dimensions. The same technique was also used in depositing highly oriented multilayered films of $Ca_2Nb_3O_{10}$ nanosheets exfoliated

from $KCa_2Nb_3O_{10}$ on $SrRuO_3$ and Pt substrates (Akatsuka et al., 2009, p. 1097; Osada et al., 2010, p. 5225). In LB depositions of single-layered/multilayered thin films, the amphiphilic TBA^+ molecules when attached to the anionic metal oxide nanosheets start floating at the air–water interface. Further compression of the floating layer by reducing the trough area made the nanosheets to reorganize themselves into a perfectly packed monolayer thin films that were transferred to the substrate under appropriate surface pressure conditions. For instance, precursor was prepared by delamination of protonated $K_{0.8}$ $[Ti_{1.2}Fe_{0.8}]O_4$ in tetra butyl ammonium hydroxide (TBAOH) by stirring at room temperature followed by filtration, washing, and drying of $H_{0.8}$ $[Ti_{1.2}$ $Fe_{0.8}]$ $O_4.H_2O$ compound. The dilute stock of $H_{0.8}$ $[Ti_{1.2}$ $FeO_{0.8}]$ $O_4.$ H_20 in TBAOH in 4:1 molar ratio of OH^- and H^+ added to the LB trough for stabilizing the surface pressure before lowering the clean Si substrate. The surface pressure adjustment facilitated the coverage of clean substrate by monolayer film during its slow removal (Timmerman, 2015).

Another technique of nanosheet preparation employed the Iayer-by-layer assembly based on the sequential deposition of nanosheets and other materials with opposite charges on the substrate. It was a simple and effective method for preparing multilayer composite thin films comprising of polymer layers along with nanosheets. For example, multilayered thin films of MnO_2 nanosheets and poly(diallyldimethyl ammonium) (PDDA) were prepared sequentially by repeated dipping silicon wafer with cationic surface into the suspension of MnO_2 nanosheets and PDDA solution. It was also found that hetero-structured thin films comprising of TiO_2 and MnO_2 nanosheets could be produced by Iayer-by-layer self-assembly technique as reported elsewhere (Omomo et al., 2003, p. 2837; Sakai et al., 2008, p. 5197).

A number of 3*d* hierarchical architectures were produced for surface-active applications such as catalysts, lithium-ion batteries, and supercapacitors. These nanosheet assemblies were found important due to nominal surface area reductions during restacking or dense aggregation of the materials involved. Freeze-drying of metal oxide nanosheets containing colloidal suspensions could produce porous 3*d* networks of the nanosheets with much larger surface areas. For example, porous TiO_2 aggregates were prepared by freeze-drying of liquid exfoliated TiO_2 nanosheets in colloidal suspension followed by heat treatment. With great progress already made in synthesizing various kinds of metal oxide nanosheets, ample opportunities became available for building hierarchical superstructures for numerous surface-active applications (Sasaki et al., 1997, p. 602; Yang et al., 2012, p. 166).

A combination of protonation followed by larger organic molecule intercalations was found reducing the inter-layer electrostatic attraction that could particularly replace the slower processes of delamination observed earlier. In this process, the parent precursor is protonated in acidic solution enabling the entry of water molecules into the inter-layer spaces by ion exchange involving counterions present there. The structural features of these exfoliated nanosheets remained identical to those of the parent crystal although having a wide variation in their lateral dimensions. Solid-state and flux-synthesized $Ti_{0.91}O_2{}^{0.36-}$, and $Ti_{0.87}O_2{}^{0.52-}$ nanosheets acquired lateral dimensions in the range of 100–500 nm and 10 μm, respectively, and those of $MnO_2{}^{0.4-}$ and $Cs_4W_{11}O_{36}{}^{2-}$ were 0.45 and 2.2 nm thick, respectively. A variety of

shapes comprising of flat, corrugated, and step-type geometries were also reported in $MnO_2^{0.4-}$, $Nb_3O_8^-$, and $Ti_4O_9^{2-}$, respectively. Similarly, in-plane dense $MnO_2^{0.4-}$ nanosheets were found quite different from those of the TaO_3^- nanosheets with holes. Unilamellar 0.7-nm-thick ZnO sheets were exfoliated successfully using dodecyl sulfate ion intercalations. Thicker ZnO sheets (e.g., 10–40 nm) were produced in aqueous solution with phosphate anions. Similarly, thicker $BiVO_4$ nanosheets were hydrothermally grown from $Bi(NO_3)_3$ and NH_4VO_3 using sodium dodecyl benzene sulfonate (Kim et al., 2014, p. 4149; ten Elshof et al., 2015, p. 1,600,355).

Complex organic molecular intercalations via acid–base reactions were found producing faster swellings compared to the cases taking weeks to protonate $Cs_{0.54}$ ($Ti_{1.825}$ $Li_{0.175}$) O_4 into $H_{0.7}Ti_{1.825}O_4.H_2O$ (HTO). The other parameters like nature and concentration of the exfoliating agent, pH, and temperature along with the stirring conditions were found affecting the synthesis besides the counterion charge balancing and improving dispersion due to TBA^+ ions. In a systematic study, TBAOH was found better than the other analog such as TMA^+, TEN^+, and TPA^+ for improving the nanosheets dispersions. The swelling efficacies of these electrolytes including dimethyl ethanolamine (DMAE), tertiary amines (trimethylamine *N*, *N* dimethylethylamine,3-dimethylamino-1-propanol and *N*,*N*-dimethylbutylamine) and quaternary amines [tetramethylammoniumhydroxide (TMAOH), diethyldimethyl ammonium hydroxide (DEDMAOH) and tetrabutylammonium hydroxide (TBAOH)], were examined in terms of exfoliating $H_{0.8}[Ti_{1.2}Fe_{0.8}]O_2$. At $N/H^+ = 0.5$, maximum swelling of ~90 nm was noted in DMAE and the tertiary amines. In case of quaternary ammonium hydroxide, the maximum swelling occurred at a lower concentration of $N/H^+ = 0.3$. For TBAOH, the maximum swelling was ~98 nm. DMAE with higher polarity and smaller size, however, helped in stabilizing the swollen structures. Using species of lower polarity and more bulky sizes like TBAOH facilitated faster exfoliation by causing quicker crystal delamination. The *in-situ* measurements during TBAOH-assisted exfoliation in HTO showed that acid/base reactions annihilating the protons at the internal surfaces of titanate nanosheets while completing the process within seconds/minutes resulting in much faster OH^-/TBA^+ ions-based delamination. This process of fast acid/base reaction-based delamination using TBAOH was applied successfully to most of the layered metal oxides. TMAOH did better in place of TBAOH in exfoliating $W_2O_7^{2-}$ nanosheets. The complex nature of acid–base reactions involved in the above-mentioned processes of exfoliation still needs further study for better understanding of the mechanisms involved. Alternately, supercritical *N*, *N*-dimethyl formamide (SC-DMF)-assisted HTO exfoliation was realized via DMF intercalations. Moreover, sonication with controlled pH was also found helpful in producing the metal oxide nanosheets by first protonating $Bi_2CaNaNb_3O_2$ to form $H_{1.8}Bi_{0.2}CaNaNb_3O_{10}$ before delayering. A single-step synthesis of manganese oxide nanosheets was reported using solid-state synthesis instead of conventional approach of protonation and exfoliation. The hydrothermal synthesis was also found viable for producing molecularly thin nanosheets in quantity (ten Elshof et al., 2016, p. 1,600,355; Hu et al., 2012, p. 59; Sun et al., 2017, p. e1602629).

2.2 Characterization

Various physicochemical properties of metal oxide nanosheets were found changing with their morphology and crystal structures as discussed in the following to highlight their emerging importance in developing the future applications.

i. **Crystal Structure and Electronic Conductivity**

The crystal structure of the metal oxide nanosheets using advanced TEM revealed a number of effects that were found invariably present. For instance, some sort of structural collapse was observed because of the elastic nature of the TiO nanosheets caused by adsorptions of the organic molecules from the solution during syntheses. On the other hand, the $Ti_{1-x}O_2$ nanosheets formed out of $K_y(Ti, Li)_2O_4$ precursor showed higher concentrations of lattice defects due to Li-ion substitutions of Ti followed by their subsequent removal during protonation. Similarly, $Ti_{1-x}O_2$ nanosheets were prepared by converting $Cs_yTi_{2-y/2}Zn_{y/2}O_4$ precursor into $K_{0.8}Ti_{1.73}Li_{0.27}O_4$ followed by delamination of $Ti_{0.87}O_2$ nanosheets with lattice defects of Ti vacancies. Direct observation of atomic arrangements and Ti vacancies in titania nanosheets using low-voltage TEM combined with first principles calculations indicated the desorption of two oxygen atoms around each Ti vacancy, as reported in the enclosed references (Ohwada et al., 2013; ten Elshof et al., 2016, p. 1600355).

Estimating the electronic conductivity of nanosheets/assemblies is necessary for using them in preparing photovoltaic solar cell (PVSC) electrodes, Li-ion batteries, supercapacitors, and photo-catalysts. Poorer in-plane conductivity of these multilayered nanosheet films show insulating behavior as noted in case of $Ti_{0.91}O_2$ and $Ca_2Nb_3O_2$ sheets possessing non-ohmic behavior in comparison to those of RuO_2 and MoO_2 with varying conductivity. The sheet resistance of the RuO_2 and MoO_2 nanosheet films was estimated as 1 K and 35 M Ω/sq, respectively. It was further noted that the nanosheet conductivity was strongly influenced by the inter-layer presence/absence of organic quaternary ammonium ions and water molecules. For example, the presence of inter-layer octadecyl ammonium cations resulted in a resistive film, while the much shorter TMA^+ counterions facilitated forming the semiconducting films of $Sr_2Nb_2O_{10}$. Irreversible insulator-to-semiconductor transition was also noted during UV irradiation led decomposition of these complex organic molecules in these thin films. Moreover, the enhanced hydrophilicity after UV irradiation was more pronounced in Nb_3O_8 than in titania nanosheet films. The above-mentioned phenomenon of photo-induced hydrophilicity could produce reproducible structural changes in the titania nanosheets due to the presence of surface hydroxyl groups during protonation of the surface O atoms as concluded from the experimental data (Shibata et al., 2009, p. 12).

Controlling the phenomena of inter-layer charge separations was found feasible in the absence of inter-layer organic molecules of MnO_2–TiO_2 nanosheet multilayer assemblies. For example, a partial reduction of Mn^{1+} to Mn^{3+} was noted after optical illumination of the TiO_2 nanosheets. The excited electrons injected into the MnO_2 layer could reduce it to Mn layer. Similarly, UV irradiation-induced charge injection from $Ti_{0.87}O_2$ into GO was found increasing the electron concentration to 7.6 ×

$10^{13}/cm^2$ along with significant improvement in carrier mobility. The electrons/holes were assumed trapped in the titanate layers, and the removal of the UV exposure did not change the charge carriers in GO even for days. A colloidal system of semiconducting Nb_3O_8 nanosheets with MV^{2+} ions adsorbed on the clay nanosheets behaved like an electron acceptor allowing the stable formation of holes in Nb_3O_8 (ten Elshof et al., 2016, p. 1,600,355; Mei et al., 2018, p. 117).

ii. **Mono-/Multilayered Films, Superlattices, and Nanocomposites**

Negatively charged nanosheets prepared from the protonated tantalates, titanates, and niobates were used for producing mono-layered nanosheet films either by adsorption on a cationic polymer substrate or by layer-by-layer depositions of cationic polymer and anionic nanosheets. The non-cations sandwiched between titania nanosheets were, subsequently, removed via thermal/photo-catalytic decompositions accompanied by 1/3rd reductions in the inter-sheet distances. Similarly, unilamellar titania crystals ($Ti_{1-\delta}O_2^{4\delta-}$; $\delta = 0.0875$) and polydiallyl dimethyl ammonium chloride were layer-by-layer deposited onto various substrates resulting in efficient surface coverage with multilayered repeat distance of 1.4–1.7 nm depending on the surrounding humidity (Sasaki et al., 2001, p. 4661; Sasaki et al., 2002, p. 3524).

The presence of electrostatic attraction between negatively charged oxide nanosheets and amphiphiles was put to use in LB deposition of densely covered multilayered nanosheet films from accumulation of the amphiphiles at the liquid/air interface leading formation of barrier compressed monolayers (e.g., 97–99% packing density) transfer to various substrates. The liquid–air interface of LB deposition was replaced with hexane/water interface as demonstrated in case of $Ti_{0.91}O_2$, $Ca_2Nb_3O_{10}$ and $Ti_{1-x}M_xO_2$ (where M = Co, Ni, Fe)-based films on Au, ITO, and mica substrates though addition of ripples did help in increasing the interface concentration of nanosheets further. Densely packed exfoliated nanosheet films of $Ti_{0.91}O_2$, $Ti_{0.8}M_{1.2}O_2$ (where M = Co, Ni), $Ti_{0.4}Fe_{0.}6O_2$, and $Ca_2Nb_3O_{10}$ on solid substrates were reported using LB transfer without amphiphilic additives at the air–water interface with almost 95% surface coverage with minimum overlapping. This kind of LB transfer of the $Ti_{0.91}O_2$ nanosheet multilayered film was successfully carried out on substrates like quartz, silicon, ITO, and Au because of adsorption of the hydrophobic $Ti_{0.91}O_2$ nanosheets available at the air–water interface. The addition of tetra butyl ammonium bromide into the sub-phase could further assist in adsorption, causing an increase in the adsorbed amount of $Ti_{0.91}O_2$ nanosheets at the air–water interface (Muramatsu et al., 2005, p. 6590; ten Elshof et al., 2016, p. 1600355).

Micropatterning of the nanosheets was reported using 25 μm wide alternate lines of $Ti_{1-x}O_2$ and $Ca_2Nb_3O_{10}$. Such multilayered films were prepared from regularly shaped $Co(OH)_2$ nanosheets by tiling into a densely packed film due to the regular hexagonal shape of the LDH-derived crystallites that could be used in fabricating humidity sensors using these LB-transferred multilayered films. The conversion of Nb_3O_8 nanosheets films (LB) into a crystalline phase of $NaNb_3O_8$ was observed after Na^+ diffusion from the glass into the films, which was ultimately transformed into $NaNbO_3$ at a temperature >450 °C. LB-deposited multilayered films were employed as seed layers to direct the subsequent growth of functional oxide films as noted in

case of perovskite phase of $Ca_2Nb_3O_{10}$ nanosheets similar to $Pb(Zr,Ti)O_3$, $SrTiO_3$, $LaNiO_3$, $SrRuO_3$, and various others. Growing such functional oxides on top of a $Ca_2Nb_3O_{10}$ LB film by sol–gel or pulsed laser deposition could produce (001)-oriented growth with coherent interface between nanosheet and perovskite film. Similarly, hexagonal ZnO was grown on 2D hexagonal MnO_2 and $Cs_4W_{11}O_{36}$ nanosheets. In contrast, the $Ti_{0.87}O_2$ and MoO_2 nanosheets with different lattice parameters compared to those of the perovskites initiated (110) and (111)-oriented growth altering the film properties. On 10% covered substrates with $Ca_2Nb_3O_{10}$ nanosheets, one could grow (001) oriented epitaxial Nb-doped anatase TiO_2 thin films with lateral sizes up to 10 μm even with much smaller dimensions of the nanosheet seeds. Low-temperature phases were observed in case of growing ZnO directly onto nanosheets covered plastic substrates in which thermal anneal could crystallize the functional films. The LB layer and perovskite film could be deposited first onto a sacrificial substrate such as mica, after which the sheets along with the film were subsequently transferred to a thermally sensitive substrate for characterization and further uses (ten Elshof et al., 2016, p. 1600355).

Many 2D nanomaterials available in colloidal form are ultimately arranged in the form of thin films onto a substrate for realizing useful device structures. It is, therefore, necessary to develop a method of eliminating the inter-sheet gap/overlapping for realizing the multilayered films or superlattice structures. Neatly tiled nanosheets were also organized for such purposes in LB-deposited films. However, the formation of multilayered films by LB method is not up scalable as it is fairly complex and quite slow. Because of these limitations, the development of a simpler, faster, and industrially viable technique was evolved for this purpose as reported already elsewhere (Matsuba et al., 2017, p. e 1700414).

There are several advantages of using exfoliated inorganic nanosheets in hybridization experiments as highlighted here. For instance, almost full exposure of all the constituents in a 2D nanosheet gives rise to very strong interactions compared to those in NPs, QDs, NWs, and NTs. This feature of nanosheets could, thus, provide numerous opportunities of not only controlling the electronic structure and physicochemical properties of such nanostructured species but also in optimizing their functional properties during hybridization.

In a typically observed morphological similarity of inorganic exfoliated 2D nanosheets with those of graphene, strong interactions were expected to improve the functionality of inorganic solids via graphene conjugation. In addition, the self-assembly of the exfoliated 2D nanosheets and other nanostructured species could offer much wider synthesis techniques of stacked structures of sheet-like crystallites. Possibility of synthesizing a variety of mesoporous hybrid materials was also explored by reorganizing their micro-pores formed during intercalations of such hybrid materials. These hierarchical porous structures were found quite effective in improving their adsorption, and catalytic/electrochemical activities. The feasibility of changing the chemical compositions of the host precursors by cation and anion substitutions during their syntheses at elevated temperatures could make their

substituted derivatives in the form of layered materials possessing tunable chemical compositions and crystal structures with enhanced matching of their electronic structures in the hybridized forms.

Except the cationic nanosheets of layered double hydroxides, most of the inorganic nanosheets are negatively charged hydrophilic structures similar to rGO. The mixed suspension of the inorganic nanosheets and rGO could, thus, be used as an effective precursor for designing inorganic carbon hybrid nanocomposites, multilayer films, freestanding membranes, and so on. The exfoliated nanosheets with wider surface areas available for attaching diverse functional groups as well and the immobilization of many nanostructured materials made it easier to tailor their surface properties like hydrophilicity/hydrophobicity, surface charges, and surface structures leading to tunable functionality of these hybrid materials (Kim et al., 2014, p. 4149). A number of molecules, ions, nanoparticles, and nanosheets were accordingly sandwiched between parallel nanosheets. Sonication of $Ti_{1-x}O_2$ and MnO_2 in toluene could, for instance, produce amine intercalated compounds like $C_nH_{2n+1}–NH_2$, $Ti_{1-x}O_2$ and $C_nH_{2n+1}–NH_2$, MnO_2 that were further used for preparing composites like $[AlO_4Al_{12}(OH)_{24}(H_20)_{12}{}^{7+}(Al_{13})$ in this process. Layered hybrid compounds were, thus, synthesized involving electrostatic interactions of the nanosheets and the cations by mixing of colloidal solutions of anionic nanosheets to that of metal ions, biological species, and organic cations such as Cr^{3+}, Al_{13} ions, $Zn_2{}^+$, Ag^+, Co^{2+}, Au^{3+}, 1,1 '-diethyl-2, 2'-cyanine, $[(NH_3)_5Ru(iii)–O–(NH_3)_4Ru(iv)–O–Ru(iii)–(NH_3)_5]^{6+}$, and myoglobin proteins. The process of self-assembly could be initiated in some cases by cationic polymer like polyallyl amine hydrochloride (PAH) or polyethylene-imine (PEI). In many other cases, the presence of cations could produce hybrids consisting of intercalated metal oxides, metal nano-clusters, or nanoparticles. The layer-by-layer deposition of nanocomposite films was accomplished in many cases involving LDH-derived cationic $Co_{0.66}$ $Al_{0.34}$ $(OH)_2$ and poly(sodium styrene 4-sulfonate) polymers. Species like myoglobin and MV^{2+} could also be used in synthesizing electro-active hybrid materials enabling electron transfers from the nanosheets to the intercalated species under the influence of bias voltage or UV radiation (ten Elshof et al., 2016, p. 1600355). However, the inter-sheet incorporation of the nanoparticles has been found difficult in absence of electrostatic interactions. Intercalation of poly(allyl amine) into protonated calcium niobate ($HCa_2Nb_3O_{10}$) followed by addition of 2–6 nm diameter Au-NPs at high pH prevented the amine protonation leading to intercalated hybrid materials. Binding of metal oxide nanosheets to mesoporous silica-NPs was, however, not that easy as both systems were negatively charged at pH > 2. Subsequently, electrostatic binding of cationic species, and porphyrin derivative onto nanosheets, and silica-NPs, respectively could form hybrid films demonstrating photo-induced electron transfers. Similarly, titania nanosheet/nanoparticle-layered composites were prepared using a cationic polymer to enable favorable interactions between alternating nanoparticles/nanosheet layers. Nanocomposites of titania nanosheets and polymerized vinyl monomers were able to photo-catalytically decompose water molecules under UV radiation (>260 nm). In a follow-up study, an aqueous dispersion of titania nanosheets, when placed in a magnetic field (10-12 T), was noted affecting the nanosheets aligned perpendicular to the applied flux lines, in contrast

to other metal oxide nanosheets that aligned parallel to the flux lines instead. Using gelation or in situ polymerization, such structures could form hybrid nanocomposites with anisotropic mechanical properties as reported earlier (Bai et al., 2013, p. 12058; ten Elshof et al., 2016, p. 1600355;).

A variety of interfaces were formed during syntheses of a number of nanocomposites involving undoped/doped metal oxide nanosheets forming *p–n* junctions (e.g., titania nanosheet and CdTe@CdS-NCs), Schottky junctions (e.g., graphene/titania/titanium hybrid films), and heterojunctions (e.g., titania nanosheets onto rGO surface). CN nanosheets formed onto TiO_2–NPs demonstrated improved photo-catalytic properties especially due to enhanced generation and separations of electrons and holes under different conditions (Shang et al., 2014, p. 749; Bai et al., 2015; Li et al., 2016, p. 211, Xu et al., 2017, p. 2193; Merenda et al., 2018, p. 8154).

LbL deposition of nanosheet multilayers and heterostructures was successfully prepared using alternate layers of anionic nanosheets, and polycation like α zirconium phosphate or niobates. This process was extended in preparing other functional nanosheet multilayered films. Titania nanosheet films having >5 layers got transformed into anatase phase after thermal anneal at 400–500 °C. It was also noted that the crystallization temperature was found increasing with decreasing number of nanosheets, reaching to 800 °C for monolayer films followed by strong preferential growth of anatase along its *c*-axis.

Multilayered heterostructures were formed using LbL assembly of anionic metal oxide, and cationic LDH nanosheets such as ($Ti_{0.9}O_2$, $Ca_2Nb_3O_{10}$), and $Mg_{2/3}AI_{1/}3(OH)_2$, respectively. Mixing K^+ ion and anionic nanosheets induced flocculation resulting in dual-phase hybrids. A more viable technique of ensuring the alternate stacking of dissimilar nanosheets was shown by modifying one of the nanosheets prior to mixing with a cationic PEI for rendering it positively charged. The LbL deposition was found effective in preparing high-quality nanosheet multilayers of different components stacked on various substrates, e.g., $LaNb_2O_7$, $Ca_2Nb_3O_{10}$, and $Sr_2Nb_3O_{10}$. A multilayer powder of alternate $Ti_{1-x}O_2$ and W_2O_7 nanosheets was prepared showing enhanced photo-catalytic activity for methylene blue degradation (Osada & Sasaki, 2011).

iii. **Nano-tubules, Spheres, Shells, and Cones**

The process of curling up of as-formed nanosheets in a solution involving Nb_6O_{17} exfoliated from $K_4Nb_6O_{17}$ driven by strain relief in the asymmetric sheets could produce nano-tubular structures (i.e., 15–30 nm diameters, and 100–1000 nm lengths). Bilayers were formed by protonation of $K_4Nb_5O_{17}$ followed by TBAOH treatment yielding bilayer colloids initially in which two sheets were sandwiched with an intermediate layer comprising of K^+ and H^+ ions, which ultimately produced unilamellar sheets and tubules. These nano-tubules behaved as very active photocatalyst in dye-sensitized H_2 evolution. The symmetrical structure of tantalates without internal strain behaved differently than Nb_6O_{17}. Although, the driving force behind tubule formation was possibly the partial flocculation in NaOH resulting in partial substitution of TBA^+ that caused restacking of the nanosheets, but the gradual de-intercalation/extraction of Na^+-ions in water altered the local inter-sheet bonding

character, which could initiate rolling up of the peeled off nanosheets into nanotubes or other irregular structures. A similar process was also observed in symmetric MnO_2 and $Ca_2Nb_3O_{10}$ nanosheets could suggest this as a generalized process. Formation of scrolls in the absence of Na^+-treatment was observed in several cases but not in all tantalates and titano-tantalates (Rostamzadeh, 2016; Ji et al., 2018, p. 26).

The photo-catalytic degradation of hexavalent chromium using GO-ZrO_2 composite was shown using hydrothermally prepared ZrO_2 nanoparticles densely coated on the GO nanosheets that could enhance the photo-catalytic reduction with 98% removal rate under UV irradiation. The experimental results confirmed the improved efficacy of GO–ZrO_2 photo-catalyst because of increased light absorption as well as the reduction of photo-electron–hole pair recombination in ZrO_2 resulting in the highest removal rate. GO–ZrO_2 was thus found effective in Cr(Vl) removal from the wastewater (Prashanti & Damodharam, 2017, p. 256).

For synthesizing core–shell and hollow particles, LbL assembly of metal oxide/hydroxide nanosheet was reported on polystyrene and polymethyl acrylate beads (400–1300 nm diameter). Employing nanosheets instead of bottom-up condensation chemistries like sol–gel processing to coat these beads provided additional advantages of inducing more complete crystallization, avoiding destruction of mesoporosity, and stopping crack formation during crystallization, in which the nanosheet adsorption using cationic polymers could tune the surface charge density of the polymer beads. The embedded beads were removed by thermal annealing at 400 °C forming hollow shells with a smooth curvature and extremely thin crystalline walls (i.e., 5–20 nm). In several cases, the thermal processing could convert the nanosheets into a 3*d* metal oxide phase as well. Incorporating Al_{13} particles between the layers could, however, retard the phase transformation. Recently, block copolymer micelles of (styrene-b-2-Vinyl pyridine-b-styrene) were used as spherical templates. Other ways of producing hollow shells using nanosheets as building blocks involved during spray drying in which the water vaporization inside the droplet was found responsible for swelling of the droplets during drying. The dispersed nanosheets expelled to the outer aqueous crust by a bubble inside of the droplet could restack producing a thin solid shell upon drying (Xie et al., 2018). Other morphologies including nanocones, corrugated nanospheres, and large surface area flower-like nanostructures were prepared from the oxides of Zn, Sn, or Ti using hydrothermal syntheses to produce thickness in the range of 5–35 nm.

iv. Quantum Confinement, Excitons, and Electron–Hole Separations

It is necessary to know the energy band structure and the resultant charge carrier transport properties of the basic metal oxide nanosheets and assemblies including mono-/multiple layers, *p-n*/heterojunctions, and superlattice structures involving the pristine nanosheets before examining their usability in different electronic applications. DFT-based theoretical studies were found useful in providing information for their experimental validations in such nano-entities. Having these objectives under consideration, an effort has been made here to highlight the relevant aspects of the

investigations carried out for assessing the energy band structure and charge carrier transport in ultrathin 2D metal oxide nanosheets and the related structures as follows.

Preliminary assessment of the electronic properties of 2D nanosheets starts with determining the modified energy band structure of the nanoassembly under consideration involving both the contributions from the constituent lattice, and the discrete energy levels introduced by the hybridized atomic orbitals in the transverse direction. In addition, the electronic properties, so assessed, are also influenced significantly by the presence of atomic/molecular species close to the surface that adds environmental dependence. For instance, the concentration and mobility of the charge carriers in such nanoassemblies were particularly found modified by the adsorbed species as dopant, while charges and fields within the oxide nanosheets were screened by the counterions and the polarizability of the surrounding medium. The absence of the space-charge layers in 2D nanosheets led to anisotropic conductivity with enhanced in-plane charge carrier mobility, while supporting out of plane electron transfers (ten Elshof, 2017, p. 312).

Monolayer and stacked lepidocrocite TiO_2 phases were DFT investigated after validating the simulation technique by reproducing the known properties of the bulk TiO_2 (i.e., rutile and anatase phases) to ensure the reliability of the simulation results of their crystal/electronic structures, dielectric, and mechanical properties. The optimized structural parameters were, however, found agreeing well with the reported data of an exfoliated nanosheet of $Ti_{0.91}O_2$ or $Cs_{0.7}Ti_{1.825}O_4\underline{\mathbf{Vac}}_{0.175}$ (where $\underline{\mathbf{Vac}}$ = vacancy). Single-layered TiO_2 was found inferior in stability to rutile and anatase phases. The band gap of TiO_2 monolayer (3.15 eV) was larger than those of rutile and anatase phases due to a quantum size effect in a 2D structure with a thickness <1 nm (Sato et al., 2003, p. 9824).

The phenomena of insertion/extraction of the Li^+-ions into/from the nanosheet galleries were caused by the reduction/oxidation of the Ti^{4+}/Ti^{3+} ions in the titania nanosheet electrodes as observed during electrochemical and photoelectrochemical investigations of the self-assembled monolayer films of titania nanosheets onto ITO substrate. These processes caused reversible changes in UV–vis absorption of the titania nanosheet electrodes. The estimated fiat-band voltage and band gap were found as 1.3 and 3.84 eV, respectively. The onset potential for photocurrent generation from the titania nanosheet electrode was around −1.27 V, and the band gap energy estimated from the photocurrent spectra was estimated as 3.82 eV, in excellent agreement with the values obtained from the spectroelectrochemical data. The lack of difference in the band gap energies for titania nanosheets electrodes with varying numbers of layers suggested that a nanosheet was electronically isolated in multilayer assemblies without affecting the electronic states of the neighboring nanosheets (Sakai et al., 2004, p. 5851).

A comprehensive study of electronic structures of 51 semiconducting monolayers of TMDCs and oxides in 2H and 1 T hexagonal phases was carried out in calculating their band structures with spin–orbit coupling in GoWo approximation and compared to different DFT descriptions. The sensitivity of the band structures to the in-plane lattice constant was analyzed and rationalized. The dielectric function, effective electron and hole masses were estimated from the band structure for computing the

binding energies of the excitons in a 2D hydrogenic model as reported in the cited reference (Rasmussen & Thygesen, 2015, p. 13169).

The quasi-particle band structure, carrier mobility, and optical response of TiO_2 monolayer were studied in detail using many-body perturbation theory of GnWo + BSE calculations predicting a direct band gap of 5.3 eV in lepidocrocite TiO_2, different from the indirect band gap in anatase TiO_2 nanosheet. Because of the dispersive valence band maxima from the strong overlap between O-2*p* orbitals, a high hole mobility of 1069 cm^2/Vs was estimated for the lepidocrocite TiO_2nanosheets with significantly anisotropic behaviors in effective mass, mobility, optical response, and exciton binding energy. The strong anisotropic excitons were noted originating from the crystal-dependent effective mass in the lepidocrocite TiO_2 nanosheet due to asymmetric orbital overlaps (Zhou et al., 2018, p. 6449).

The underestimation of the bulk material band gaps in DFT simulation was noted as a major drawback of this technique in the context of developing methods for predicting correct band gap. Another approach known as Wannier–Koopmans method (WKM) was recently reported for predicting the band gap of extended 3*d* bulk systems. Though, WKM method has been successful in case of the isolated molecules, it was still not certain whether it would succeed in predicting the behavior of 2D nanomaterials that lie in between the 0D molecules and 3*d* bulk systems. WKM was, however, extended to 16 commonly known 2D nanomaterials indicating that the WKM predicted band gaps were on par with their GW calculated ones (Wong et al., 2018, p. 281).

Comparative phase stabilities of freestanding 2D TiO_2 monolayers formed out of octahedral (o), hexahedral (h), pentahedral (p), and tetrahedral (t) lattices of Ti–O blocks were reported based on first principle calculations recently indicating the variation of their enthalpies in the following order: o-ML (α) < h-ML (β) < t-ML (δ) < p-ML (γ). Except δ-phase, all other phases were found thermodynamically stable. The lepidocrocite-type multiple-layered sheets were found most stable freestanding 2D TiO_2 nanosheet configuration possessing full or partial band gaps in their phonon spectrum that could be the feature of phononic crystals. All these direct band gap semiconducting phases showed wider energy gaps > 3 eV. The order of their band gaps and thickness variations were noted as: o-ML (α-phase) > h-ML (β-phase) > *p*-ML (γ-phase). Comparatively better insulation and normal optical absorption properties were observed compared to the bulk state. The h-ML and o-ML phases possessed the strongest photo-catalytic reducibility and oxidizability, respectively (Wang et al., 2018).

Taking the example of titanium oxide nanosheets (e.g., $Ti_{1-x}O_2$, $x = 0.09$–0.13), the main contribution to the valence and conduction bands come from the interaction of 3*d* and 2*p* orbitals of Ti and O atoms, respectively, in the form of anti-bonding states. Taking into account the split in the conduction band due to octahedral oxygen ligand shell surrounding Ti at the center, the band structure of the oxide nanosheet could be assumed as 2*d* analog of the structurally similar 3*d* oxides. The calculated energy band structure of the stacked nanosheet monolayers was, thus, found similar to that of the anatase phase. The band gap of 0.75-nm-thick 2D titanate crystals was, for instance, found larger than that of the bulk. The experimental band gaps of $Ti_{1-x}O_2$

nanosheets, estimated from electrochemical, photochemical, optical characterizations, conductive atomic force, and STEM methods, fell in the range of 3.8–4 eV, compared to ~3.2 eV for the bulk. A difference of ~0.6 eV was reported between the band gaps of the protonated-layered titanates ($H_yTi_{1-x}O_2$), and their exfoliated 2D counterparts. The larger band gaps in nanosheets were attributed to the influence of quantum confinement in quasi-2D arrangements, although the additional influence of structural changes caused by exfoliation could not be ignored in the practical cases.

The characterization of valence electron energy loss spectroscopy (VEELS) was used in estimating the band gap of exfoliated $[TBA_xH_{1-x}] + [Ca_2Nb_3O_{10}]$ monolayer from the bulk $KCa_2Nb_3O_{10}$ with tetra-n-butyl ammonium hydroxide (TBAOH) intercalations. These anionic perovskite nanosheets surrounded by cationic ligands exhibited 2.9 eV band gap in the freely suspended samples with optical band gap >3.8 eV. The band gap of an individual monolayer was found practically unchanged compared to the bulk phase as observed in this study (Virdi et al., 2016, p. 11170).

However, attaching a monolayer of $C_{14}H_{29}–NH_3^+$ ions to the negatively charged surface of $Ti_{1-x}O_2$ nanosheet was found to increase its band gap by 0.22 eV. Dihydroxy-naphthalene (DHN) coadsorption onto $C_{14}H_{29}–NH_3^+$ was similarly found modifying the electronic structure of the $Ti_{1-x}O_2$ nanosheet. Accordingly, the doping of the anionic surface with different cations was noted modulating the nanosheet electronic properties. The XPS characterization could examine the possible changes that occurred onto the surfaces of ultrathin metal oxide nanosheets involving the different chemical states from the core atoms. The core levels of the elements like Ti (2*p*), Zn (2*p*), Co (2*p*), and W(4*f*) showed lower binding energies (0.5–2.0 eV shift) compared to those of the corresponding bulk crystals as the result of metal atoms gaining electrons from the surrounding oxygen atoms (e.g., converting Ti^{4+} into Ti^{3+} state). This could cause distortions in the crystal structure in the surface-dominated metal oxide nanosheets as predicted by DFT calculations. The metal atoms of ZnO nanosheet were found surrounded by higher electron densities giving rise to 'reduction' states compared to the corresponding bulk materials that introduced changes including new bond formations/breakings/distortions between the metal–oxygen atoms in the crystal structures reflected in the XPS state shifts. This kind of redistribution of the electron density and resulting electron transfer from metal atoms to O atoms was found leading to slightly reduced chemical states of the transition metal atoms in the 2D metal oxide nanosheets (Dou, 2016; ten Elshof, 2017, p. 312).

The energy band structures of the compounds ($A_{1-n}M_nO_{10}$; A = monovalent; A^0 = divalent; M = tetra/pentavalent cation) were found too complex to analyze. The DFT and impedance spectroscopy-based estimates of the band gaps and the flat band potentials of the layered perovskites nanosheets ($A_2M_3O_{10}$; A = Ca, Sr; M = Nb, Ta) were, although, found lower than their absolute values, but it did indicate the trend. The M-site cations when substituted exerted maximum influence on their electronic structures as they otherwise contributing to the conduction and valence bands. Comparison of DFT data of $Sr_2Nb_3O_{10}$ and $Ca_2Nb_3O_{10}$ nanosheets indicated that A-site cations influenced via the A-O bonds. The 0.35 eV difference in the band gaps of $Sr_2Nb_3O_{10}$ and $Ca_2Nb_3O_{10}$ could thus be attributed to the more ionic character of the Ca–O bond compared to the longer Sr–O bond. The larger size of Sr compared

to Ca possibly could distort the relaxation of the NbO_6 octahedron in the nanosheet, thereby leading to more delocalization of the excited states causing band gap reduction. Experimental optical band gaps in restacked protonated niobates nanosheets ($A_2Nb_3O_{10}$; A = Ca, Sr) showed a reduction of ~0.20 eV upon substitution of Ca by Sr.

The band gaps of $Ca_2Nb_3O_{10}$ (3.44 eV), $TiNbO_5$ (3.68 eV), and Ti_2NbO_7 (3.64 eV) nanosheets were found larger than those of their parent bulk materials prior to exfoliation, i.e., $KCa_2Nb_3O_{10}$ (3.33 eV), $TiNbO_5$ (3.51 eV), and Ti_2NbO_7 (3.56 eV). In contrast, the electronic structures and the optical band gaps of TMA-stabilized $Ca_2Nb_3O_{10}$ nanosheets and bulk $KCa_2Nb_3O_{10}$ were almost identical within experimental error showing practically no change during delamination. Taking simple estimate from the particle in a box model, $Ca_2Nb_3O_{10}$ nanosheet being 2 times thicker (1.44 nm) than titanate (0.7 nm) should have 1/4th of the titanate ΔE_G under similar conditions.

The applications of nanosheets in photovoltaic solar cells, photo-catalysts, supercapacitors and lithium-ion batteries have primarily been decided by their corresponding energy band structures. For instance, the semiconducting $T_{1-x}O_2$, $Ca_2Nb_3O_{10}$ Nb_4O_{17}, and MnO_2 nanosheets showed the energy band gap of titania nanosheet ($Ti_{0.91}O_2$) as ~3.85 eV against theoretically estimated value of 3.15 eV, which went up to 4.06 eV after absorbing the tetradecane amines ($C_{14}H_{29}$–NH_2). No influence of photochemical removal of organic polyelectrolyte confirmed that these nanosheets were isolated from the adjacent ones without affecting the electronic states in the neighborhood. The energy band structures of semiconducting nanosheet multilayered films of $Ca_2Nb_3O_{10}$, $TiNbO_5$, Ti_2NbO_7, Ti_5NbO_{14}, and Nb_3O_8 showed indirect band gaps between 3.44 and 3.68 eV during electrochemical and photoelectrochemical characterizations.

The conductivity of the single MnO_2 nanosheet was found higher than that of the $Ti_{1-x}O_2$ having direct optical band gap of 2.23 eV corresponding to the difference between Mn (3_d–t_{2g}) and Mn (3_d–e_g) states. This value was found smaller than expected from the thickness of MnO_2 (0.45 nm) and the effect of quantum confinement. The layered and intercalated parent compound (Na_xMnO_2) showed a direct and indirect band gaps of 2.7, and 2.1 eV, respectively. DFT modeling of the structure and electronic properties of bulk and single-layer MnO_2 exhibited tunable direct and indirect band gaps due to the nature of the intercalated cations including alkali, earth alkali, Zn^+, B^{3+}, Al^{3+}, Ga^+, Sc^{3+} and Y^{3+}. The influence of the counterions in distorting the edge-shared MnO_2 octahedron in the sheets, and the ordering of Mn (Ill) centers, made the indirect and direct band gaps to vary between 1.96–2.73 eV and 2.65–3.00 eV, respectively. Although the electronic structure of the MnO_2 surface layer differed only slightly from the bulk due to the subtle effects of Mn–O bonding and cation coordinations, loss of one of the prominent surface bonds effectively blocked an indirect transition present in bulk crystal, while promoting a direct one. The exfoliation of the bulk material into a monolayer, consequently, led to an indirect-to-direct band transition. In addition, the vacancy defect engineering could also be used in modifying the electronic structures of MnO_2 nanosheets further (Mei et al., 2018, p. 117). The band gaps of the compounds having compositions

of $Nb_xTa_{1-x}WO_6$ ($x = 0 - 1$) were modified from 3 to 5 eV by altering the Ta/Nb ratio, whereas the pure TaO_3 exhibited an even larger band gap. WO_3 nanosheets and platelets (i.e., 4–15 nm thick) exhibited band gaps in the range of 2.75–2.88 eV without noticing any significant influence of the quantum confinement on the degree of band splitting.

The phenomenon of exciton formations and electron–hole separations in 2D nanosheets has been of interest as compared to those in the corresponding bulk materials. For example, the photo-generated electron–hole pairs in titanate nanosheets were expected to be confined within the nanosheets as the estimated Bohr radius of an exciton (e.g., 0.37 nm) was only half of the thickness of a titanate nanosheet. Any electric field generated within the oxide nanosheet would thus be completely shielded from the ions present in the surrounding matrix in the absence of any space-charge layer. In a 2D system, therefore, electron and hole separations could only be allowed via in-plane diffusion or electron transfers to the adjacent nanosheet or the electrolyte species as noted in case of the photo-catalytic activity of the compound (TBA^+,H^+)-$Ca_2Nb_3O_{10}$ that was particularly attributed to the transfer of electrons or holes into the adjacent electrolyte. Similarly, the opposite process of electron injections from the adsorbed molecules into the conduction band of titanate nanosheets was also observed and reported (ten Elshof, 2017, p. 312).

The associated anisotropy and reduced dimensionality as well as the phenomenon of dielectric screening in 2D nanosheet assemblies were found responsible for supporting excitons, trions, and biexcitons. Subsequent further theoretical investigations confirmed the feasibility of higher binding energy excitations as a result of stronger many-body interactions. Moreover, the realization of a number of optoelectronics devices was also suggested including LEDs, lasers, and optical modulators. For instance, quasi-1D excitons and trions, observed in 2D phosphorene, were noted possessing much higher binding energies than those in the TMDC monolayers. Such experimental observations did confirm the formations of robust quasi-particles in anisotropic materials at room temperature. The role of extrinsic defects in phosphorene was found initiating localized exciton emissions in the NIR region that was also explored for optical communications. Future applications were particularly foreseen in realizing devices based on exciton–polariton interactions, polariton lasers, single photon emitters, and tunable light emitting diodes (Yuan et al., 2014, p. 856).

v. **Electron Transport**

The nature of inter-layer interactions was investigated during in-plane stacking of the nanosheets in LB depositions that were found giving the highest quality oxide films. The nanosheet films, such as $Ti_{1-x}O_2$, $Ca_2Nb_3O_{10}$ and TaO_3 were high k dielectric insulators compared to conducting sheets of RuO_2 and MoO_2. The higher conductivity of RuO_2 nanosheet was possibly due to basic conducting nature of rutile RuO_2. The layered forms of K and Na-doped nanosheets like $K_{0.2}RuO_2$ and $NaRuO_2$ exhibited the metallic behavior. RuO_2 and MnO_2 nanosheets together could improve the conductivity of MnO_2 stack for their use in supercapacitors. The RuO_2 nanosheets were found better than rGO due to their higher hydrophilicity that made

chemical interaction with MnO_2 better. In general, it was noted that LB-deposited (TBA^+-stabilized) multilayer films, or layer-by-layer deposited negatively charged nanosheets and positively charged polydiallyl-dimethyl ammonium ($PDDA^+$), were non conducting along the normal to the substrate because of the insulating layers present there between the consecutive sheets. This was, for instance, also confirmed in the thickness-independent band gaps of CaNbO/$PDDA^+$ multilayer films exhibiting clear isolations between the consecutive layers, which were reconfirmed once again by noting the thickness-independent UV–vis absorption intensity of MnO_2/PDDA multilayer films without any spectral change. Similarly, UV–vis absorption in multilayer films of $Ti_{0.91}O_2$ and MnO_2 nanosheets in different stacking orders was found dependent only on the total number of layers giving further evidence of inter-Iayer isolations as mentioned above. In another study, Zn–porphyrin complexes, embedded between the titanate nanosheet layers as visible light sensitizer, not showing any performance improvement was another proof in this context.

A number of experiments conducted independently did confirm the removal of the intervening organic layers either by heating the samples at elevated temperature or UV irradiation influencing the measured optical absorptions, and band gap reductions. Enhanced optical absorption intensity (>350 nm wave lengths) in the $MnO_2{}^+$ intercalated between $TaWO_6$ nanosheets was observed after heating the as-precipitated powder at 300 °C that led to possible hybridization of the 3*d*, 5*d*, and 4*f* orbitals of Mn, Ta, and W atoms accompanied by band gap reduction from 3.22 to 2.38–2.54 eV. Extensive UV irradiation experiments of the multilayer films not only confirmed the existence of excitons but also helped in oxidizing and eliminating the intervening organics without raising the temperature and enabling the protons to remain in the film as counterions. While measuring the impedance response of the titanate multilayer nanosheet films as a function of exposure to 280 nm UV irradiation, the trend of decreasing resistive component was attributed to the removal of $PDDA^+$ causing improvement in electron transfers. In another study, the relationship between the photo-catalytic activity of a multilayer titanate film and the UV intensity was shown to scale with the number of layers in the film, suggesting that photo-excited carriers formed in the internal part of the film could migrate to the surface and participate in the photo-oxidation reactions. Metallic nanparticles, intercalated between nanosheet layers, offered another method of improving the electron exchanges between two subsequent layers as observed in the improved electrode conductivity after using Ag (5 nm) and Au_{20} (5–15 nm) nanoparticles loading of MnO_2 used in supercapacitors in the following order $MnO_2 < Ag_2O–MnO_2 < Ag–MnO_2$.

The phenomenon of easier in-plane electron/hole transfers in the nanosheet films was put to use in enhancing the current extraction from the multilayer nanosheet films via edge connections than employing the top and bottom of the layers to the outer electrodes that resulted into a 2.5 times increased photocurrent in case of a 10-layer titanate film. This kind of improvement was observed despite the presence of large number of 2D grain boundaries in the lateral packing of nanosheet layers acting as resistive sites for the lateral charge carrier transport. Ohmic contacts were, accordingly, established between $Ca_2Nb_3O_{10}$ layers and PEDOT: PSS, while $Ti_{1-x}O_2$

and PEDOT: PSS showed a highly resistive and non-ohmic contact with an injection barrier. Further details of these observations summarized above were taken from the enclosed references (Yamaki & Asai, 2001, p. 2564; Sugimoto et al., 2003, p. 4092; Wang et al., 2003, p. 2873; Sugimoto et al., 2004, p. 4542; Shikano et al., 2004, p. 1214; Muramatsu et al., 2005, p. 6590; Saruwatari et al., 2005, p. 1999; Izawa et al., 2006, p. 4645; Sakai et al., 2006, p. 6198; Shibata et al., 2007, p. 2413; Akatsuka et al., 2007, p. 6730; Sakai et al., 2008, p. 5197; Akatsuka et al., 2009, p. 1097; Sato et al., 2010, p. 18049; Kim et al., 2011, p. 2700; Akatsuka et al., 2012, p. 12426; Chang et al., 2012, p. 20443; Itoh et al., 2012, p. 02BK13; Lin et al., 2012, p. 166; Zhang et al., 2012, p. 618; Ida et al., 2013, p. 23357; Wang et al., 2014, p. 2658; Ma & Sasaki, 2015a, 2015b, p. 111; Lee et al., 2016, p. 11786; Sharma et al., 2018, p. 1164).

A number of changes in the conductivity and UV photo-sensitivity were observed experimentally across the hetero-interfaces of different nanosheet assemblies primarily due to carrier transfers occurring from the orbital reconstructions and intimate contacts formed in the layered structures. Such charge transfers were reported in self-assembled $(Ti_{0.8}Co_{0.2}O_2/Ti_{0.6}Fe_{0.4}O_2)_n$ superlattices and the multilayers of alternating WO_x and $Ti_{1-x}O_2$, TaO_3, or Nb_3O_8 nanosheets in which the nanosheets were modified with alkenes/thiols groups and coupled by alkene-thiol click reactions, in which the C-chain lengths of the modifiers could vary the intersheet distances. The stacking of *p*- and *n*-type nanosheets could effectively produce the fully crystalline junctions without any amorphous intermediate layer. Further additions of graphene/GO/rGO to these nanosheet assemblies led to improved conductivity as noted in superior performance of the supercapacitor electrodes made out of rGO/MnO_2 nanosheets based heterostructures. Such improvements could be attributed to the high conductivity of the rGO, and the good pseudo-capacitance of the MnO_2 leading to large interfacial surface area with more intimate contacts offering efficient electron transfers. The theoretical prediction of semi-metallic behavior of the MnO_2/graphene/MnO_2 system is yet to be realized experimentally as discussed in the enclosed references (Jiang & Zhao, 2011, p. 6448; Osada et al., 2011, p. 6871; Mochizuki et al., 2014, p. 22968; Ida et al., 2014, p. 1872; Ano et al., 2016, p. 1111; Kishimoto et al., 2016, p. 73830; Zhang et al., 2016, p. 2119).

Photoconductivity of mono/multilayer titanate nanosheet films on graphene substrate and $(rGO/Ti_{0.87}O_2)_n$ superlattices could initiate irreversible reduction of the sheet resistance due to the combined effect of oxidative degradation of PDDA linker molecules present there between adjacent rGO and $Ti_{0.87}O_2$ sheets, and partial reductions of rGO during initial UV irradiation of the as-prepared rGO/$Ti_{0.87}O_2$ multilayer structures. The energetic electrons injected from the titanate phase into the rGO layers could produce highly conducting superlattices. The rGO component in $(rGO/Ti_{0.87}O_2)_{10}$ heterostructures showed n-type RT conductivity with high carrier density and mobility of $7.6 \times 10^{13}/cm^2$ and 0.22 cm^2/V s, respectively. Features like holes remaining trapped in the titanate layers, and the state of higher conductance remained there for several days even after removing the UV irradiation (Sun et al., 2012a, 2012b, p. 4518; Cai et al., 2014, p. 14419; Cai et al., 2015, p. 11436).

3 Electronic Applications

After discussing about the structural details of single-/multilayered metal oxide nanosheets, superlattices, and nanocomposites; synthesis protocols, and characterizations of their physicochemical properties; formations of various nanostructured species from these nanosheets, energy band structures, excitons, electron–hole separations and many other miscellaneous features, mentioned in the earlier sections, few electronic applications are described in the following.

3.1 Sensors

The compact and low-cost solid-state metal oxide-based gas sensors have frequently been used in monitoring the environmental pollutions and public health hazards, besides their many other industrial applications. Further improvements in their sensor performances were foreseen by incorporating morphological and structural changes in the basic materials at the receiving surfaces. The future developments, thus, need strong support from the first principle studies of various nanomaterials and their composites with super-sensitive detection capabilities along with fast responses and recovery features.

The polycrystalline and monocrystalline materials used in recent gas sensors have met the requirements of higher response and good stability, respectively, to a reasonable extent. In this context, the porous metal oxide nanosheets were found retaining their crystalline structure with relatively larger surface areas. Accordingly, porous monocrystalline nanostructured species turned out as the ideal gas-sensing materials as noted in monocrystalline SnO_2 nanowires that demonstrated both high sensitivity and long-term stability. However, the difficulty in large-scale synthesis of porous monocrystalline nanowires shifted the choice toward using nanosheets that were rather easier to synthesize in monocrystalline form along with lots of pores. For instance, porous ZnO nanosheets made after thermal treatment of ZnS $(ethylenediamine)_{0.5}$ exhibited higher pore density enabling the gas sensors exhibit good response and short response as well as recovery times with long-term stability (Sun et al., 2012a, 2012b, p. 2610).

A quick overview of the physicochemical properties responsible for gas-sensing characteristics of bulk materials like ZnO, NiO, and CuO could be taken as reference while discussing the related nanomaterials (Khun, 2015).

Porous MO resistive sensors operating at elevated temperatures (e.g., 300–450 °C) have been use since long for early warning of the gas leaks in homes. Further developments in this context have been related to including more number of gases such as H_2S, CO, NO_2, volatile organic compounds (VOCs), O_3, and others. Varying relative humidity has been interfering invariably posing a major challenge in making quality MO gas sensors.

MO semiconductors have been used in detecting gaseous analytes via surface reactions involving gas adsorption, impinging upon the active area and diffusing across the exposed surface, causing charge carrier transfers via surface reactions on the MO film experiencing adsorption, surface reactions, and desorption of the reaction products simultaneously leaving the surface. The whole sequence is, consequently, found affected by the gas surface adsorption–desorption processes, surface diffusions, and surface redox reactions. In the absence of a surface reaction assisting catalyst, gas diffusion alone decides the rate of response. The surface chemistry particularly involving interactions of either adsorbed oxygen species or oxidation of the reducing gases (e.g., alcohols, CO, hydrocarbons) or the adsorption of the oxidizing gases (e.g., NO_2, and O_3) induces the charge transfers, occurring between the adsorbed gas molecules and the semiconducting material during surface interactions that changes the sensor resistance. The charge transfer involved herein occurs partly in the conduction band and partly on the localized traps changing the surface conductance as a function of material reactivity, grain size, microstructure, free charge concentration, sensitive layer morphology, and the geometry. The charge transfer to the conduction band, for instance, produces a surface depletion layer at the semiconductor, to establish equilibrium between the trapping of the electrons in the surface states and their releases due to desorption and reaction with target gas. For instance, reducing molecules react with surface-adsorbed oxygen, leaving behind electrons that enhance the conductivity, whereas oxidation, occurring at the vacancy sites via adsorption of the oxidizing molecules, withdraws electrons depleting the conduction band causing conductivity reduction. Adsorption of the incoming gas molecules on the MO semiconductor surface causes negative change in free energy of the system, because the reduced translational freedom of the adsorbate once adsorbed. Adsorption proceeds from physisorption—the weak adsorption involving dipole interactions and van der Waals forces and leads to chemisorption—the strong bonding that causes charge transfer between gas molecules and the sensing film. Under thermal equilibrium, the process of gas adsorption increases with decreasing temperature. The physical adsorption of the gas molecules onto the surface of metal oxide occurs without a chemical change in the nature, geometrical structure, or change in the electronic structure of the gas molecule and the film surface. This occurs at the initial interaction of the gas molecules with surface comprising of electrostatic interaction between the adsorbates and the surface, described by van der Waals forces or dipole–dipole interaction. Physisorption is characterized by a high surface coverage at low temperatures (<100 °C) and low surface coverage at higher temperatures. Chemisorption has stronger bonding between the gas and the surface. Hydrogen bonding is another electrostatic interaction with binding energy between physisorption and chemisorption (~0.1 eV). The associated inter-molecular forces are composed of van der Waal's and covalent parts in a symmetrical or asymmetrical form. More detailed discussions on these energetic processes are available elsewhere (Bassey, 2014).

The reducing gas detection-based surface reactions at temperatures <500 °C, generally involve changes in the concentration of surface oxygen species O_2^-, O^- or O_2^- that act as stable electron traps. In case of an *n*-type MO semiconductor, the electrons, drawn from the ionized donors, reduce the carrier density at inter-granular

surfaces creating a potential barrier to the charge transport. The introduction of even a low concentration of a reducing gas like CO releases CO_2 and return the electrons to the conduction band. Within the normal operating temperature range of 300–450 °C, the predominant surface oxygen ions (O^-) result in increasing the conductivity related to the local concentration of the reducing gas. In case, such an *n*-type structure is exposed to small concentrations of an oxidizing gas, a competitive adsorption of molecules like NO_2 result in an increase in the density of charge carriers trapped at the oxide surface that decreases the conductivity. In a *p*-type MO semiconductor, oxygen adsorbed from atmosphere acts as a surface acceptor state involving extraction of electrons from the valence band increasing the hole concentration in the near-surface region (Bassey, 2014).

Employing low-dimensional nanostructured MOs in place of porous bulk material was found far better for developing thin film-based gas-sensing devices because of improved sensitivity and reproducibility witnessed during recent developments of conductometric sensors as discussed later.

A brief overview of synthesizing a large variety of nanospecies including nanowires, nanobelts/nanoribbons, sandwiched nanoribbons, nanosheets, nanodiskettes, nanoblocks, and nano-dendrites using powders of SnO/SnO_2 will be worth examining along with their crystal structures, morphology, growth orientations, and cross sections achieved therein. This information could be made use of in exploring the possible improvement in the sensor characteristics of nanostructured MO-based nanocomposites for preparing films for detecting still larger varieties of hazardous gases produced industrially. Some of the salient features are briefly described in the following from this angle (Dai et al., 2003).

A number of nanobelts/ribbons were synthesized from several MOs including oxides of Zn, S, In, Cd, Ga, and Pb. These transparent conductive oxides are now finding increasing applications in gas sensors, flat panel displays, and optoelectronic devices. Nanobelts (e.g., mm lengths, rectangular cross section with width-to-thickness ratio of 5–10) of rutile structure were found growing along (Sakai et al., 2008) direction. Rutile-structured SnO_2-nanowires were produced from layered Sn-foil/SnO mixture on a cold plate introduced into the system and were found structurally similar to nanobelts with a rectangular cross section along (Sakai et al., 2008) direction. SnO_2-nanowiress were invariably found straight though with broad range of diameters. Some of the high-pressure synthesized SnO_2 nanowires were of orthorhombic structure besides the normal rutile structure and were considered as a superstructure of rutile-type SnO_2. Orthorhombic SnO_2 nanowires were found growing along the [010] direction with rectangular cross section. Sandwich types of nanoribbons were synthesized with two 20-nm thick side layers along with 120 nm wide rectangular cross section of the core layer and smaller aspect ratio than that of the nanobelts. The nanoribbons of uniform width over their entire lengths had core, and side layers of rutile and orthorhombic structures, respectively. The surface of the SnO_2 nanoribbon edge was not flat on the atomic sale. Diskette-like nanospecies were also synthesized from SnO/SnO_2 powders under high pressure with typical diameters of 8–10 μm and thicknesses varying from several 10s to several 100s of nm. Each diskette was found having a single crystal tetragonal structure and out

of their two types, type-I was of uniform thickness with flat surfaces, while type-II diskettes possessed terraces and spirals culminating into a cone-like peak on the top. For example, in case the (001) surfaces of the SnO crystals were clean and the arriving droplets could wet the entire surfaces constantly during the growth, type-I diskettes were formed. In case of having some deposited impurity onto the diskette around which the cone peak could form, it resulted into type-II diskettes. In all these cases, the substrate temperature influenced the morphology and phase structures. In the low-temperature region, the deposited structures were found more complex. The SnO diskettes were, for instance, always found attached to the SnO_2 nanobelts. Raising the source temperature to 1100 °C at 500–600 torr pressure, a dendrite-like structure was found growing in the low-temperature region covering the SnO diskettes. These nano-dendrites were orthorhombic SnO_2 crystals, and the main and sub-branches were found growing along (Shang et al., 2014) and ± (Shang et al., 2014) directions, respectively. The processes, including hydrothermal, sol–gel, and precipitation techniques, facilitated synthesizing nanostructured metal oxides by converting the precursors into nanostructured species. The overall processing duration could further be reduced significantly using microwave heating. MO nanomaterials were produced in the form of nanoparticles, nanorods, nanosheets, 'flower-like' structures as well as core–shell types involving two oxide materials forming heterostructures (e.g., MO and rGO) in addition to that described earlier (Dai et al., 2003).

A second layer added to the mother oxide surface imparted better sensing properties, as reported recently, causing local changes in the electronic charges. Formation of 'heterojunctions' after decoration of the oxide surface with metal particles, and addition of a second oxide layer (e.g., either same as the base material or another semiconductor) could disturb the native charge distributions. Due to different Fermi levels of the two materials, the charge carriers could diffuse across the interface to establish equilibrium resulting in tuning of the surface response for specific gas detections.

Metal decorated SnO_2 surfaces with metal particle of Pt or Pd showed improved performance in gas detection after a dip in their aqueous salt solutions followed by heat treatment causing partial surface covered by hexagonally arranged monolayers. Creation of depletion layers due to the formation of Schottky junctions at the interfaces between the metal and MO layers caused by different work functions and the presence of a catalytic metal could also facilitate shifting the maximum response temperature to lower values. For instance, in CH_4 sensing, the maximum response temperature was reduced from 500 to 310 °C after Pt decoration in addition to reducing RH variations caused interferences. Au/Ag decorations were added, more recently, on a number of metal oxides improving particularly their low-temperature sensitivity. One study compared the effects of Pd and Ag decoration of SnO in place of SnO_2 showing good responses to H_2 and CO, but poor for NO_2, as they offered catalytic and electronic functionalization of the surfaces, respectively. The introduction of Ag–NPs to the surfaces of indium oxide nanospheres exhibited sensitivity toward NO_2 with 0.5 ppb minimum detection limit. The space-charge layers formed at the *n*-type MO semiconductors were modified after depositing a second n-type oxide layer permitting the electron transfers from the higher Fermi level side to that

with the lower one. Having proper combinations of the metals, either accumulation or depletion layers were formed in the backbone oxide in the two different configurations (i.e., *p*-type backbone modified with *n*-type materials or *n*-type backbones with *p*-type materials) used in gas sensors. Adding *p*-type material to *n*-type backbone could increase the sensor resistance by widening the space-charge layer close to *n–p* junction. It has been known, since long, that the addition of silver oxide could reduce the maximum response temperature of SnO_2 sensors for CO detection from 400 to 250 °C. In another study, sulfonated graphene + SnO_2 could eliminate the influence of varying humidity altogether. Promising results were reported using pairings like NiO/CdO and SnO_2/Ag_2O in low-temperature H_2S detection, with no interference from changing RH. The developments of MO nanocomposites for conductometric gas sensors, in the recent past, showed that with careful selections of the *n*/*p* material ratios and the composite structures at the nano-levels, highly sensitive heterostructures were realized for their reduced temperature applications.

Using impedance spectroscopy of the signal of MO-based gas sensors after AC excitation was also examined but with additional cost of the analytical set up. However, more recent developments in IC designs did offer better methods of signal extraction for improving selectivity and/or sensitivity including unambiguous gas detection signatures.

Better understanding of the changes occurring due to water adsorption during gas detection is expected to show better promises in future. The performance of ZnO sensors, for instance, was found affected significantly by water chemisorption causing an increase in the electron concentration due to the OH^- ions released after water dissociations. The reaction of the H^+ ions with the lattice oxygen forming hydroxyl group, creating O vacancies, and producing additional electrons affected its conductivity. A core–shell-type nanostructure of ZnO + silica, exhibited better ethanol response with only a minor degradation due to moisture at 56% RH. Finally, by taking care of the associated problems like interference and/or response distortions with varying RH, these MO sensors would certainly surpass the other sensors that had sensitivity limitations worsened by operating temperatures (Khun, 2015; Moseley, 2017).

While extending the usage of MO nanosheets in developing various kinds of high-performance sensors, as described above, it would not be out of place to add something briefly about yet another fast upcoming area of applications, particularly, in food processing, packaging and storage sectors as discussed in the following.

The controllable properties of MO nanosheets, synthesized and functionalized with numerous other molecular species, have started offering detection possibilities of toxins and volatile organic compounds produced in food stuffs during aging, and transportation besides helping in food processing, packaging, and the preservation-related industrial applications. Food packaging materials with antimicrobial properties causing oxygen scavenging, enzyme immobilizations, and mechanical strengthening, particularly, needed for enhancing the stability and shelf life of the food by offering protections against humidity, temperature, and other physiological factors. From these detailed considerations included in a recent review, some of the salient

features are discussed in the following for highlighting the roles of such sensors (Galstyan et al., 2018).

Oxides of Ti, W, and Zn were successfully put to use in detecting trimethylamine (TMA) formed during biodegradation of fish and animal products. Further functionalizations by introducing Cr^{3+} in 1D oxides of Zn, Cr and In heterostructures formed between *p*-type Cr_2O_3 and SnO_2 nanowires, and hierarchical heterostructures of α-Fe_2O_3/TiO_2 could improve the responses and recovery times as noted in enhanced response and selectivity of TMA detection. It is further expected to improve the performance of these sensors with better understanding of the processes involved.

The detection of NH_3 was used in determining the shelf life and spoilage of the other meat products and the oxide materials used there offered improved sensitivity by adding polypyrrole polymerized SnO_2 nanosheets and ZnO nanorods. Lower concentration of NH_3 were detected using *p–n* junctions formed at the interface causing enhanced interaction between the polypyrrole chains and the ZnO nanorods giving better charge transfer in the composite. Selective RT detection of NH_3 by these composites was realized in producing low power devices in which mixing of the oxides of Ti and Zn coupled to polyaniline, Au functionalized ZnO nanorods, and SnO_2/SnS_2 composites could improve their RT responses and selectivity with reduced recovery times. Monitoring the changes occurring in the fresh fruits and vegetables during their transport and storage employed the detection of VOCs by MO sensors. The detection of ethanol and acetone was achieved using oxides of Sn, Zn, Ti, Cr, W, Co, Ni, and In with different morphologies. It has been a general observation that the functionalization and introduction of specific dopants in above-mentioned nanostructured metal oxides could improve their responses, selectivities, and recovery times.

The recent development of oxide materials in the present context has been focusing on employing the nanostructures based thin films, with special purpose of improving the sensor performance at relatively lower operating temperatures in the prototype sensors. However, the formation of water molecules on the surface due to adsorptions of some reducing gases made it almost mandatory to operate these sensors at elevated temperature for stable and reversible responses. The objective of having accurate control of the structures, shapes, compositions, and dimensions of the nanostructured sensor elements would, thus, be a driving force in synthesizing newer nanomaterials, which will open up many unexplored possibilities for future sensing technologies in food quality control applications (Galstyan et al., 2018).

Nanoparticulate TiO_2 behaves as photo-catalyst and antimicrobial agent frequently used in food packaging for acting upon the food spoiling bacteria through lipid peroxidation leading to generating reactive oxygen species (ROS) under visible and UV irradiation, and DNA damage via hydroxyl radicals resulting in cell death. TiO_2 used in preparing bio-nanocomposites was used as the efficient packaging materials for various oxygen-sensitive food products as noted in case of TiO_2-based nanocomposite film as a packaging material for soft white cheese. The nanomaterials comprising of chitosan (CH), poly(vinyl alcohol) (PVA), and TiO_2-NPs (CS/PVA/TiO_2) exhibited strong mechanical properties for packaging with antimicrobial activities against gram ± ve bacteria, fungi, and coliform.

In another study, nanoparticulate ZnO, CH, and carboxymethyl cellulose (CMC) forming CH/CMC/ZnO nanocomposite was found useful in cheese packaging. The CS/PVA/TiO_2 bio-nanocomposite displayed hydrophobic property, and when used as a packaging material for soft white cheese, the moisture content of the cheese significantly increased with enhanced storage period. In case of CH/CMC/ZnO packaged cheese, the cheese texture cheese got reduced with the storage time and few changes were also reported as compared to the blank. These films affected the pathogenic microbes presented with 5–15 mm inhibition zones. A PVC/TiO_2 nanocomposite film exhibited an efficient food packaging property possessing adequate mechanical strength, and antimicrobial properties. A TiO_2-protein/polysaccharide nanocomposite film showed an antimicrobial action against the food pathogen bacteria *E. coli* and *S. aureus*, and maintained the quality and shelf life of cherry tomatoes when used as a coating material. By increasing the TiO_2 content in starch/TiO_2 bio-nanocomposite, its hydrophobicity was improved along with its better thermal, mechanical, and UV light-shielding properties.

Nanoparticulate TiO_2-blended low-density polyethylene (LDPE) films were noted maintaining the quality and shelf life of white shrimps by inhibiting the growth of spoilage bacteria besides lowering the polyphenol oxidase (PPO) activity, and slowing down the whiteness reductions, and water holding capacity. The ability of TiO_2 LDPE nanocomposite films was found effective against bacteria spoiling the fruits and vegetables. LDPE/clay TiO_2 nanocomposite films showed better mechanical and barrier properties, besides acting against microorganisms, which made them useful in horticulture product packaging. Similarly, mesoporous TiO_2/SiO_2 nanocomposites with different concentrations of NPs were found useful in ethylene degradation under UV exposure as a measure to ensure the shelf life of mature green tomatoes besides acting as photo-oxidative film for packaging the fresh fruits, vegetables, and postharvest management. Chitosan/TiO_2 nanocomposite films caused ethylene photo-degradation that helped in prolonging the life of tomato storage. Nanoparticulate TiO_2 was used in fabricating biodegradable nanocomposite films for preserving the microbial and sensory qualities of lamb meat storage. The combination of whey protein isolate (WPI)/cellulose nanofiber (CNF)/TiO_2-NPs/rosemary essential oil (REO) in a nanocomposite film was able to reduce the bacterial load containing food pathogens, and increasing the meat shelf life. Other biodegradable nanocomposite films that were fabricated by incorporating jackfruit filum polysaccharide (JFPS) TiO_2 nanoparticles displaying reduced moisture content, transparency, and total soluble matter possessing an excellent antimicrobial feature that was very useful for food packaging.

AgCl–TiO_2 nanocomposite could preserve fresh lettuce by affecting the bacteria as UV irradiation-induced charge carriers initiated redox reactions on the microbial cell surface. The paper packages containing Ag/TiO_2–SiO_2, Ag/N–TiO_2, Au/TiO_2, or Ag–NPs composites could extend the shelf life of white bread by inhibiting the growth of yeast, molds, and Gram + ve bacteria. The Ag/TiO_2–SiO_2 papers were the best out of the above-mentioned combinations. Polylactic acid (PLA) nanocomposite films (PLA/TiO_2 and PLA/TiO_2 + Ag) showed antimicrobial behavior by extending the shelf life of cottage cheese. TiO_2 + potato starch blended films could reduce water

solubility, water vapor permeability, and moisture uptakes. Soybean polysaccharide-based (SSPS)/TiO_2 bio-nanocomposite showed heat-sealing and biocidal properties desirable in many food coating and packaging materials. Other TiO_2-based nanocomposites films including fish gelatin/agar with TiO_2, wheat gluten/cellulose nanocrystal (CNCs)/TiO_2 nanocomposites, and TiO_2/LDPE films assured food safety and quality. A chitosan-TiO_2 nanocomposite could protect red grapes by extending their shelf life. Wheat gluten, nanocellulose, and TiO_2-NPs-coated paper sheets found very useful packaging applications.

It is worth noting that the above-mentioned nanocomposites showed better mechanical properties and enhanced hydrophilicity besides being efficient against both Gram +ve/−ve bacteria. Similarly, TiO_2- and Ag-doped-TiO_2–NPs showed photo-catalytic antibacterial properties under visible light irradiation in which TiO_2 offered a good supporting material for doping of Ag-nanoparticles (Galstyan et al., 2018).

A 2D molybdenum trioxide (MoO_3) FET-based biosensing platform was reported using bovine serum albumin as a model protein along with conduction channel of nanofilm of 2D α MoO_3 nanoflakes ($\leq$2.8 nm thickness). The response time was reduced to <10 s offering a competitive solution for future biosensing applications (Balendhran et al., 2013).

A. Energy Harvesting and Storage

The unique physicochemical properties of the 2D MO nanosheets have been put to use in finding extremely useful applications in various fields. Some of the cases of common interest are discussed here in the following with special reference to their uses in energy harvesting and storage to highlight the extraordinary importance of their advanced features in various other fields of industrial importance as well.

I. Li-Ion and Other Batteries

The current demands of mobile electronics and electric vehicles need high-quality rechargeable LIBs, with higher capacity, enhanced rate capability, long cycle life, and higher stability. Besides using graphite anodes, the transition metal oxides (TMOs)-based anodes are currently showing alternative promises because of their higher theoretical capacity. Metal oxide anodes, however, have low rate capability and poor cycling stability due to inherently poor electronic conductivity, slow reaction kinetics, and severe volume expansion during repeated discharge–charge cycles. Graphene, on the other hand, possessing large surface area, higher intrinsic electrical conductivity, and excellent mechanical flexibility, is being incorporated more to enhance electron transfers, accelerate reaction kinetics, and alleviate volume expansion, thereby leading to improved electrochemical performance.

The strong affinity between two types of layer-by-layer deposited nanosheets makes the TMO/graphene composites as an effective architecture for LIBs. However, the insufficient coupling is still relatively small fraction of surface atoms of MOs bonded with graphene. Recently, 2D inorganic graphene analog (IGAs) with single/few layer stacking are proving as better alternatives with structural disorder

on their surfaces, produce increased density of states near the Fermi level, leading to improved electrical conductivity and accelerated reaction kinetics. They possess, in addition, a large percentage of coordinated unsaturated surface atoms that after hybridizing with graphene involving more carbon atoms through oxygen-containing functional groups achieve enhanced synergistic coupling. Therefore, it is necessary to develop an ideal nanostructure of 'atomic layer-by-layer' transition metal oxide/graphene to deliver high-performance LIBs.

In this context, mesoporous Co_3O_4 nanosheets/graphene composites (ATMCNs-GE) were successfully developed and employed as anode material, delivering high discharge capacities of 2014.7 and 1134.4 mAh/g at 980 and 2000 mA/g, respectively. These features exhibited ultra-long cycle life and enhanced cycling stability with 92.1% capacity retention after 2000 cycles, surpassing the performances of bare ATMCNs and any existing Co_3O_4/C (i.e., graphene, carbon nanotubes, and porous carbon) composites. Such performance was attributed to the atomic thickness and mesoporous nature of Co_3O_4-nanosheets providing adequate electrode/electrolyte contact and shortened lithium-ion diffusion lengths along with higher electrical conductivity, and flexibility of graphene for enhanced electronic/ionic transportation and improved stability. Extra lithium storage was achieved due to higher specific surface area with abundant surface atoms; mesopores, grain boundaries, edges, and defects in the Co_3O_4 + graphene composites. The unique atomic layer-by-layer deposited structures in which Co_3O_4 and graphene acted as Li^+ and electron accepting phases, respectively, provided excellent lithium storage (Dou, 2016).

A generalized method of scalable synthesis of cobalt-/nickel-based oxides/hydroxides was reported replacing the existing methods with several shortcomings observed during the study of sodium and lithium storage capabilities of Co_3O_4 nanosheets. The excellent rate capabilities and cycling performances observed in case of 2D cobalt-/nickel-based hydroxides/oxides were also expected to have applications in supercapacitors, electrocatalysis and other energy storage/conversion fields (Zhang et al., 2016, p. 18060). The uniform hexagonally layered morphologies of α-NiOH and NiO were produced solvothermally for lithium storage in NiO nanosheets accompanied by high charge capacity of 1109 mAh/g (66% efficiency). The NiO–NS-based electrodes showed excellent cycling stability and high specific capacity of 1314 mAh/g and sustaining 99% efficiency over 60 cycles. $NiCo_2O_4$ nanosheets, possessing a higher electrical conductivity than NiO and Co_3O_4, found better uses in energy storage/conversion and catalysis applications.

A flexible morphology of $NiCo_2O_4$ nanosheets was synthesized from $Ni(OH)_2$–$Co(OH)_2$ precursor and as-prepared $NiCo_2(OH)_6$ got converted into cubic $NiCo_2O_4$ after 300 °C anneal. $NiCo_2O_4$nanosheets based electrodes showed stable cycling performance for lithium storage, delivering 1346 mAh/g during the 60th cycle at 200 mA/g. For the synthesis of cobalt hydroxide and Co_3O_4 nanosheets, a solution consisting of 1.8 mMol $Co(NO_3)_2{\cdot}6H_2O$ and 3.6 mMol hexamethylene tetramine (HMT) dissolved in 16 mL DI water and 24 mL ethylene glycol (EG) produced a pink solution for autoclaving at 120 °C. Cobalt hydroxide nanosheets were obtained after freeze-drying of the final products for two days, and Co_3O_4 nanosheets were

produced by annealing the cobalt hydroxide in air at 300 °C. For synthesizing nickel hydroxide and NiO nanosheets, a similar procedure was used with a precursor of 1.8 mmol $Ni(NO_3)_2{\cdot}6H_2O$. For the synthesis of nickel/cobalt hydroxide and $NiCo_2O_4$ nanosheets, 0.6 mMol $Ni(NO_3)_2{\cdot}6H_2O$ and 1.2 mMol $Co(NO_3)_2{\cdot}6H_2O$ were used as the precursors accordingly (Zhang et al., 2016). Some recent developments of nanomaterial improvements for Li-ion batteries utilized the nanospaces in preparing high-performance electrodes are reported elsewhere (Abdel Hamid et al., 2017, p. 1,701,427; Minamisawa et al., 2018, p. 23).

It was generally observed that whatever new features were observed in other 2D nanomaterials, graphene did also offer something similar once examined in more detail because of its unique energy band structure that is easily amenable to chages incorporated therein. For example, graphene electrodes are ultralight, conductiing, and anti-corrosive and thus qualify as ideal alternative to Al or Cu foils in manufacturing batteries. A graphene electrode could, thus, be employed as both a nonmetallic current collector with/without adding a number of active materials resulting in binder-free, and self-standing anode without involving complex processing steps. Moreover, traditional batteries usually do not possess flexibility, miniaturization, and stimuli-responsive features, in contrast to the batteries involving graphene that could provide all the above-mentioned functions. For instance, graphene electrodes with superior structural stability against repeated deformations due to their unique mechanical strength, are promoting extensive R&D efforts to produce graphene-based batteries with flexible, compressible, or stretchable functions. Moreover, 3*d* printing of colloidal solution of graphene sheets might be used in fabricating interdigitated and arrayed electrode structures that might offer significant ease in fabricating the microsized batteries that are difficult to realize via conventional methods. In addition, graphene electrodes, being responsive to a range of stimuli-like electrical field, mechanical strain, pH, temperature, and gas/bio-molecules, graphene-based materials, are certainly destined to be used in developing smart batteries of future (Ye et al., 2018).

For instance, wearable and portable electronics applications in future would certainly need deformable batteries with flexible, foldable, and/or stretchable features. GF has been found useful as a flexible and conductive nonmetallic current collector to firmly anchor active materials to get rid of the problems with the conventional slurry-casting method of battery manufacturing. GFs would make batteries with outstanding deformability due to the excellent conductivity, flexibility, and compressibility. A thin, lightweight, and flexible LIB was reported using 3*d* GFs as conductive substrates to load a $Li_4Ti_5O_{12}$ (LTO) anode and $LiFePO_4$ (LFP) cathode that exhibited excellent cyclic stability in both the flat and bent states. An all-stretchable-component sodium-ion full battery (NIB) was reported to show good electrochemical and mechanical stability even after hundreds of stretch release cycles. The NIB was made using stretchable cathode (PDMS sponge/rGO/$VOPO_4$), an anode (PDMS sponge/rGO/hard carbon), gel electrolyte, and elastic substrate. This kind of battery maintained a steady energy output while stretched at 20 and 50% strain. A graphene-based microsize LIB comprising of 3*d* printed anode, cathode, and solid-state gel electrolyte with arranged interdigitated configuration was reported

recently involving LFP/rGO and LTO/rGO with a capacity of 100 mAh/g at current density of 50 mA/g. These observations confirmed the utility of rGO as a printable material that could be blended with various components to prepare microbatteries (Ye et al., 2018, p. 245).

Stimuli-responsive smart batteries are made to proact to the changes in the surrounding environments and offer electrical signals responsive to variations of pressure, moisture, light, temperature, and magnetic field that would be usable in numerous fields such as self-powered sensors, energy management, smart optical systems, and clinical diagnosis. Recently, a responsive zinc-air battery (ZAB) with energy management function was reported by sandwiching a KOH-based hydrogel electrolyte between Zn foil and a pressure-sensitive sponge electrode. By attaching RuO_2 nanoparticles to the surface of the solid-state electrolyte could catalyze the oxygen evolution during the charging process, and the ZAB could spontaneously, timely, and reliably control the power output in response to external pressure changes. During the compression state, the ZAB could, however, light up an LED. The dependence of energy output on external pressure showed that the output voltage increased with increasing pressure. When the ZAB was subjected to compressions at 4, 8, 16, and 32 times per unit of 50 s at a pressure loading of 140 kPa, the dynamic output voltage could remain stable and uniform at arbitrary test cycles without detectable variation (Ye et al., 2018, p. 245).

II. **Photovoltaic Solar Cells**

The metal oxide nanosheets are generally mixed with sensitizers and other photoactive phases for meeting the requirements in fabricating advanced photovoltaic materials. For instance, porous titania nano-hybrids prepared by mixing exfoliated titania nanosheets with TiO_2 nanoparticles led to an ICPE of 10.1%. Normally, the electronic state of the neighboring nanosheets being unaffected, the connecting individual layers into a percolate network were found necessary to improve the conversion efficiency of the related solar cells. Several methods were proposed in this context. Concept of inserting conductive materials between semiconductor nanosheets was found useful for making lateral interconnects.

Metal oxide nanosheets have been investigated as electron transport layers (ETL) in multi-junction PV solar cell (MJPSC) fabrications. It was found that calcium niobate (CNO) nanosheets have properties useful for ETL that could enhance the efficacy of recombination stack. TiO_2 nanosheets were found improving the cell performance in an inverted MJPSC when employed as ETL and could reduce the leakage current, increasing the open-circuit voltage, and the fill factor. A system having TiO_2 nanosheets, cationic porphyrins ($MTMPyP^{4+}$; $M = H_2$, Zn, and Co) and MV^{2+} demonstrated longer living charge separations (i.e., half-life time >2.5 h). Similar stable charge separations were also observed in colloidal dispersions of inorganic layered niobate semiconductors and viologens. Moreover, it was found that nanosheets could modify and adjust the photochemical properties of the dyes via the electrostatic host–guest interactions in dye-sensitized solar cells. When Au nanoparticles were assembled with monolayer TiO_2 nanosheets into multilayer films, the

photoelectric conversion properties were enhanced due to the plasmon resonance of the Au nanoparticles on the TiO_2 nanosheets. Exfoliated MO nanosheets were used in dye-sensitized solar cells (DSSC) and multi-junction polymer solar cells (MJPSC) using $Ti_{0.91}O_2$ nanosheets for increasing the light scattering by forming a porous structure that increased the dye adsorption (Su et al., 2017).

The potential benefits of using graphene and its derivatives as well as TMDCs as electron and hole transport layers (E/HTLs) were examined recently in all solution-processed low-cost photovoltaic devices such as DSSCs, QDSSCs, OSCs and PSCs with not only very useful and comprehensive observations but also showing the future research directions as summarized below in brief (Wang & Sasaki, 2014).

Graphene in every layer of PV solar cell enabled alternative and facile fabrications although not surpassing its counterparts. TMDCs were, on the other hand, found as efficient E/HTLs in OSCs, though still lagging behind graphene in meeting the scalability and commercialization criteria for the third-generation high-efficiency solar cell production using solution processing resulting in long-term stability, low-cost manufacturing and compatibility with flexible substrates. Compatibility of the 2D nanomaterials with large-scale solution-based printing, along with work function tunability, and ambipolar charge carrier transport was found useful despite efficiency and stability issues being there to take care of. For instance, graphene photoanode as a highly conductive host backbone for DSSCs and QDSCs could facilitate their commercializations. The graphene and its derivatives with enhanced surface area and porosity demonstrated improved dye adsorption causing better charge extraction. Such materials could promote electron transport, retard charge recombination, and function as intermediate energy cascade materials that finally increased J_{SC} due to the optical scattering. TMDCs, being used only as Pt-free counter electrodes in DSSCs, when incorporated into photoanode, could also offer advantages due to higher carrier mobilities. In the perovskite solar cells (PSCs), graphene could provide faster charge transport and higher transparency. Considering the fact that low-temperature processing is essential toward having highly efficient flexible PSCs, the application of graphene and other 2D nanomaterials in OSCs has been widely explored in hole extraction and transport, where graphene is found quite competitive against PEDOT:PSS and metal oxides due to their excellent solution processability, work function tunability, ambipolar carrier transport, and improved stability. Unlike PEDOT:PSS that suffers from higher acidity and hygroscopicity, graphene is highly stable. Employing transition metal oxides with poor mechanical flexibility and needing high temperature annealing or vacuum deposition are not compatible with plastic and flexible substrates. Development of suitable surface modification techniques became necessary to render them compatible with large area solution-processable OSCs in future. Although GO offers higher solubility, its insulating nature does not allow forming good ohmic contacts. For preparing the electron extraction, graphene derivatives were mostly combined with state-of the-art metal oxides to improve the charge carrier mobility. Nonetheless, graphene MO composites still have to compete with the other highly efficient solution-processable materials, like poly[(9,9-bis(30 -(*N*,*N*-dimethylamino)propyl) 2,7-fluorene)-alt-2,7-(9,9 dioctylfluorene)], Ca and LiF. In the field of tandem OSCs, graphene offers higher transparency

and lower electrical and optical losses. The MoS_2 as OSCs inter-layers were found satisfactory as the efficiency obtained was comparable to PEDOT: PSS-based cells with added stability features. TaS_2, WS_2, and $NbSe_2$ were found as effective inter-layers with tunable work functions for good ohmic contacts. The materials like WSe_2, $MoTe_2$, and $MoSe_2$ could also be used as HELs within OSCs for better work function tuning. TaS_2 has to date been the only TMDC tested as EEL, though efforts are going on to insert MoS_2, or WS_2 with suitably located energy levels. TMDCs have not yet been used as charge transport inter-layers in PSCs. In DSSCs and QDSSCs, investigations have mostly been concentrating on doping the metal oxide scaffold with highly conductive graphene derivatives. The same principle was attempted with the graphene-like TMDCs. An alternate approach could use multilayered TMDCs considering that their optoelectronic properties were different from those of the pristine TMDC layers. In this context, band gap engineering of TMDs hetero-bilayers might provide further advantage in realizing efficient carrier extraction layers (Wang & Sasaki, 2014; Balls et al., 2016, p. 580; Wen et al., 2016; Xiong et al., 2018, p. 1768).

III. **Piezoelectric Energy Generation**

The piezoelectric and semiconducting properties of wurtzite family of crystalline materials brought a revolution in the field of energy harvesting recently. Lateral bending of a ZnO nanowire, for instance, could produce positive, and negative voltages on its tensile, and compressive strained sides, respectively.

Electrical energy generation in a piezoelectric material was noted to occur due to external forces induced disturbances in its crystal symmetry producing piezoelectric potentials. In case of ZnO, for instance, the layer-by-layer stacking of tetrahedrally coordinated Zn^{2+} and O^{2-} ions form an electric dipole due to separation of the charge centers of the cations and anions that gives rise to piezopotential once disturbed by the external force applied. Such a deformed crystal, when connected to an external circuit, allowed current flow after partial screening of the piezopotential, and establishing a new equilibrium state. Continuously changing dynamic straining affected in a piezoelectric nanogenerator (PENG) could produce a steady stream of current pulses through the external circuit. PENG power generation being dependent on the coupling of piezoelectric material, selection of the right material and appropriate structural configuration became the main concern in optimizing the energy harvesting in this process. A repeated bending and releasing of ZnO nanowire fixed at both the ends to the electrodes when placed laterally on a flexible substrate could produce a piezoelectric potential along the wire under uniaxial tensile strain enabling the electrons to flow along the external circuit in the form of alternating current pulses with open-circuit voltage and short circuit current of 20–50 mV and 400–750 pA, respectively.

The output power of PENG was enhanced significantly by integrating a large number of nanowires placed in parallel on a flexible substrate, e.g., an assembly of 700 rows (i.e., each row containing ≈20 000 lateral ZnO nanowires) could generate a maximum voltage and current of 1.26 V and 28.8 nA, respectively. The output

performance of PENGs was scaled up by transferring the separately grown vertically aligned ZnO nanowires onto a flexible substrate forming horizontal arrays (i.e., maintaining the crystallographic orientations) and interconnecting them with metal electrodes that exhibited open-circuit voltage and peak output power density of 2.03 V and 11 mW/cm^3, respectively. Capacitor-stored PENG electricity could run a commercial LED, demonstrating its potential for applications in electronic devices. In another alternate approach, a PENG involving composite structure was reported by dispersing conical ZnO nanowires onto a flat polymer film that generated a potential difference of 2 V at 50 nA between the top and bottom electrodes during mechanical deformations. Subsequently, high-output PENGs were realized using solution grown vertically aligned ZnO nanowires at 80 °C on a variety of substrates with sputter-coated seed layer to facilitate the growth of well-aligned nanowires forming a quasi-continuous film at low cost, and on large scale for applications. A fully flexible and transparent PENG involving vertically aligned ZnO nanowires was reported in 2009 in which a Schottky barrier at the interface between ZnO nanowires and the metal electrode, could control the electrons flow. Conductive SW-CNT network sheets were alternately used for contact electrodes that could not only improve the output current density significantly but also imparted exceptional durability and stability. Consequently, the combinations of graphene and ZnO nanowires could produce fully rollable and transparent PENG using epitaxially grown ZnO nanowires on graphene sheets in a solution growth technique producing output current density 2 μA/cm^2 with no fluctuations even after several times of device rolling.

A new alternating current PENG was reported using vertical ZnO nanowires arrays by coating a thin layer of PMMA on top of the ZnO film before depositing a metal electrode. The coupling of piezoelectric potential and electrostatic induction in a cyclic deformation resulted in the back-and-forth flow of electrons through the external load with a measured 20 V output at 8 μA current representing a maximum power density of 0.16 W/cm^3. Another super-flexible PENG was reported using 18 μm thin Al foil as the substrate and electrode, and this arrangement could also be used as an active sensor to detect the wrinkling of a human face. Under the blinking motion, the output voltage and current were measured to be 0.2 V and 2 nA, respectively.

Simple integration of NGs in parallel and series combinations could produce a maximum output voltage and current up to 3.2 V and 195 nA, respectively, when coupled with human walking.

A fiber-based PENG was prepared for converting vibrations into electricity using piezoelectric ZnO nanowires radially grown around textile fibers. A cyclic relative sliding motion between the two fibers could produce power output due to deflection and bending of the nanowires. A hybrid-fiber piezoelectric generator comprising of ZnO nanowires and PVDF coating on a conducting fiber could convert low-frequency mechanical energy into usable electricity as seen in placing a PENG device on a human arm, the folding-releasing motion of the elbow produced an output voltage, current, and power density of 0.1 V, 10 nA/cm^2, and 16 μW/ cm^3, respectively. In another version of flexible fiber NG based on carbon fibers that were cylindrically covered by textured ZnO thin films, when subjected to uni-compression under an

applied pressure, the thin film could generate a piezopotential across its inner and exterior surfaces giving an output peak voltage of 3.2 V and average current density of 0.15 $\mu A/cm^2$ (Fan et al., 2016).

In an experimental validation of piezoelectric energy generation concept, a 600 nm long ZnO–NW (50 nm diameter) was fixed at one end on a Si substrate with conducting epoxy and using AFM tip to create positive and negative strains for measuring the corresponding potentials with respect to grounded end contact. The piezoelectric potential produced was noted ~ 0.4 V in case of a lateral force of 80 nN. The maximum potential at the NW's surface was directly proportional to its lateral displacement and inversely proportional to its length-to-diameter aspect ratio. The piezopotential was found constant as long as the deformation was in place, and no external free charges were injected. Once AFM in contact with the stretched side, the negative bias across the tip-ZnO interface allowed very little current flow across. Similarly, in case, the tip was in contact with the compressed side, the interface was forward biased causing significant output current. However, the free electrons flowing inside the loop through the nanowire to the tip could neutralize the ionic charges distributed in the volume reducing the magnitudes of the potentials along compressed and stretched sides.

For demonstrating a practical nanogenerator employing this combination of piezoelectric semiconducting features of wurtzite materials, a large numbers of vertically aligned ZnO-NWs were grown on a substrate and placed below a Pt-electrode formed on a corrugated silicon substrate. Using sound wave or vibration for exciting the nanogenerator with a zigzag Pt-electrode could create individual Schottky contacts with each tip of ZnO-NWs. During excitations, the zigzag electrode could move down and push the NWs to bend laterally creating tensile and compressive strains. The electrode in contact with the NW's stretched surface produced very little current (reversely biased Schottky). Further pushing the electrode down enabled the bent NWs reaching the other side of the zigzag electrode's adjacent tooth making the contact with the compressed side creating forward-biased Schottky resulting in sudden rise of the output current flowing from the top electrode into the NW. For further increasing the output power to usable ranges, it simply needed parallel connections of the identical nanogenerators as noted experimentally (e.g., 1.8 nA output current from one unit was increased to 5.9 nA by combining three nanogenerators). Contributions from 500 to 1000 NWs could cumulatively produce 10 $\mu W/cm^2$, which was subsequently improved to double output current density (20 $\mu A/cm^2$) (Wang et al., 2008).

Interactions between piezoelectric and semiconducting properties of wurtzite family of materials such as ZnO, GaN, InN, and CdS were further explored for fabricating PENGs, piezoelectric diodes, and FETs, piezoelectric chemical sensors, and piezo-photo-tronic devices using their nanostructured species as the building blocks. This created a new field of 'piezotronics,' which enabled controlling the charge carrier transport for realizing mechanical–electronic devices that make use of the piezoelectric potential created in the crystal. The potential applications of these devices are expected in several areas like MEMS/NEMS, nano-robotics, human–computer interfacing, and sensors (Zhang et al., 2011, p. 1).

The strained ZnO-NWs experience two types of major changes that are related to the material features including band gap, carrier density, and the density of states in the conduction band influencing the two-end contacts equally, and the piezoelectric effect that comes from the polarization of ions in the crystal with an asymmetric effect on the local contacts due to polarity. The negative piezopotential, for instance, raises the barrier height at the metal n-type semiconductor contact changing it from ohmic to Schottky contact, whereas the positive piezopotential lowers the local barrier height, changing the Schottky to an ohmic contact. These barrier height modifications depend on the doping type and density in the NW. The piezoelectric charges are located at the ends of the wire, and thus directly affect the contacts. The piezotronic effect is limited to the wurtzite family of semiconductors including ZnO, GaN, CdS, and InN. The polarity of the piezopotential is modified by changing the tensile strain to the compressive strain (Zhang et al., 2011, p. 1).

AC power generation was observed in vertically stacked NW assembly between two electrodes when pushed and released in vertical position or stretched and released in lateral position on flexible substrates driving the electrons flow across the Schottky contacts formed at the electrodes. The piezopotential enables the electrons to flow through the external circuit across the electrode in contact with the negative potential on the NWs and get accumulated at the interface between the opposite electrode and the NWs with positive potential side. The piezoelectric potential inside the NWs disappeared, while the accumulated electrons flow back via an external circuit. Alternately, DC power is generated after applying a force perpendicular to the axis of the NWs. The stretched and compressed parts of the NW exhibited positive, and negative potentials, respectively. Consequently, the NW with its tip with an electrical potential was grounded at the bottom. Schottky contact formed between electrode and the NW tips enabled electrons to pass to the counter electrode, which is in contact with the negative potential and the current started flowing. In case the counter electrode was in contact with positive potential, no current flowed resulting in DC output (Kumar & Kim, 2011, p. 18,946).

Biomechanical energy harvesting was realized using flexible/foldable substrates responding to low-frequency excitations (<10 Hz) and converting biomechanical/hydraulic energy of the human body, such as flow of blood or body fluid, heartbeat, and contraction of blood vessels, muscle stretching or eye blinking, into electrical energy. Growing ZnO-NWs radially around the textile fiber was, for instance, used in fabricating fiber-based PENG in which the relative brushing of the NWs rooted at the two fibers produced electrical energy. The flexibility and transparency of these devices show potentials for artificial skins or touch sensor applications, such as full touch screens and deformable displays. An integrated transparent flexible NG was subsequently reported with ZnO-NWs grown on a flexible ITO-coated polyethersulfone (PES) substrate. This device generated current via the deformation of the ZnO NWs giving output current density of 3.7 mA/cm^2 under a compressive force of 0.9 kgf. Subsequently, using ML graphene with extraordinary electrical and mechanical properties (26,000 cm^2/Vs mobility and 1TPa elastic modulus) fully rollable transparent NGs were reported by taking care of the problems of earlier versions using ITO-based devices. A PENG assembly was, thus, made by growing ZnO nanowires

on graphene electrode followed by capping with another graphene sheet at the top. This arrangement produced current density of 2 mA/cm^2 for pushing force of 1 kgf in the vertical direction. The output current was enhanced further either by connecting a number of them in parallel or enhancing the work function and reducing the resistance of the graphene electrodes via the controlled doping (Kumar & Kim, 2011, p. 18946).

Strong piezoelectric effect was noted in PENG made out of ZnO nanosheets grown on Al substrate in aqueous solution of zinc nitrate hexahydrate [Zn $(NO_3)_2$ $6H_2O$, 0.025 M], hexamethylene tetramine (0.025 M), and de-ionized water at 95 °C and covering the assembly with 100-nm-thick Au-coated PES substrate as top electrode. The measurements confirmed the formation of Zn- and Al-mixed oxide and Zn-Al-layered hydroxide between the ZnO nanosheets and Al electrode. Gold-coated PES electrode placed above the ZnO nanosheets network exhibited nonlinear I-V characteristics when subjected to 1 kg cyclic force resulting in current density and output voltage of 6.5 $\mu A/cm^2$ and 0.44 V, respectively, and it increased to 8.1 and 11.8 $\mu W/cm^2$ for the forces of 3 and 4 kgf, respectively. The combined effect of buckling of ZnO nanosheets, coupled with semiconducting and piezoelectric properties of ZnO nanosheet network generated +ve and −ve potentials across the stretched, and the compressed sides of the sheet, respectively. A Schottky contact formed between Au and ZnO nanosheets could preserve the piezoelectric potential generated in the ZnO nanosheets for storing the charges in the layered hydroxide capacitor having positive charges balanced by NO_3^- anions involved in anion exchange. When +ve charges in the layered hydroxide facing the nanosheets were compensated with electrons from the ZnO nanosheets, the overall large negative charges were built up at the nanosheet/layered hydroxide interface generating strong potential difference with the negative charges in layered hydroxide. ZnO nanosheets buckling under an external force generated piezoelectric potential that remained constant for the constant force without any change. The positive potential in the ZnO nanosheets at the interface with the Au electrode starts decaying until the electrons screen the piezoelectric potential in the ZnO nanosheets. The absence of the piezoelectric potential causes full recovery of the layered hydroxide as a neutral layer after releasing the force, and the device returns to the initial condition. A strong potential difference developed involving negative charges at the layered hydroxide/Al electrode could thus drive the electrons from the bottom side of the Al electrode to the top side of the Au electrode (Kim et al., 2013).

IV. **Super-capacitors**

The energy storage and release in supercapacitors has been involving phenomenon of ion adsorption/desorption and redox reactions occurring on transition metal oxides and layered double hydroxide nanosheets of RuO_2, $Ni(OH)_2$, MnO_2,$Co(OH)_2$, MoO_3, $VOPO_4$, exfoliated Co-Al and Zn-Al; and on conductive surfaces comprising of activated carbon, CNTs, and graphene. These pseudo-capacitors employing redox reactions via chemical binding to store energy using transition metal oxides/hydroxides of Fe, Co, Ni, Mn, Ru, and V. Although RuO_2 is best among

all these materials, the associated factors like higher cost and rare availability have continuously been asking for a more economical and readily available alternative. Unfortunately, non-precious transition metal oxides/hydroxides, being insulators, are not useful for electrodes. Accordingly, more investigations on super-capacitor materials are badly needed in increasing their electronic conductivity.

$Ti_{1-x}O_2$, with high permittivity/low-leakage current is more preferred in high *k* capacitors realized by reducing defect concentrations in layered materials at elevated temperature. The thermodynamic equilibrium of crystallites makes these materials acquire higher permittivity since the ionic and electronic defects reduce the permittivity due to charge pinning, electronic conductivity, and grain boundary effects. For instance, monocrystalline nanosheets grown at 1100–1200 °C and assembled into a multi-layered thin films perform better as high *k* dielectrics.

Although $Ni(OH)_2$ nanosheets were found useful in replacing RuO_2 in pseudo-capacitors, but easy pulverization of these electrodes caused due to large specific volume changes in the host matrix during cycling and the associated higher resistivity of both the phases of $Ni(OH)_2$ were found as major drawbacks. Exfoliated $Ni(OH)_2$ nanosheets were used in preparing hexagonally tiled monolayer films, but their structure and performance degraded after 250 charge/discharge cycles due to breakage of the large size platelets (500–600 nm lateral size) into much smaller ones during repeated exchange reactions. Nevertheless, $Ni(OH)_2$ nanosheets based porous micro-spheres in a bottom-up process aggregating as wrinkled α-$Ni(OH)_2$ nanosheet-like structures could exhibit capacitances up to 1500 F/g with cycling stability exceeding 500 cycles. Another assembly of submicron-scale morphology after adding Al into $Ni(OH)_2$ nanosheets could produce specific capacitance better than 2100 F/g by lowering the charge transfer and ion diffusion resistances, and increasing the reaction kinetics (Kumar et al., 2018. p. 482).

Addition of alkali metal or quaternary ammonium ions was found improving the porosity during freeze-drying and flocculation of the exfoliated nanosheets resulting in specific capacitances of 140–180 F/g with very high recyclability up to 10,000 cycles. Introducing Ru- into Li-layered MnO_2 structure (i.e., $Mn_{1-x}Ru_xO_2$; x = 0.05–0.10) was found improving the capacitance up to 330–360 F/g by enhanced conductivity. RuO_2 nanosheets being good electronic conductors, the specific capacitance of exfoliated ruthenic acid nanosheets was found 10 × higher than nanocrystalline rutile (i.e., 658 F/g versus 68 F/g with a similar surface area of 52 m^2/g). The creation of surface redox charges was found enhancing specific capacitance of restacked ruthenic acid nanosheets. Phase-pure RuO_2 nanosheet-based electrodes drop casted from an exfoliated $H_{0.2}RuO_2$/TBAOH solution exhibited specific capacitance of 700 F/g. Introducing GO/rGO in Ni-Co-Al-layered hydroxide and MnO_2 nanosheets could further increase the conductivity via electrostatic aggregation and precipitation leading to specific capacitances up to 650–900 F/g with very good cyclic stability. In another case, Li^+-induced flocculation of rGO and MnO_2 nanosheets could produce porous disordered nanocomposite structures in this context. Multi-walled-carbon nanotubes were also used in preparing more disordered and porous microstructures upon mixing layered hydroxides with MoO_3 nanosheets. Ag–NPs sandwiched between metal oxide nanosheets could offer a disordered porous phase

with easy access for the ionic species in such Ag-nanoparticles loaded MnO_2 nanosheet electrodes offering capacitance of 272 F/g. Ultrathin 2D NiO flakes on GO sheets could offer specific capacitance of 525–882 F/g. LbL deposited 40 layers of Co–Al hydroxide/rGO films could display long cycle life with specific capacitance of 1200 F/g.

Hybrid electrodes made out of nanowires nanosheets using sequential depositions onto a conductive substrate of MnO_2 nanosheet via electrostatic assembly, followed by a CoOOH nanowire layer by potentiostatic deposition resulted in a micro-porous network with a large surface area and effective diffusion paths. A porous α_1-vanadyl phosphate/graphene nanocomposite film was reported with very high specific capacitance of 8.3 mF/cm^2 with cycle life better than 2000 cycles. Similarly, porous graphene with surface area of 3100 m^2/g and 500 S/m conductivity was fabricated by KOH activation of exfoliated GO with higher capacitance and energy density in both organic and ionic liquid electrolytes. An all-solid-state, flexible, stretchable, and fiber-shaped supercapacitor was accordingly designed using all-graphene core–sheath fiber woven into a textile for wearable electronics. A highly compressible supercapacitor using polypyrrole-G foam electrode was also reported that were found tolerating large compressive strains with higher specific capacitance without detereoration during long-term compression/decompression cycles.

By using self-healable polymer substrate for loading the active materials for supercapacitors, it was demonstrated the damaged electrode could make it conductive again enabling the supercapacitor to function normally. Alternately, a stretchable, fiber-shaped, and self-healable supercapacitor was reported using two parallel spring electrodes containing polypyrrole-decorated rGO/MWCNTs wrapped with gel electrolyte and encapsulated with polyurethane (PU) in constructing supercapacitors that exhibited self-healing features by involving interfacial hydrogen bonding of PU resulting in extended lifetimes of the broken electronics.

In contrast to conventional supercapacitors, stimuli-responsive devices offer electricity in response to a variety of inputs like electricity, pressure, heat, light, magnetic field, pH, and ions. For example, charge/discharge states of reversible electrochromic supercapacitor were reported via color changes. The PET-loaded devices exhibited an in situ reversible electrochromicity during charge–discharge cycles between 0 and 1 V. These devices not only exhibited the energy storage states visually but also represented a further step in human–device interactions.

Three microchannels carrying the solutions of GO and alginate calciumpolyvinyl alcohol (ACa-PVA) were passed through a microfluidic spinneret for appropriate mixing and extrusion in a one-step spinning for fabricating a continuous fabric of rGO/ACa-PVA/rGO fiber, which was hydrazine vapor reduced for fabricating supercapacitor. In this integrated structure, rGO served as the electrodes while ACa-PVA gel acted as the separator and electrolyte reservoir. Such devices exhibited a capacity of 35 mF/cm^2 with good electrochemical stability. A flexible, all-in-one, fiber-shaped supercapacitor was also developed by region-specific reduction of GO fiber into the rGO-GO-rGO configuration under controllable laser writing for fabricating integrated devices, in which the bilateral rGO and central GO acted as the active electrodes and separator, respectively. The capacitance of the integrated fiber

supercapacitor reached up to 1.2 mF/cm^2 at a current density of 80 mA/cm^2. A flexible, compressible, integrated, foam-type supercapacitor of rGO/GO/rGO structure was laser written showing outstanding mechanical properties and superior electrochemical performance of ~1 mWh/cm^3 under 90% strain (Ye et al., 2018, p. 245).

C. Photo-detectors

The fabrication of transparent, flexible UV photo-detectors was reported recently by depositing metal oxide nanosheets on a graphene back-electrode. These photo-detectors, covering UV-A band (320–400 nm), are currently being used in health care, climate control, agriculture, astronomy, and aeronautics. The metal oxide nanosheets prepared with wide band gaps allow the transmission of visible light along with high response to UV light and are also very promising high-performance UV photo-detectors. In the fabrication of these devices single-layer graphene was transferred on PET substrate via a roll-to-roll production method. Well-dispersed metal oxide nanosheets in ethanol was, thereafter, spin-coated onto the graphene substrate to form a 50 nm thin transparent and flexible photo-electrode. This assembly, with a graphene PET counter electrode, could provide transparent and flexible UV photo-detectors, exhibiting mA/cm^2 photocurrent densities at 325 nm UV irradiation. Except for WO_3 photo-detectors (i.e., *p*-type Schottky barrier type), the other detectors showed linear I-V response under the UV irradiation with ohmic behavior enhancing their photo-sensitive properties. The linear characteristics of these detectors made out of TiO_2, ZnO, and Co_3O_4—nanosheets are promising devices with large output signals in tens of 'on–off' switching cycles, confirming the excellent stability and fast response. The WO_3 photo-electrodes, on the other hand, offered enhanced photocurrents with prolonged irradiation time, due to its photochromic feature under UV irradiation. All these experimental results show the promising potentials of these metal oxide nanosheets for their practical applications in photoelectric and photochemical devices (Xie et al., 2018).

D. Nano-electronic/Magnetic Devices

The recent experiments confirmed the possibility of creating a highly conducting nano-channel across insulating oxide interfaces for their possible applications in FET devices. Out of numerous reports, only two are included in the following discussion to highlight the importance of this oxide nano-electronics in the future.

About a decade ago, some oxide multilayers confirmed the formation of a highly conducting quasi-two-dimensional electron gas (Q-2DEG) sheet at the interface between two insulating perovskites ($LaAlO_3$—$SrTiO_3$) endowed with high electron mobilities of 10^4 cm^2/Vs (4.2 K) and orders of magnitude higher carrier densities than those found in III–V-based HEMT devices. These charge sheets showed modified properties by changing the unit cell level thickness of the $LaAlO_3$ sheets though $LaAlO_3$ layers exhibiting highly insulating interfaces up to 3 unit cell thickness. The discontinuity present in the TiO_2–LaO^+ sequence could result in modulation doping in such a nano-channel, and a critical thickness of 4 unit cell was

found adequate for transition from insulating to highly conducting state The electron energy loss measurements showed that Q-2DEG was around ~2-nm-thick layer in which the interface was doped by transfer of electrons from the $LaTiO_3$ to $SrTiO_3$. While exhibiting three orders of magnitude lesser charge carrier mobilities compared to the modulation-doped semiconductor interfaces, the carrier densities in these heterostructures exceeded those of their III-V semiconductor counterparts by orders of magnitude that enabled realization of room temperature FET devices with large 'on/off' ratios. Although it remains to be seen whether the resultant device parameters, stability, and their integration would be practically implemented in producing usable devices. These heterostructures are expected to result in newer device designs based on oxide nanosheets. Subsequently, a reconfigurable nanoscale conducting region was created at the polar/nonpolar $LaAlO_3/SrTiO_3$ (LAO/STO) interface using the conductive atomic force microscopy that offered an attractive platform for oxide-based nano-electronic devices including FETs, SET, ballistic electron waveguides, photo-detectors, and THz sources and detectors (Akatsuka et al., 2009, p. 1097; Sato et al., 2010, p. 18,049; Thiel et al., 2006, p. 1942; Cen et al., 2009, p. 1026).

Another room temperature Q-2DEG system was reported using c-AFM lithography producing stable conductive structures with 1.2 nm length across the nonpolar/nonpolar oxide interface of $CaZrO_3/SrTiO_3$ by strain-induced polarization in $CaZrO_3$ layer. A number of low-temperature devices produced and characterized gave further insight into the electron-confinement across such interfaces (c, p. 113,002). In this work, pulsed laser-assisted LbL deposited films were patterned by lithography and dry etching to create trenches that were filled with Ti/Au contacts to the interface and bonding pads onto the top surface. Nanoscale conducting channels were created by applying +20 V on the AFM tip during contact mode scanning that exhibited a sharp conductance jump after completing the path that indicated the channel formation at the interface. This process could be reversed after applying − 20 V to c-AFM tip and moving across the existing wire causing steep drop in the conductance. Even channel was reduced to 1.2 nm from 2.8 nm by applying reduced bias of 10 V. These nanowires, created at the interface, remained extremely narrow at all writing voltages tested, in contrast to those formed at the $LaAlO_3/SrTiO_3$ interface. Repeating a similar experiment in vacuum exhibited no jump in conductance compared to that carried out in air (RH ~43% at 22 °C) confirming that the presence of H_2O-mediated surface protonation was necessary to create conducting channel at the interface. The $CaZrO_3$ layer being nonpolar and no lattice matching with the $SrTiO_3$ substrate, the polarization discontinuity could be strain-induced enabling switching between conducting and insulating state through surface protonation during c-AFM lithography. Moreover, low-temperature measurements of $CaZrO_3/SrTiO_3$ nanostructures confirmed the existence of a superconducting state with a critical current ~0.9 nA, which disappeared at higher temperatures or magnetic fields. A broad transition from the superconducting to the normal state was concluded with tunable features caused by varying gate voltages as observed experimentally. Hall charge carrier mobility and charge density were found as 3600 cm^2/Vs and $2.47 \times 10^{13}/cm^2$, respectively. Such a method of realizing arbitrary-shaped conducting nanostructures with tunable electronic properties of the complex oxide interface would certainly

evolve into newer pathways for exploring their further applications as discussed recently (Chen et al., 2018, p. 113,002).

Based on these observations, a number of more novel device structures were conjectured besides *p-n* junctions, photoconducting devices, and field-effect transistors. Heterojunctions of $Sr_2Nb_3O_{10}$ and *p*-type Zn-saponite exhibited diode characteristics. Similarly, field-switching behavior of oxide nanosheets in an accumulation-type FET using titania nanosheets exhibited carrier mobility of 500 cm^2/Vs and 'on/off' ratio of 10^3. Although, further developments are needed for improving these performances explored so far as these results only indicated the proof of concept for fabricating more flexible and transparent nanosheet-based optoelectronic devices in future (Yui et al., 2006, b. 4585; Miyamoto et al., 2007, p. 4123; Sato et al., 2008, p. 035,001). Using oxide nanosheets as seed layers specifically oriented 1 nm-thick monolayer crystalline films could be produced due to their extraordinary thermal stabilities at higher temperatures even in the monolayer form. This method has greater future potentials in furthering the associated thin-film technology for their better applications (Fukuda et al., 2003, p. 281;Li et al., 2007, p. 8000; Shibata et al., 2008, p. 231).

In connection with exploring the possibilities of introducing magnetic effects in oxide nanosheets for realizing magnetic devices, some recent efforts were made as briefly described below (Shi et al., 2018, p. 24). Room temperature ferromagnetic properties of nanosheets were first noted during exfoliation of $Ti_{0.8}Co_{0.2}O_2$ from $K_{0.8}Ti_{1.6}Co_{0.4}O_4$ with a maximum magnetic moment of 1.4 mB/Co. Similar ferromagnetic properties were also reported in other 3*d* transition metal oxide nanosheets, including $Ti_{1-x}Co_xO_2$ ($x \leq 0.2$), $Ti_{1-x}Fe_xO_2$ ($x \leq 0.4$), $Ti_{1-x}Mn_xO_2$ ($x \leq 0.4$), $Ti_{0.8-x/4}Fe_{x/2}Co_{0.2-x/4}O_2$ ($x = 0.2,0.4,0.6$), and $Co_{0.33}\ Al_{0.66}\ (OH)_2$. Ferromagnetic nanosheets are currently being examined for fabricating magneto-optical and magneto-electronic devices as their low-dimensional features facilitating their integration for using the ferromagnetic properties of spin-polarized electrons along with their nano-electronic features. A gigantic magneto response was also reported much superior to that of the bulk systems. Multilayer films of $Ti_{0.8}Co_{0.2}O_2$ and $Ti_{0.6}Fe_{0.4}O_4$-NSs exhibited magneto-optical effect at the shortest wavelength of 280 nm (Ohno, 1998, p. 951; Matsumoto et al., 2001, p. 854; Coey et al., 2005, p. 173; Priour et al., 2005, p. 037,201; Osada et al., 2006a, 2006b p. 295; Osada et al., 2006a, 2006b, p. 153,301; Liu et al., 2006, p. 4872; Osada et al., 2008, p. 253,110).

The magnetic properties of these devices were found tunable by employing different forms of superlattices and/or controlled doping as well. For example, the superlattice of $Ti_{0.8}Co_{0.2}O_2$ and $Ti_{0.6}Fe_{0.4}O_2$-NSs subunits exhibited either enhanced or suppressed magneto-optical responses according to the inter-layer couplings. Alternate stacking of $(Ti_{0.8}Co_{0.2}O_2/Ti_{0.6}Fe_{0.4}O_2)_5$ exhibited a strong response at 400–550 nm. A similar magneto-optical response at 400–750 nm was observed in (Co/Fe)-co-substituted titania nanosheets of $Ti_{0.8-x/4}Fe_{x/2}Co_{0.2-x/4}O_2$ ($x = 0.2$, 0.4, 0.6). All these results confirmed that such band engineering of transitions in titania nanosheets might be usable in obtaining a gigantic magneto-optical response in the short wavelength region for its applications in optical isolators and data storage devices.

These ferromagnetic nanosheets would be useful in preparing spintronics devices, along with the transparent electronic and molecular devices. A tunnel junction was, for instance, used in fabricating spin-tunneling switches, spin valves and optical interconnects. In this context, first principles studies demonstrated that the room temperature operating semi-metallic ferromagnetic combinations were realized in optimally doped nanosheets of $Ti_{1-x}Co_xO_2$ (Co^{3+}; $x = 0.125$) and $Ti_{0.5}Fe_{0.25}Co_{0.25}O_2$ for further exploration of their spin transport (Kotani et al., 2008, p. 093,112).

While assessing the introduction of magnetic properties into the nonmagnetic 2D layered crystals, the available first principles based techniques were employed along three different directions of magnetic dopant adsorption; defect engineering; and a combination of doping-absorption in the species like MoS_2, $MoSe_2$, WS_2, BN, ZnO, and g-C_2N. This study could confirm besides the structural stability and electric properties of the host matrices, the tailoring of the magnetic properties with the general observation that the origin of magnetism in such cases went beyond the conventional models.

Tunable electronic and magnetic properties of graphene-like (g-ZnO) and SW-ZnO-NTs were realized after transition metal doping. The ferromagnetic monolayers when doped with Co (i.e., substituting the Zn atoms) were found modified accordingly. Placing the Mn atoms over the center of the lattice hexagon was found most favorable site according to theory for adsorption. The total magnetic moment per Mn atom in Mn-doped g-ZnO-ML was estimated ~ 5 μB with spin polarization. It was noted that some of the 3*d* transition metals such as Sc, Ti, V, Cr, Mn, Fe, Co, Ni and Cu could efficiently dope the g-ZnO-monolayers by substituting the Zn atoms affecting their electronic and magnetic properties. The theoretical calculations showed that Cr ions could influence the nearest-neighbor O ions causing antiferromagnetic interactions, whereas the ions like Mn, Fe, Co, Ni, and Cu participated in ferromagnetic interactions. The local moment for the Cr and Mn dopant were found as − 3.2 and 4.7 μB, respectively. The major contribution to the total magnetic moments of transition metal-doped g-ZnO monolayers came from the strong *p*–*d* orbital mixing of O and transition metal besides affecting the electronic structure by doping. For instance, doping of Sc, Ti, and V exhibited the band gaps of 2.084 (direct), 0.134 (semi-metal), and 0.561 eV (indirect), respectively. However, Cr-doped g-ZnO monolayers were metallic, whereas Mn, Fe, Co, Ni, and Cu-doped monolayers were semiconductors with band gaps of 0.689, 1.057, 1.518, 1.648, and 1.798 eV, respectively, for the majority spin state and 2.164, 0.516, 1.142, 0.181, and 0.780 eV, respectively, for the minority spin state.

The doped g-ZnO was found undergoing transitions from nonmagnetic to antiferromagnetic to ferromagnetic and semiconductor to semi-metal phases, with increasing distance between two C and B atoms. Similarly, 2 N atoms/super-cell doping of g-ZnO-ML formed a *p*-type semiconductor with an antiferromagnetic state, while the magnetic properties were not affected by the distance between the two N atoms (Ta et al., 2016, p. 100).

Despite successful theoretical study of the above-mentioned transition metals doping strategies, experimental realizations are still awaited. Substitutional doping via ion bombardment was not found easy as noted experimentally. On the other hand,

in wet chemical synthesis, the reactions took place on the sides rather than within the layer.

Continuing efforts in this context showed that the magnetic property of the transition metal impurity atoms was not affected by the ZnO substrate. The spin coupling of in TM@ZnO-ML exhibited optimal properties when their adsorption sites coincided with the positions right above the O atoms while maintaining their spin states. The magnetic moment was found similar to the 3*d* unpaired electrons such as 5 μB for Mn, and 4 μB for Fe, except in Cr@ZnO system, where the 4 s electron from Cr was excited to the 3*d*-orbit turning the spin direction to minimize the total energy. Consequently, TM@ZnO generated magnetic moments from 1 to 5 μB per/unit cell for different transition metals without affecting their semiconducting features. Theoretical studies predicted that TM@ZnO materials (where TM = Sc, Ti, V, Cr, Mn, Fe, Co, Ni) could be used as new dilute magnetic semiconductors with tunable magnetic properties (Ta et al., 2016, p. 100). A variety of such properties were explored while introducing the magnetic effects in oxide monolayers due to strong interactions with charge, spin, and orbital degrees of freedom in oxides. For instance, ZnO and SnO_2 could be heavily doped up to 30%. Oxides doped with 3*d* transition metals became ferromagnetic suitable for spintronics, spin valves and magnetoresistive devices. Room temperature ferromagnetism was reported in Co-doped ZnO; Cr-doped Fe_2O_3; and $BaTiO_3$-doped with Sc, V, Cr, Mn, Fe, Co, Ni, and Cu (Nakayama and Katayama-Yoshida 2001, p. L1355; Chambers, et al., 2006, pas; Bibes and Barth'el'emy, 2007, p. 1003; Ali et al., 2009, p. 456,005; Li et al., 2012, p. 174,430; Apostolova et al., 2013, p. 203,904; Kumar et al., 2013, p. 221,903; Ren et al., 2013, p. 2243; Riaz et al., 2014, p. 2,200,704; Albar, 2017).

The spin polarization in SnO added more values to its already existing novel applications in transparent and strain sensitive p-type semiconducting behavior with very high hole mobility. Substitutionally doped SnO (i.e., 1 and 5% Fe), for instance, exhibited room temperature paramagnetism with the antiferromagnetic interactions becoming weaker with increasing dopant concentration. In order to explore further, first principles calculations were made to understand about the electronic and magnetic properties of this unique material in a recent doctoral program (Albar, 2017).

The semiconducting *g*-ZnO-ML was found suitable for preparing dilute magnetic semiconductors by 3*d* transition metal ion doping and adsorptions in two modes. In one, the Mn dopant was accompanied with adsorbate varying from Sc to Zn, whereas in the other, the dopant and adsorbate were reversed. First principles calculations showed that the stable adsorbed − doped systems could possess a lower bandgap than that of the host. System magnetic moments could be tuned to $|5 - x|\mu B$, where x refers to the magnetic moment of the individual 3*d* atom. A ferromagnetic system was demonstrated using Mn-adsorbed/doped configuration. This theretical study offered a way to tailor the electronic and magnetic properties of g–ZnO–ML via doping and sequentially adsorbing transition metal atoms appeared feasible experimentally as discussed elsewhere (Zhang et al., 2017, p. 1192).

4 Some Recent Applications

A number of composite porous materials were examined for sensor applications in a doctoral thesis from where some of the salient features are summarized here for highlighting their importance in gas-sensing. CuO@SnO_2 nanowire-based H_2S sensors exhibited interesting features. Although, SnO_2 nanowires showed moderate NH_3 sensitivity that was degraded further in the presence of moisture, but using CuO@SnO_2-heterostructure nanowires could significantly enhance its sensitivity to H_2S detection showing larger resistance variations due to typical reaction between CuO and H_2S forming the metallic CuS that eliminated the depletion layer formations. In the case of p-type CuO nanowire, the dominant role of surface O was noted while testing the three gases namely—NH_3, H_2S and NO_2 from their resistance changes caused by the analyte exposure. While NH_3 response could be assigned to electron injection in SnO_2 nanowires, the H_2S response did not follow the sulfurization process proposed for the CuO particles in CuO@SnO_2-nanowires possibly due to different property of the two kinds of CuO materials. Similarly, the relative selectivity of ZnO nanowires toward NH_3 against CO was assigned to its intrinsic surface/bulk properties that exhibited remarkable features when operated in the pulsed-temperature mode. The enhanced sensitivity at the lower temperatures was found influenced by surface O/H_2O/NO_2 modulation effects by the fast temperature transitions. The NiO@SnO_2 heterostructures were found sensitive toward H_2S with better stability. More recently, adding an organic molecule sensitizer to the metal oxide could offer higher sensitivity and selectivity confirming the promising features of the hybrid materials. The ZnO nanowires showed NH_3 selectivity against CO with sensitivity deterioration after 500 °C anneal. On the other hand, the sensors showed interesting features, when working in the temperature-pulsed mode, which are not yet explained properly. Those involved parameters capable of manipulating the sensor responses included: longer or shorter pulse period, and different temperature combinations.

This study could conclude that for optimizing the metal oxide gas sensors, it was necessary to run the combined simulations of the surface processes by DFT and the surface/bulk charge carrier transport for better understanding of the experimental observations. The interfacing of the charge transport model of the semiconductor physics with that of DFT, is still a challenge in it self.

Higher sensitivity, more stable, reproducible, and reliable selective ethanol sensors were reported using ternary metal oxide system of CdO/ZnO/Yb_2O_3 nanosheets in alkaline phase. A thin layer of CdO/ZnO/Yb_2O_3 nanosheets was deposited onto a glassy carbon electrode with conducting binder showing linear range of ethanol detection (i.e., from 0.35 nM to 3.5 mM), with a minimum detection limit of 0.127 $\pm$ 0.006 nM and system sensitivity of 7.4367 $\mu A/mM.cm^2$ (Rahman et al., 2017, p. 22,627).

A number of observations made in a recent review are summarized below for highlighting the importance of nanomaterials in gas sensor fabrications (Neri, 2017, p. 21). Although, LDHs offer very good opportunity for gas sensing but are not

yet investigated in detail in this context. The experimental investigations carried out showed that different concentrations could be differentiated even at room temperature using an Al-

LDHs materials in detecting the volatile compounds like CH_4, CO, and NO. LDHs are, though, used as precursors for preparing the gas-sensing materials in the form of metal oxides that are prepared by roasting the layered nanosheets, showing higher stability against sintering, homogeneous dispersion between the elements, and contributing to better gas-sensing characteristics. Using a soft-chemical process, various nanosheets of $Ti^{\delta-}O_2$, $Ti_{1-x}Co_xO_2$, MnO_2, and perovskites were synthesized by delaminating their corresponding precursors into their molecular single sheets. Others, including oxides of Zn, Sn, Ti, ln, W, Fe, and Mo were used in preparing cost-effective conductometric gas sensors with reasonable chemical stability, and electrical properties for their further commercial productions as noted in case of SnO; and ZnO during the last five decades. By reducing their dimensionalities, e.g., in 2D MoO_3 nanosheets, a band gap opening induced blue shift was observed. ZnO nanosheets based gas sensors were produced using monocrystalline ZnO-= nanosheets with porous structures prepared from annealing the $ZnS(en)_{0.5}$ (where en = ethylenediamine) precursors containing numerous mesopores (~26 nm diameter) suitable for detecting 5–100 ppm formaldehyde at 240 °C. WS_2 nanosheets were used as a sensing material in fabricating humidity sensors on an interdigitated set of Al electrodes on Si/SiO_2 substrates resulting in sensor response varying from 11.9 to 37.5 for a change in RH from 40 to 80%, respectively. Recently, the gas-sensing performance of MoS_2-rGO hybrid 2D nanosheets prepared using exfoliated MoS_2 and graphene in which the gas-sensing properties were retained even under mechanical deformation of the flexible substrate used. Such devices are found extremely useful in flexible electronic applications (Neri, 2017, p. 21).

Self-standing pinhole free 180 μm thick GO membranes were prepared using colloidal suspension of GO nanosheets for fabricating room temperature H_2 sensors (i.e., 50–300 ppm in air with 35%RH) by attaching Pt/C and Pt black to the membrane as sensing and reference electrodes, respectively. Susceptibility of the sensor response to humidity, to a large extent, could not exhibit stable response under dry conditions. Further analyses of the samples revealed that the electrochemical reactions were not favored in the absence of water causing the response to be unstable. A planar-type GO sensor fabricated using solid reference electrodes made out of a perovskite-type oxide that was not sensitive to hydrogen but showed good room temperature responses (Miyamoto et al., 2017, p. 2994).

A variety of hierarchical superstructures were synthesized comprising of graphene/2D metal oxide composites using nanotubes, nanowires, nanorods, and nanofibers in template-assisted processes for improving the gas-sensing capabilities of these materials due to their higher surface-to-volume ratios and abundant surface states as reviewed recently (Xie et al., 2018, p. 1456). Despite the attractive features of these template-assisted hybrid syntheses, some problems were also noted such as the difficulty in implementing the protocols, costly templates, and residual impurities that could be problematic. Graphene functionalized 3*d*-WO_3 hemitubes, for instance, were reported involving nonwoven fiber of polyvinylpyrollidone (PVP)/poly(methyl

methacrylate) (PMMA) composite as template under O_2 plasma for preparing Cu_2O nanowires based mesoporous hybrids in the presence of GO and o-anisidine in a one-pot hydrothermal process. This porous 3*d* framework interspersed in 2D rGO nanosheets led to self-organization of 3*d* mesoporous architectures, in which GO was simultaneously reduced leading to an efficient multistep process for producing many 3*d* hybrid composites. Another core–shell-type composite of 3*d* rGO/metal oxide nanosheets for sensors was reported by preparing rGO nanosheets loaded ZnO core–shell nanofibers using electrospinning of ZnO/rGO precursors. A similar technique was reported for conjugating rGO along with the oxides of Sn, ln, Fe, and other metals as well in an efficient two-step synthesis. Synthesis of 3*d* mesoporous rGO/ZnO nanorods composite was realized by using $Zn(Ac)_2$ methanol solution with GO to absorb Zn ions onto the surfaces of GO nanosheets. Thereafter, ZnO nanoseed layer was formed on the GO nanosheets in NaOH methanol solution added to an aqueous suspension containing NaOH/$Zn(OH)_2$ precursor for further extension of the ZnO nanoparticles into ZnO nanorods with in-situ GO reduction. Gram scale production of 3*d* mesoporous rGO/ZnO nanorod composite materials in 10 min showed the commercial viability of this process.

The problem of high energy consumptions in operating gas sensors based on 3*d* graphene/metal oxide nanocomposites at higher temperatures (>100 °C) for detecting gases like NO_2, NH_3, HCHO, and H_2S that were also susceptible to explosions, was taken care by controlling the structures of the composites materials for enhanced room temperature NO_2 sensors based on synergy between graphene and metal oxide species. A 3*d* nano-flower-like Cu_xO was reported comprising of 5–9 nm nanoparticles/multilayer graphene composites for room temperature operation. Further efforts are, however, still needed in achieving green, cost-effective, and commercially viable methods for producing these 3*d* graphene-based sensing materials by controlling the number of graphene layers and in-situ growth of metal oxide nanosheets on graphene that is still a challenge. Besides, the interaction mechanisms involved between building units and gas adsorption/diffusion requires more systematic studies for optimal performances as discussed in more detail in a recent review (Xia et al., 2018, p. 1456).

The performance of metal oxide gas sensors comprising of high density porous ZnO nanosheets were grown on an aluminum substrate for realizing MEMS gas sensors for ozone detection, in which the improved performance was found depending on oxygen vacancy adsorption, as measured by photoluminescence emission. This method could produce a low temperature, hydrothermally grown novel porous ZnO nanosheets based ozone gas sensor that measured O_3 responses of 96.1 and 53.4% at 300 and 150 °C, respectively (Tsai et al., 2018, p. 5559).

The demands of real-time and on-site environmental monitoring for detecting the hazardous chemical species with the help of high-performance gas sensors are currently being considered important as discussed in detail in a current review with following observations (Choi & Kim, 2018). The improved sensing characteristics of heterogeneous composites were examined by taking different nanosheet combinations of graphene/ZnO, rGO/NiO, and rGO/hexagonal WO_3 for gas sensing. About 100-fold increase in sensitivity and selectivity of NO_2 sensors was observed

compared to those using pristine NiO nanosheets, and for this, rGO layer was formed on a substrate followed by vertical growth of NiO nanosheets to form the rGO/NiO composites. Hydrothermally formed and calcined nanosheets of rGO/hexagonal WO_3 exhibited fourfold improved response compared to that of pristine WO_3 at 330 °C in case of 40 ppm of H_2S. The properties of graphene and TMDC composites were also explored using a hybrid structure comprising of patterned graphene as a charge collector along with the sensing layer of MoS_2 flakes on polyimide films by using CVD-grown graphene layer onto the patterned MoS_2 flakes that exhibited high sensitivity detection (5 ppm) of NO_2 at 150 °C. Moreover, this flexible sensor was found stable even after 5000 bending cycles during characterization. Similar combinations of MoS_2/graphene hybrid aerogels possessing very high porosity (700 m^2/g) could result in enhanced surface reactions.

Continuing the effort of designing more nanocomposites further, two different 2D TMDC nanosheets of $NbSe_2$ and WSe_2 were combined together by one-step CVD for better detection of NO_2 gas. The hybrid $NbSe_2/WSe_2$- nanosheets were synthesized by selenization of pre-patterned WO_3 and Nb_2O_5 to produce $NbSe_2$–$Nb_xW_{1-x}Se_2$-WSe_2 heterojunctions comprising of the inter-layer structure of $Nb_xW_{1-x}Se_2$ that showed decreasing resistance upon exposure to 1.2–5 ppm of NO_2 and the improvement in performance was assigned to reduction in the Schottky barrier height due to the inter-layer alloy junction formation that affected the charge carrier transfers induced by the chemical reactions. Integrating the $NbSe_2/WSe_2$ nanosheets on PET film could form a flexible sensor that maintained its response up to 10,000 bending cycles (i.e.5 mm bending radius). Another sensor involving hexagonal-BN (h-BN) and BP nanosheets was fabricated tunneling thin-film transistors having different configuration such as h-BN/graphene nanosheets, and WSe_2-h-BN graphene multilayered structures for transparent TFTs.

Promising results are expected from using 2D nanosheets as gas-sensing materials, especially by introducing reversible selectivity features in gas sensors by employing chemical doping of graphene. The sensing properties of multi-compositional 2D layers could also be improved by introducing porosity necessary for enhanced analyte gas penetrations. Moreover, nano-pores would also provide the active reaction sites additionally by increasing density of edge sites. Flexible sensors fabricated by integrating the nanosheet materials on a flexible substrate for future applications in having real-time wearable devices with improved performance in terms of sensitivity and reliability under mechanical stress. New synthesis techniques appropriate for flexible substrate would provide novel wearable sensing platforms for future applications (Choi & Kim, 2018, p. 221).

A chemical potential energy harvesting system was reported recently using graphene oxide (GO) film by incorporating gradient distribution of oxygen-related groups (g-GO) that generated electricity when exposed to moisture. In this process, the water molecules created free and H^+ and O^- species attached to GO film, respectively. The diffusion of such H^- ions from the higher concentration to the lower one could induce electrical potential causing current flow in the external circuit. When exposed to RH variation (75%), such films could generate an asymmetric electric output pulse of 0.26 V. Four such units connected in series could illuminate

a LED at the moist part (RH = 80%). In another variant, a layered GO nanoribbon membrane having a gradient distribution of oxygen-related groups exhibited ion transport leading to chemical potential energy harvesting system based on moisture exposure to produce voltage and current outputs of 40 mV and 0.35 mA/cm^2, respectively. In 1D version of graphene fiber power generator, laser processed composition of rGO/g-GO/rGO fiber of 1 mm length and 80 mm diameter could produce 355 mV and 1.06 mA/cm^2 under RH = 65%. Four such units connected in series could produce a maximum voltage ~1.32 V, while in parallel, exhibiting a maximum current ~3.6 mA/cm^2. These highly flexible but strong GO-based energy harvesting systems could easily be integrated into textile fabric to power wearable electronic devices (Ye et al., 2018, p. 245).

Moisture sensitive GO/Li-battery was reported for supplying electrical power and detecting the human respirations. It was fabricated by combining a lithium foil with GOF to prepare a button-type cell without additional electrolytes and was called Li-GOF battery. The presence of punched holes on one side of the cell in touch with the GOF enabled moisture entry, whereas Li acted as anode and GOF played the roles of proton carrier and separator, which eliminated the phenomenon of short-circuiting. The water molecules trapped by the GOF layer were transported to the surface of the Li-foil that served as a micro-reactor to trigger the redox reactions. Accordingly, the electrons so produced could flow in the external circuit, and the resultant electrical signal reflected the real-time rate and depth of respiration. When the Li-GOF battery was placed just below the nose of a person, abundant moisture from the exhaled breath could induce the redox reactions between Li and H_2O, which changed the output current from an initial value of zero to a maximum value of ~1.8. When the person inhaled, the reduced supply of moisture made the induced current gradually return to 0. In the same way, the Li-GOF battery could accurately detect blowing by the person. This kind of Li-GOF battery provided new possibility in the field of clinical diagnosis field and construction of similar electrochemical power sources for other applications as well (Ye et al., 2018, p. 245).

5 Discussion and Conclusions

A number of layered metal oxide nanosheets based composites possess such unique physico-chemical properties that make them qualified for further detailed studies for developing their technological applications in future. For instance, a rising number of these chemically exfoliated metal oxide nanosheets based assemblies that are, in general, transparent, flexible, semiconducting, photosensitive, and pH-stable besides having larger specific surface area to volume ratios, is continuously growing with the explorations of the newer types of metal oxide nanosheets involving different layered functional materials. This is regularly adding newer members to the existing list of a variety of these nano-architectures that are easy to modify in their layered precursors providing better-optimized functional properties.

Despite a number of breakthroughs reported already in this area of nanostructured materials, some challenges are still there in almost all the cases examined primarily due to the lack of precise control of the shapes and sizes of the individual metal oxide nanosheets for which newer techniques are necessary to be explored and optimized. More regular shapes of the metal hydroxide nanosheets, however, do not allow the preparation of densely packed films involving them as building blocks besides possessing the limited mechanical strength, for which, the nanosheet colloids must be protected from their exposure to the stronger shear forces that break them into the smaller fragments during processing, as noted in case of very thin (<1 nm) nanosheets of $Ti_{1-x}O_2$ and MnO_2, which are very sensitive to their cohesive breaks. Although the heterogeneous size distributions of these metal oxide nanosheets help them in forming densely packed multiple-layered films, nevertheless the sheet morphology control has still been practically difficult to achieve because of their fragile nature. Similarly, the thermal stability of the metal oxide nanosheets poses a problem by restricting their uses in different ways. For example, while a LB-deposited thin film of $Ti_{0.87}O_2$ monolayer nanosheets needs temperature > 800 °C to transform it into anatase phase, a stack of 5 monolayers of the same material was found transforming into anatase phase at 400–500 °C, which is the normal crystallization temperature of the bulk reactants.

While extending the realizations of the nanostructured building blocks for preparing more varieties of nanocomposites, it was found feasible to combine the nanosheet films with superlattices as constituent components. Relatively lower conductivity of nanosheet assemblies comprising of mono- and multiple-layered films due to the existence of poor ohmic contacts between the individual sheets has been an important issue requiring further improvement, in particular, because the majority of the energy-related materials discussed above in the context of Li-ion batteries, supercapacitors, photo-catalysts, and photovoltaic solar cells, invariably, require electrodes with a higher electronic conductivity to ensure good performance.

Considering the case of the enhanced conductivity observed in hybridizing the metal oxide nanosheets with graphene monolayers or their other compositions, the synergistic effects observed there appear to be of significant importance for extending a similar approach to many more compositions of such nanomaterial species to achieve the targeted properties under active consideration. In this respect, the recent development of a large number of other 2D nanomaterials like WS_2, MoS_2, BN, and many others, offer excellent opportunities for designing novel functional layered nanocomposites for device explorations. Artificial lattices might also be included offering more novel properties and phenomena that are not found in the bulk materials individually.

For realizing the experimentally viable devices using metal oxide nanosheets as the main constituent along with other inorganic, organic and biomolecular species, the main hurdle lies in the nonavailability of a suitable method of producing larger quantities of these constituent materials with identical physical characteristics like size and shape, as they invariably possess statistically varying lateral sizes and morphologies. Furthermore, there is no reliable way to produce the large-scale devices that will be needed in more advanced integrated systems. However, sufficiently promising

indications are there to show that these technological obstacles will be taken care of quite soon during the upcoming developments.

Further development in evolving better theoretical simulation models would certainly facilitate providing better insights into the processes involved with the help of the computed results, which will be helpful in resolving the problems that are currently being faced.

Acknowledgements The authors are thankful to the faculty and research graduates of the JCB University of Science & Technology, YMCA, Faridabad, Haryana, for their kind encouragements while conducting these studies in a congenial academic environment. Active support of the Vice Chancellor, JCB University of Science and Technology, YMCA, extended throughout, has been one of the major motivating factors behind this ongoing study of Intelligent Materials for Sensors and Devices undertaken currently in the ECE Department.

References

Abdel Hamid, A. A., Yu, Y., Yang, J., & Ying, J.Y. (2017). Generalized synthesis of metal oxide nanosheets and their application as Li-Ion battery anodes. *Advanced Materials, 29*(32), 170142.

Ahmad, F., Mansoori, A., Bansal, S., Dhahi, T. S., & Ahmad, S. (2018). Device applications of metal-2D-materials interfaces—A short review. *European Journal of Engineering and Technology Research, 3*(4), 1.

Ahmad, S. (2016). Band-structure-engineered materials synthesis nanocrystals and hierarchical superstructures—Current status and future trend. *International Journal Material Science, 6*(1), 1.

Ahmad, S. (2017). Role of 2D-material in engineered nanomaterials -Editorial. *MOJ Polymer Science., 1*(4), 00024.

Akatsuka, K., Ebina, Y., Muramatsu, M., Sato, T., Hester, H., Kumaresan, D., Schmehl, R. H., Sasaki, T., & Haga, M. A. (2007). Photo-electro-chemical properties of alternating multilayer films composed of Titania nanosheets and Zn Porphyrin. *Langmuir, 23*, 6730.

Akatsuka, K., Haga, M. -A., Ebina, Y., Osada, M., K. Fukuda, K., & Sasaki, T. (2009). Construction of highly ordered lamellar nanostructures through Langmuir-Blodgett deposition of molecularly thin Titania nanosheets tens of micrometers wide and their excellent dielectric properties. *ACS Nano, 3*, 1097.

Akatsuka, K., Takanashi, G., Ebina, Y., Haga, M.-A., & Sasaki, T. (2012). Electronic band structure of exfoliated Titanium and/or Niobium-based oxide nanosheets probed by electrochemical and photo-electrochemical measurements. *Journal of Physical Chemistry C, 116*, 12426.

Akinwande, D., Brennan, C. J., Bunch, J. S., Egberts, P., Felts, J. R., Gao, H., Huang, R., Kim, J. S., Li, T., Li, Y., Liechti, K. M., Lu, N., Park, H. S., Reed, E. J., Wang, P., Yakobson, B. I., Zhang, T., Zhang, Y. W., Zhou, Y., & Zhu, Y. (2017). A review on mechanics and mechanical properties of 2D materials—Graphene and beyond. *Extreme Mechanics Letter, 13*, 42.

Albar, A.A. (2017). Defect engineering and interface phenomena in Tin Oxide. *Dissertation for the degree of Doctor of Philosophy*. Kingdom of Saudi Arabia March: King Abdullah University of Science and Technology Thuwal.

Ali, B., Shah, L.R., Ni, C., Xiao, J. Q., & Shah, S. I. (2009). Lnterplay of dopant, defects and electronic structure in driving ferromagnetism in Co-doped oxides: $Ti0_2$, CeO_2 and ZnO. *Journal of Physics: Condensed Matter, 21*, 456005.

Androulidakis, C., Zhang, K., Robertson, M., & Tawfick, S. (2018). Tailoring the mechanical properties of 2D-materials and hetero structures. *2D Mater, 5*, 032005.

Ano, T., Kishimoto, F., Mochizuki, D., Tsubaki, S., Maitani, M. M., Suzuki, E., & Wada, Y. (2016). Distance-depending photo induced electron transfer at two-dimensional interface in alternate stacked structures of Tantalate nanosheets and Tungstate nanosheets. *Chemistry Letters, 45*, 1111.

Apostolova, I. N., Apostolov, A. T., Bahoosh, S. G., & Wesselinowa, J. W. (2013). Origin of ferromagnetism in transition metal doped $BaTiO_3$. *Journal of Applied Physics, 113*, 203904.

Bai, Y., Wang, L., Xing, Z., Zong, X., Zhu, Y., & Wang, L. (2015). Bismuth-rich Bi4O5X2 (X = Br, and l) nanosheets with dominant {101} facets exposure for photo-catalytic H2 evolution. *Catalysis Today, 264*. DOI: https://doi.org/10.1016/j.cattod.2015.08.007.

Bai, Y., Xing, Z., Yu, H., Li, Z., Amal, R., & Wang, L. (2013). Porous Titania nanosheet/nanoparticle hybrids as photo-anodes tor dye- sensitized solar cells. *ACS Applied Materials & Interfaces, 5*(22), 12058.

Balendhran, S., Walia, S., Alsaif, M., Nguyen, E. P., Ou, J. Z., Zhuiykov, S., Sriram, S., Bhaskaran, M., & Kalantar-zadeh, K. (2013). Field effect biosensing platform based on 2D α-MoO(3). *ACS Nano, 7*(11), 9753.

Balis, N., Stratakis, E., & Kymakis, E. (2016). Graphene and transition metal di chalcogenide nanosheets as charge transport layers for solution processed solar cells. *Materials Today, 19*(10), 580.

Bassey, E. F. (2014). *Development and characterization of metal oxide gas sensors*. Ph.D. thesis submitted to Auckland University of Technology.

Bibes, M., & Barth'el'emy, A. (2007). Oxide Spintronics. *IEEE Transactions on Electron Devices, 54*, 1003.

Cai, X., Ma, R., Ozawa, T. C., Sakai, N., Funatsu, A., & Sasaki, T. (2014). Superlattice assembly of graphene oxide (GO) and titania nanosheets: Fabrication, in situ photo catalytic reduction of GO and highly improved carrier transport. *Nanoscale, 6*, 14419.

Cai, X., Sakai, N., Ozawa, T. C., Funatsu, A., Ma, R., Ebina, Y., & Sasaki, T. (2015). Efficient photo induced charge accumulation in reduce graphene oxide coupled with titania nanosheets to show highly enhanced and persistent conductance. *ACS Applied Materials & Interfaces, 7*, 11436.

Cen, C., Thiel, S., Mannhart, J., & Levy, J. (2009). Oxide nanoetectronics on demand. *Science, 323*, 1026.

Chambers, S. A., Droubay, T. C., Wang, C. M., Rosso, K. M., Heald, S. M., Schwartz, D. A., Kittilstved, K. R., & Gamelin, R. G. (2006). Ferromagnetism in oxide semiconductors. *Materials Today, 9*, 28.

Chang, L., Holmes, M. A., Waller, M., Osterloh, F. E., & Moulé, A. J. (2012). Calcium niobate nanosheets as a novel electron transport material for solution-processed multi-junction polymer solar cells. *Journal of Materials Chemistry, 22*, 20443.

Chen, C., Fan, Y., Gu, J., Wu, L., Passerini, S., & Mai, L. (2018). One-dimensional nanomaterials for energy storage. *Journal of Physics D: Applied Physics, 51*, 113002.

Chen, X., Zhou, Y., Liu, Q., Li, Z., Liu, J., & Zou, Z. (2012). Ultrathin, single-crystal WO(3) nanosheets by two-dimensional oriented attachment toward enhanced photo catalytic reduction of CO(2) into hydrocarbon fuels under visible light. *ACS Applied Materials & Interfaces, 4*, 3372.

Cheng, W. (2016). *Design of functional metal oxide nanostructures with high aspect ratio*. D.Sc thesis submitted to ETH, Zurich, Switzerland.

Cheng, W., He, J., Yao, T., Sun, Z., Jiang, Y., Liu, Q., Jiang, S., Hu, F., Xie, Z., He, B., Yan, W., & Wei, S. (2014). Half-unit-cell α-Fe_20_3 semiconductor nanosheets with intrinsic and robust ferromagnetism. *Journal of the American Chemical Society, 136*, 10393.

Choi, B., Yu, J., Paley, D. W., Trinh, M. T., Paley, M. V., Karch, J. M., Crowther, A. C., Lee, C.-H., Lalancette, R. A., Zhu, X., Kim, P., Steigerwald, M. L., Nuckolls, C., & Roy, X. (2016). van der Waals Solids from seIfassembled nanoscale building blocks. *Nano Letters, 16*(2), 1445.

Choi, S.-J., & Kim, L.-D. (2018). Recent developments in 2D- nanomaterials for chemiresistive-type gas sensors. *Electronic Materials Letters, 14*(3), 221.

Coey, J. M. D., Venkatesan, M., & Fitzgerald, C. B. (2005). Donor impurity band exchange in dilute ferromagnetic oxides. *Nature Mater, 4*, 173.

Dai, Z. R., Pan, Z. W., & Wang, Z. L. (2003). Novel nanostructures of functional oxides synthesized by thermal evaporation. *Advanced Functional Materials, 13*(1), 9.

Dou, Y. (2016). *Atomically thin transition metal oxides for energy conversion and storage.* Ph.D. thesis submitted to University of Wollongong.

Erba, A., Baima, J., Bush, I., Orlando, R., & Dovesi, R. (2017). Large-scale condensed matter DFT simulations: Performance and capabilities of the CRYSTAL code. *Journal of Chemical Theory and Computation, 13*(10), 5019.

Fan, F.R., Tang, W., & Wang, Z.L. (2016). Flexible nanogenerators for energy harvesting and self-powered electronics. *Advanced Materials, 28*. https://doi.org/10.1002/adma.201504299.

Fukuda, K., Sasaki, T., Watanabe, M., Nakai, I., Inaba, K., & Omote, K. (2003). Novel crystal growth from titania nanosheets studied by total reflection fluorescence XAFS. *Crystal Growth and Design, 3*, 281.

Galstyan, V., Bhandari, M. P., Sberveglieri, V., Sberveglieri, G., & Comini, E. (2018). Metal oxide nanostructures in food applications: Quality control and packaging. *Chemosensors, 6*, 16.

Gao, S., Sun, Y., Lei, F., Liu, J., Liang, L., Li, T., Pan, B., Zhou, J., & Xie, Y. (2014). Freestanding atomically-thin cuprous oxide sheets for improved visible-light photo electro chemical water splitting. *Nano Energy, 8*, 205.

Hu, G., Yi, L., & Liu, C. (2012). Supercritical N, N-dimethylformamicle exfoliation of the layered bulk titanate material into titania nanosheets. *The Journal of Supercritical Fluids, 72*, 59.

IC. (2018). *Structures of Simple Ionic Compounds.* Text @ www.everyscience.com/Chemistry/Inorganic/Ionic_Solids/b.1297.php

Ida, S., Takashiba, A., & Ishihara, T. (2013). Self-ordering of disorderly arranged 2D crystal layers to 3D regular arrangement using a heat- induced chemical reaction between 2D crystal layers. *Journal of Physical Chemistry C, 117*, 23357.

Ida, S., Takashiba, A., Koga, S., Hagiwara, H., & Ishihara, T. (2014). Potential gradient and photo catalytic activity of an ultrathin p-n junction surface prepared with two-dimensional semiconducting nanocrystals. *Journal of the American Chemical Society, 136*, 1872.

Ikhmayies, S. J. (2014). Characterization of nanomaterials. *JOM Journal of the Minerals Metals and Materials Society, 66*(1), 28.

Itoh, E., Maruyama, Y., Fukuda, K. (2012), "Fabrication of inverted bulk-hetero junction organic solar cell with ultrathin Titanium Oxide nanosheet as an electron-extracting buffer layer. *Japanese Journal of Applied Physics, 51*, 02BK13.

Izawa, K., Yamada, T., Unal, U., Ida, S., Altuntasoglu, O., Koinuma, M., & Matsumoto, Y. (2006). Photo electro chemical oxidation of methanol on oxide nanosheets. *The Journal of Physical Chemistry B, 110*, 4645.

Ji, E., Son, J., Kim, J. H., & Lee, G. H. (2018). Rolling up two-dimensional sheets into nanoscrolls. *FlatChem, 7*, 26.

Khun, K. (2015). *Synthesising metal oxide materials and their composite nanostructures for sensing and optoelectronic device applications.* Linköping University.

Kim, D. S., Ozawa, T. C., Fukuda, K., Ohshima, S., Nakai, I., Sasaki, T. (2011). Soft-chemical exfoliation of $Na_{0.9}Mo_2O_4$ Preparation and electrical conductivity characterization of a Molybdenum oxide nanosheet. *Chemistry of Materials, 23*, 2700.

Kim, H. -J., Osada, M., Ebina, Y., Sugimoto, W., Tsukagoshi, K., & Sasaki, T. (2016). Hunting for monolayer oxide nanosheets and their architectures. *Scientific Reports*, 6 (Article number: 19402).

Kim, H. -J., Osada, M., Ebina, Y., Sugimoto, W., Tsukagoshi, T., & Sasaki, T. (2016). Hunting for monolayer oxide nanosheets and their architectures. *Scientific Reports, 6* (Article number: 19402).

Kim, I. Y., Jo, Y. K., Lee, J. M., Wang, L., & Hwang, S. J. (2014). Unique advantages of exfoliated 2D-nanosheets for tailoring the functionalities of nanocomposites. *Journal of Physical Chemistry Letters, 5*, 4149.

Kim, K. -H., Kumar, B., Lee, K. Y., Park, H. -K., Lee, J. -H., Lee, H. H., Jun, H., Lee, D, Kim, S. -W. (2013) Piezoelectric two-dimensional nanosheets/anionic layer hetero junction for efficient direct current power generation. *Scientific Reports, 3* (Article number: 2017)(2013).

Kishimoto, F., Ano, T., Mochizuki, D., Terauchi, T., Maitani, M. M., Suzuki, E., & Wada, Y. (2016). Specific electronic absorptions of alternate layered nanostructures of two metal oxides synthesized via thiolene click reaction. *RSC Advances, 6*, 73830.

Kotani, Y., Taniuchi, T., Osada, M., Sasaki, T., Kotsugi, M., Guo, F.Z., Watanabe, Y., Kubota, M., & Ono, K. (2008). X-ray nano spectroscopic characterization of a molecularly thin ferromagnetic $Ti_{1-x}Co_xO_2$ nanosheet. *Applied Physics Letters, 93*, 093112.

Kumar, B., & Kim, S.-W. (2011). Recent advances in power generation through piezoelectric nano generators. *Journal of Materials Chemistry, 21*, 18946.

Kumar, D., & Ahmad, S. (2017). *Green intelligent nanomaterials by design (Using nanoparticulate/2D-materials building blocks) Current developments and future trends, Chapter 8;* Text available @ https://doi.org/10.5772/intechopen.68434

Kumar, K. S., Choudhary, N., Jung, Y., & Thomas, J. (2018). Recent advances in two-dimensional nanomaterials for super capacitor electrode applications. *ACS Energy Letters, 3*(2), 482.

Kumar, N., and Kumbhat, S. (2016). Characterization tools for nanomaterials. In N. Kumar & S. Kumbhat (Eds.), *Essentials in nanoscience and nanotechnology*. https://doi.org/10.1002/9781119096122.ch3

Kumar, P., Malik, H. K., Ghosh, A., Thangavel, R., & Asokan, K. (2013). Band gap tuning in highly c-axis oriented $Zn_{1-x}Mg_xO$ thin films. *Applied Physics Letters, 102*, 221903.

Lee, S., Jin, X., Kim, I. Y., Gu, T. H., Choi, J.-W., Nahm, S., & Hwang, S.-J. (2016). Superior additive of exfoliated RuO_2 nanosheet for optimizing the electrode performance of metal oxide over graphene. *Journal of Physical Chemistry C, 120*, 11786.

Lei, F., Sun, Y., Liu, K., Gao, S., Liang, L., Pan, B., & Xie, Y. (2014). Oxygen vacancies confined in ultrathin indium oxide porous sheets for promoted visible-light water splitting. *Journal of the American Chemical Society, 136*(19), 6826.

Li, D. J., Huang, Z., Hwang, T. H., Narayan, R., Choi, J. W., & Kim, S. O. (2016). Atomic thin titania nanosheet-coupled reduced graphene oxide 2D heterostructures for enhanced photo catalytic activity and fast lithium storage. *Electronic Materials Letters, 12*(2), 211.

Li, L., Guo, Y., Cui, X. Y., Zheng, R., Ohtani, K., Kong, C., Ceguerra, A. V., Moody, M. P., Ye, J. D., Tan, H. H., Jagadish, C., Liu, H., Stampfl, C., Ohno, H., Ringer, S. P., & Matsukura, F. (2012). Magnetism of Co- doped ZnO epitaxially grown on a ZnO substrate. *Physical Review, B 85*, 174430.

Li, L., Ma, R., Ebina, Y., Fukuda, K., Takada, K., & Sasaki, T. (2007). Layer-by-layer assembly and spontaneous flocculation of oppositely charged oxide and hydroxide nanosheets into inorganic sandwich layered materials. *Journal of the American Chemical Society, 129*, 8000.

Lin, B. Z., He, L. W., Zhu, B. L., Chen, Y. L., & Gao, B. F. (2012). Visible-light photo catalytic activity of mesoporous nanohybrid assembled by tantalotungstate nanosheets and manganese ions. *Catalysis Communications, 29*, 166.

Liu, Z., Ma, R., Osada, M., Iyi, N., Ebina, Y., Takada, K., & Sasaki, T. (2006). Synthesis, anion exchange, and delamination of Co-Al layered double hydroxide: Assembly of the exfoliated nanosheet/polyanion composite films and magneto-optical studies. *Journal of the American Chemical Society, 128*, 4872.

LP. (2018). *Chemical structure of layered perovskites.* Text @ https://chemicalstructure.net/portfolio/layered-perovskites/

Ma, R., & Sasaki, T. (2010). Nanosheets of oxides and hydroxides: Ultimate 2D charge-bearing functional crystallites. *Advanced Materials, 22*, 5082.

Ma, R., & Sasaki, T. (2015a). Two-dimensional oxide and hydroxide nanosheets: Controllable high-quality exfoliation, molecular assembly, and exploration of functionality. *Accounts of Chemical Research, 48*(1), 136.

Ma, R. Z., Sasaki, T. (2015). Organization of artificial superlattices utilizing nanosheets as a building block and exploration of their advanced functions. In D. R. Clarke (Ed.), The Annual Review of Materials Research, 45, p. 111.

Matsuba, K., Wang, C., Saruwatari, K., Uesusuki, Y., Akatsuka, K., Osada, M., Ebina, Y., Ma, R., & Sasaki, T. (2017). Neat monolayer filing of molecularly thin two-dimensional materials in 1 min. *Science Advances, 3*(6), e1700414.

Matsumoto, Y., Murakami, M., Shono, T., Hasegawa, T., Fukumura, T., Kawasaki, M., Ahmet, P., Chikyow, T., Koshihara, S., & Koinuma, H. (2001). Room-temperature ferromagnetism in transparent transition metal-doped titanium dioxide. *Science, 291*, 854.

Mei, J., Liao, T., & Sun, Z. (2018). Two-dimensional metal oxide nanosheets for rechargeable batteries. *Journal Energy Chemistry, 27*(1), 117.

Minamisawa, T., Oshida, K., Kobayashi, N., Ando, A., Misawa, D., Itaya, T., Moriyama, M., Osawa, K., Hata, T., Sugiyama, Y., Iguchi, H., & Kobayashi, N. (2018). Development of electrode materials of Lithium-Ion battery utilizing nano spaces. *Journal Carbon Research, 4*, 23.

Miyamoto, A., Kuwaki, Y., Sano, T., Hatakeyama, K., Quitain, A., Sasaki, M., & Kida, T. (2017). Solid electrolyte gas sensor based on a proton-conducting graphene oxide membrane. *ACS Omega, 2*, 2994.

Miyamoto, N., Yamada, Y., Koizumi, S., & Nakato, S. (2007). Extremely stable photo induced charge separation in a colloidal system composed of semiconducting Niobate and Clay nanosheets. *Angewandte Chemie, 46*, 4123.

Mochizuki, D., Kumagai, K., Maitani, M. M., Suzuki, E., & Wada, Y. (2014). Precise control of photo induced electron transfer in alternate layered nanostructures of Titanium Oxide-Tungsten Oxide. *The Journal of Physical Chemistry C, 118*, 22968.

Moseley, P. T. (2017). Progress in the development of semiconducting metal oxide gas sensors: a review. *Measurement Science and Technology, 28*, 082001.

Muramatsu, M., Akatsuka, K., Ebina, Y., Wang, K., Sasaki, T., Ishida, T., Miyake, K., & Haga, M. (2005). Fabrication of densely packed titania nanosheet films on solid surface by use of Langmuir-Blodgett deposition method without amphiphilic additives. *Langmuir, 21*(14), 6590.

Nakayama, H., & Katayama-Yoshida, H. (2001). Theoretical prediction of magnetic properties of $Ba(Ti_{1-x}\ M_x)O_3$ (M=Sc, V, Cr, Mn, Fe Co, Ni, Cu). *Japanese Journal of Applied Physics, 40*, L1355.

Neri, G. (2017). Thin 2D: The new dimensionality in gas sensing. *Chemosensors, 5*, 21.

Ohno, H. (1998). Making nonmagnetic semiconductors ferromagnetic. *Science, 28*, 951.

Ohwada, M., Kimoto, K., Mizoguchi, T., Ebina, Y., & Sasaki, T. (2013). Atomic structure of Titania nanosheet with vacancies. *Scientific Reports, 3*. (Article Number: 2801)(2013).

Omomo, W. Y., Sakai, N., Fukuda, K., Nakai, I., Ebina, Y., Takada, K., Watanabe, M., & Sasaki, T. (2003). Fabrication and characterization of multilayer ultrathin films of exfoliated MnO_2-nanosheets and polycations. *Chemistry of Materials, 15*, 2873.

Osada, M., Akatsuka, K., Ebina, Y., Funakubo, H., Ono, K., Takada, K., & Sasaki, T. (2010). Robust high-k response in molecularly thin perovskite nanosheets. *ACS Nano, 4*, 5225.

Osada, M., Ebina, Y., Fukuda, K., Ono, K., Takada, K., Yamaura, K., Takayama-Muromachi, E., Sasaki, T. (2006). Ferromagnetism in two-dimensional $Ti_{0.8}Co_{0.2}O_2$ nanosheets. *Physical Review B, 73*, 153301.

Osada, M., Ebina, Y., Takada, K., & Sasaki, T. (2006b). High-K dielectric nano films fabricated from Titania nanosheets. *Advanced Materials, 18*, 295.

Osada, M., Itose, M., Ebina, Y., Ono, K., Ueda, S., Kobayashi, K., & Sasaki, T. (2008). Gigantic magneto-optical effects induced by (Fe/Co) co-substitution in Titania nanosheets. *Applied Physics Letters, 92*, 253110.

Osada, M., & Sasaki, (2011). *Chemical nano manipulation of two-dimensional nanosheets and its applications.* Chapter 5. Dr. Y. Masuda (Ed.), Nanofabrication. ISBN:978-953-307-912-7; InTech.

Osada, M., Sasaki, T., Ono, K., Kotani, Y., Ueda, S., & Kobayashi, K. (2011). Orbital reconstruction and interface ferromagnetism in self- assembled nanosheet superlattices. *ACS Nano, 5*, 6871.

Powers, K. W., Brown, S. C., Krishna, V. B., Wasdo, S. C., Moudgil, B., & Roberts, S. M. (2006). Research strategies for safety evaluation of nanomaterials. Part VI. Characterization of nanoscale particles for toxicological evaluation. *Toxicological Sciences, 90*(2), 296.

Prashanti, B., & Damodharam, T. (2017). Development of GO-ZrO_2 nanocomposite: Enhanced photo-catalytic degradation of Cr(Vl) under Sunlight irradiation. *Journal of Nanoscience and Technology, 3*(2), 256.

Priour, Jr., D.J., Hwang, E.H., & Sarma, S. D. (2005). Quasi-two-dimensional diluted magnetic semiconductor systems. *Physical Review Letters, 95*, 037201.

Rahman, M. M., Alam, M. M., Asiri, A. M., & Islam, M. A. (2017). Ethanol sensor development based on ternary-doped metal oxide (CdO/ZnO/Yb_2O_3) nanosheets for environmental safety. *RSC Advances, 7*, 22627.

Rasmussen, F. A., & Thygesen, K. S. (2015). Computational 2D materials database electronic structure of transition-metal dichalcogenides and oxides. *Journal of Physical Chemistry C, 119*(23), 13169.

Ren, J., Zhang, H., & Cheng, X. (2013). Electronic and magnetic properties of all 3d-transition-metal-doped ZnO monolayers. *International Journal of Quantum Chemistry, 113*, 2243.

Riaz, S., Akbar, A., & Naseem, S. (2014). Ferromagnetic effects in Cr- doped Fe2031hin films. *IEEE Transactions on Magnetics, 50*, 2200704.

Rostamzadeh, T. (2016). *Engineering nanoarchitectures from nanosheets, nanoscrolls, and nanoparticles.* Ph.D. dissertation submitted to the University of New Orleans in Chemistry Nano-Materials.

Sakai, N., Ebina, Y., Takada, K., & Sasaki, T. (2004). Electronic band structure of titania semiconductor nanosheets revealed by electrochemical and photo electro chemical studies. *Journal of the American Chemical Society, 126*(18), 5851.

Sakai, N., Fukuda, K., Omomo, Y., Ebina, Y., Takada, K., & Sasaki, T. (2008). Hetero-nanostructured films of Titanium and Manganese oxide nanosheets: Photo induced charge transfer and electrochemical properties. *Journal of Physical Chemistry C, 112*, 5197.

Sakai, N., Fukuda, K., Shibata, T., Ebina, Y., Takada, K., & Sasaki, T. (2006). Photo induced hydrophilic conversion properties of titania nanosheets. *The Journal of Physical Chemistry B, 110*, 6198.

Saruwatari, K., Sato, H., Kameda, J., Yamagishi, A., & Domen, K. (2005). An evidence for role of organic layers in photo conductivity of organic/inorganic hybrid nanosheets as prepared by Langmuir-Blodgett methods. *ChemComm*, 1999.

Sasaki, T., Ebina, Y., Fukuda, K., Tanaka, T., Harada, M., & Watanabe, M. (2002). Titania nanostructured films derived from a titania nanosheet/polycation multilayer assembly via heat treatment and UV irradiation. *Chemistry of Materials, 14*(8), 3524.

Sasaki, T., Ebina, Y., Tanaka, T., Harada, M., Watanabe, M., & Decher, G. (2001). Layer-by-layer assembly of Titania nanosheet/polycation composite films. *Chemistry of Materials, 13*(12), 4661.

Sasaki, T., Nakano, S., Yamauchi, S., & Watanabe, M. (1997). Fabrication of Titanium dioxide thin flakes and their porous aggregate. *Chemistry of Materials, 9*, 602.

Sato, H., Okamoto, K., Tamura, K., Yamada, H., Saruwatari, K., Kogure, T., & Yamagishi, A. (2008). First-principles study of two-dimensional Titanium dioxides. *Applied Physics Express, 1*, 035001.

Sato, H., Ono, K., Sasaki, T., & Yamagishi, A. (2003). First-principles study of two-dimensional Titanium Dioxides. *The Journal of Physical Chemistry B, 107*(36), 9824.

Sato, J., Kato, H., Kimura, M., Fukuda, K., & Sugimoto, W. (2010). Conductivity of ruthenate nanosheets prepared via electrostatic self- assembly: Characterization of isolated single nanosheet crystallite to mono- and multilayer electrodes. *Langmuir, 26*, 18049.

Shang, X., Zhang, M., Wang, X., & Yang, Y. (2014). Sulfur, nitrogen-doped TiO_2-graphene oxide composites as a high performance photo catalyst. *Journal of Experimental Nanoscience, 9*(7), 749.

Sharma, A., Yan, H., Zhang, L., Sun, X., Liu, B., & Lu, Y. (2018). Highly enhanced many-body interactions in anisotropic 2D-semiconductors. *Accounts of Chemical Research, 51*(5), 1164.

Shi, X., Huang, Z., Huttula, M., Li, T., Li, S., Wang, X., Luo, Y., Zhang, M., & Cao, W. (2018). Introducing magnetism into 2D nonmagnetic inorganic layered crystals: A brief review from first-principles aspects. *Crystals, 8*, 24.

Shibata, T., Fukuda, K., Ebina, Y., Kogure, T., & Sasaki, T. (2008). One-nanometer-thick seed layer of unilamellar nanosheets promotes oriented growth of oxide crystal films. *Advanced Materials, 20*, 231.

Shibata, T., Sakai, N., Fukuda, K., Ebina, Y., & Sasaki, T. (2007). Photo catalytic properties of titania nanostructured films fabricated from titania nanosheets. *Physical Chemistry Chemical Physics: PCCP, 9*, 2413.

Shibata, T., Sakai, N., Fukuda, K., Ebina, Y., & Sasaki, T. (2009). Well- controlled crystal growth of zinc oxide films on plastics at room temperature using 2D nanosheet seed layer. *Materials Science and Engineering B, 161*(1–3), 12.

Shikano, M., Delmas, C., & Darriet, J. (2004). $NaRuO_2$ and $Na_xRuO_2{\cdot}yH_2O$: New oxide and oxyhydrate with two dimensional RuO_2 layers. *Inorganic Chemistry, 43*, 1214.

Su, P., Fu, W., Yao, H., Liu, L., Ding, D., Feng, F., Xue, Y., Liu, X., & Yang, H. (2017). Enhanced photovoltaic properties of perovskite solar cells by TiO_2 homogeneous hybrid structure. *Royal Society Open Science, 4*, 170942.

Sugimoto, W., Iwata, H., Yasunaga, Y., Murakami, Y., & Takasu, Y. (2003). Preparation of ruthenic acid nanosheets and utilization of its interlayer surface for electrochemical energy storage. *Angewandte Chemie International Edition, 42*, 4092.

Sugimoto, W., Omoto, M., Yokoshima, K., Murakami, Y., & Takasu, Y. (2004). Electrical and magnetic properties of ion-exchangeable layered ruthenates. *Journal of Solid State Chemistry, 177*, 4542.

Sun, M., Liu, H., Liu, Y., Qu, J., & Li, J. (2015). Graphene-based transition metal oxide nanocomposites for the oxygen reduction reaction. *Nanoscale, 7*, 1250.

Sun, P., Ma, R., Bai, X., Wang, K., Zhu, H., & Sasaki, T. (2017). Single-layer nanosheets with exceptionally high and anisotropic hydroxyl ion conductivity. *Science Advances, 3*(4), e1602629.

Sun, P. Z., Ma, R. Z., Osada, M., Sasaki, T., Wei, J. Q., Wang, K. L., Wu, D. H., Cheng, Y., & Zhu, H. W. (2012a). The formation of graphene-titania hybrid films and their resistance change under ultraviolet irradiation. *Carbon, 50*, 4518.

Sun, Y.-F., Liu, S.-B., Meng, F.-L., Liu, J.-Y., Jin, Z., Kong, L. T., & Liu, J.-H. (2012b). Metal oxide nanostructures and their gas sensing properties: A review. *Sensors, 12*, 2610.

Sun, Y., Liu, Q., Gao, S., Cheng, H., Lei, F., Sun, Z., Jiang, Y., Su, H., Wei, S., & Xie, Y. (2013). Pits confined in ultrathin cerium (IV) oxide for studying catalytic centers in carbon monoxide oxidation. *Nature Communications, 4*, 2899.

Sun, Z., Liao, T., Dou, Y., Hwang, S. M., Park, M.-S., Jiang, L., Kim, J. H., & Dou, S. X. (2014). Generalized self-assembly of scalable two-dimensional transition metal oxide nanosheets. *Nature Communications, 5*, 3813.

Ta, H. Q., Zhao, L., Pohl, D., Pang, J., Trzebicka, B., Rellinghaus, B., Pribat, D., Gemming, T., Liu, Z., Bachmatiuk, A., & Rümmeli, M. H. (2016). Graphene-like ZnO: A mini review. *Crystals, 6*, 100.

ten Elshof, J. E. (2017). Electronic band structure and electron transfer properties of two-dimensional metal oxide nanosheets and nanosheet films. *Current Opinion in Solid State and Materials Science, 21*(6), 312.

ten Elshof, J. E., Yuan, H., Rodriguez, P. G. (2016). Two-dimensional metal oxide and metal hydroxide nanosheets: Synthesis, controlled assembly and applications in energy conversion and storage. *Advanced Energy Materials*, 1600355.

Thiel, S., Hammerl, G., Schmehl, A., Schneider, C. W., & Mannhart, J. (2006). Tunable quasi-two-dimensional electron gases in oxide heterostructures. *Science, 313*(5795), 1942.

Timmerman, M. (2015). *Rapid exfoliation of metal oxides.* Bachelor Thesis, University of Twente. Text available @ https://essay.utwente.nl/68430/1/Bachelor_Thesis_Melvin_Timmerman%20s1243500%20%20openbaar.Pdf

Tsai, Y., Chang, S., Tang, I., Hsiao, Y., & Ji, L. (2018). High density novel porous ZnO nanosheets based on a micro heater chip for ozone sensors. *IEEE Sensors Journal, 18*(13), 5559.

Virdi, K. S., Kauffmann, Y., Ziegler, C., Ganter, P., Blaha, P., Lotsch, B. V., Kaplan, W. D., & Scheu, C. (2016). Band gap extraction from individual two-dimensional Perovskite nanosheets using valence electron energy loss spectroscopy. *Journal of Physical Chemistry C, 120*, 11170.

Wang, C., Osada, M., Ebina, Y., Li, B. W., Akatsuka, K., Fukuda, K., Sugimoto, W., Ma, R., & Sasaki, T. (2014). All-nanosheet ultrathin capacitors assembled layer-by-layer via solution-based processes. *ACS Nano, 8*, 2658.

Wang, L., & Sasaki, T. (2014). Titanium oxide nanosheets: Graphene analogues with versatile functionalities. *Chemical Reviews, 114*(19), 9455.

Wang, L., Wei, D., Kang, S., Xie, X., Shi, Y. (2018). Two-dimensional Titania: Structures and properties predicted by first principle calculation. *The Journal of Physical Chemistry C, 122*. (Article ASAP). https://doi.org/10.1021/acs.jpcc.8b05412

Wang, L. Z., Omomo, Y., Sakai, N., Fukuda, K., Nakai, I., Ebina, Y., Takada, K., Watanabe, M., & Sasaki, T. (2003). Fabrication and characterization of multilayer ultrathin films of exfoliated MnO_2 nanosheets and polycations. *Chemistry of Materials, 15*, 2873.

Wang, Z.L., Wang, X., Song, J., Liu, J., Gao, Y. (2008). PERVASIVE computing.Text @http://www.nanoscience.gatech.edu/paper/2008/08_PVC_1.pdf

Wen, L., Zhou, M., Wang, C., Mi, Y., & Lei, Y. (2016). Functional nanostructuring for efficient energy conversion and storage. *Advanced Energy Materials, 6*(23) (2016). 7 December 2016 (Special Issue). https://doi.org/10.1002/aenm.201670132.

Xia, Y., Li, R., Chen, R., Wang, J., & Xiang, L. (2018). 3D architectured graphene/metal oxide hybrids for gas sensors: A Review. *Sensors, 18*, 1456.

Xie, W., Li, Z., Shao, M., & Wei, M. (2018). Layered double hydroxide- based core-shell nanoarrays for efficient electrochemical water splitting. *Frontiers of Chemical Science and Engineering*. Text @. https://doi.org/10.1007/s11705-018-1719-6

Xiong, P., Ma, R., Sakai, N., & Sasaki, T. (2018). Genuine unilamellar metal oxide nanosheets confined in a superlattice-like structure for superior energy storage. *ACS Nano, 12*(2), 1768.

Xu, Z., Zhuang, C., Zou, Z., Wang, J., Xu, X., & Peng, T. (2017). Enhanced photo catalytic activity by the construction of a TiO_2/carbon nitride nanosheets hetero structure with high surface area via direct interfacial assembly. *Nano Research, 10*(7), 2193.

Yamaki, T., & Asai, K. (2001). Alternate multilayer deposition from Ammonium amphiphiles and Titanium dioxide crystalline nanosheets using the Langmuir-Blodgett technique. *Langmuir, 17*, 2564.

Yang, M.-C., Lee, Y.-Y., Xu, B., Powers, K., & Meng, Y. S. (2012). TiO_2 flakes as anode materials for Li-ion-batteries. *Journal of Power Sources, 207*, 166.

Ye, M., Zhang, Z., Zhao, Y., & Qu, L. (2018). Graphene platforms for smart energy generation and storage. *Joule, 2*, 245.

Yuan, H., Lubbers, R., Besselink, R., Nijland, M., & ten Elshof, J. E. (2014). Improved Langmuir-Blodgett titanate films via in situ exfoliation study and optimization of deposition parameters. *ACS Applied Materials & Interfaces, 6*, 8567.

Yui, T., Kobayashi, Y., Yamada, Y., Tsuchino, T., Yano, K., Kajino, K., Fukushima, Y., Torimoto, T., Inoue, H., & Takagi, K. (2006). Photo chemical electron transfer though the interface of hybrid films of titania nanosheets and mono-dispersed spherical mesoporous silica particles. *Physical Chemistry Chemical Physics: PCCP, 8*, 4585.

Zhang, D., Sun, W., Chen, Z., Zhang, Y., Luo, W., Jiang, Y., & Dou, S. X. (2016). Two-dimensional Cobalt-Nickel-based oxide nanosheets for high-performance Sodium and Lithium storage. *Chemistry A European J., 22*(50), 18060.

Zhang, G., Zheng, L., Zhang, M., Guo, S., Liu, Z.-H., Yang, Z., & Wang, Z. (2012). Preparation of Ag-nanoparticle-loaded MnO_2 nanosheets and their capacitance behavior. *Energy & Fuels, 26*, 618.

Zhang, J. T., Jiang, J. W., & Zhao, X. S. (2011). Fundamental theory of piezotronics. *Journal of Physical Chemistry C, 115*, 6448.

Zhang, M., Shi, X., Wang, X., Li, T., Huttula, M., Luo, Y., & Cao, W. (2017). Transition metal adsorbed-doped ZnO monolayer: 2D-dilute magnetic semiconductor, magnetic mechanism, and beyond 2D. *ACS Omega, 2*, 1192.

Zhong, Y., Yang, Y., Ma, Y., & Yao, J. (2013). Controlled synthesis of ultrathin lamellar EU_2O_3 nanocrystals: Self-assembly of 1D-nanowires to 2D-nanosheets. *Chemical Communications, 49*, 10355.

Zhou, W., Umezawa, N., Ma, R., Sakai, N., Ebina, Y., Sano, K., Liu, M., Ishida, Y., Aida, T., & Sasaki, T. (2018). Spontaneous direct band gap, high hole mobility, and huge exciton energy in atomic-thin TiO_2 nanosheet. *Chemistry of Materials, 30*(18), 6449.

Ziegler, C. (2015). *Two-dimentional transition metal oxide nanosheets for nanoarchitechtronics* (Ph.D. thesis) submitted to Ludwig-Maximilians-Universität München, Germany.

Chapter 9
Modeling and Simulation of Nano-Structured 2D Materials

Neha Ahlawat and Vinay Panwar

1 Introduction

The development of nanomaterials has invoked multidiscipline-oriented approach due to their multifunctional properties. Diversified properties of 2D nanomaterials make them suitable for wide range of applications which includes biotechnology, electronic devices, energy storage, optical devices, sensors, etc. (Yang et al., 2013; Xu et al., 2013; Choi et al., 2017; Liu et al., 2011; Zhang, 2015; Ping et al., 2017; Zhu et al., 2017). This led to the design and development of new materials for improving the performance of typical devices and structures. Two-dimensional (2D) nanomaterials are typical nanostructures having two dimensions higher than nanoscale range i.e., 0–100 nm. Though experimental characterizations have attested the incredible properties of 2D nanomaterials but it has been very challenging, time-consuming, and cost-ineffective to choose typical experimental techniques for synthesis and processing of such nanomaterials.

Modeling and simulation methodologies employ investigative tools for development of reliable mathematical and computational models, predicting the existence of typical nanostructures and analyzing the properties (e.g. mechanical, electrical, thermal, etc.) of nanomaterials. In early 2000, when carbon nanotubes (CNTs) and graphene were emerged as multifunctional 2D materials, researchers realized the need to understand changes in properties of similar basic nanostructures through their modification at atomic/molecular levels. Some of such characteristic nanomaterials include hexagonal boron nitride (hBN), germanium phosphide (GeP), silicon

N. Ahlawat
Department of Mathematics, Jaypee Institute of Information Technology, Noida, Uttar Pradesh 201304, India

V. Panwar (✉)
Mechanical Engineering Department, Netaji Subhas University of Technology, Dwarka, New Delhi 110078, India

S. Singh et al. (eds.), *Advanced Applications of 2D Nanostructures*,
Materials Horizons: From Nature to Nanomaterials,
https://doi.org/10.1007/978-981-16-3322-5_9

arsenide (SiAs), 2D oxides, phosphorene, 2D chalcogenides, different graphene derivatives, etc. (Geim & Grigorieva, 2013; Mortazavi & Rabczuk 2018). Though the realistic applicability of such nanomaterials can be accurately defined by experimentations, but it is unrealistic to try for various possible nanostructures. The investigative tools used in theoretical approaches have been found very helpful for saving time, cost, and efforts for conducting unfruitful experimentations. Therefore it is highly essential to mark for the accuracy and efficiency to such modeling and simulation tools/techniques. The development of technology in addition to the advancements in modeling framework is the only way for betterment of computational methods. Nanotechnology is actually based on the applicability of facts into real technologies.

Application of modeling and simulation has increased the opportunities for development in electronics, biomedical, aerospace, energy, and various other areas. The study of physicochemical properties of various molecular and condensed phase systems involves the analysis of their dynamic behavior at atomistic/molecular scale. This phenomenon is also acceptable for the regenerative materials and life sciences which include organic solids, virtual screening, macromolecular complexes, drug development and delivery, etc. It has been noticed that the use of typical simulation techniques which were developed for bulk materials can be applied to nanomaterials with modification in those original methods. The use of advanced computer systems has provided multiple opportunities to the researchers for reconfiguration of the modeling and simulation tools to study the size-dependent properties and behavior of nanoscale materials. A brief overview regarding different simulation methods has been provided in the next section.

2 Simulation Methodologies

Molecular Dynamic (MD) and Monte Carlo (MC) simulations are two basic approaches which had been widely used for computational materials research from nano- to meso-scale. In these computational methods, the atoms or molecules are confined in a small geometrical region which is considered as a cell. The fundamental difference between these two methods is that MD method analyzes the molecular movements within the cells using Newton's equations of motion, whereas MC method employs probabilistic approach for accepting or rejecting the movements of atoms or molecules. In this regard, MC simulations represent molecular chains as simpler models and thereby reduce the simulation time to a considerable extent. These basic approaches are really essential to understand the broad classification of different tools and techniques employed for the computer-based simulation of nanomaterials. In this section, a brief discussion about these basic methodologies has been included which may help to choose a suitable approach while analyzing desirable properties of the nanostructures. This section includes a brief introduction about the general approaches used for MD and MC simulation techniques which are commonly used to analyze the properties of materials at atomic/molecular scale.

2.1 Molecular Dynamic Method

The modeling of molecular systems using MD approach enables nearly accurate calculations regarding various functional and structural properties of the nanomaterials. MD simulations provide the details about behaviour of materials at atomic/molecular level to resolve molecular structure and localized interactions. The physicochemical properties of atomic structures obtained from typical MD simulation techniques are also helpful in determining different possibilities for surface modification of the nanostructures which may sometimes considered as a part of design and development of new nanomaterials.

The molecular modeling has been initiated by E. Schroedinger on the basis of equation commonly known as Schroedinger equation (SE), which is given as,

$$H\psi = E\psi \tag{1}$$

Here, ψ represents the waviness of wave-like particles using wavefunctions obtained by solving the Eq. 1. SE generally describes the locations of electrons and nuclei of the molecules within confined space as well as their constrained energies under the given set of conditions. Due to limited technological development, it was very difficult to find the analytical solutions of the SE for the molecular system comprised of number of electrons. The approximate solutions of SE were categorized as ab-initio and semiempirical. The main difference between the two methods was that semiempirical methods neglect some of the time-consuming mathematical terms, whereas ab-initio methods include all the terms in SE. The introduction of computers has made it possible to solve the SE including all the simplifying terms for the molecular systems with large number of electrons. With developments in computer technology, the remaining hurdles and time for the analytical solution of such molecular system have significantly reduced which simplified the modeling of molecular systems (Berendsen, 2007). Though it has only provided an idea regarding the location of electrons and their energies, but at the same time provided an idea to the researchers regarding possibility for developing different analytical methods to study different properties of such molecular systems. The main drawback of this approach was indistinguishable details regarding differently charged particles (i.e. electrons and neutrons) of the molecular system. In this regard, Max Born and J. Robert Oppenheimer introduced an approximation method which makes it possible to separate the motion of nuclei and electrons. This method is popularly known as Born–Oppenheimer approximation which consists of separable components of wavefunction and energy, as highlighted by Eqs. 2 and 3, respectively.

$$\psi_{\text{total}} = \psi_{\text{electronic}} \times \psi_{\text{nuclear}} \tag{2}$$

$$E_{\text{total}} = E_{\text{electronic}} + E_{\text{vibrational}} + E_{\text{rotational}} + E_{\text{nuclear}} \tag{3}$$

It has been found that the motion of particles (i.e. electrons and neutrons) can be described with the help of laws of classical mechanics which introduces the need for exposing the mechanical and dynamic (bonding between atoms) properties of the molecular models/structures. These methods are recognized as molecular dynamic methods. Observations have proved that the calculation time using Born–Oppenheimer approximation is significantly less than the quantum mechanics approach. In 1959, Alder and Wainwright (1959) first time reported the use of this method to study simple fluid models with atoms represented as rigid spheres. This simulation study was considered as first molecular dynamic simulation method. Similar research articles have been published in subsequent years where simulations on polar molecule (such as water) (Rahman & Stillinger, 1971; Berendsen et al., 1981; Jorgensen et al., 1983), polymer chain (Ryckaert & Bellemans, 1978), macromolecule (Karplus, 2003), nucleic acids (Levitt, 1983), and biological membrane (Vander Ploeg & Berendsen, 1982) have been performed. Such types of simulation studies have attested the ability of MD simulations for investigating typical physical and chemical properties of materials at molecular level. In addition, these methods enabled a close physiochemical examination of structures without performing real-time experimental methods using harsh chemicals and experimental conditions. The results of MD simulations of nanomaterials and biomaterials have accelerated the need of simulation in different fields of basic sciences (Lee et al., 2009; Dror et al., 2012).

MD simulations are based on potential energy function which allows calculation of forces experienced by atoms located at particular positions. The effect of forces on motion of atoms is studied using Newton's law of motion (2nd law), i.e.

$$F = ma \tag{4}$$

where, F is force on an atom, m is mass of the atom, and a is the atom's acceleration.

For a molecular system comprising of 'N' atoms, the Newton's law for MD simulation is shown by Eq. 5,

$$m_i \frac{\partial^2 r_i}{\partial t^2} = F_i; i = 1, 2, \ldots, N \tag{5}$$

Here, r_i represents the position vector of particle 'i'.

Also, the force on particular particle equals the negative derivative of potential function (V) for that particle. Mathematically, this can be represented using Eq. 6,

$$F_i = -\frac{\partial V}{\partial r_i} \tag{6}$$

Using Eqs. 5 and 6, the relation between potential energy function and time can be shown as,

$$m_i \frac{\partial^2 r_i}{\partial t^2} = -\frac{\partial V}{\partial r_i} \tag{7}$$

Further, the trajectory of an atom is mainly dependent on its initial position and velocity. This is particularly due to the deterministic equations of motion which help to calculate the position and velocities of different atoms at selective time intervals. The momentum 'P' of molecular system, i.e. product of mass and velocity of different atoms, at particular time instant and constant temperature are always zero.

$$P = \sum_{i=1}^{N} m_i v_i = 0 \tag{8}$$

The probability 'p' for velocity 'v_x' in x-direction of a particular atom 'i' at specific temperature 'T' is given on the basis of Maxwell–Boltzmann or Gaussian distribution. While, considering the movement in one direction, it follows Maxwellian distribution function as shown in Eq. 9,

$$p(v_{ix}) = \left(\frac{m_i}{2\pi k_B T}\right)^{1/2} \exp\left[-\frac{1}{2}\frac{m_i {v_{ix}}^2}{k_B T}\right] \tag{9}$$

This approach predicts the material's behavior on the basis of movement of atoms or molecules. Initially, the equations of motion for interacting particles are integrated to define the atomistic position of the molecules comprising those particles. Thereafter, the pathway of molecules w.r.t. time domain is reflected as the result of particular simulation. Subsequently, the pathway assists for analyzing typical structural and dynamic properties of the system which describes the kinetic and thermodynamic behavior of the molecular structure.

The equations of motion needed to depict the potential energy of the atoms comprising the molecular system do not have analytical solution. Such equations are numerically solved using various algorithms e.g. Verlet algorithm, Leap-frog algorithm, Velocity-Verlet algorithm, Beeman's algorithm. The choice of particular algorithm depends upon its computational efficiency, provision of long time step for integration, and ability to conserve energy and momentum. In addition, energy minimization is a particular part in MD simulation which is mostly required in two particular cases. First, when it becomes difficult to stabilize (bring equilibrium) the initial configuration of molecular system. Another reason is presence of kinetic energy in the molecular system which develops the thermal noise in the structures as well as potential energies of the system.

2.2 Monte Carlo Method

Monte Carlo simulation is a mesoscopic approach which provides a timely solution using the generated chance variables, exhibiting random behavior. Herein, stochastic transitions are used instead of deterministic equations used in MD simulation, to study the effect of slow processes in molecular system. It is also known as a coarse-grained method. Although these methods do not include the atomistic details required for resolving the molecular structure and analyzing the localized interactions, they provide necessary details about the chemical structure which help to simulate the behavior of nanomaterials (Kremer & Muller-Plathe, 2001). The systematic procedure for MC simulations is well explained in the book authored by Dierk Raabe (1998). The basic steps involved in that procedure are as follows:

(i) To generate samples from the random variables which are selected as input values for the simulation experiments. It involves the generation of random variables and transformation of these variables to another random variables using the given distribution function.
(ii) To solve the distribution function using selected samples and evaluate performance functions. This process is generally termed as 'numerical experimentation'.
(iii) Analysis of the resultant data or output performance functions for extracting probabilistic information by using appropriate statistical methods.

On the basis of above discussion, simulation using Monte Carlo approach is mainly based on random numbers which may exhibit the random walk of particular particles or macroscopic objects. Some of the examples based on MC simulation methods include modeling of polymers, diffusion-limited aggregation (DLA) of colloidal particles, study of motion of fluids by considering blocks of fluid as individual particles, etc. (Gates et al., 2005; Landau & Binder, 2009). Using MC simulation approach, Hendren et al. (2013) have developed a mass balance model which has shown that the coating on silver nanoparticles can be useful for its stabilization in the suspension and shown its effectiveness for application in wastewater treatment plant. Recently in 2016, Paro et al. (2016) have carried out a comparative study between analytical and MC simulation to study the dose enhancement factors in nanoparticle-enhanced X-ray radiation therapy, based on source of energy deposition, nanoparticle materials, and concentration regime. In this research work, authors have attested the superior ability of MC simulation overanalytical approach for the selected problem. Angelescu et al. (2010) have examined the structural features of Platinum-Bismuth (PtBi) bimetallic nanoparticles synthesized in water–oil microemulsion using a coarse model solved by MC simulations. This study evident the experimental conditions required for designing specific bimetallic structures.

2.3 Ab Initio Methods

Ab initio or first principle based methods are mainly used to study the behavior of materials having length scale of 10^{-10} m with the help of complex SE. However, it has been difficult to use the SE for solving the complex many-body systems eg., condensed phase materials, nanotubes, clusters, nanowires, etc. Hohenberg have proposed a theory in 1964, popularly known as Density Functional Theory (DFT), by replacing the electrons with effective electrons in such a way that the total density can be expressed according to the relation given in Eq. 10 (Karakasidis & Charitidis, 2007),

$$\rho(r) = \sum_{i=1}^{n} |\psi_i(r)|^2 \tag{10}$$

where, ψ_i can be obtained as the solution of the Eq. 11 given below,

$$\left[-\frac{\hbar^2}{2m}\nabla^2 + V_{eff}\right]\psi_i(r) = \varepsilon_i \psi_i(r) \tag{11}$$

Herein, V_{eff} is the effective potential due to Coulomb and exchange–correlation contributions.

Still, DFT was unable to provide the solution for above equations. Local density approximation (LDA) has been provided more accurate solution of the equation but with certain limitations of system equilibrium and non-uniform charge densities which were further improved by generalized gradient approximation (GGA). These DFT-LDA approximations were used for calculating band structures, cohesive and chemisorption energies, activation barriers, etc. Vienna Ab Initio Simulation Package (VASP) is one of the popular DFT simulation programs. Ab initio molecular dynamics (AIMD) has become an advanced approach to study the physical and chemical behavior of nanomaterials in a broad sense. This is generally performed by employing the MD (i.e. considering the interatomic forces) with DFT codes using typical simulation tools e.g. VASP, LAMMPS, etc.

3 Significant Tools/Techniques Used for Molecular Dynamic Simulation

This section includes a brief discussion about various tools which can be used for the MD simulation of nanomaterials. These tools are basically the computer programs developed by researchers which have similar basic features. The choice of particular technique depends upon the material/structure, force field parameters and typical properties needed to define the applicability of corresponding material.

3.1 GROMACS

GROningen MAchine for Chemical Simulations (GROMACS) is mainly designed for the simulation of bio-based systems including proteins, membranes, DNA, RNA, nucleic acids, and lipids. It is very rapid and user friendly in comparison to other softwares. The compatibility of GROMACS is certainly due to user-friendly command line interface, flexible force field, real-time calculation progress, and broad trajectory library.

3.2 AMBER

Assisted Model Building with Energy Refinement (AMBER) is another suitable program for simulation of biomolecules. This software applies forcefields to the biomolecules using a set of programs which includes typical force field parameters i.e. force constants, charges equilibrium bond lengths, and angles.

3.3 LAMMPS

Large-scale atomic/molecular massively parallel simulator (LAMMPS) is one of the popular MD simulation tools which enable the modeling of materials using typical simulation codes. LAMMPS is free and open-source software. The codes are designed on the basis of force fields and boundary conditions. LAMMPS is generally used to model the particles which may be present in any state of matter and constituting atomic to macroscopic systems including polymers, metals, ceramics as well as oxides. This simulation tool integrates Newton's equations of motion for modeling a collection of interacting particles.

3.4 Desmond

Desmond is one of the MD simulation tools which is used to calculate the absolute and free energy of biological systems. The fixed-charged force fields generated in such system is used to compute the energy and forces in the system. Some examples of supported force fields are CHARMM, AMBER, OPLS, etc. the trajectory of particles can be viewed and analyzed in this software during the simulation process. The calculations of energy and forces are performed on the basis of Ewald techniques. This software includes various tools for the energy minimization, position restoring, and molecular configurations.

3.5 Tinker

Tinker software contains algorithms for molecular mechanics as well as dynamics. It may use the force field setup parameters included in AMBER, CHARMM, OPLS, AMOEBA, etc. the built-in special features in Tinker supports the simulation of biopolymers. This simulation software includes various programs for energy minimization, vibration analysis, free energy calculations, single point potential energies, intermolecular potential parametric fitting, locating transition state between two minima, building bio-based structures (e.g. protein and nucleic acid), annealing under controlled cooling behavior, etc.

3.6 ESPResSo

ESPResSo is used for simulation of coarse-grained models of liquid crystals, ferrofluids, polymers, colloids, and biological systems based on physics, molecular biology, and chemistry. Coarse-grained models constitute a system composed of group of atoms/molecules which show the qualitative behavior of desired properties. The algorithms in this software contain hydrodynamic and electrostatic interactions. Therefore, it is generally used to describe the theoretical models. ESPResSo is also free and open-source software.

3.7 CHARMM

CHARMM stands for Chemistry at Harvard Macromolecular Mechanics. CHARMM is primarily focused on the simulation of biological elements such as carbohydrates, peptides, lipids, proteins, nucleic acids, etc. using the tools available for energy minimization, path sampling, free energy calculations, and molecular modeling. This software can be easily used for simulating the multi-particle systems.

3.8 GROMOS

GROMOS stands for Groningen Molecular Simulation. It simulates the multi-particle systems using MD simulation based on Newtonian equations of motion. GROMOS can be used for simulating the systems comprising of complicated bonded as well as nonbonded interactions. This makes it applicable for both the biological and non-biological systems. GROMOS is gaining attention of researches due to user-friendly interface, non-scripting language, display of expected time for completion of simulation run, trajectory viewer, storage of trajectory data, trajectory analysis,

improving the accuracy by extending the time steps in simulation, fully automated topology builder for small molecules to structures and free availability.

3.9 NAMD

NAMD stands for Nanoscale Molecular Dynamics. The force field in NAMD includes bonded interactions and pairwise interactions (electrostatic and van der Waals forces). The force field is same as that in CHARMM. Herein, simulation algorithms are designed for constant energy/temperature/pressure dynamics, boundary conditions, energy minimization, harmonic restraints, etc. Some important features of NAMD include multiple time stepping to describe the positions and velocities of the atoms in time; compatible input and output file formats; ease to modify and extend the algorithm; interactive simulation system; and load balancing.

4 Investigation of Nano-Structured Materials Using Typical Simulation Techniques

The studies related to typical properties of nanomaterials are commonly explored using atomistic methods of simulations i.e. Ab initio methods and molecular dynamics methods. This section is mainly focused towards discussion of some significant achievements in study of different carbon-based (carbonous) and non-carbonous nanomaterials' properties using particular modeling and simulation methods/tools.

4.1 Carbonous Nanomaterials

The investigation of carbon-based nanomaterials has initiated with fullerenes but the promising diversified properties of carbon nanotubes (CNTs) and graphene captured the attention of researches to explore their structure, properties, and various opportunities to tune their properties. Although significant initial experimentation have attested the promising ability of these carbonous nanomaterials (Iijima, 1991; Iijima & Ichihashi, 1993; Dresselhaus et al., 1995), use of sophisticated equipments and development of particular chemical/physical approaches restrict the researchers to invest time and resources in conducting unproductive trials for tuning the properties of such nanomaterials. In this regard, modeling and simulation have attested its effectiveness for proposing their possible structural modification and random properties.

In 2000, Lier et al. (2000) have conducted the first ab initio study to calculate the Young's modulus and Poisson's ratio of closed single-walled nanotubes and

graphene 2D nanostructures. It was observed that the theoretically calculated values of Young's moduli were in close approximation with the values reported on the basis of experimentations. Thereafter in 2010 Ni et al. (2010) conducted an advanced study using MD to analyze the anisotropic behavior of 2D graphene nanosheets loaded in different directions. They noticed that the Young's modulus and third-order elastic modulus in the longitudinal mode was higher than in the transverse mode which causes the failure of nanosheets in longitudinal mode. Moreover, it has also been noticed that the cyclic (loading and unloading) stress–strain curves obtained for nanosheets unloaded before the fracture point, were overlapped. Thereby, authors have attested the elastic and reversible deformation behavior of graphene nanosheets. Grantab et al. (2010) studied the mechanical strength tilt grain boundaries i.e. zigzag- and armchair-oriented graphene sheets, using MD and DFT calculations. They have reported that strain generated in critical bonds decrease with increase in grain boundary angle due to which the ultimate strength of nanosheets increases. Shen et al. (2010) investigated the elastic properties of graphene nanosheets with different aspect ratio under different loading conditions and varying temperature using MD simulation. In addition to the size-dependent and temperature-dependent properties of graphene nanosheets, their calculations have also confirmed the anisotropic behavior of such nanosheets. Further, authors have also reported that the effective thickness of zigzag sheets is larger than that of armchair sheets.

Nowadays researchers have become more interested to study the possibilities and effects of change in structure of carbon nanotubes and graphene. In one of such research works, Mortazavi et al. (2016) investigated the temperature-dependent mechanical properties and thermal conductivity of 2D nitrogenated holey graphene having C_2N stoichiometry with the help of first principles calculations based on DFT and MD simulations. They reported values of elastic modulus, tensile strength, thermal conductivity, and effective phonon mean free path at particular temperatures and offered a promising nanomaterial for experimental synthesis and application.

4.2 Non-Carbonous Nanomaterials

Besides carbon-based nanomaterials the scope of modeling and simulation is increasing towards analysis of 2D nanostructured materials based silicon (Si), titanium (Ti), germanium (Ge), etc. Manjanath et al. (2014) have reported the stability for planer form of nickel (Ni) doped silicene using first principles DFT calculations. The stability of its planer structure was confirmed on the basis of higher in-plane stiffness than buckled structure of silicene. Authors have also compared the effect of other dopants, i.e. iron (Fe), and cobalt (Co), and the structural stability of doped Ge and tin (Sn) based 2D nanomaterials. Study revealed that doped Sn nanosheets show planer stability but transition metal-doped Ge-based nanostructures are unstable for both planer as well as buckled forms. Mortazavi et al. (2017) have reported similar research work in 2016 which includes stress–strain properties of 2D allotropes of Si, Ge, and Sn i.e. silicene, germanene and stanene, respectively. Here again, authors

have calculated mechanical properties of these 2D structures through uniaxial tensile and compressive simulations based on first principles DFT calculations. In addition the calculations of electronic density of state (DOS) have also been carried out to explore the variation in electronic properties of nanosheets with loading intensity.

In one of the experimental-computational approach by Cao et al. (2017) DFT and Finite element modeling (FEM) have been used to identify the fact for improvement in Young's modulus of titania (TiO_2)/graphene hetrostructure after introduction of graphene layer. Simulation studies have suggested the reinforcing ability of graphene layer and strong adhesion at the interface between TiO_2 and graphene being the reason for improvement in stress-bearing ability of synthesized hetrostructure. Recently in 2018, Mortazavi and Rabczuk (2018) have explored the possibilities of engineering in band gap of Si and Ge based nanostructures using DFT simulations. This study suggests the strain tuneable band-gap character of 2D nanostructures of GeP, GeAs, SiP, and SiAs with change in mechanical loading conditions. In this way, computer simulation has provided a direction for conducting experimentation for the synthesis of nanomaterials with required properties. Various tools/packages used for MD simulations as well as ab initio methods are very helpful to suggest possibility of typical nanostructures and sometimes to explain characteristic properties of synthesized nanomaterials.

5 Summary and Future Prospects

The importance of modeling and simulation for exploring the magnificent properties of nanostructures has been discussed in this chapter. Multiscale simulation techniques enable researchers with integrated analysis tools that are required to predict the material's behavior. Various methodologies and techniques used for simulation provide an opportunity to study desirable properties of nanomaterials and to think about possibility for new nanostructures. It has been very helpful to minimize the high cost of synthesis of nanomaterials which are prepared through complicated experimental setups. In addition, this chapter provides an idea related to tools/softwares which are available for simulation. A close examination of these techniques may be helpful to modify or develop the algorithms for further examination of typical nanostructures.

References

Alder, B. J., & Wainwright, T. E. (1959). Studies in molecular dynamics.1. General method. *The Journal of Chemical Physics, 31*, 459–466.

Angelescu, D. G., Magno, L. M., & Stubenrauch, C. (2010). Monte Carlo simulation of the size and composition of bimetallic nanoparticles synthesized in water in oil microemulsions. *The Journal of Physical Chemistry C, 114*, 22069–22078.

Berendsen, H. J. C. (2007). *Simulating the physical world: Hierarchical modeling from quantum mechanics to fluid dynamics*. Cambridge University Press.

Berendsen, H. J. C., Postma, J. P. M., van Gunsteren, W. F., & Hermans, J. (1981). Interaction models for water in relation to protein hydration. In B. Pullman (Ed.), *Intermolecular forces* (pp. 331–342). Springer.

Cao, C., Mukherjee, S., Liu, J., Wang, B., Amirmaleki, M., Lu, Z., Howe, J. Y., Perovic, D., Sun, X., Singh, C. V., Sun, Y., & Filleter, T. (2017). Role of graphene in enhancing the mechanical properties of TiO_2/Graphene heterostructures. *Nanoscale, 9*, 11678–11684.

Choi, W., Choudhary, N., Han, G. H., Park, J., Akinwande, D., & Lee, Y. H. (2017). Recent development of two-dimensional transition metal dichalcogenides and their applications. *Materials Today, 20*, 116–130.

Dresselhaus, M. S., Dresselhaus, G., & Eklund, P. C. (1995). *Science of fullerenes and carbon nanotubes*. Academic Press.

Dror, R. O., Dirks, R. M., Grossman, J. P., Xu, H., & Shaw, D. E. (2012). Biomolecular simulation: A computational microscope for molecular biology. *Annual Review of Biophysics, 41*, 429–452.

Gates, T. S., Odegard, G. M., Frankland, S. J. V., & Clancy, T. C. (2005). Computational materials: Multi-scale modeling and simulation of nanostructured materials. *Composites Science and Technology, 65*, 2416–2434.

Geim, A. K., & Grigorieva, I. V. (2013). Van der waals heterostructures. *Nature, 499*, 419–425.

Grantab, R., Shenoy, V. B., & Ruoff, R. S. (2010). Anomalous strength characteristics of tilt grain boundaries in graphene. *Science, 330*, 946–948.

Hendren, C. O., Badireddy, A. R., Casman, E., & Wiesner, M. R. (2013). Modeling nanomaterial fate in wastewater treatment: Monte Carlo simulation of silver nanoparticles (nano-Ag). *Science of the Total Environment, 449*, 418–425.

Iijima, S. (1991). Helical microtubules of graphitic carbon. *Nature, 354*, 56–58.

Iijima, S., & Ichihashi, T. (1993). Single-shell carbon nanotubes of 1-nm diameter. *Nature, 363*, 603–605.

Jorgensen, W. L., Chandrasekhar, J., & Madura, J. D. (1983). Comparison of simple potential functions for simulating liquid water. *The Journal of Chemical Physics, 79*, 926–935.

Karakasidis, T. E., & Charitidis, C. A. (2007). Multiscale modeling in nanomaterials science. *Materials Science and Engineering C, 27*, 1082–1089.

Karplus, M. (2003). Molecular dynamics of biological macromolecules: A brief history and perspective. *Biopolymers, 68*, 350–358.

Kremer, K., & Muller-Plathe, F. (2001). Multiscale problems in polymer science: Simulation approaches. *MRS Bulletin, 26*, 205–210.

Landau, D. P., & Binder, K. (2009). *A guide to Monte Carlo simulations in statistical physics* (3rd ed.). Cambridge University Press.

Lee, E. H., Hsin, J., Sotomayor, M., Comellas, G., & Schulten, K. (2009). Discovery through the computational microscope. *Structure, 17*, 1295–1306.

Levitt, M. (1983) Computer simulation of DNA double-helix dynamics. In *Cold Spring Harbor symposia on quantitative biology*. Cold Spring Harbor Laboratory Press.

Lier, G. V., Alsenoy, C. V., Doren, V. V., & Geerlings, P. (2000). Ab initio study of the elastic properties of single-walled carbon nanotubes and graphene. *Chemical Physics Letters, 326*, 181–185.

Liu, M., Yin, X., Ulin-Avila, E., Geng, B., Zentgraf, T., Ju, L., Wang, F., & Zhang, X. (2011). A graphene-based broadband optical modulator. *Nature, 474*, 64–67.

Manjanath, A., Kumar, V., & Singh, A. K. (2014). Mechanical and electronic properties of pristine and Ni-doped Si, Ge, and Sn sheets. *Physical Chemistry Chemical Physics, 16*, 1667–1671.

Mortazavi, B., & Rabczuk, T. (2018). Anisotropic mechanical properties and strain tuneable band-gap in single layer SiP, SiAs, GeP and GeAs. *Physica E: Low-Dimensional Systems and Nanostructures, 103*, 273–278.

Mortazavi, B., Rahaman, O., Makaremi, M., Dianat, A., Cuniberti, G., & Rabczuk, T. (2017). First-principles investigation of mechanical properties of silicene, germanene and stanene. *Physica E: Low-Dimensional Systems and Nanostructures, 87*, 228–232.

Mortazavi, B., Rahaman, O., Rabczuk, T., & Pereira, L. F. C. (2016). Thermal conductivity and mechanical properties of nitrogenated holey graphene. *Carbon, 106*, 1–8.

Ni, Z., Bu, H., Zou, M., Yi, H., Bi, K., & Chen, Y. (2010). Anisotropic mechanical properties of graphene sheets from molecular dynamics. *Physica B, 405*, 13010–21306.

Paro, A. D., Hossain, M., Webster, T. J., & Su, M. (2016). Monte Carlo and analytic simulations in nanoparticle-enhanced radiation therapy. *International Journal of Nanomedicine, 11*, 4735–4741.

Ping, J., Fan, Z., Sindoro, M., Ying, Y., & Zhan, H. (2017). Recent advances in sensing applications of two-dimensional transition metal dichalcogenide nanosheets and their composites. *Advanced Functional Materials, 27*, 1605817.

Raabe, D. (1998). *Computational materials science.* Wiley-VCH.

Rahman, A., & Stillinger, F. H. (1971). Molecular dynamics study of liquid water. *The Journal of Chemical Physics, 55*, 3336–3359.

Ryckaert, J. P., & Bellemans, A. (1978). Molecular dynamics of liquid alkanes. *Faraday Discussions of the Chemical Society, 66*, 95–106.

Shen, L., Shen, H. S., & Zhang, C. L. (2010). Temperature-dependent elastic properties of single layer graphene sheets. *Materials and Design, 31*, 4445–4449.

Vander Ploeg, P., & Berendsen, H. (1982). Molecular dynamics simulation of a bilayer membrane. *The Journal of Chemical Physics, 76*, 3271–3276.

Xu, M., Liang, T., Shi, M., & Chen, H. (2013). Graphene-like two-dimensional materials. *Chemical Reviews, 113*, 3766–3798.

Yang, Y., Asiri, A. M., Tang, Z., Du, D., & Lin, Y. (2013). Graphene based materials for biomedical applications. *Materials Today, 16*, 365–373.

Zhang, H. (2015). Ultrathin two-dimensional nanomaterials. *ACS Nano, 9*, 9451–9469.

Zhu, C., Dua, D., & Lin, Y. (2017). Graphene-like 2D nanomaterial-based biointerfaces for biosensing applications. *Biosensors and Bioelectronics, 89*, 43–55.

Chapter 10
Novel Corrosion Properties of 2D Nanostructures for Advanced Applications

Tushar Banerjee

1 Introduction

The term 'corrosion' generally refers to 'eating away' or degradation of materials by a variety of processes like oxidation of metals, galvanic corrosion, microbial corrosion, dusting of metals and chemical degradation. Corrosion is a major cause for loss of economy, amounting to approximately 3–4% of GDP of the industrialized countries (El-Meigi, 2010; Raman & Tiwari, 2014), and around 4.2% only for USA (Lilly et al., 2007). Such degradation of materials also negatively impacts the environment. Therefore, any effort to mitigate this process will not only curtail loss of money but will also have a beneficial impact on the environment. It is also noted that failure of materials due to corrosion can be broadly classified into two categories, viz. *uniform* corrosion which covers 30% of the failure cases and *localized* corrosion which caters for 70% of the cases.

Three fundamental strategies, as mentioned below, can be adopted to minimize the occurrence of corrosion (Stoot et al., 2016).

(i) Alloying: Additional material (s) is alloyed with the original metal, thereby forming a more corrosion resistant or self-passivating product, which will be able to counter the corrosion attack.

(ii) Anodic protection: Here the original metal (to be protected) is made a cathode in a galvanic system and thereby will not give up electrons. It will reduce the tendency of the metal (cathode) to combine with other negatively charged atoms to form corrosion products. However, another metal piece is made the anode which will act in a sacrificial mode to protect the cathodic material.

T. Banerjee (✉)
Department of Production and Industrial Engineering, National Institute of Technology Jamshedpur, Jharkhand 831014, India

S. Singh et al. (eds.), *Advanced Applications of 2D Nanostructures*,
Materials Horizons: From Nature to Nanomaterials,
https://doi.org/10.1007/978-981-16-3322-5_10

(iii) Surface coating: A protective coating is deposited over the material, which will act as a barrier to prevent direct contact of corrosive media, oxygen, or movement of electrons/ions to/from the material.

The above-mentioned strategies however have their own limitations. Alloying will alter the mechanical properties of the bulk material which may not be allowable/desirable in certain circumstances. Alloys which are considered to be highly corrosion resistant such as duplex stainless steels, SAF 2507 and 2205 possess high content of expensive elements like chromium and nickel. In anodic protection strategy, there is degradation of the sacrificial material, which itself is a corrosion process. Also, the anodic material needs additional space as well as periodic replacement. Surface coatings, though, do not alter the bulk material properties and however may significantly impact surface properties like thermal conductivity of the material concerned. The adhesion of the protective coating with the bulk material is another issue which needs proper attention. Wear and tear of the protective coating may also open up sites for localized corrosion. Too thick a coating will also interfere with the tolerance of the dimensions of the part concerned. Nevertheless, out of the above three options, surface coatings appear to be the most feasible. However, it is necessary to visualize and develop coating which will mitigate the above-mentioned limitations of conventional coatings. Therefore, a suitable coating for corrosion protection should have the following essential properties.

(a) Should have sufficiently good adhesion with the part
(b) Should be a perfect barrier, thereby restricting contact of corrosive media with the part
(c) Should be chemically stable
(d) Should not be harmful to environment
(e) Should be sufficiently wear-resistant
(f) Thin enough so as to not interfere with the dimensions of the part.

2-D coatings in monolayer or multilayer configurations can cater to most of the needs listed above. A suitable candidate in this respect is graphene which is an atomically thin honeycomb structure of carbon atoms. The anti-corrosion property of graphene stems from the fact that it is non-reactive to most chemicals (Raman & Tiwari, 2014), impermeable to most gases as well as liquids (Raman & Tiwari, 2014) and thermally stable up to 400 °C (Prasai et al., 2012). It also possesses high mechanical strength (Papageorgiou et al., 2017) as well as transparency (Raman & Tiwari, 2014). Graphene grown by chemical vapour deposition (CVD) process is a promising thin corrosion protection coating for various metals. Another promising candidate for this purpose is 2-D hexagonal boron nitride (hBN) which also exhibits a honeycomb structure containing alternate boron and nitrogen atoms.

2 2D Materials for Corrosion Protection

2.1 Graphene

2.1.1 Comparison of Structure of Graphene and Other Allotropes of Carbon

Carbon is one of the most fascinating elements in the periodic table. It exhibits many allotropic forms, some of which like diamond and graphite are known to mankind for quite a few years. Some forms like fullerenes and nanotubes were discovered around 20–30 years back. The two-dimensional form called graphene which consists of array of carbon atoms in the form of a honeycomb structure has been discovered recently. Crystal structures of different allotropes of carbon are shown in Fig. 1 (Ding et al., 2018).

The stability of atomic arrangement of carbon in 2 dimensions is intriguing. According to the theorem by Mermin-Wagner (Mermin, 1968), long range order in two dimensions should not be possible. Also, 2D membranes in space should not be stable because of bending fluctuations in long range. However, theoretical calculations have shown that such detrimental fluctuations can be suppressed by non-linear coupling between bending and stretching modes (Nelson & Peliti, 1987).

The energy states of s- and p-electron orbitals in carbon atoms are close to each other which makes hybridization possible. In case of diamond, hybridization of all three p orbitals, results in an sp^3 structure with four chemical bonds, giving rise to an insulating material. However, in case of sp^2 hybridization, there will be three

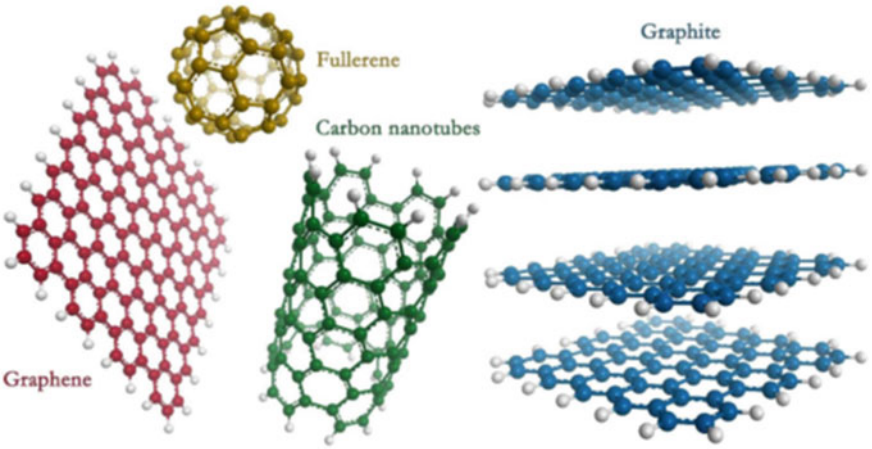

Fig. 1 Crystal configurations of different allotropes of carbon: Graphite in 3D form, Graphene in 2D form, Carbon nanotube in 1D form and Fullerene structure (balls) in 0D form (Reproduced with permission from Ding et al., 2018)

chemical bonds with availability of an additional p-electron. This electron though participates in covalent bonding, yet makes the material conducting which is the case with graphite and graphene.

2.1.2 Corrosion Protection Property of Graphene

Limited permeability to most gases and liquids is one of the most significant features of graphene which leads to its corrosion prevention property. In the graphene 2D structure, as shown in Fig. 2, the sp^2 hybridized carbon atoms are arranged in the form of hexagonal honeycomb lattice. The Van der Waals radius of the carbon atoms are 0.11 nm while the C–C bond length is 0.142 nm. The geometric pore is 0.064 nm. Such dimensions make the lattice impermeable to most gases and liquids, even helium (Kakaei et al., 2019).

This property of impermeability has also been illustrated in Fig. 3. Further, graphene also possesses dense electron cloud which repels reactive atoms and molecules. Such features basically enable graphene to act as an effective physical barrier between the underlying substrate and the outer corrosive medium.

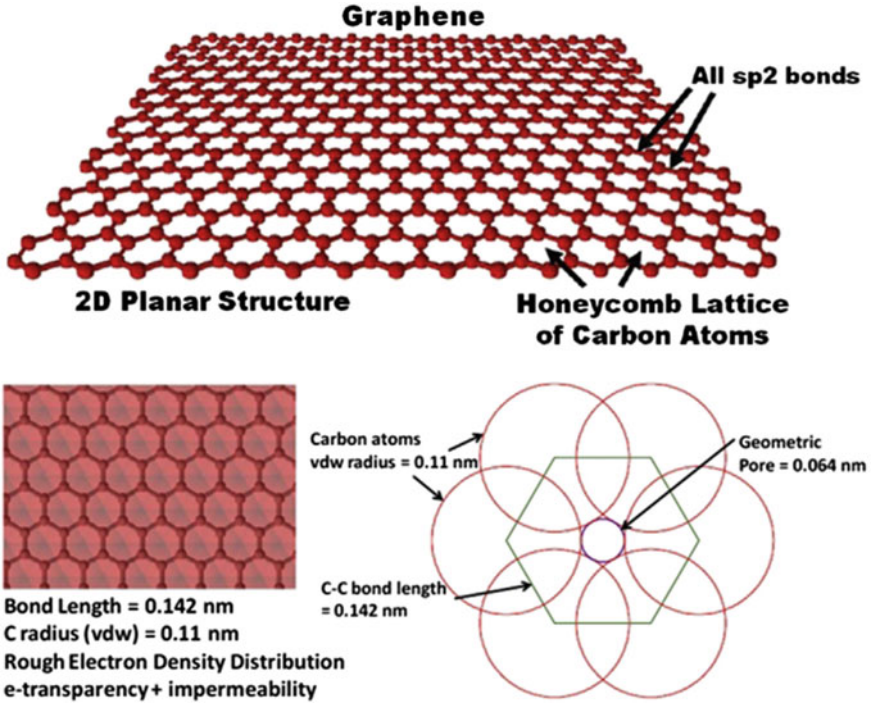

Fig. 2 Graphene lattice structure and dimensions of hexagonal lattice. Reproduced from Kakaei et al., 2019

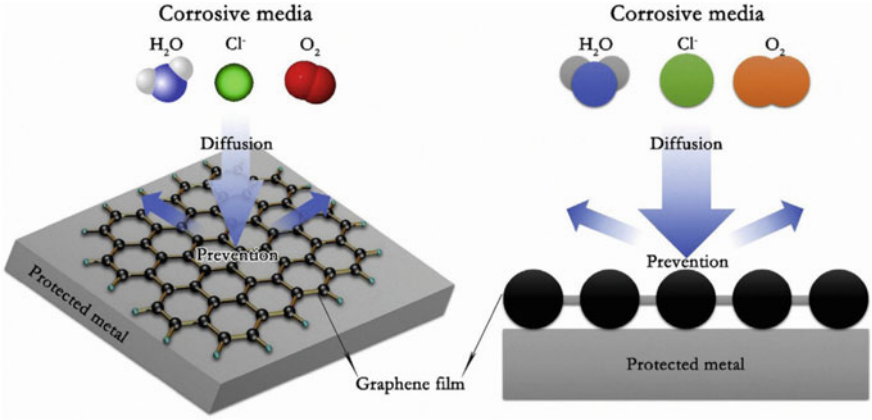

Fig. 3 Graphene acting as barrier to corrosive media. Reproduced from Ding et al., 2018

The permeability of different gases through graphene sheets of different thickness was experimentally determined by Bunch et al. (2008) as shown in Fig. 4. The experiment was done by placing graphene wafers/flakes on a cavity made in a silicon wafer. No significant difference in gas escape rates could be observed for helium, argon or air up to graphene film thickness of around 10 nm.

Kirkland et al. (2012) studied the electrochemical response of graphene coated nickel (99.9% Ni) and copper (99.9% Cu) of 1 mm thickness. The graphene film was grown on the substrates using chemical vapour deposition (CVD) process in an environment of H_2 and CH_4. The structure of graphene was studied by Raman spectroscopy. It was observed that almost 80% for Cu and 60% of Ni surface was covered with single or few layer graphene. Formation of graphene was further confirmed by Scanning Electron Microscopy. Potentiodynamic polarization tests were performed in three-electrode configuration with 0.1 M NaCl solution as the corrosive medium. Figure 5 shows the anodic and cathodic polarization curves for different uncoated and

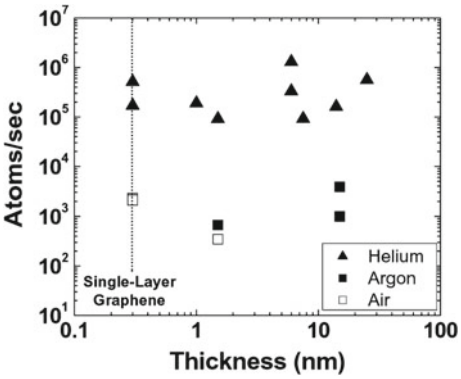

Fig. 4 Gas leak rates at different layer thickness of graphene. Reproduced from Bunch et al., 2008

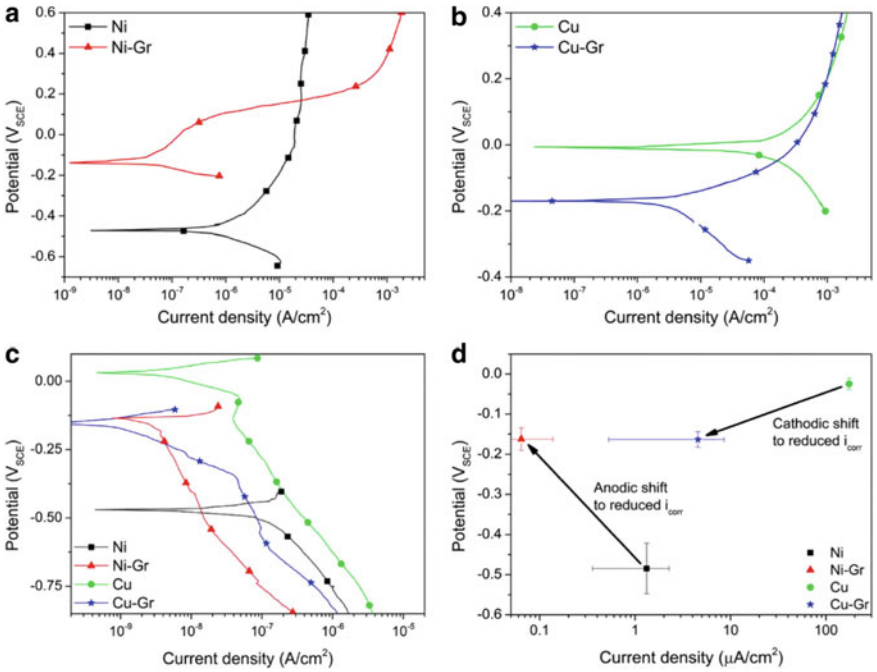

Fig. 5 Polarization curves for graphene coated nickel and copper. (**a**) Polarization curves for Ni and Ni-Gr in anodic mode, (**b**) Polarization curves for Cu and Cu-Gr in anodic mode, (**c**) Polarization curves for Ni, Ni-Gr, Cu, Cu-Gr in cathodic mode (**d**) E_{corr} versus I_{corr} for uncoated and Gr-coated Ni and Cu Reproduced from Kirkland et al., 2012

graphene coated samples. The anodic and cathodic tests were performed separately so that they do not influence each other. This was important considering the fragile nature of graphene. Deposition of graphene coating on Ni resulted in a drastic decrement in anodic and cathodic reaction phenomenon indicating decrement in charge transfer (Fig. 5a and c). A decrease in corrosion current density for graphene coated Ni was also observed (Fig. 5d). Simultaneously the corrosion potential was also shifted in the positive direction. The results indicated that graphene was basically acting as an anodic (ionic) barrier which resisted the formation of Ni^{2+} from Ni.

Polarization curves corresponding to graphene coated graphite however, showed a different behaviour. Though the corrosion current reduced, the corrosion potential shifted to the negative direction (Fig. 5b, c and d) suggesting that graphene prevented cathodic reaction, which was in contrast to that for Ni substrate. Nevertheless, it was established that depositing a graphene coating could reduce the corrosion rates of Ni and Cu substrates.

In another study, Prasai et al. (2012) also reported that rate of corrosion of graphene coated copper was 7 times slower in aerated Na_2SO_4 solution as compared to its uncoated counterpart. It was also observed that nickel coated with CVD grown multilayer graphene corroded 7 times slower as compared to nickel with a coating

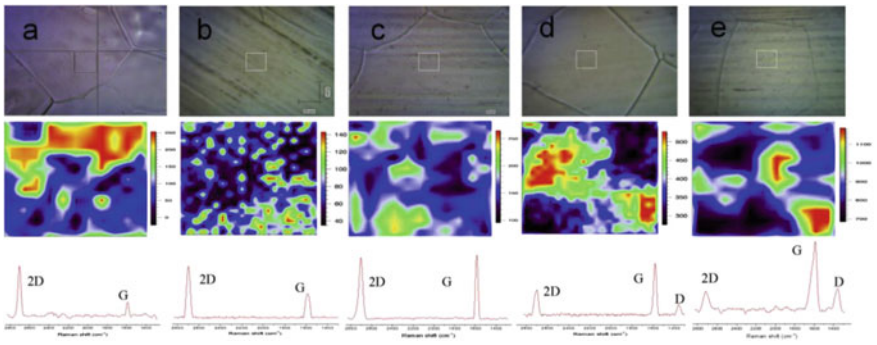

Fig. 6 Optical images, Raman mapping and Raman spectra of different layer of graphene synthesized on Cu substrate. Reproduced from Wu et al., 2019

of four layered mechanically transferred graphene. The study also indicated the supremacy of chemical vapour deposition (CVD) method to synthesize graphene films for anti-corrosion application.

Wu et al. (2019) reported the effect of different defect levels and conductivity of graphene on corrosion protection property for Cu substrate. It included the corrosion performances of monolayer, bilayer and multilayer graphene. Mechanism of failure of graphene coating was particularly studied. Graphene films were deposited by chemical vapour deposition (CVD). The quantity of defects and layer numbers were assessed by Raman spectroscopy. Electrochemical tests (potentiodynamic polarization tests) were performed in a three-electrode configuration using 3.5 wt.% NaCl solution as the corrosive medium. Figure 6 shows optical images (top row) and corresponding Raman maps (middle row) and spectra (bottom row) of different layered structures of graphene. The intensity ratio of G/2D and full width at half maximum (FWHM) values of the 2D band corresponded to mono-layered, bi-layered, tetra-layered, hexa-layered and octa-layered coated Cu. Optical images and Raman mapping after corrosion tests (Fig. 7) showed some regions where graphene was peeled off. This phenomenon was particularly observed for multi-layered graphene coatings.

Electrochemical studies revealed that the bilayer graphene coated Cu displayed the best anti-corrosion performance as it displayed the highest impedance, phase angle and lowest corrosion current density. Graphene basically acted as a barrier to ion-transport towards the under lying Cu substrate. The corrosion was initiated owing to permeation of corrosive medium through the defects in graphene structure. It resulted in the formation of a galvanic cell which further promoted the corrosion process. Progressive corrosion and accumulation of corrosion products resulted in exfoliation or peeling of graphene layers into the electrolyte (corrosive medium) as shown in Fig. 8. This suggested that though graphene itself can act as barrier to corrosive media, defects in graphene layer can actually promote the corrosion process by galvanic means.

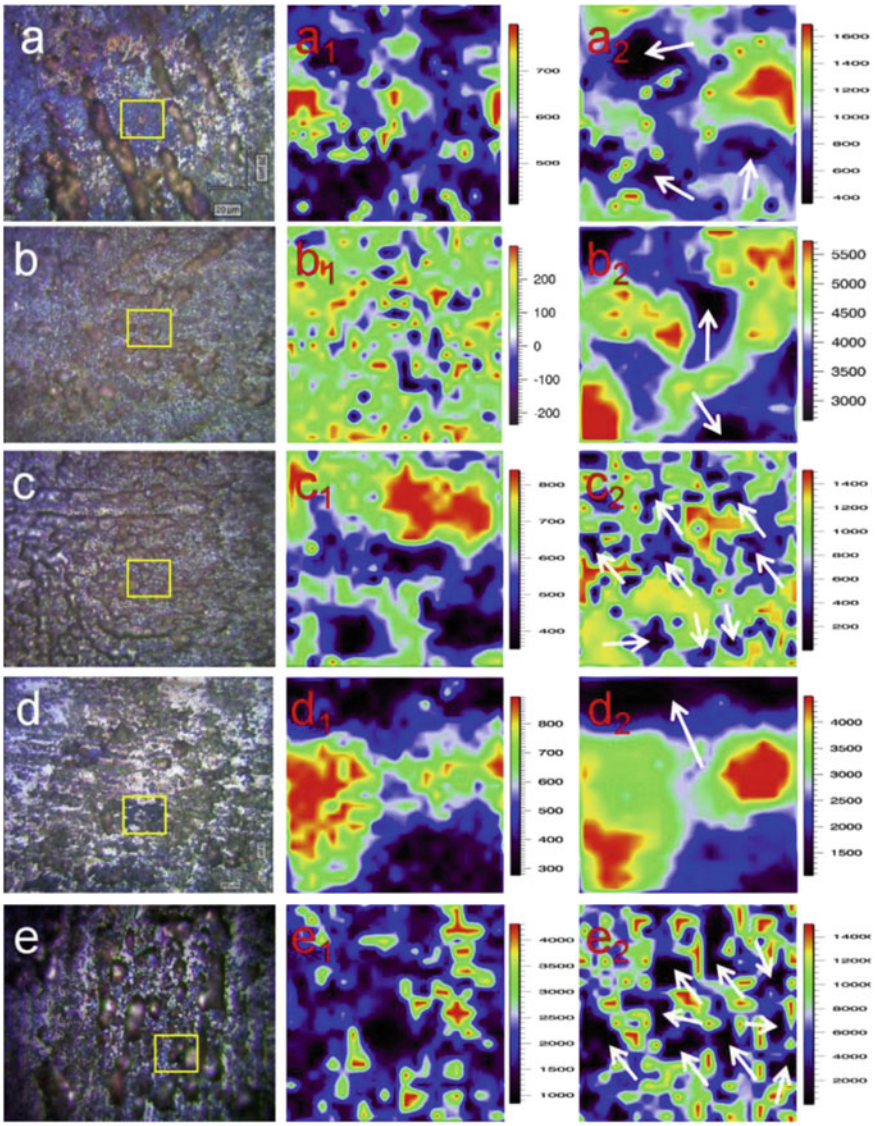

Fig. 7 Optical images and Raman mapping of graphene coating on Cu substrate after corrosion tests. Reproduced from Wu et al., 2019

Earlier, Schriver et al. (2013) also reported that graphene was able to protect copper from thermal oxidation at temperatures as high as 250 °C, but only for short duration of the order of minutes. However, with increase in duration, graphene coated Cu was oxidized possibly due to migration of oxygen through defects in graphene layer.

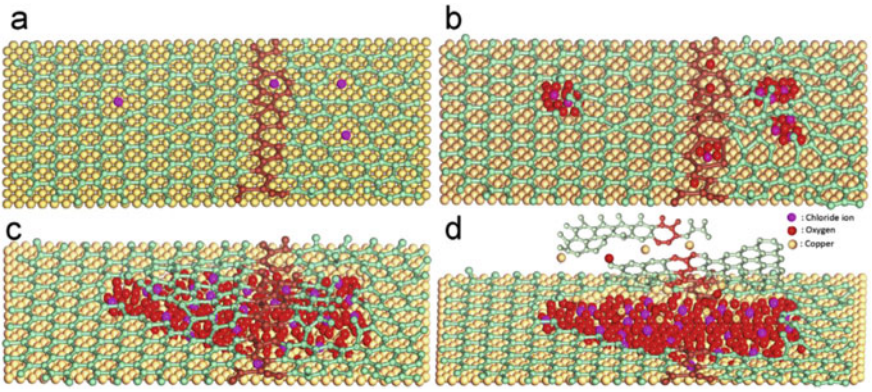

Fig. 8 Schematic of corrosion mechanism of graphene coated Cu and the exfoliation of graphene into electrolyte. Reproduced from Wu et al., 2019

2.2 Graphene Oxide

Apart from pristine graphene coating, attempt has also been made by researchers to investigate the anti-corrosion properties of graphene-based coating, particularly graphene oxide.

Yadav et al. (2018) reported anti-corrosion property of graphene oxide coating for protection of iron particles (microspheres) in saline water. The substrate was carbonyl iron which is a highly pure (~99%) bcc phase iron and has wide applications in the areas of catalysis, drug delivery, sensors, etc. Graphene oxide sheets were obtained from graphite flakes by improved Hummer's method (Yadav et al. 2018). The graphene oxide coating on CI micro-particles was synthesized using 4-aminobenzoic acid as grafting agent. Corrosion resistance was measured by cyclic voltammetry method using graphene oxide coated and bare carbonyl graphite electrodes in 1 mol/L KCl solution. Coated samples showed better resistance to charge transfer as compared to uncoated counterparts. Shifting of corrosion potential towards positive direction also suggested better passivity of the coated electrodes. Also, the corrosion current was less than that of bare samples. The results implied excellent corrosion protection behaviour of graphene oxide coating on iron micro-particles.

Nayak and Mohana (2018) also reported that incorporation of graphene oxide in epoxy resin coating improved the corrosion resistance while protecting mild steel substrate. Before incorporation graphene oxide was functionalized using 4-nitro aniline to ensure uniform distribution inside the epoxy. Electrochemical impedance spectroscopy and potentiodynamic polarization tests showed that composite containing 0.5 wt.% of functionalized graphene oxide had better anti-corrosion property as compared to that with graphene oxide. It was suggested that graphene oxide effectively blocked micro-pores and defects in the epoxy coating thereby increasing the pathway of the corrosive media to the substrate.

Ho et al. (2019) reported the anti-corrosion performance of graphene oxide films synthesized on stainless steel substrate by electrophoretic deposition. Though chemical vapour deposition has been proven to a very effective means of depositing corrosion resistant graphene layers, it suffers from drawbacks like process complexity, high cost and high temperature, the latter being detrimental to form stability of steel substrates. Electrophoretic deposition, on the other hand, is a simpler and cost effective means. Graphene oxide films were synthesized through electrophoretic deposition using strong oxidizing agents like $NaNO_3$ and Na_2SO_4, control of temperature and a variety of drying processes. Corrosive agent was aqueous hydrochloric acid. Use of strong oxidizing agents along with freeze drying created high oxygenated functional groups in graphene oxide which led to good corrosion resistance due to higher resistance to carrier pathway.

2.3 Hexagonal Boron Nitride

Hexagonal boron nitride (hBN) is a two-dimensional atomically thin material. It exhibits excellent thermal (stable up to 1500 °C) stability, chemical stability, low permeability, mechanical property and thermal conductivity. Such properties make it a front runner as a candidate for corrosion protection coating. Different methods have been explored to synthesize boron nitride sheets, which includes pulsed laser deposition, mechanical exfoliation, chemical vapour deposition. However, pulsed laser deposition produces amorphous boron nitride films and has high cost. Mechanical exfoliation method, on the other hand, produces small area hBN, limiting its application. Chemical vapour deposition though have its own drawbacks regarding process complexity and relatively high cost, however, produces highly crystalline hBN.

Liu et al. (2013) synthesized highly crystalline and large area hBN atomic layers on Ni substrate by chemical vapour deposition method. Oxidation tests suggested that such coatings can act as an ultra-effective barrier to oxidation of nickel at temperatures up to 1100 °C. Also few layers of hexagonal boron nitride can prevent oxidation of graphene layer at similar high temperatures.

Shen et al. (2016) conducted a comparative study on anti-corrosion property of graphene and boron nitride deposited on copper substrate. Schematic of corrosion mechanism in presence of these two layers have been illustrated in Fig. 9. Oxygen attacks underlying copper substrate through pits/defects in the films for both graphene and boron nitride. The highly conducting nature of graphene will allow progress of oxidation of underlying copper by allowing transport of electron through it. However, boron nitride being an insulator will prevent such charge transport and thereby oxidation will be suppressed. Therefore, in comparison with graphene, boron nitride is a much better candidate for anti-corrosion application particularly for long term application.

Huang et al. (2019) incorporated different concentrations of hexagonal boron nitride into zinc phosphate coating in a quest to improve anti-corrosion property

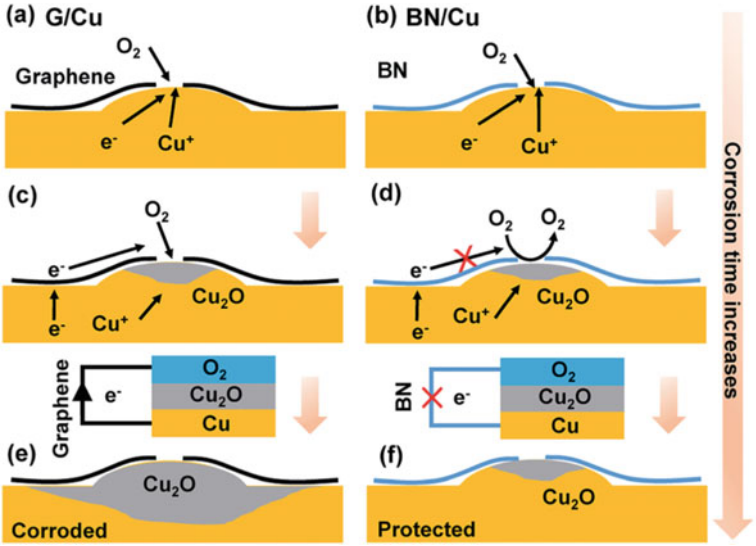

Fig. 9 Mechanism of corrosion protection by graphene and boron nitride. Reproduced from Shen et al., 2016

of the latter on mild steel sheets. hBN proportion of 0.5 to 6 g/L was added to the phosphating deposition bath. Potentiodynamic polarization tests were carried out in three-electrode configuration using Ag/AgCl as reference electrode, graphite as counter electrode and coated steel sample as the working electrode. 3.5% NaCl solution was used as the corrosive medium. It was observed that incorporation of hBN restricted the grain size of phosphate coating making it denser. In electrochemical tests, coatings with hBN showed significantly less corrosion current as compared to that without hBN.

3 Conclusion

Anti-corrosion property of 2-dimensional nanostructures in the form of thin films or coatings has been discussed in this chapter. Fundamental strategies for corrosion protection have been briefly reviewed, followed by exploration on role of protective coatings for corrosion prevention. Keeping in view different functional requirements, essential characteristics for an ideal anti-corrosion coating has been chalked out. Synthesis and anti-corrosion characterization of graphene, graphene oxide and hexagonal boron nitride has been thoroughly discussed. Owing to its hexagonal honeycomb structure with restricted opening, graphene acts as a barrier to movement of most chemical species, which has led to its anti-corrosion property. However, research reports also suggested that defects in graphene structure actually augmented

corrosion of the underlying substrate in long term. This occurred due to the formation of galvanic cell promoted by conductivity of graphene layer. Graphene oxide was also reported to provide corrosion protection in medium like KCl, NaCl, aqueous HCl. Comparison of hexagonal boron nitride with graphene showed superiority of the former in terms of corrosion protection (oxidation) of underlying copper substrate owing to its non-conductivity as compared to graphene.

References

Bunch, J. S., Verbridge, S. S., Alden, J. S., van der Zande, A. M., Parpia, J. M., Craighead, H. G., & McEuen, P. L. (2008). Impermeable atomic membranes from graphene sheets. *Nano Letters, 8*, 2458–2462.

Ding, R., Li, W., Wang, X., Gui, T., Li, B., Han, P., Tian, H., Liu, A., Wang, X., Liu, X., Gao, X., Wang, W., & Song, L. (2018). A brief review of corrosion protective films and coatings based on graphene and graphene oxide. *Journal of Alloys and Compounds, 764*, 1039–1055.

El-Meligi, A. A. (2010). Corrosion preventive strategies as a crucial need for decreasing environmental pollution and saving economics. *Recent Patents on Corrosion Science, 2*, 22–33.

Ho, C. Y., Huang, S. M., Lee, S. T., & Chang, Y. J. (2019). Evaluation of synthesized graphene oxide as corrosion protection film coating on steel substrate by electrophoretic deposition. *Applied Surface Science, 477*, 226–231.

Huang, H., Wang, H., Xie, Y., Dong, D., Jiang, X., & Zhang, X. (2019). Incorporation of boron nitride nanosheets in zinc phosphate coatings on mild steel to enhance corrosion resistance. *Surface and Coatings Technology, 374*, 935–943. https://doi.org/10.1016/j.surfcoat.2019.06.082

Kakaei, K., Esrafili, M. D., & Ehsani, A. (2019). Graphene and anticorrosive properties. *Interface Science and Technology, 27*, 303–337.

Kirkland, N. T., Schiller, T., Medhekar, N., & Birbilis, N. (2012). Exploring graphene as a corrosion protection barrier. *Corrosion Science, 56*, 1–4.

Lilly, M. T., Ihekwoaba, S. C., Ogaji, S. O. T., & Probert, S. D. (2007). Prolonging the lives of buried crude-oil and natural-gas pipelines by cathodic protection. *Applied Energy, 84*, 958–970.

Liu, Z., Gong, Y., Zhou, W., Ma, L., Yu, J., Idrobo, J. C., Jung, J., MacDonald, A. H., Vajtai, R., Lou, J., & Ajayan, P. M. (2013). Ultrathin high-temperature oxidation-resistant coatings of hexagonal boron nitride. *Nature Communications*. https://doi.org/10.1038/ncomms3541

Mermin, N. D. (1968). Crystalline order in two dimensions. *Physical Review, 176*, 250–254.

Nayak, S. R., & Mohana, K. N. S. (2018). Corrosion protection performance of functionalized graphene oxide nanocomposite coating on mild steel. *Surfaces and Interfaces, 11*, 63–73.

Nelson, D. R., & Peliti, L. (1987). Fluctuations in membranes with crystalline and hexatic order. *Journal of Physique, 48*, 1085–1092.

Papageorgiou, D. G., Kinloch, I. A., & Young, R. J. (2017). Mechanical properties of graphene and graphene-based nanocomposites. *Progress in Materials Science, 90*, 75–127.

Prasai, D., Tuberquia, J. C., Harl, R. R., Jennings, G. K., & Bolotin, K. I. (2012). Graphene: corrosion-inhibiting coating. *ACS Nano, 6*, 1102–1108.

Raman, R. K. S., & Tiwari, A. (2014). Graphene: The thinnest known coating for corrosion protection. *The Journal of The Minerals Metals & Materials Society, 66*, 637–642.

Schriver, M., Regan, W., Gannett, W. J., Zaniewski, A. M., Crommie, M. F., & Zettl, A. (2013). Graphene as a long-term metal oxidation barrier: Worse than nothing. *ACS Nano, 7*, 5763–5768.

Shen, L., Zhao, Y., Wang, Yi., Song, R., Yao, Q., Chen, S., & Chai, Y. (2016). A long-term corrosion barrier with an insulating boron nitride monolayer. *Journal of Materials Chemistry A, 4*, 5044–5050.

Stoot, A. C., Bøggild, P., & Camilli, L. (2016). *Protective coatings based on 2D-materials.* Dissertation, Technical University of Denmark.

Wu, Y., Zhu, X., Zhao, W., Wang, Y., Wang, C., & Xue, Q. (2019). Corrosion mechanism of graphene coating with different defect levels. *Journal of Alloys and Compounds, 777*, 135–144.

Yadav, A., Kumar, R., Choudhary, H. K., & Sahoo, B. (2018). Graphene-oxide coating for corrosion protection of iron particles in saline water. *Carbon, 140*, 477–487.

Chapter 11
Nanostructured 2D Materials for Biomedical, Nano Bioengineering, and Nanomechanical Devices

Arpita Roy and Chandan Kumar Maity

1 Introduction

In modern era, the developments of nanobiotechnology and clinical biomedicine have significantly increased the demand of 2D materials as a preferential choice. As dimensionality influences the properties of materials, likewise 2D materials possess planner structure and ultrathin thickness with high surface area which helps in boosting the use of these 2D materials in biomedical applications (Chen et al., 2015). Nanomaterials with different topologies like ellipsoidal, cages, wire, and tube have been successfully used for biomedical purpose like drug delivery, imaging, theranostics agent for cancer treatment, tissue engineering, and so on. (Chen et al., 2015). Also, the unique features of 2D materials such as one dimension in nanometer, planer structure, high surface area, specific physicochemical properties, and tunable functionalities make them potential candidates not only in the field of energy storage, sensor, optical, and electronics but also in different biomedical as well as pharmaceutical works, (Jayakumar et al., 2018), and Fig. 1 Jayakumar et al. (2018) represents the different types of 2D materials used in biomedical, nano bioengineering, and nanomechanical devices.

Biocompatibility and bioactivity are two major concerns which have been associated with 2D materials for biomedical technology. In the family of 2D materials, graphene has already drawn a significant attention for the development of biotechnology in last few decades. Biocompatible graphene and its derivatives have been recently exhibited as an effective potential candidate for biomedical applications, introducing the biosensing, photothermal therapy, anticancer drug delivery, gene transportation, photodynamic therapy, and even in tissue engineering. Somehow this wonder material displays better performances as compared to other topologies such as nanoparticles, cages, tubes, and wires. Graphene-based nanohybrid materials have

A. Roy (✉) · C. K. Maity
Department of Chemistry, IIT (ISM), Dhanbad, Dhanbad 826004, India

S. Singh et al. (eds.), *Advanced Applications of 2D Nanostructures*,
Materials Horizons: From Nature to Nanomaterials,
https://doi.org/10.1007/978-981-16-3322-5_11

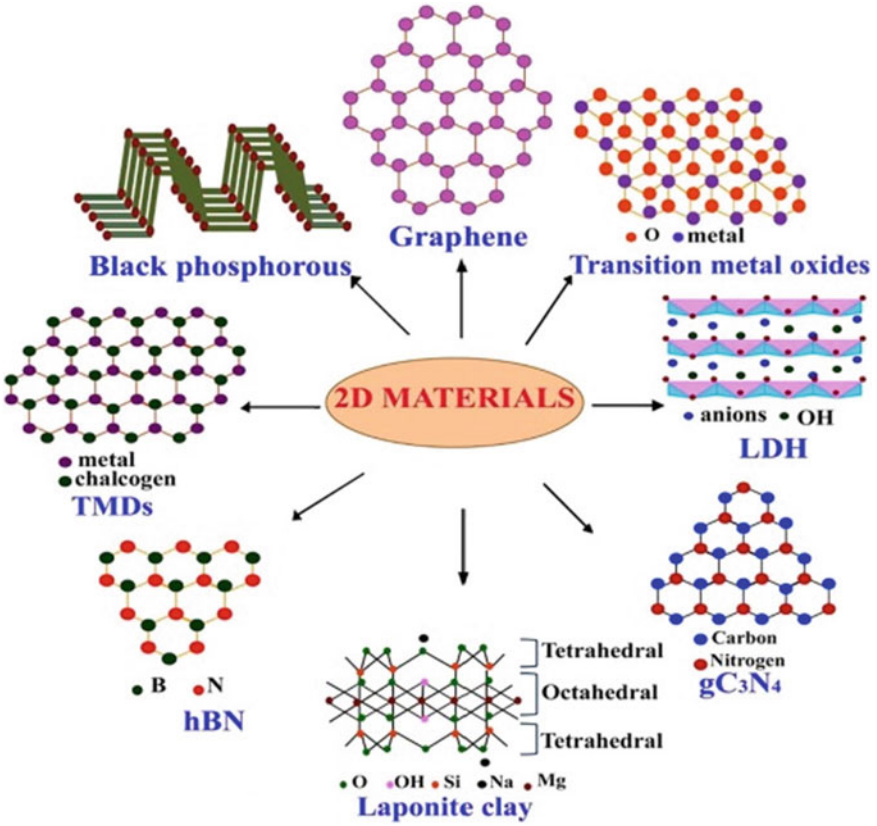

Fig. 1 Structure of different 2D materials (Jayakumar et al., 2018)

also been successfully established for radionuclide imaging, fluorescent imaging, computed tomography (CT), and magnetic resonance imaging (MRI) by integrating graphene with some other active materials (Chen et al., 2015). But, including all of these advantages there are some major concerns associated with these materials that are they somehow demonstrate cytotoxicity, excretion problems, biodistribution, and a little hemo and histocompatibility. For example, due to the existence of defects in graphene, photothermal conversion efficiency of graphene becomes very low during photothermal therapy (PTT). In case of *in-vivo* drug delivery, these carbonaceous materials demonstrate very low biodegradation rate resulting in a long-term accumulation of graphene in body which may lead to health hazards (Chen et al., 2015). So, it became very essential to find some new methods for the modification graphene or to find out some other new 2D materials. So, these researches have drawn noteworthy attention for futuristic development of potential candidates for biomedical applications.

In addition with graphene, other 2D materials like reduced graphene oxide (rGO), hexagonal boron nitrides (hBN), black phosphorous (BP), 2D clay materials, 2D transition metal oxides (TMOs), 2D Transition metal dichalcogenides (TMDs), and graphitic carbon nitride (g-C_3N_4) are gaining much recognition for health care. Like, Chen et al. worked on the therapy for the treatment of cancer as well as bioimaging with 2D TMD nanosheets. Chimene et al. used TMDs and TMOs in various biomedical applications (Chen et al., 2018). Graphene analogous 2D materials are mainly inorganic materials with planner structure as like graphene and also possess high surface area with single or several atomic layers. These materials are also associated with similar structural properties as graphene, but they exhibit some unique physicochemical/biological behavior with different surface status and composition. In this respect, recently these bioactive and biocompatible graphene analogous 2D materials are widely used as a complementary or alternative of graphene and graphene-based nanohybrids for diagnostic imaging, drug delivery, biosensing, and photothermal/photodynamic therapy. Summary of biomedical applications of biocompatible graphene analogous 2D materials (2D-GAs) is depicted in Fig. 2 (Yang et al., 2018).

Easy functionalization and modification of these 2D materials can also tune their properties to improve biocompatibility and reduce its toxic effects. So, the recent trend is growing to explore the potentiality of these 2D materials which mainly emphasizes on biosafety and eco-friendly nature. Owing to their large surface area, these materials offer higher interaction with cells leading to huge chances in toxicity effect (Jayakumar et al., 2018). In this regards recently, new 2D materials have been developed. Among them graphene, graphyne, graphdiyne, fluorinated graphene, and

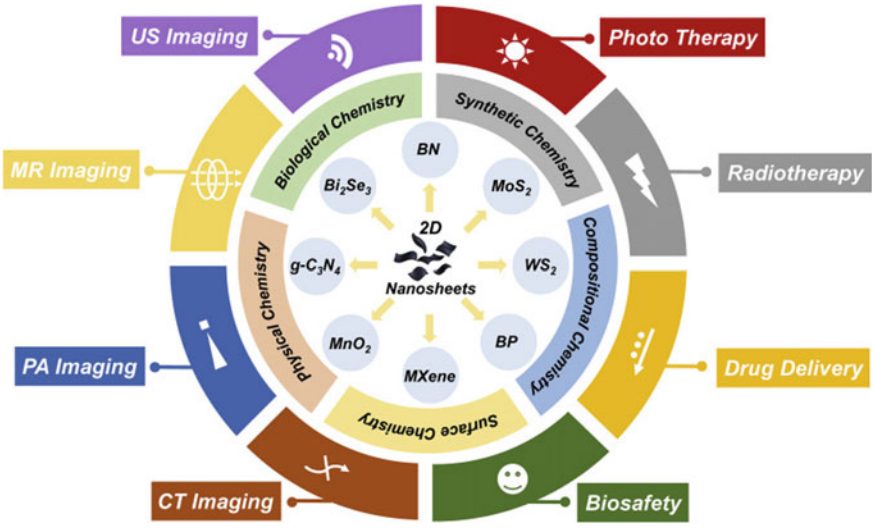

Fig. 2 Summary of versatile biomedical applications of biocompatible graphene analogous 2D materials (2D-GAs) (Yang et al., 2018)

elemental 2D materials such as silicene, germanene, arsenene, and antimonene are new members (Vargas-Bernal, 2016). Chen et al. have reported graphdiyne-based drug delivery device for cancer treatment (Jin et al., 2018). So, in this chapter, we have focused on the uses of different 2D materials in biomedical, bioengineering, and mechanical device along with their synthetic strategies and other properties.

2 Synthesis of 2D Materials

For layered materials, synthetic pathway plays an important role to tune its properties. For example, the direct band gap of bulk MoS_2 is 1.3 eV, but it becomes 1.8 eV for its single layer form. MoS_2, WS_2, and such types of single- or few-layered TMDs have been successfully synthesized for different application as like catalysis, electronic/optoelectronic devices, energy harvesting, and storage. In addition, synthetic procedures of other 2D materials such as graphene g-C_3N_4, Bi_2Se_3, BN, and transition metal oxide have been widely investigated in different way. Usually, these synthetic techniques are divided into two different categories, one is top-down approach, and another one is bottom-up approach.

2.1 Top-Down Approach

Top-down approach generally refers to the production of micro/nanoscale materials from bulk materials (macro). Mainly exfoliation techniques are associated with this approach. Exfoliation can split the bulk-layered materials into thin sheets. Thin sheet of graphene and other graphene analogous 2D materials can be synthesized from their initial bulk materials, which are stacked with their strongly bonded interlayers through Van dar Waals force of attraction. Generally, surfactant-assisted exfoliation, mechanical treatments, ion intercalation, etc., are the methods that are generally involved to synthesize 2D materials through direct exfoliation. Exfoliation may be carried out in both liquid and solid phases. For example, mechanical exfoliation is carried out in solid phase to split the interlayer force of attraction. Mechanical exfoliation was used to produce graphene from graphite first by Novoselov et al. (2004). Using this mechanical exfoliation, the thin sheets of other 2D materials such as hBN and MoS_2 have been synthesized successfully. Low energy ball milling is a well-known process by which few-layered sheets can be produced; for example, this ball milling technique is potentially able to synthesize BN nanosheets in large scale with a high yield. Thermal exfoliation is another solid phase exfoliation technique to produce thin sheets. It proceeds via very high internal pressure as well as fast gas generating breakdown. This high internal pressure and fast gas generating dissociation in turn help in overcoming the Van der Waals force present on the bulk materials and generate thin layers. This procedure is mostly used for the synthesis of thin graphene sheets from graphene oxide (GO). But thermal exfoliation process suffers

from numerous difficulties like very low yield and defects in structures. Among solid-state exfoliations as well as adhesive-assisted mechanical exfoliation are often used methods for the generation of high quality large sheets of thin 2D materials, though it also suffers from low yield and large-scale synthesis problem.

Exfoliation in liquid phase is reasonably more useful and effective and somehow able to solve the demerits related to solid phase exfoliation process. Yield and better dispersed layered can be obtained using liquid-phase exfoliation. Here, solvent layer interaction helps to overcome the layer–layer interaction more efficiently, and this solvent layer interaction can be enhanced by means of surfactant or organic solvent instead of water only. Liquid-phase exfoliation can produce high quality of materials in large amount; though these products are polydisperse mixture of sheets with different lateral size and thickness with unwanted residual elements. Chemical exfoliation in liquid to synthesize graphene analogous other 2D materials is one of the most extensively used pathways for biomedical applications as this process leads to large-scale production and crucial structural/compositional factors. As an example, recently an electrochemical Li intercalation and exfoliation process has been developed to control the intercalation and increase the yield of product in a desirable way (Zeng et al., 2011). By this strategy, single- and few-layered TMD nanosheets like BN, MoS_2, TiS_2, WSe_2, TaS_2, WS_2, ZrS_2, Sb_2Se_3, Bi_2Te_3, and $NbSe_2$ can be synthesized in large amount with very high yield of product. Also, H_2SO_4-supported liquid-phase exfoliation method has been used to formulate highly dispersed WS_2 nanosheets (Zeng et al., 2011).

2.2 Bottom-Up Approach

Bottom-up method is an alternative approach for synthesizing 2D nanomaterials. Wet synthesis and chemical vapor deposition (CVD) are most commonly used method for bottom-up approach. CVD refers the growth of thin film or layer on an appropriate substrate consuming vapor of the precursor. High-quality 2D materials such as graphene, WS_2, MoS_2, and hBN can be synthesized with high surface area, controllable thickness, and in high yield with the help of CVD method. But the finding of proper substrate and reaction condition is the major factors as well as limitations of this process. For example, single-layered MoS_2 films can be deposited on the amorphous SiO_2 via CVD process using MoO_3 and S powders as the precursors at 650 °C (Lee et al., 2012). However, CVD technique is widely used for large-scale device fabrication, but it is not suitable for the fabrication of 2D materials for biomedical applications. Recently, some new techniques such as atomic layer deposition technique (ALD) and metal–organic CVD have been introduced to synthesize 2D materials.

In wet synthesis, hydro as well as solvo-thermal treatment is widely used to fabricate good quality 2D TMDs and TMOs that may be used for biomedical as well as pharma applications. Elemental and composition ratios can easily be tuned

in this process, which is one of the most desirable advantages of this process. Co-precipitation method is extensively used for LDH synthesis, and this co-precipitation is associated with reconstruction and ion-exchange technique. These are comparatively eco-friendly and low-cost processes. In the co-precipitation process, the solution of anticipated metal cations (divalent and trivalent) is mixed slowly to the solution having anion to be intercalated, and the precipitate is created by fine-tuning of pH of that solution to acquire LDH. Temperature, pH as well as the aging time significantly change the size and crystallinity of the synthesized particles.

3 Functionalization and Modification of 2D Materials

To overcome the poor stability, toxicity, and less aqueous solubility, functionalization and modification of 2D materials are important. It has become brilliant techniques for making it suitable for biomedical and mechanical device application. Surface modification of 2D materials through functionalization is capable to tailor the chemical, electronic, and optical properties of these materials. In physiological conditions, sometimes exfoliated thin sheets of 2D materials are not stable, and thus, functionalization is essential to modify its surface which will help to gain high stability and dispersity in physiological systems, improved biocompatibility, and site-specific targeting capability. Effective aqueous solubility and biocompatibility are required for better interaction of these materials with cellular system and biocomponents during targeted *in-vivo* drug delivery and imaging system. Thus, modification can indeed help to enhance its biocompatibility, water solubility and also helps to reduce its toxicity significantly. Covalent and non-covalent modifications have been introduced recently for the modification of 2D materials. In this way, the improvement of the 2D materials has been explored for real-time biomedical applications.

Hydrophobic character of graphene restricts its use for biomedical applications. Desirable dispersion of graphene is very crucial for administration to cells. So, to find a way to solve this issue, covalent modification of graphene by using L-lysine has been prepared and reported which is able to disperse it effectively in water, and this modification enhances the biocompatible nature as well as interaction behavior with other bioactive molecules (Shan et al., 2009). In addition, this L-lysine functionalized graphene can be used as biosensors. Liu et al. (2011) reported gelatin functionalized biocompatible graphene. This gelatin functionalized graphene has no toxicity toward cells even up to usage of 200 mg/ml concentration. Again, due to low solubility of hBN, it is restricted from its use in drug delivery, but this hBN when composed with fluorescence active graphene quantum dots then exhibits water solubility, very low cytotoxicity, and better stability in HeLa cells. Recently, using thermal substitution of carbon atoms in g-C_3N_4 with boron, more efficient water dispersible hBN has been developed. Hydroxyl (-OH) functionalized hBN has also been produced with high biocompatible and porous character which enhances its drug loading capability (Weng et al., 2014). Functionalization of g-C_3N_4 enhances its electrical and optical properties mainly. Modification of g-C_3N_4 using fluorine can tune its bandwidth

and improve its potentiality in optoelectronics. Ma et al. (2014) synthesized 2–4 nm thick protonated g-C_3N_4 with increased stability in water via dispersion, and this protonated g-C_3N_4 demonstrates enhanced fluorescence intensity for sensing heparin even to a very minute concentration. When doxorubicin (Dox) was taken as a model drug and loaded in PEGylated MnO_2 nanosheets, it showed a better drug loading capacity, and this matrix was then used as a carrier of Dox for targeted drug delivery to the cancer cells. PEGylated MnO_2 systems have an advantage that, when this matrix is administered *in-vivo*, shows an increment of MRI signal due to Mn (II) ion which generates from the breakdown of MnO_2 nanosheets. Solubility property of TMDs in ionic solvent can be triggered through its modification. To prepare water-soluble WS_2 nanosheets, a sonication-assisted simple *in-situ* exfoliation method has been developed with poly(acrylic acid) (PAA) through the coordination interaction with carboxyl groups of PAA and tungsten (Yuan et al., 2014), and this PAA-modified stable WS_2 can be stored in normal temperature for long period of time. Likewise, the adsorption of bovine serum albumin (BSA) on WS_2 nanosheet surface might help to improve their dispersity as well as stability in phosphate-buffered saline (PBS). BP shows better properties with respect to biocompatibility and low toxicity, but the oxophilic nature of this material somehow restricts its application. Due to rapid chemical reactivity with water and oxygen, BP surface goes to rapid degradation in the presence of water and air. Doping, surface modification, and encapsulation have been introduced to overcome the rapid degradation of BP. By means of incorporation of anionic surfactants into the interlayer of LDH, the hydrophilic nature of LDH surface may be changed to hydrophobic. In 2002, biosensors made up of LDH and laponite clay matrix were established.

4 Biomedical Application of 2D Materials

Various chemical arrangements and exclusive 2D planar structure created some unique properties to 2D-GAs which makes them suitable for the use in biomedical field. So far, these types of nanosheets have been used in various biomedical purposes like drug and gene delivery, photothermal or photodynamic remedy, theranostics imaging, biosensing, and so on. Still the behavior and effects of these 2D nanosheets on biological systems are also under wide exploration. Till date, the research on 2D materials for these applications includes layered double hydroxide (LDH), transition metal chalcogenides, layered silicates, and metal oxides. These are generally nontoxic or very minute amount of toxic which as such does not affect the biological system. Besides, various chemical techniques are nowadays used to increase the biocompatibility of these materials such as coating with some biocompatible polymers. As there are very limited numbers of studies are available for this filed so, it is increasing its demand. Many researchers now are focusing in this field being aware of high potential and opportunities associated with 2D materials. So, the research to improve 2D materials and making them friendlier to the biological

systems is picking up high acceleration and will be more emerging in forthcoming years.

4.1 Biosensors

Due to exfoliation process, the electronic structures of many layered bulk materials which are semiconductor in nature often change. Change in thickness can help to modulate the band gap of 2D materials as well as there are several other processes also to modify the band gap like intercalating appropriate ions and alternating the lateral dimensions, etc. These tunings help them to become a potential candidate to develop innumerable types of electronics as well as biosensors. These biosensors are generally consisting of two major components, one is recognition element, and the other is transducer. Generally, biomolecules such as proteins, oligonucleotides, or some live cells or tissues which generally exhibit changes when they bind or come closer to targets act as recognition elements. Whereas transducers are the moieties which have some special features that they are able to transform the changes of recognition sites to such type of signals that can be detected and processed by means of modern electronics. One example of the most frequently used biosensors developed using 2D materials is field effect transistor (FET). By virtue of the sheet-like geometry of 2D materials, thin film is straightforwardly deposited on FET, but as transition metal dichalcogenides like MoS_2 (intrinsic semiconductors), they do not need further alternation to be used in FET biosensors. Another important kind of biosensors is fluorescence/photoluminescence (PL)-based biosensors. Many 2D materials are capable of adsorbing biomolecules by physisorption. When some fluorescent tags are attached to the biomolecules, their fluorescent activity can be quenched due to their adsorption by 2D materials via Forster resonance energy transfer, which thus develops fluorescence quenching-based biosensing. Such as Zhu et al. (2013) reported that a targeted DNA with complimentary sequence can be identified using MoS_2 nanosheets adsorbed with probe DNA. In case of biosensing, as compared to NP-based sensors, 2D materials-based sensors possess two key advantages. One advantage is that, by virtue of high surface area and 2D planner skeletons, they offer immobilization of higher amount of molecules to be sensed which helps to create a lower detection limit and a shorter duration of sensing assay. Another advantage is that 2D nanosheets have some uncommon properties like they can quench the fluorescent emission by means of photoinduced electron transfer (PET) from the excited state of fluorophore to the conduction band of 2D nanosheets. Another example of biosensors made up of 2D g-C_3N_4 nanosheet is DNA biosensor designed using change of affinity between g-C_3N_4 and DNA probes. They also work on the principal of analytes targeting and the measurement of corresponding PET-based fluorescence quenching effect (Wang et al., 2013).

4.2 Drug and Gene Delivery

2D nanosheets have a very noteworthy structural feature that they possess very high surface-to-volume ratio which leads to generate more spaces and interaction sites for incoming guest molecules. By virtue of its ultrahigh superficial area and exclusive sp^2-bonded carbonaceous surface, 2D graphene and its derivatives offer supramolecular π-π staking interaction and hydrophobic interaction which lead to high amount of adsorption of anticancer drugs. There are some advantages to using inorganic 2D-GAs materials as drugs carrier like as compared to micelles and organic liposomes inorganic 2D-GAs materials exhibit relatively higher chemical and physiological stability. So, they help to release the drugs in a sustained or controlled manner and sidestep the problem of burst release of drug which is generally created by breakage of conventional organic nanocarriers. Another advantage is that 2D-GAs endows huge amount of drug encapsulation and entrapment efficiency as they contain large surface-to-volume ratio. Due to some unique features of the 2D materials, they enhance the interaction ability of the drug moluecles with them. This helps in high amount of drug loading as well as in the release of the drugs accordingly, responding to the external stimuli. g-C_3N_4 nanosheets are the semiconductor materials, which have been introduced newly for its catchy performance in the field of photochemical and electrochemical catalysis. These g-C_3N_4 nanosheets have been synthesized via chemical oxidation afterword ultrasonic exfoliation bulk g-C_3N_4. These synthesized g-C_3N_4 nanosheets have only 1.1 nm thicknesses and 55 nm hydrodynamic diameter, and they are capable of delivering anticancer drugs (Dox) to the targeted area in an anticipated as well as act as the photosensitizer in photodynamic therapy. Incorporation of Dox in g-C_3N_4 is also much higher than other conventional mesoporous NPs. This release of Dox from g-C_3N_4 matrix is also pH-dependent, so rate of drug release is modulated by change of acidity. In case of chemotherapy, as nanocarriers of drugs, biocompatible transition metal oxide nanosheets can be utilized. pH-responsive drug delivery study has also been carried out using MnO_2 nanosheets-based carrier. Specifically, MnO_2 nanosheets have a special property of being breakdown when impregnated in mild acidic condition. So, Dox-loaded MnO_2 nanosheets when exposed to acidic environment exhibit a higher rate of drug release. This research if further modified by assembling 2D nanosheets to create 3D porous materials to carry the drug molecules. For anticancer drug delivery, a porous, biocompatible, and highly water-soluble BN-based material has been introduced. These BN nanostructures are inherently light in nature and also help in generation of extra p–p interactions between the BN network frame which in turn offers extremely high amount of drug loading efficiency, e.g., 309 wt % Dox has been loaded in this framework. Generally, for drug or gene delivery purpose, LDH used contains no toxic metal as component, and hence, they show a nontoxic behavior. There are several methods available for synthesizing LDH like hydrothermal growth reaction, hydrolysis, and precipitation of precursors or solid-state diffusion. Though LDH exhibits more biocompatibility toward biological systems as compared to other viral or organic nanocarriers (cationic liposomes, polycations, etc.), but the transfer efficacy to the cells and systems is very

low compared to them. This relatively lower transfer efficacy may be utilized for highly selective delivery to target sites via appropriate molecular engineering. Many experiments have confirmed that LDHs can demonstrate pH-responsive drug release (Hu et al., 2019). For example, an excellent research has been described by Peng et al. (2018). They have used LDHs to fabricate a biocompatible nano drug delivery system (Fig. 3). As drug carriers, MLDH nanosheets achieved the co-loading of DOX and indocyanine green and exhibited an exceptionally high loading of both DOX and ICG. The synthesized material exhibited both pH as well as NIR-induced DOX release along with a higher synergetic anticancer activity as well as excellent biocompatibility.

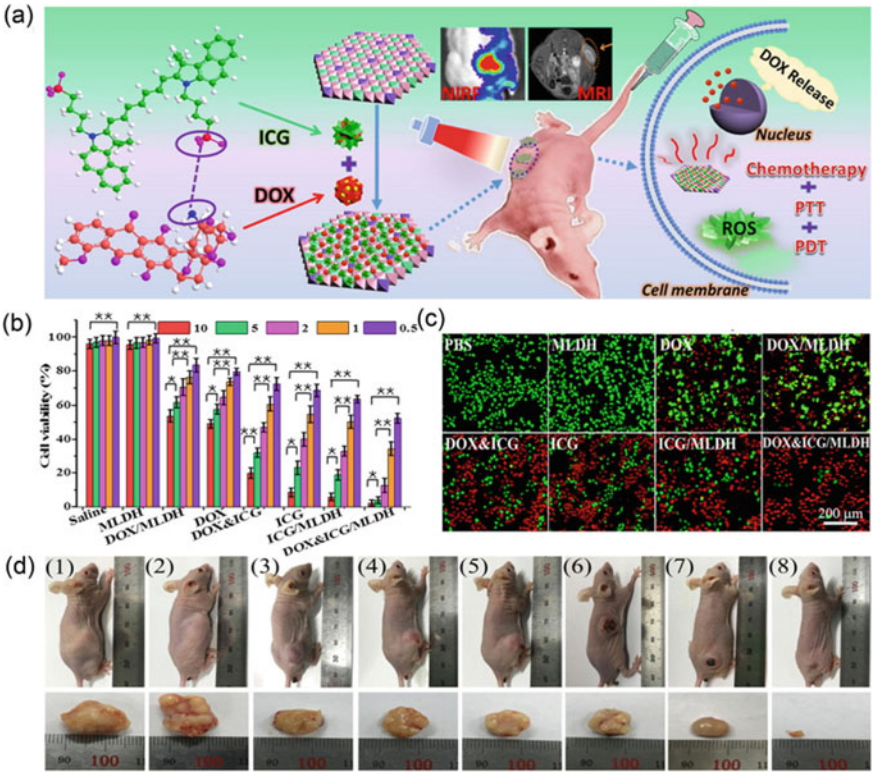

Fig. 3 Schematic diagram of cancer drug delivery system based on MLDH, its toxicity study results using HepG2 cells, and corresponding live dead assay images. Real digital photographs of *in-vivo* antitumor studies of day 14 after different treatments (Hu et al., 2019)

4.3 Bioimaging

2D materials are now extensively used as very good contrast agents (CAs) in medical imaging using the combination their various properties. They are generally used in magnetic resonance imaging (MRI), photoacoustic tomography (PAT), X-ray computed tomography (CT), and PL imaging.

4.3.1 Magnetic Resonance Imaging (MRI)

MRI is widely used techniques in medical imaging for diagnostic purpose. It is helpful as it offers very large spatial resolution, very good contrast difference in 3D tissues, and also non-invasive in nature. So, as MRI contrast agent, 2D materials associated with some magnetic properties are very promising, especially 2D materials exfoliated from layered rear earth hydroxides (LRH). LRH possess a higher layer charge density compared to that of LDH. Again, compared to LDH, LRH has a low solubility in water which also minimizes the CO_2 contamination. Gd is the rare earth element which has been so far extensively used in clinical diagnostics, and hence, Gd-based LRH are suitable to be used in MRI (Lee et al., 2009). But there is a problem associated with Gd-based LRH that when they fragmented, they generate highly toxic Gd ions. So, to improve this problem, as MRI contrast agent, 2D MnO_2-based exclusive compound has been introduced. Mn is an important element of human body, and it is less toxic in nature as compared to Gd (Chen et al., 2014). Dispersed MnO_2-based nanosheets were synthesized with the help of normal chemical exfoliation process. The superficial area was improved using PEGylation. This in turn also increases their strength in various physiological conditions. The *in-vitro* dynamic assessment of T1-weighted MRI indicated that, the T1 signal provided a significant enhancement after the incubation of MnO_2 nanosheets in the slightly acidic condition (pH 4.6) while the soaking of PEG–MnO_2 nanosheets in mild alkaline media (pH 7.4) did not generate any noticeable positive increment in the signal. Such a highly sensitive pH-responsive MRI increment was observed because of the gradual breakdown of MnO_2 nanosheets. This exclusive disintegration behavior of these 2D MnO_2 nanosheets may also simplify the process of excretion of these nanosheets from the human body. Owing to the ultra-small size of generated Mn^{2+} ions, they can easily be removed by kidney. Many inorganic 2D nanosheets with various functional moieties are recently used in oncological applications. As an explanatory model, for MRI-guided higher sonodynamic therapy (SDT) against cancer cells (Fig. 4), Dai et al. (2017) have effectively fabricated multimodal nanocomposites like MnO_x/TiO_2-GR-PVP. Owing to high electrical conductivity, very thin and planar structures, rich surface modification capability, and high photothermal conversion ability of reduced graphene oxide (GR) nanosheets, it is successfully used and exerted very good theranostics effects. The high electroconductivity of graphene facilitates the separation of the electron (e^-) and hole (h^+) pairs from the energy band of TiO_2 and restricts their recombination when they are exposed under external ultrasound irradiation.

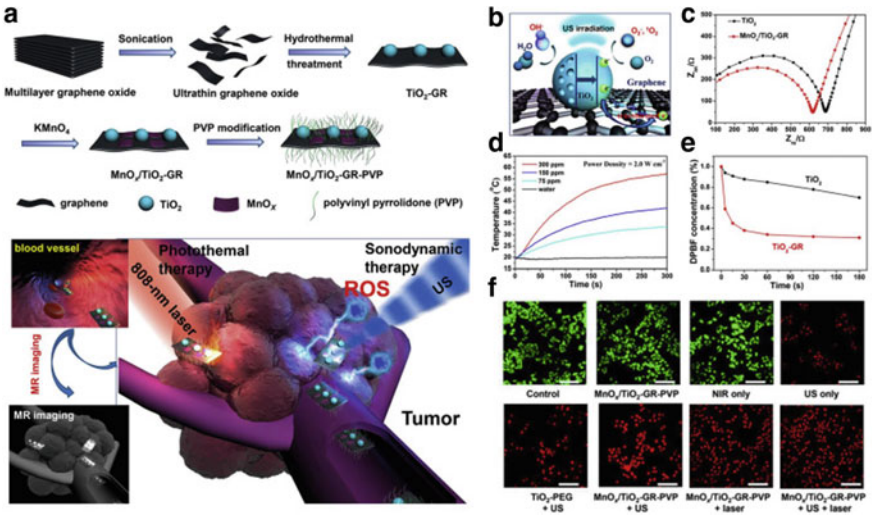

Fig. 4 MnOx/TiO_2-GR-PVP nanocomposite on 2D nanosurface for MRI-guided synergetic PTT and SDT against cancer. **a** Synthetic techniques for the fabrication of the nanocomposite and the cancer treatment through tumor microenvironment (TME) sensitive MRI-guided cancer therapy using the nanocomposite. **b** Illustration of the important principle for the GR-boosted SDT using TiO_2 nanoparticles as sonosensitizers. **c** Nyquist plot of TiO_2 and MnO_x/TiO_2-GR acquired from electrochemical impedance spectroscopic values for comparison. **d** Photothermal assessment of the nanocomposites at raised concentrations under 808 nm laser treatment. **e** Decay curves of DPBF at 410 nm with various extents of irradiation in existence of MnOx/TiO_2-GR or TiO_2 for more study of their sonocatalytic behavior. **f** Confocal microscopic images of live dead assay of 4T1 cells and also images of propidium iodide staining (Dai et al., 2017)

Thus, they significantly improved therapeutic efficacy of TiO_2 nanosonosensitizers for SDT against cancer.

4.3.2 Photoacoustic Tomography (PAT)

Recently, PAT has engrossed abundant consideration in the field of diagnostic imaging because of its precise properties of extremely good imaging depth and spatial resolution. As diagnostic imaging modality, PAT also involves the contrast agents (CAs) for further advancement of their imaging process. For this purpose, as CAs for PAT, nanoprobes associated with strong NIR absorbance property are preferred. Based on the outstanding NIR absorbance maxima of PEGylated WS_2 nanosheets, for PAT imaging, Liu et al. utilized this material as the CAs (Cheng et al., 2014). Employing a 700 nm laser excitation source in PAT imaging 4T1 tumor can be detected by strong photoacoustic signals, after intra-tumor or intravenous injection of WS_2–PEG (Chen et al., 2015).

4.3.3 Computed Tomography (CT)

An element having larger atomic number (Z) may also act as contrast agent in CT. So, 2D-GAs materials containing elements with higher atomic number are likely to work as CAs in CT imaging. WS_2–PEG has already been used as CA for CT imaging owing to the higher Z value of W ($Z = 74$) associated with the clinically used one, i.e., I ($Z = 53$) (Cheng et al., 2014). The higher efficiency in *in-vitro* CT imaging of WS_2–PEG was observed compared to commercially used I based CT CAs (Iopromide). Moreover, after the intravenous administration of WS_2–PEG, it is helpful that WS_2–PEG can enter and gather within the tumor tissues which provide the enhanced contrast in case of CT. Till now among various metallic elements, Bismuth ($Z = 83$) is considered to be an element with highest Z value with an acceptable biocompatibility (Chen et al., 2015). Though Bi_2S_3 NPs for CT imaging has widely been explored, but 2D topological insulator of Bi_2Se_3 nanoplates owns some specific functions in photothermal therapy as well as CT imaging (Liu et al., 2012; Rabin et al., 2006). Consequently, maximum 2D materials are normally perfect CAs for X-ray CT scanning and have been confirmed from some current reports. Nowadays, as several imaging ways are available, so a particular 2D material may be employed for multimode scanning and imaging. This can also be associated with therapeutics, which leads to an extremely promising property for 2D materials.

4.3.4 Fluorescent Imaging

Inorganic quantum dots (QDs) have been extensively studied compared to that of conventional organic fluorescein, in regards of their superior properties which includes tunable wavelength, enhanced photostability, and extraordinary quantum yields (Choi et al., 2007; Gao et al., 2004; Medintz et al., 2005; Michalet et al., 2005). Nevertheless, such inorganic QDs naturally comprise lethal heavy metal atoms (e.g., Cd-based QDs), and therefore, their clinical translations are restricted. Recently studied metal-free fluorescent nanomaterial is graphene QDs, which have displayed prospective application in fluorescent imaging (Liu et al., 2013; Zhang et al., 2010). Nonetheless, a low photo-response and intrinsically hydrophobic nature of these graphene QDs make their applicability restricted. More consistent inorganic fluorescent nanomaterials are ultrathin g-C_3N_4 nanosheets having π-conjugated electronic assembly, and rigid C–N planes can act as probes for two-photon fluorescence imaging of cellular nucleus (Zhang et al., 2014). Such g-C_3N_4 QDs display characteristic TPA feature by simultaneously absorbing and emitting two near-infrared photons and bright fluorescence in the visible-light region, respectively. Even though the bioimaging of g-C_3N_4 nanosheets is effective for intracellular imaging, *in-vivo* fluorescent imaging is strictly limited since they emit blue fluorescence, and thus, they fall out of the NIR window of wavelengths (700–1300 nm) (Chen et al., 2015). Some 2D transition metal dichalcogenides have been demonstrated for bioimaging using PL.

4.4 Therapeutic Applications of 2D Materials

Two main promises by the emerging bionanotechnology are highly precise therapeutics.

4.4.1 Photothermal Therapy (PTT)

Photothermal therapy (PTT) is a technique which characteristically utilizes laser to generate heat for inducing hyperthermia within the tumor tissues. Such therapy causes the denaturation of proteins, leading to the rupturing of cell membrane, and consequently damages the cancer cells permanently. On introducing photothermal agent (PTA), the low power density laser selectively heats a confined microenvironment of the tumor tissue (Jin et al., 2003; Li et al., 2012; Ma et al., 2012). One such widely studied PTA is graphene that has been employed for *in-vitro* and *in-vivo* photothermal ablation of cancer cells (Robinson et al., 2011; Yang et al., 2012). The strong light absorbance property of graphene in the near-infrared (NIR) window (700–1300 nm) makes its applicability in this field (Robinson et al., 2011; Yang et al., 2012). Chemically exfoliated MoS_2 (designated as $ceMoS_2$) having 2D planar morphology was produced via the Morrison method (Cheng et al., 2014). Bulk MoS_2 exfoliated through ultrasonication causes breaking the interlayer Van der Waals force resulted in synthesized $CeMoS_2$, which showed an average sheet size of 800 nm and thickness of 1.54 nm (Cheng et al., 2014). The synthesized $ceMoS_2$ displayed a mass extinction coefficient of 29.2 Lg^{-1} cm^{-1} via NIR absorbance, which is much better than that of GO nanosheets (3.6 Lg^{-1} cm^{-1}) and rGO nanosheets (24.5 Lg^{-1} cm^{-1}). A rapid increase in temperature to above 40 °C can be achieved at $ceMoS_2$ concentrations in the range of 38–300 ppm. In-vitro photothermal assessment against HeLa cells demonstrated that after NIR irradiation ($\lambda = 800$ nm, 20 min) and co-incubation with $ceMoS_2$, the cells could be totally destroyed as the temperature of the solution could be rapidly elevated over thermal-ablation thresholds. like MoS_2, WS_2 nanosheets show favorable photothermal transformation competence for PTT (Chen et al., 2015). Significantly, the proficiency of WS_2–PEG for PTT was thoroughly studied *in-vivo*. It was established that a 5 min-irradiation by an 808 nm laser could rapidly increase the superficial temperature of the tumor to about 65 °C within at the power density of 0.8 W cm^{-2}, regardless of the intra-tumor or intravenous administration of WS_2–PEG into mice. Specifically, a combination of both the administration of WS_2–PEG along with laser irradiation could considerably increase *in-vivo* photothermal therapeutic efficacy, and the tumors could be totally destroyed without any reoccurrences. Again, 2D Bi_2Se_3 nanoplates are also established to efficiently absorb the NIR laser and transform it into heat for PTT (Chen et al., 2015). 2D TMDs nanosheets, such as MoS_2 and WS_2, have also been verified as effective therapeutic agents for photothermal therapy. It is predicted that these 2D nanosheets can anchor anticancer agents onto their surface and synergistically combine chemotherapy as well as photothermal therapy. Such synergism is

hard to be attained by using Au NPs as a photothermal agent. Therefore, extensively chemical-exfoliated 2D MoS_2 nanosheets were produced, which was supplementary modified by lipoic acid conjugated PEG (LA–PEG) for improved stability in PBS (Liu et al., 2014). Apart from encapsulation as well as delivery of anticancer drugs at the targeted cells for chemotherapy, 2D-layered nanosheets can also deliver other therapeutic cargos like photosensitizers. Methylene blue (MB) as a photosensitizer was attached onto the surface of WS_2 nanosheets to generate the cytotoxic singlet oxygen for photodynamic therapy (PDT) (Yong et al., 2014). These outcomes give the robust confirmation that 2D-GA nanosheets can also act as the matrix to carry the photosensitizers for PDT. Also, chemically exfoliated MoS_2 nanosheets showed exceptional antibacterial property because of their 2D planar assembly and high conductivity that could induce the membrane /oxidative stress and generate reactive oxygen species.

5 Toxicology and Biocompatibility of 2D Materials

Only few studies have been explored to understand the toxicity of 2D materials, and till now, these studies are going on to properly investigate the toxicity of these materials. Studies on 2D materials demonstrate the toxicity effects of these 2D materials above 100 ppm concentration level (Anh Tran et al., 2014; Song et al., 2014). For example, the practicality of 293 T, HeLa, and 4T1 cells downs to ca. 50% after 100 ppm exposure of WS_2 (Kalantar-zadeh et al., 2015). Above 100 ppm PEG-coated MnO_2 nanoplates, the practicality of MCF-7 cells downs to 45% during 24 h treatment (Qiu, 2016). The environmental and biological belongings of 2D ultrathin materials on living system can be primarily separated into three types: mechanical, physical, chemical, and redox effects (Qiu, 2016). Mechanical and physical effects are mostly the mechanical stress due to the folding or bending of 2D material, when these 2D materials are integrated within a tiny biological system. These possessions could alter the biological paths through disturbing the transportation of biomolecules or triggering compensations to functional cell organelle. Mechanical and physical effects are identified for graphene and can possibly disturb lipid removal and facilitate corner-first lipid bilayer diffusion if the energy barrier is low. Chemical effect is the conversion of 2D materials into other species and the belongings of converted species to biological system. The converted species are not essentially sheet-like structure. These may be dissolved ions, precipitates, aggregates, nanoparticles, or mixture of these forms. The converted components may be biocompatible; however, sometimes these components are toxic and may be responsible for toxicity. 2D MoS_2 undergoes oxidative dissolution and creates soluble MoO_4^{2-} ion, which is primarily accountable for the experiential toxicity of MoS_2 in cell culture medium. The chemical characteristics of few exfoliated 2D materials are still very comparable to their bulk crystal structure, and consequently, it may be a good option to know the historical knowledge of their bulk crystal structure to envisage the toxicity of these 2D materials. For Example, in aqueous acidic solution, both 2D MnO_2 nanosheets and bulk

MnO_2 gradually dissolve. Redox effects are not well recognized for 2D materials. Histological evaluation after 7 and 28 days of post-implantation reported that LDH tempted no swelling or cytotoxicity, signifying that LDH was extremely biocompatible (Jayakumar et al., 2018). Cytotoxicity investigation of hydroxyl functionalized BN on mouse embryonic fibroblast cell and human prostrate tumorous cell exhibited 92% and 70% cell existence, respectively, after 24-h acquaintance with 100 μg/ml. Bulk TMDs are testified having low toxicity. Chng et al. (2014) reported that with decreasing the number of layers the toxicity of TMDs increases. Due to exfoliation, defects and surface area of TMDs increase which enhance the toxicity because of greater contact with cell. So far, very lesser number of studies on the genotoxic effect of 2D materials are accessible. Usually, chromosomal aberrations and monitoring DNA damage analyze the genotoxicity of 2D materials. Limited data is accessible on environmental toxic effect of 2D material. Bio safeties for the use of 2D resources are yet not been studied properly. Contact of many of the 2D materials with environment desires to be examined. Solubility, composition, particle size, and distribution are responsible to control the destiny of nanoparticles in environment. Regular risk assessment and toxicity assessment of 2D materials are essential due to the enhanced exposure for demands. To develop the materialistic characteristics according to the importance for upcoming research on 2D materials in biomedical field, environmental impacts must be focused.

6 Conclusion and Outlook

2D materials having unique characteristics have opened up a platform for biomedical application. Carbonaceous 2D materials such as graphene, rGO, GO, and fluorographene are intensely studied. Some new carbonaceous 2D materials such as graphdyine and graphyne are still in their early progress stage. Other various 2D materials such as TMOs, LDH, and TMDs have concerned the attention on biomedical research. 2D clay materials like laponite and LDH have drawn its significant interest on biomedical application, although these materials still have a possibility in broad biomedical field. LDH exposed possible application in gene transfer, tissue engineering, targeted drug delivery, and ion-exchange. TMDs and TMOs find their potential applications toward drug delivery, bioimaging, cancer therapy, and biosensing. Again 2D TMOs have not been discovered much and hold an opportunity for progress. Black phosphorous has opened up an opportunity for using them in thermal, electrical, mechanical, and optical application for bioengineering. Hexagonal boron nitride and g-C_3N_4 having some unique properties such as tunable bang gap and thermal stability are promising candidate for biosensors. Thus, 2D materials have opened up an opportunity for next generation biomedical device application. However, the investigations of these 2D-GAs in biomedical field are in their early development stage, and some severe problems are yet to be addressed to further enable the progress.

(i) Most of the studied 2D materials were synthesized from bulk crystals through exfoliation. Thus, suitable methodologies to synthesize 2D-GAs nanosheets in a standard and control way having satisfactory hydrophilicity, dispersity, surface functionalities, and sheet size are very difficult, which limit their application *in-vivo* biological application and diagnostic/therapeutic performances.

(ii) For clinical testing, details biosafety and biological evaluations of these 2D-GAs materials are instantly required. However, primary evaluations have established the potentiality of some 2D-GAs (such as MoS_2, WS_2, MnO_2, and g-C_3N_4), although their efficacy should be further revealed and determined for long-lasting toxicity assessment. The evaluations should be focused on the excretion, biodegradation, biodistribution, and potential toxicity to specific organs, which may influence the primary development of real-time biomedical device.

(iii) Because of the limited research on 2D-GAs for biomedical application, the practical application of these 2D-GA has been explored partially as compared to 2D graphene/rGO. As evident from the reported studies, 2D-GA materials show significant potentiality in other biomedical field like radio sensitization, tissue engineering, and gene therapy along with diagnostic imaging, biosensing, and drug delivery.

(iv) Lastly, 2D-GA materials can be smartly integrated with other biocompatible systems, which can be further used for several therapeutic and diagnostic purposes. With the understandable distinction between the great promises of 2D materials and the incomplete studies and applications, more studies speciously are essential to be carried out in this field to endorse its progress additionally. We hope the biomedical applications deliberated here only mark the commencement of a new era of applying these interesting new 2D materials to help fight challenging diseases and recover the life quality of human lives

References

Anh Tran, T., Krishnamoorthy, K., Song, Y. W., Cho, S. K., & Kim, S. J. (2014). Toxicity of nano molybdenum trioxide toward invasive breast cancer cells. *ACS Applied Materials & Interfaces, 6*(4), 2980–2986.

Chen, H., Liu, T., Su, Z., Shang, L., & Wei, G. (2018). 2D transition metal dichalcogenide nanosheets for photo/thermo-based tumor imaging and therapy. *Nanoscale Horizons, 3*(2), 74–89.

Chen, Y., Tan, C., Zhang, H., & Wang, L. (2015). Two-dimensional graphene analogues for biomedical applications. *Chemical Society Reviews, 44*(9), 2681–2701.

Chen, Y., Ye, D., Wu, M., Chen, H., Zhang, L., Shi, J., & Wang, L. (2014). Break-up of two-dimensional MnO_2 nanosheets promotes ultrasensitive pH-triggered Theranostics of cancer. *Advanced Materials, 26*(41), 7019–7026.

Cheng, L., Liu, J., Gu, X., Gong, H., Shi, X., Liu, T., Wang, C., Wang, X., Liu, G., Xing, H., & Bu, W. (2014). PEGylated WS_2 nanosheets as a multifunctional theranostic agent for in vivo dual-modal CT/photoacoustic imaging guided photothermal therapy. *Advanced Materials, 26*(12), 1886–1893.

Chng, E. L. K., Sofer, Z., & Pumera, M. (2014). MoS_2 exhibits stronger toxicity with increased exfoliation. *Nanoscale, 6*(23), 14412–14418.

Choi, H. S., Liu, W., Misra, P., Tanaka, E., Zimmer, J. P., Ipe, B. I., Bawendi, M. G., & Frangioni, J. V. (2007). Renal clearance of quantum dots. *Nature Biotechnology, 25*(10), 1165–1170.

Dai, C., Zhang, S., Liu, Z., Wu, R., & Chen, Y. (2017). Two-dimensional graphene augments nanosonosensitized sonocatalytic tumor eradication. *ACS Nano, 11*(9), 9467–9480.

Gao, X., Cui, Y., Levenson, R. M., Chung, L. W., & Nie, S. (2004). In vivo cancer targeting and imaging with semiconductor quantum dots. *Nature Biotechnology, 22*(8), 969–976.

Hu, T., Mei, X., Wang, Y., Weng, X., Liang, R., & Wei, M. (2019). Two-dimensional nanomaterials: Fascinating materials in biomedical field. *Science Bulletin, 64*(22), 1707–1727.

Jayakumar, A., Surendranath, A., & Mohanan, P. V. (2018). 2D materials for next generation healthcare applications. *International Journal of Pharmaceutics*.

Jin, R., Cao, Y. C., Hao, E., Métraux, G. S., Schatz, G. C., & Mirkin, C. A. (2003). Controlling anisotropic nanoparticle growth through plasmon excitation. *Nature, 425*(6957), 487–490.

Jin, J., Guo, M., Liu, J., Liu, J., Zhou, H., Li, J., Wang, L., Liu, H., Li, Y., Zhao, Y., & Chen, C. (2018). Graphdiyne nanosheet-based drug delivery platform for photothermal/chemotherapy combination treatment of cancer. *ACS Applied Materials & Interfaces, 10*(10), 8436–8442.

Kalantar-zadeh, K., Ou, J. Z., Daeneke, T., Strano, M. S., Pumera, M., & Gras, S. L. (2015). Two-dimensional transition metal dichalcogenides in biosystems. *Advanced Functional Materials, 25*(32), 5086–5099.

Lee, B. I., Lee, K. S., Lee, J. H., Lee, I. S., & Byeon, S. H. (2009). Synthesis of colloidal aqueous suspensions of a layered gadolinium hydroxide: A potential MRI contrast agent. *Dalton Transactions, 14*, 2490–2495.

Lee, Y. H., Zhang, X. Q., Zhang, W., Chang, M. T., Lin, C. T., Chang, K. D., Yu, Y. C., Wang, J. T. W., Chang, C. S., Li, L. J., & Lin, T. W. (2012). Synthesis of large-area MoS2 atomic layers with chemical vapor deposition. *Advanced Materials, 24*(17), 2320–2325.

Li, M., Yang, X., Ren, J., Qu, K., & Qu, X. (2012). Using graphene oxide high near-infrared absorbance for photothermal treatment of Alzheimer's disease. *Advanced Materials, 24*(13), 1722–1728.

Liu, Y., Ai, K., & Lu, L. (2012). Nanoparticulate X-ray computed tomography contrast agents: From design validation to in vivo applications. *Accounts of Chemical Research, 45*(10), 1817–1827.

Liu, Q., Guo, B., Rao, Z., Zhang, B., & Gong, J. R. (2013). Strong two-photon-induced fluorescence from photostable, biocompatible nitrogen-doped graphene quantum dots for cellular and deep-tissue imaging. *Nano Letters, 13*(6), 2436–2441.

Liu, T., Wang, C., Gu, X., Gong, H., Cheng, L., Shi, X., Feng, L., Sun, B., & Liu, Z. (2014). Drug delivery with PEGylated MoS_2 nano-sheets for combined photothermal and chemotherapy of cancer. *Advanced Materials, 26*(21), 3433–3440.

Liu, K., Zhang, J. J., Cheng, F. F., Zheng, T. T., Wang, C., & Zhu, J. J. (2011). Green and facile synthesis of highly biocompatible graphene nanosheets and its application for cellular imaging and drug delivery. *Journal of Materials Chemistry, 21*(32), 12034–12040.

Ma, M., Chen, H., Chen, Y., Wang, X., Chen, F., Cui, X., & Shi, J. (2012). Au capped magnetic core/mesoporous silica shell nanoparticles for combined photothermo-/chemo-therapy and multimodal imaging. *Biomaterials, 33*(3), 989–998.

Ma, T. Y., Tang, Y., Dai, S., & Qiao, S. Z. (2014). Proton-functionalized two-dimensional graphitic carbon nitride nanosheet: An excellent metal-/label-free biosensing platform. *Small (weinheim an Der Bergstrasse, Germany), 10*(12), 2382–2389.

Medintz, I. L., Uyeda, H. T., Goldman, E. R., & Mattoussi, H. (2005). Quantum dot bioconjugates for imaging, labelling and sensing. *Nature Materials, 4*(6), 435–446.

Michalet, X., Pinaud, F. F., Bentolila, L. A., Tsay, J. M., Doose, S. J. J. L., Li, J. J., Sundaresan, G., Wu, A. M., Gambhir, S. S., & Weiss, S. (2005). Quantum dots for live cells, in vivo imaging, and diagnostics. *Science, 307*(5709), 538–544.

Novoselov, K. S., Geim, A. K., Morozov, S. V., Jiang, D., Zhang, Y., Dubonos, S. V., Grigorieva, I. V., & Firsov, A. A. (2004). Electric field effect in atomically thin carbon films. *Science, 306*(5696), 666–669.

Peng, L., Mei, X., He, J., Xu, J., Zhang, W., Liang, R., Wei, M., Evans, D. G., & Duan, X. (2018). Monolayer nanosheets with an extremely high drug loading toward controlled delivery and cancer theranostics. *Advanced Materials, 30*(16), 1707389.

Qiu, Y. (2016). Two-Dimensional materials beyond graphene: emerging opportunities for biomedicine. *Nano Life., 6*(03n0), 1642008.

Rabin, O., Perez, J. M., Grimm, J., Wojtkiewicz, G., & Weissleder, R. (2006). An X-ray computed tomography imaging agent based on long-circulating bismuth sulphide nanoparticles. *Nature Materials, 5*(2), 118–122.

Robinson, J. T., Tabakman, S. M., Liang, Y., Wang, H., Sanchez Casalongue, H., Vinh, D., & Dai, H. (2011). Ultrasmall reduced graphene oxide with high near-infrared absorbance for photothermal therapy. *Journal of the American Chemical Society, 133*(17), 6825–6831.

Shan, C., Yang, H., Han, D., Zhang, Q., Ivaska, A., & Niu, L. (2009). Water-soluble graphene covalently functionalized by biocompatible poly-L-lysine. *Langmuir, 25*(20), 12030–12033.

Song, S. S., Xia, B. Y., Chen, J., Yang, J., Shen, X., Fan, S. J., Guo, M. L., Sun, Y. M., & Zhang, X. D. (2014). Two dimensional TiO_2 nanosheets: In vivo toxicity investigation. *RSC Advances, 4*(80), 42598–42603.

Vargas-Bernal, R. (2016). Graphene against other two-dimensional materials: A comparative study on the basis of electronic applications. *Two-Dimensional Materials: Synthesis, Characterization and Potential Applications; Nayak, PK, Ed*, (pp. 103–121).

Wang, Q., Wang, W., Lei, J., Xu, N., Gao, F., & Ju, H. (2013). Fluorescence quenching of carbon nitride nanosheet through its interaction with DNA for versatile fluorescence sensing. *Analytical Chemistry, 85*(24), 12182–12188.

Weng, Q., Wang, B., Wang, X., Hanagata, N., Li, X., Liu, D., Wang, X., Jiang, X., Bando, Y., & Golberg, D. (2014). Highly water-soluble, porous, and biocompatible boron nitrides for anticancer drug delivery. *ACS Nano, 8*(6), 6123–6130.

Yang, B., Chen, Y., & Shi, J. (2018). Material chemistry of two-dimensional inorganic nanosheets in cancer theranostics. *Chem, 4*(6), 1284–1313.

Yang, K., Hu, L., Ma, X., Ye, S., Cheng, L., Shi, X., Li, C., Li, Y., & Liu, Z. (2012). Multimodal imaging guided photothermal therapy using functionalized graphene nanosheets anchored with magnetic nanoparticles. *Advanced Materials, 24*(14), 1868–1872.

Yong, Y., Zhou, L., Gu, Z., Yan, L., Tian, G., Zheng, X., Liu, X., Zhang, X., Shi, J., Cong, W., & Yin, W. (2014). WS_2 nanosheet as a new photosensitizer carrier for combined photodynamic and photothermal therapy of cancer cells. *Nanoscale, 6*(17), 10394–10403.

Yuan, Y., Li, R., & Liu, Z. (2014). Establishing water-soluble layered WS_2 nanosheet as a platform for biosensing. *Analytical Chemistry, 86*(7), 3610–3615.

Zeng, Z., Yin, Z., Huang, X., Li, H., He, Q., Lu, G., Boey, F., & Zhang, H. (2011). Single-layer semiconducting nanosheets: High-yield preparation and device fabrication. *Angewandte Chemie International Edition, 50*(47), 11093–11097.

Zhang, H. G., Hu, H., Pan, Y., Mao, J. H., Gao, M., Guo, H. M., Du, S. X., Greber, T., & Gao, H. J. (2010). Graphene based quantum dots. *Journal of Physics: Condensed Matter, 22*(30), 302001.

Zhang, X., Wang, H., Wang, H., Zhang, Q., Xie, J., Tian, Y., Wang, J., & Xie, Y. (2014). Single-layered graphitic-C_3N_4 quantum dots for two-photon fluorescence imaging of cellular nucleus. *Advanced Materials, 26*(26), 4438–4443.

Zhu, C., Zeng, Z., Li, H., Li, F., Fan, C., & Zhang, H. (2013). Single-layer MoS2-based nanoprobes for homogeneous detection of biomolecules. *Journal of the American Chemical Society, 135*(16), 5998–6001.

Chapter 12
2D Nanomaterials Based Advanced Bio-composites

Md. Manzar Iqbal, Amaresh Kumar, and Subhash Singh

1 Introduction

In recent years, 2D nanomaterial has been receiving significant interest in biomedical field for drug delivery, imaging, cancer therapy, and bone tissue engineering purposes, due to its exclusive physiochemical and biological properties. It is an encouraging field from material science for offering high-technological materials to improve the present confines in biomedicine. Nowadays, nanomaterials have found wide acceptance as a reinforced material possessing high mechanical properties; for instance, essential strength along with high Young's Modulus value. After invention of graphene, researchers have shifted their focus to more 2D materials such as hexagonal boron nitride, silicates, trans-metal dichalcogenides (TMDs) and black phosphorus (BP). This growing family of 2D nanomaterial shows an extensive spectrum of properties in implant therapy such as bone and teeth implant as they played a vital function for promoting the differentiation of stem cells into fibroblast and osteoblast in addition to implant-osteointegration and implant tissue interaction. These properties might help in clinical application to remove the difficulties in the successful placement of implants and reduce the problems that occurred later.

In bone tissue engineering, different types of biomaterials (bio-ceramics and polymers) are used which have similar chemical composition to the apatite (found in bone) but reduced mechanical properties. The most appropriate key solution is incorporation of second phase in the base material. Researchers have been implementing the prospect of enhanced mechanical properties of materials while retaining the biocompatibility of the composite. Graphene-based nanomaterials have unique properties: promotes stem cell attachment; improves osteogenic differentiation; acts as substitute

Md. M. Iqbal · A. Kumar · S. Singh (✉)
Department of Production and Industrial Engineering, National Institute of Technology Jamshedpur, Jharkhand 831014, India

S. Singh et al. (eds.), *Advanced Applications of 2D Nanostructures*,
Materials Horizons: From Nature to Nanomaterials,
https://doi.org/10.1007/978-981-16-3322-5_12

material in bone regeneration investigation (Bentini, 2015). Graphene is mostly categorized by number of layers & by chemical composition, for instance, graphene oxide (GO) or reduced graphene oxide (rGO). The Graphene family is a group of nanomaterials with specific physiochemical properties, remarkably high mechanical strength, and high Young's Modulus value, which is compatible with bone regeneration.

2 Application of 2D Bio-Composite

2D nanomaterials are most potentially used in biomedical applications due to its unique biochemical properties. It can be used in biosensing and bioimaging because of properties of high resolution of micrograph imagery. It exhibits high strength as well as biocompatibility, thus it is used as bone implants. The bio-nanocomposite materials also possess antibacterial properties. Because of its strong optical absorption into NIR range can be used in photothermal therapy. It can be also used in drug delivery, because of its significant intermolecular interaction. Some of the types and application of 2D nanomaterials have been shown in Fig. 1.

The percentage usage of 2D nanomaterials in various sectors is illustrated in Fig. 2.

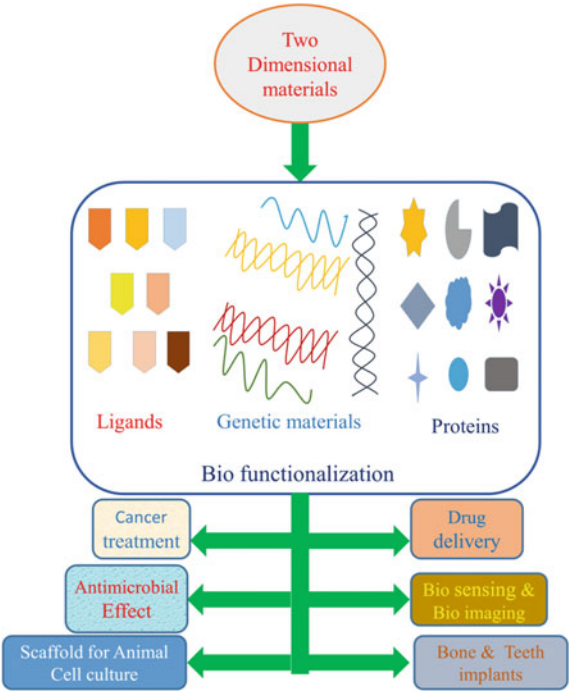

Fig. 1 Biomedical applications of 2D materials

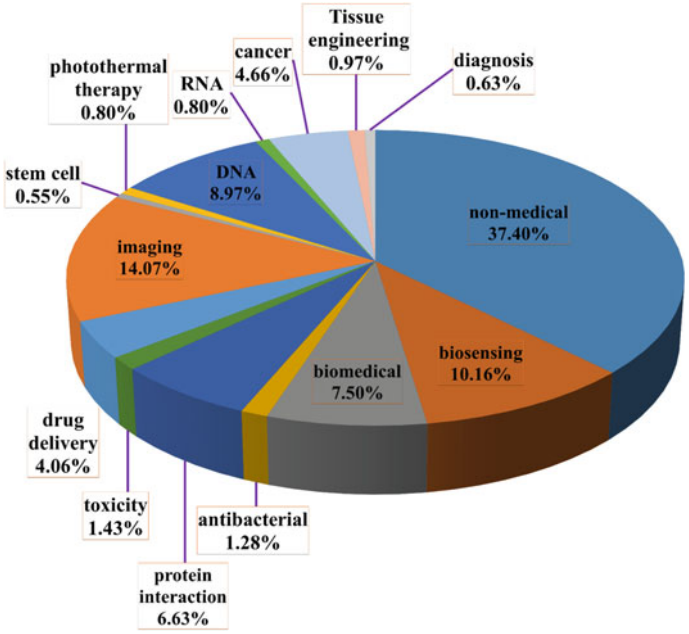

Fig. 2 Various percentage of graphene-based nanomaterial is used in biomedical application (Mao et al., 2013)

2.1 Bone Implants

Bone reconstruction has an important role in universal research on health issues. However, the matching of mechanical, physical, and chemical properties with host bone properties is rather challenging. Fu et al. (2017) improved the osteogenesis and promoted bone regeneration successfully by restraining Bone morphogenetic protein-2 (BMP-2) at GO-included poly (lactide-co-glycolide) (PLGA) with Hydroxyapatite (HA) biodegradable microcarriers. BMP-2 is a significant feature and a biodegradable microcarriers, which is must for superior bone grafting. Rajan Unnithan et al. (2017) incorporated the graphene oxide-Chitosan (GO–CS) nanocomposites with Hyaluronic acid exhibited excellent attachment and spreading with mouse preosteoblast MC3T3 cell. Addition of hyaluronic acid improved the cell proliferation. Kumar (2016) attributed that polyethylenimine (PEI) conjugated with graphene oxide remarkably developed bioactive resorbable biomaterials for orthopedic devices which include fracture fixation and tissue engineering. Zhao (2016) prepared bone screws by graphene-reinforced nanohydroxyapatite/polyamide66 (nHA/PA66) and found that elastic modulus and tensile strength of composites had significantly enhanced by 21.2% and 49.14% respectively as well as showed better adhesion and proliferation. It was observed that this composite can be used in bone tissue engineering. Jeong (2015) examined that addition of rGO in Hydroxyapatite

Nanocomposites enhanced Osteogenesis as well as promoted the bone formation due to alkaline phosphate activity. It was concluded that rGO/Hap nanocomposites may be used in innovative dental and orthopedic implants. Depan (2014) reported that hybrid graphene oxide–chitosan shows strong electrostatic connections among the functional groups like Ca ions into the simulated body fluid. Apart from this, the proposed system showed positively modulating cellular activity and it can be considered in tissue engineering. Sayyar et al. (2013) explored that the covalent linking of the polymer to graphene chains caused the homogeneity of dispersed phase of graphene as well as enhanced mechanical properties and mark the materials prominently biodegradable for use in tissue engineering. Baradaran et al. (2013) developed nanotube hydroxyapatite composites (nHA) and reduced graphene (rGO). It was concluded that addition of rGO resulted in proliferation and osteoblast adhesion which led to the biocompatibility of composites. Rashkow et al. (2017) suggested that scaffold integrated with molybdenum disulfide nanoplatelets (MSNPs) or graphene oxide nanoplatelets (GONPs) exhibited as the promising options for bone tissue engineering.

2.2 Drug Delivery

In the last few years, curiosity has increased in application of 2D materials for drug loading and delivery. 2D materials may be used for drug delivery due to its significant interaction among hydrophobic drugs and aromatic regions of graphene sheets. Tian (2014) had functionalized nanographene oxide (NGO) for proficient drug delivery of cisplatin. The medium of NGO-PEGylated was observed nontoxic. Hyunwoo et al. (2013) developed PEG-BPEI-rGO nanocarrier which is capable to load greater quantity of drug. Wen et al. (2012) developed redox responsive PEGylated Nano-Graphene Oxide. The composites were used in Intracellular drug delivery. As a result, the formation of PEGylated nano-graphene oxide (NGO-SS-mPEG) with redox-responsive detachable PEG shell occurred. The shell was rapidly released through an encapsulated payload with tumor-relevant glutathione (GSH) levels. The surface-engineered constructions enhanced the activation of doxorubicin hydrochloride (DXR) from NGO-SS-mPEG by 1.55 times than without presence of GSH. Optimum drug loading capability, targeted delivery for nanocarrier was achieved in appropriate location. The interest has correspondingly increased in significant features to attain successful therapeutic outcome. Depan et al. (2011) explored that unique graphene mediated drug delivery system along with regulated released. GO has been surrounded by nanofiller also exhibited superior drug loading. It was mentioned that due to the presence of chitosan micromolecular chains degraded at targeted place and made a strong bond between DOX and folic acid. Rana et al. (2011) functionalized graphene oxide with CS. They found that exact release of Ibuprofen and 5-fluorouracil. The nanocomposite showed biocompatibility and can be used in biomedical application (Table 1).

Table 1 Drug delivered by 2D based materials

Carriers	Delivered drugs	Results and uses	References
nGO-PEG	Cisplatin	Inhibition cell proliferation and morphology deformation. Covalent reaction promoted effective drug loading mechanism	Tian et al. (2014)
PEG-BPEI-GO	DOX	Photothermally generated cytosolic drug delivery through Endosome Disruption	Hyunwoo et al. (2013)
PEGylated nano-graphene oxide	Doxorubicin hydrochloride	Redox-responsive drug have been developed. More ever, inhibition of cell proliferation is absolutely linked with enlarged intracellular GSH concentrations because of quick DXR discharge	Wen et al. (2012)
DOX-GO–CHI-FA nanohybrid	Doxorubicin	pH dependence drug release mechanism has been perceived. The nanohybrid exhibited an appropriate drug carrier in nanomedicine treatments	Depan et al. (2011)
Chitosan-GO	Ibuprofen, 5-fluorouracil	The composites regulated releasing behavior for chemically unlike drug	Rana et al. (2011)

2.3 Bioimaging

Various nano-devices have been enhanced by 2D-based nanomaterials for optical imaging in the field of nanomedicine. Any simple to complex biological phenomena occurring within the tissue, living cells, and whole organism can be seen by new bioimaging tools. Various techniques are used for bioimaging are explained below.

2.3.1 Raman Spectroscopy

The application of Raman spectroscopy in the biomedical has gained attention due to use of bioimaging to describe chemical configurations of cells and tissues. This technique is broadly used to characterize graphene and its derivatives because of its

characteristics band in Raman spectra. Addition of silver or gold nanoparticles on the graphene nanomaterials improved Raman intensity and sensitivity (Shin et al., 2018). A lot of research was done to exploit this characteristic as imaging probes for biological cells. Ma, X., et al. (2013) exploited the gold nanoparticles in graphene oxide. They utilized intracellular Raman imaging in Hela cell. Liu et al. (2012) examined that cells incubated Au/GO hybrids system which is shown in Fig. 3. The system demonstrated considerable Raman signals which led to attainment of a continuous and distinguishable image. Furthermore, the technique was proven harmless to living cells and appropriate for cell investigations.

2.3.2 Fluorescence Imaging

This technique is broadly utilized for bioimaging and diagnosis. But it has certain drawbacks such as photo blinking, photobleaching, and circumstantial sound because of autofluorescence from tissue and cells. But most researchers preferred this technology for bioimaging of graphene-based materials. Ji (2015) reported in their experimental studies that glycocomposite demonstrated excellent imaging capability for cancer cell due to the reason of over express glycoprotein receptor associated with the control cells. Sreejith et al., (2012) explored that hybrid materials consist of mesoporous silica nanoparticles (MSNPs), organic dyes, and GO. It has been concluded that biocompatible hybrid materials exhibited noncytotoxic and offered important in vitro fluorescence imaging for cancer cells. Pan (2012) used ultrasmall GQDs for imaging the biological cells. The GQDs showed bright as well as stable green PL which is mentioned in Fig. 4.

2.3.3 Photoacoustic Imaging

In biomedical imaging, there was an enormous requirement for a non-invasive imaging technique. Photoacoustic imaging technique is used for functional structural and molecular imaging. It works upon transformation involving light and acoustic. Nowadays, graphene and its derivatives are broadly utilized in this technique for being a photoacoustic imaging agent. Graphene-based nanomaterials are widely used in deep organ tissue imaging because it facilitates superior resolution. ME-LOGr nanosheets showed exceptionally intense photoacoustic signals produced with graphene nanosheets with NIR excitation as reported by Patel (2013). The photoacoustic conversion has independent of wavelength of NIR excitation as illustrated in Fig. 5 differ from various photoacoustic agents (Table 2).

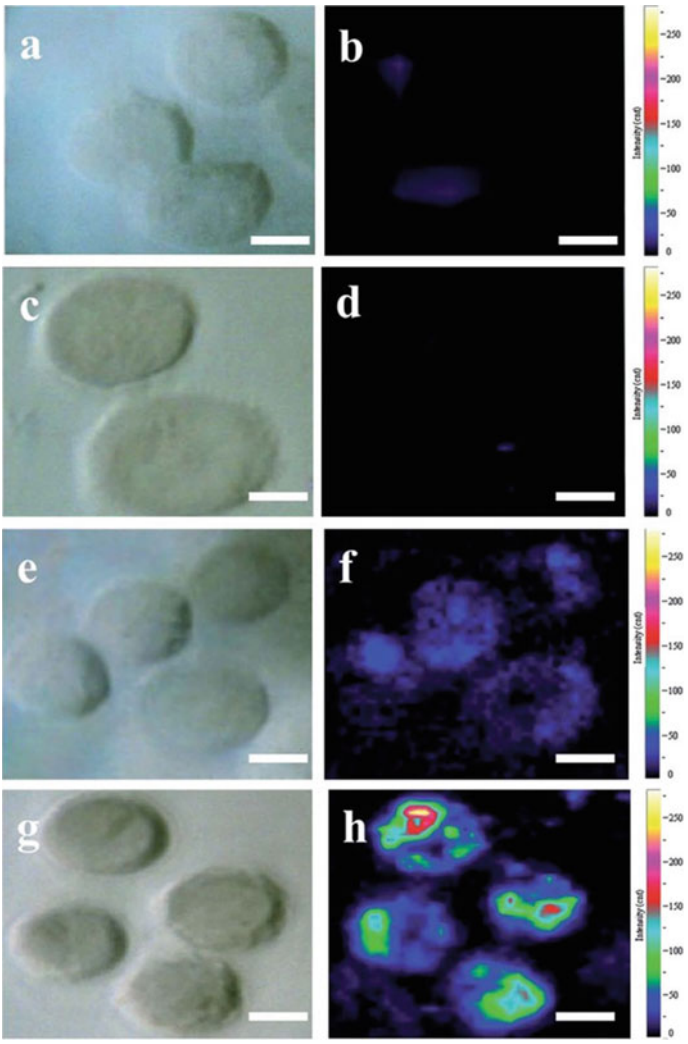

Fig. 3 Comparison among optical images (**a**, **c**, **e** and **g**) and Raman images (**b**. **d**, **f** and **h**) of Hela 229 cells. In **a** and **b**, cells were incubated in medium without GO; in **c** and **d** in medium with Silver nanoparticles; in **e** and **f**, cells were incubated with Graphene oxide; and in **g** and **h**, with Gold/Graphene oxide hybrids at a temperature of 37 °C for 24 h ahead of imaging. (Scale bar: 10 mm). Reproduced with permission from Liu (2012). Copyright 2012 Royal Society of Chemistry

2.4 Biosensors

Biosensors are analytical devices used to detect chemical substances. Graphene and its derivatives are mostly used in biosensors due its remarkable properties. In recent

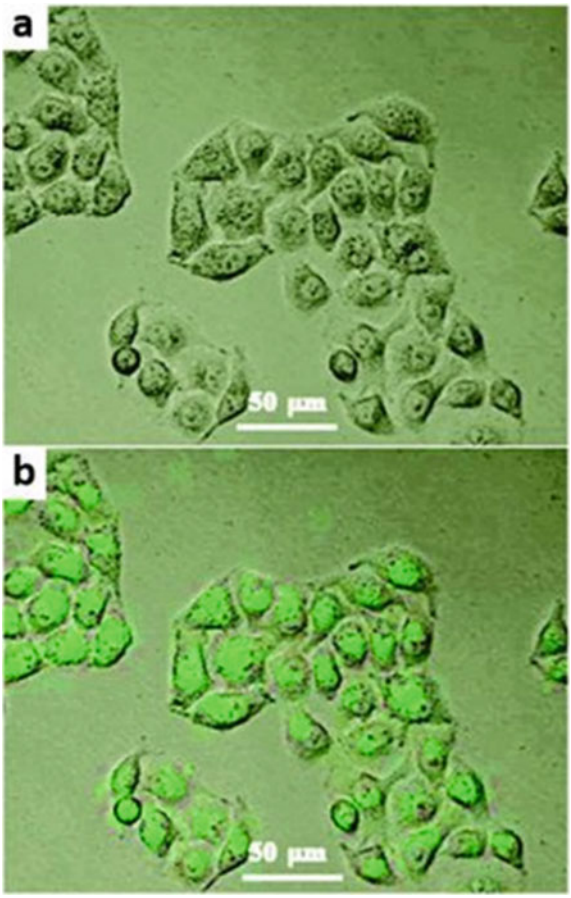

Fig. 4 Hela cell cured through Graphene Quantum dot suspension: **a** image of bright-field and **b** confocal fluorescence photomicrograph occupied at excitation wavelength at 405 nm. For detection of images, wavelength varies from 420 to 520 nm. Reproduced with from Pan et al., (2012). Copyright 2012 Royal Society of Chemistry

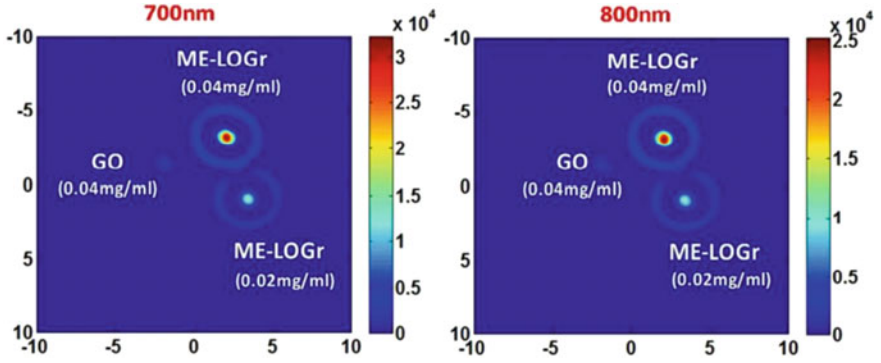

Fig. 5 Photoacoustic signal of Graphene oxide and graphene nanosheets at distinct concentrations, lightened in the wavelength of 700 nm and 800 nm laser respectively. *Y*-axis line which is at different colors denotes strength of photoacoustic signal produced. Reproduced with permission from Ref. Patel et al., (2013) Copyright 2013 American Chemical Society

Table 2 List of 2D materials-based composites used in bioimaging applications

Platform	Imaging instrument	Use	References
GO wrapped with Au nanoparticles	Raman	Imaging for Hella cells	Ma, X., et al. (2013)
GO with Au nanoparticles	Raman	Imaging of Hella cells	Liu et al., (2012)
Glycoprobe conjugated GO	Fluorescence	Imaging for Hep-G2 cells	Ji et al., (2015)
Graphene Oxide Wrapped with Squaraine-Loaded Mesoporous Silica Nanoparticles	Fluorescence	Imaging of HeLa cancer cells	Sreejith et al., (2012)
Microwave-enabled less quantity of oxygen graphene nanosheets	Photoacoustic	High photothermal, effective NIR absorption also photoacoustic conversion efficiencies	Patel et al., (2013)

time, various numbers of biosensors have been developed based on the 2D-based nanomaterial as explained below.

2.4.1 Electrochemical Biosensor

Graphene materials have high specificity and sensitivity which makes it an emerging compound for making electrochemical biosensors. The specificity depends upon various reduction or oxidation of molecules in several potential windows. Exchanges of electron occur in graphene nanomaterials through oxidation and reduction route. Heterogeneous electron transfer activity occurs either by edges or defects in basal plane (Ghosal & Sarkar, 2018). Graphene-based composites are most widely used to detect glucose since currently diabetes is a global threat.

Li (2014) synthesized graphene/NiO nanocomposites based electrochemical glucose biosensor. They found that nanocomposite sensors exhibited quick and amply sensitive response towards glucose. Istrate et al., (2016) proposed that AuNPs–ERGO–PAH composites revealed very decent analytical functioning termed by a quick response, sensitive and reproducible analysis with a decent selectivity in DPV. Also it was concluded that fabrication process is easy and simple which led to this sensors attracted transducer detection of NADH. Zheng (2015) explored that polyaniline/graphene-based DNA sensors have effectively detected complementary DNA ranges 0.01 pm to 1 μm. Luo et al., (2014) developed electrochemical sensor which is used in bivine hemoglobin (BHb). Graphene-molecular imprinted polymers composite was used like detection ingredient. The sensors demonstrated exceptional sensing behavior, excellent selectivity, low fabrication cost, and green process attracted to detection of BHb. Dinesh (2014) reported that cytochrome c immobilized GO-MWCNT sensors used in recognition of H_2O_2. These nanocomposites have

shown prominent current sensitivity of 0.533 μA pM^{-1} cm^{-2} and a very small detection range of 27.7 Pm which makes its use in bioimaging and healthcare novel. Ruecha (2014) proposed use of Graphene/polyvinylpyrrolidone/polyaniline based nanocomposite to determine the presence of cholesterol in human serum. This composite has exhibited low cost, simple process, disposability, and portability.

2.4.2 Fluorescence

Fluorescence spectroscopy is used in biomolecular detection. Graphene-based material are commonly used for fluorescence detection due to its strong fluorescence quenching property. Zhang (2014) proposed boron-doped graphene quantum dots (BGQDs) for detection of glucose using abnormal aggregation-induced photoluminescent enhancement. The sensing mechanism depends on reaction occurred on the BGQDs surface created rigid by BGQDs-glucose aggregates which restrict the intermolecular rotations, and thus result in a great boost in the PL intensity. The sensor revealed a wide functional range (0.05–10 mM) with lower least count (about 0.01 mM) at pH 10 phosphate buffer. Qian (2014) fabricated biocompatible nanosensors for DNA recognition. For that, they used GQDs and carbon nanotubes. FRET process is simply achieved via its specific Π-Π interactions. The sensor exhibited superior outcome at trace analysis.

2.4.3 Bio-Field Effect Transistor (FET)

Currently, this technique has attracted excessive courtesy for biosensing. Since it is fully approaching towards automated electronic detection. The recognition is wholly incorporated by electronic chips manufactured in semiconductor companies. Graphene is the most appropriate material for manufacturing biosensors due to its zero band gaps properties. But according to requirement, the band gap can be adjusted via surface changes. Said (2017) fabricated Graphite-oxide based FETs for glucose sensors. Incorporation of copper and silver nanoparticles improved the sensor's sensitivity for optimum functioning. The GO/Cu-NPs nanocomposite possesses good stability, and low detection sensitivity of about 1 μM, and wide range from 1 μM to 30 mM. It is difficult to operate the standard tools for optical-based sensors at a low cost with high throughput measurement. The fabrication of Nanowire based FETs for biosensors at reliable and cost-effective is a persistent task. Xu (2017) demonstrated graphene single crystal domain patterned into multiple channels can measure time and concentration-dependent DNA with a detection limit of 10 Pm (Table 3).

Table 3 Two-dimension nanostructured composites-based biosensors

Element of sensors	Forms of sensor	Sensor platform	Detection Limit (μM)	Linear range (mM)	References
Glucose	Electrochemical	GCE/NiO composites/ Graphene	1	0.005–2.8	Li et al., (2014)
NADH	Electrochemical	AuNPs–ERGO–PAH/SPE sensing	3.5	0.01–0.2 0.2–5	Istrate et al., (2016)
DNA	Electrochemical	Polyaniline/ graphene	1×10^{-8}	1×10^{-10}–1×10^{-3}	Zheng et al., (2015)
Hemoglobin	Electrochemical	Graphene-molecular imprinted polymers composite (GR-MIP)	2.0×10^{-13} g/L	1.0×10^{-12} 1.0×10^{-4} g/L	Luo et al., (2014)
Hydogen peroxide	Electrochemical	Cytc/GO-MWCNT/Au NP	27.7×10^{-6}	1.0×10^{-8}–1.4×10^{-7}	Dinesh et al., (2014)
Cholesterol	Electrochemical	Graphene/polyvinylpyrrolidone/polyaniline nanocomposite	1	0.05–10	Ruecha et al., (2014)
Glucose	Fluorescence	Br doped graphene quantum dots	10	0.05–10	Zhang et al., (2014)
DNA	Fluorescence	GQDs-cDNA-CNTs	0.0004	0.0000015- 0.000133	Qian et al., (2014)
Glucose	FET	Graphite oxide–Copper/Silver nano particles	1	0.001–30	Said et al., (2017)
DNA	FET	Only one crystal graphene domain-PBASE-Probe DNA	0.000001	2.5×10^{-7}–1×10^{-5}	Xu et al., (2017)

Table 4 Antibacterial efficiency of 2D materials

2D nanomaterials	Bacterial Strains	Concentration (μg/m)	Incubation Time (h)	Inhibition (%)	References
GO/Ag Nanocomposites	*E. coli*	10^2	4	100	Vijay Kumar (2013)
Graphene oxide–silver nanoparticle	*E. coli*	3.2/6.4	24	99.9	Ma, L., et al. (2013)
GO/Ag NPs	*S. aureus*/*B. subtilis*	N/A	24	100	Das et al., (2013)

2.5 Antibacterial Property

Graphene and its derivatives have also exposed prohibition effect against bacterial growth on their surface. This is because of synergistic effects through another substances; also oxidative stress provoked through membrane disruption (Liu, S., et al. 2011). Moreover, the antibacterial activity is regulated as per graphene size so that it causes least skin infection (Banerjee, 2018). Liu, S., et al. (2011) explored the GO–Ag nanocomposites in contradiction of gram-negative bacteria Escherichia coli. They found that antibacterial activity has been considerably improved as compared to Ag nanocomposites particles and can be used as antibacterial materials. Akhavan and Ghaderi (201)0 examined GO and rGO nanowalls deposited on stainless steel and studied the Gram-positive and Gram-negative models of bacteria. Also reported that cell membrane of bacteria was damaged because of presence of highly sharp edges of graphene sheets. Santos (2011) illustrated that graphene polymer nanocomposite film exhibited 90% more effectiveness to bacterial colonization can be used as an alternative coating in biomedical applications (Table 4).

2.6 Photothermal Therapy

Temperature is a significant factor through which feasibility of biological species are closely controlled. But with increasing temperature in controlled way on targeted tissues/organs, plentiful therapeutic improvements occurred in patients having cancer or another disease. Recently, researchers have developed smart materials as well as methodology to confine the heating. Photothermal therapy (PTT) is an emerging area due to its own astonishing characteristics for generating localized heat which can be controlled by means of optical energy exposure. In this regard, 2D nanomaterials offer the several qualities required for the fabrication for photothermal therapy because it possesses strong optical absorption into the NIR range. Also, adjustment in 2D nanomaterials would improve fabrication of composite for improved heating regulation. Shi (2013) reported graphene-based magnetic plasmonic nanocomposite for PTT. They formed multi-functional magnetic and plasmonic graphene oxide-iron

oxide nanoparticles-Gold nanocomposite by decorating IONPs and Au in GO. Dai (2011) fabricated ultrasmall nano-rGO sheet with remarkable NIR absorbance for photothermal therapy. Afterward they combined a peptide sustaining Arg-Gly-Asp (RGD) motif to promote selective cellular consumption in U87MG cancer cells and highly valuable in vitro photoablation of cells.

3 Challenges for Development of 2D Materials in Biomedical Applications

2D-based nanostructured composites have new and electrifying properties which lead to biomedical applications. But research in this field is still in infant phase and various key challenges encountered by this area cannot be wholly commercialized. The main challenges faced by biosensing and bioimaging application is the reproducibility and reliability of the materials and processes at a low cost. A lot of studies attributed that detection sensitivities are observed superior as compared to traditional methods. The batch to batch deviations of nano-biosensors has not yet been justified and need further examination (Banerjee, 2018). As far as application in drug delivery and therapy are concerned, main challenges are recognition of suitable and high drug loading capability for practical applications. For instance, graphene and its derivatives are inorganic nanomaterials which are not easily biodegradable. Therefore, several novel processes need to be experimented for attaining biodegradable nanocomposites. Also, main factors of use of 2D nanostructured materials in the tissue engineering are cell culture and antibacterial activities. In antibacterial activity, the major challenges are: (a) Proper scaling technology to determine stem cell differentiation. (b) Clear knowledge of relative antibacterial activity of the materials, (c) proper detection method for finding antibacterial effects which clarification as well as outcome. As graphene-based nanomaterials enhanced the bacterial growth rather than inhibition, which made it evident that antibacterial activity is dependent on the experiment conditions (Ruiz et al., 2011).

4 Conclusion and Future Research Recommendations

The use of 2D materials has become an exciting research area and requires suitable future perception for transformation of ideas into market-based research area. One of the most important applications is the therapeutic application through proper understanding of the toxicity profile of the material can be utilized in vitro and in vivo experimentation. Also, another future biomedical application is in vivo gene transformation. Various researchers found that 2D nanomaterials could serve like in vitro gene transformation vectors. But in vivo gene transformation by these materials are yet to be explored. For that nanomaterials with smarter design of surface chemistry

can be used in forthcoming treatment of genetic disorders. In other field, bio-imaging graphene quantum dots (GQD) had exhibited low toxicity although productivity is low. Therefore, in future, an improved technique could be developed to increase the productivity of GQD. Another application of biosensors could be to improve sensing efficiency to fit as per market usages. Hence future research in these areas to recognize the molecular mechanism of biosensors can be performed. An application in biomolecules detection and drug delivery could be development of a latest and scalable training procedure for inerratic nanomaterials synthesis. In antibacterial activities, researchers are trying to understand the mechanism of materials such as the effects of time, size, concentration, and density. A function of nanomaterial in tissue engineering is new. Nanomaterial have more strength so it can be used as a bioimplant. Meanwhile, 2D nanomaterials possess unique physiochemical and biological properties that can be investigated in interdisciplinary domains. Research work in these areas would accelerate the biomedical application of 2D nanomaterials and lead to formation of research labs for clinical application.

References

Akhavan, O., & Ghaderi, E. (2010). Toxicity of graphene and graphene oxide nanowalls against bacteria*, 4*(10), 5731–5736.

Banerjee, A. N. (2018). Graphene and its derivatives as biomedical materials: Future prospects and challenges. *Interface Focus, 8*(3). https://doi.org/10.1098/rsfs.2017.0056

Baradaran, S., et al. (2013). Mechanical properties and biomedical applications of a nanotube hydroxyapatite-reduced graphene oxide composite. *Carbon*, 1–14. https://doi.org/10.1016/j.carbon.2013.11.054

Bentini, R., et al. (2015). Graphene: A versatile carbon-based material for bone tissue engineering. *Stem Cells International, 2015*, 1–12. https://doi.org/10.1155/2015/804213

Dai, H., et al. (2011). Ultrasmall reduced graphene oxide with high near-infrared absorbance for photothermal therapy. *Journal of the American Chemical Society, 133*(17), 6825–6831. https://doi.org/10.1021/ja2010175

Das, M. R., et al. (2013). The synthesis of citrate-modified silver nanoparticles in an aqueous suspension of graphene oxide nanosheets and their antibacterial activity. In *Colloids and Surfaces B: Biointerfaces* (Vol. 105, pp. 128–136). Elsevier B.V. https://doi.org/10.1016/j.colsurfb.2012.12.033

Depan, D., Pesacreta, T. C., & Misra, R. D. K. (2014). The synergistic effect of a hybrid graphene oxide-chitosan system and biomimetic mineralization on osteoblast functions. *Biomaterials Science, 2*(2), 264–274. https://doi.org/10.1039/c3bm60192g

Depan, D., Shah, J., & Misra, R. D. K. (2011). Controlled release of drug from folate-decorated and graphene mediated drug delivery system: Synthesis, loading efficiency, and drug release response. *Materials Science and Engineering C, 31*(7), 1305–1312. https://doi.org/10.1016/j.msec.2011.04.010

Dinesh, B., et al. (2014). Direct electrochemistry of cytochrome c immobilized on a graphene oxide-carbon nanotube composite for picomolar detection of hydrogen peroxide. *RSC Advances, 4*(54), 28229–28237. https://doi.org/10.1039/c4ra02789b

Fu, C., et al. (2017). Enhancing cell proliferation and osteogenic differentiation of MC3T3-E1 pre-osteoblasts by BMP-2 delivery in graphene oxide-incorporated PLGA/HA biodegradable microcarriers. *Scientific Reports, 7*(1), 1–13. https://doi.org/10.1038/s41598-017-12935-x

Ghosal, K., & Sarkar, K. (2018). Biomedical applications of graphene nanomaterials and beyond. *ACS Biomaterials Science and Engineering, 4*(8), 2653–2703. https://doi.org/10.1021/acsbiomaterials.8b00376

Hyunwoo, K., et al. (2013). Photothermally triggered cytosolic drug delivery via endosome disruption using a functionalized reduced graphene oxide. *ACS Nano, 7*(8), 6735–6746.

Istrate, O. M., et al. (2016). NADH sensing platform based on electrochemically generated reduced graphene oxide-gold nanoparticles composite stabilized with poly(allylamine hydrochloride). *Sensors and Actuators, B: Chemical* (Vol. 223, pp. 697–704). Elsevier B.V. https://doi.org/10.1016/j.snb.2015.09.142

Jeong, C.-M., et al. (2015). Enhanced osteogenesis by reduced graphene oxide/hydroxyapatite nanocomposites. *Scientific Reports, 5*(1), 1–13. https://doi.org/10.1038/srep18833

Ji, D. K., et al. (2015). Receptor-targeting fluorescence imaging and theranostics using a graphene oxide based supramolecular glycocomposite. *Journal of Materials Chemistry B, 3*(47), 9182–9185. https://doi.org/10.1039/c5tb02057c

Kumar, S., et al. (2016). Engineering a multi-biofunctional composite using poly(ethylenimine) decorated graphene oxide for bone tissue regeneration. *Nanoscale, 8*(12), 6820–6836. https://doi.org/10.1039/c5nr06906h

Li, S. J., et al. (2014). A facile one-step electrochemical synthesis of graphene/NiO nanocomposites as efficient electrocatalyst for glucose and methanol. *Sensors and Actuators, B: Chemical*. https://doi.org/10.1016/j.snb.2013.09.047

Liu, L., et al. (2011). Facile synthesis of monodispersed silver nanoparticles on graphene oxide sheets with enhanced antibacterial activity. *New Journal of Chemistry, 35*(7), 1418–1423. https://doi.org/10.1039/c1nj20076c

Liu, Q., et al. (2012). Cell imaging by graphene oxide based on surface enhanced Raman scattering. *Nanoscale, 4*(22), 7084–7089. https://doi.org/10.1039/c2nr32525j

Liu, S., et al. (2011). Antibacterial activity of graphite, graphite oxide, graphene oxide, and reduced graphene oxide: Membrane and oxidative stress. *ACS Nano, 5*(9), 6971–6980. https://doi.org/10.1021/nn202451x

Luo, J., Jiang, S., & Liu, X. (2014). Electrochemical sensor for bovine hemoglobin based on a novel graphene-molecular imprinted polymers composite as recognition element. *Sensors and Actuators, b: Chemical, 203*, 782–789. https://doi.org/10.1016/j.snb.2014.07.061

Ma, L., et al. (2013). Preparation of graphene oxide-silver nanoparticle nanohybrids with highly antibacterial capability. *Talanta, 117*, 449–455. https://doi.org/10.1016/j.talanta.2013.09.017

Ma, X., et al. (2013). Graphene oxide wrapped gold nanoparticles for intracellular Raman imaging and drug delivery. *Journal of Materials Chemistry B, 1*(47), 6495. https://doi.org/10.1039/c3tb21385d

Mao, H.Y., Laurent, S., Chen, W., et al. (2013) Graphene: promises, facts, opportunities, and challenges in nanomedicine. *Chemical Review*, *113*, 3407–3424. https://doi.org/10.1021/cr300335p

Pan, D., et al. (2012). Cutting sp 2 clusters in graphene sheets into colloidal graphene quantum dots with strong green fluorescence. *Journal of Materials Chemistry, 22*(8), 3314–3318. https://doi.org/10.1039/c2jm16005f

Patel, M. A., et al. (2013). Direct production of graphene nanosheets for near infrared photoacoustic imaging. *ACS Nano, 7*(9), 8147–8157. https://doi.org/10.1021/nn403429v

Qian, Z. S., et al. (2014). DNA nanosensor based on biocompatible graphene quantum dots and carbon nanotubes. *Biosensors and Bioelectronics, 60*, 64–70. https://doi.org/10.1016/j.bios.2014.04.006

Rajan Unnithan, A., et al. (2017). A unique scaffold for bone tissue engineering: An osteogenic combination of graphene oxide–hyaluronic acid–chitosan with simvastatin. *Journal of Industrial and Engineering Chemistry, 46*, 182–191. https://doi.org/10.1016/j.jiec.2016.10.029

Rana, V. K., et al. (2011). Synthesis and drug-delivery behavior of chitosan-functionalized graphene oxide hybrid nanosheets. *Macromolecular Materials and Engineering, 296*(2), 131–140. https://doi.org/10.1002/mame.201000307

Rashkow, J. T., et al. (2017). In Vivo hard and soft tissue response of two-dimensional nanoparticle incorporated biodegradable polymeric scaffolds. *ACS Biomaterials Science & Engineering*. https://doi.org/10.1021/acsbiomaterials.7b00425

Ruecha, N., et al. (2014). 'Novel paper-based cholesterol biosensor using graphene/polyvinylpyrrolidone/polyaniline nanocomposite. *Biosensors and Bioelectronics, 52*, 13–19. https://doi.org/10.1016/j.bios.2013.08.018

Ruiz, O. N., et al. (2011). Graphene Oxide: A nonspecific enhancer of cellular growth—ACS Nano (ACS Publications). *ACS Nano*, (10), 8100–8107. Available at: http://pubs.acs.org/doi/abs/10.1021/nn202699t%5Cnpapers2://publication/uuid/78125D25-4DD5-4A3C-AE33-45CB88322F9B

Said, K., et al. (2017). Fabrication and characterization of graphite oxide—Nanoparticle composite based field effect transistors for non-enzymatic glucose sensor applications. *Journal of Alloys and Compounds, 694*, 1061–1066. https://doi.org/10.1016/j.jallcom.2016.10.168

Santos, C. M., et al. (2011). Antimicrobial graphene polymer (PVK-GO) nanocomposite films. *Chemical Communications, 47*(31), 8892–8894. https://doi.org/10.1039/c1cc11877c

Sayyar, S., et al. (2013). Covalently linked biocompatible graphene/polycaprolactone composites for tissue engineering. *Carbon, 52*, 296–304. https://doi.org/10.1016/j.carbon.2012.09.031

Shi, X., et al. (2013). Graphene-based magnetic plasmonic nanocomposite for dual bioimaging and photothermal therapy. *Biomaterials, 34*(20), 4786–4793. https://doi.org/10.1016/j.biomaterials.2013.03.023

Shin, D., Choi, Y. S., & Hong, B. H. (2018). Graphene-enhanced Raman spectroscopy reveals the controlled photoreduction of nitroaromatic compound on oxidized graphene surface. *ACS Omega, 3*(9), 11084–11087. https://doi.org/10.1021/acsomega.8b01285

Sreejith, S., Ma, X., & Zhao, Y. (2012). Graphene oxide wrapping on squaraine-loaded mesoporous silica nanoparticles for bioimaging. *Journal of the American Chemical Society, 134*(42), 17346–17349. https://doi.org/10.1021/ja305352d

Tian, L., et al. (2014). Functionalized nanoscale graphene oxide for high efficient drug delivery of cisplatin. *Journal of Nanoparticle Research, 16*(11). https://doi.org/10.1007/s11051-014-2709-3

Vijay Kumar, S., et al. (2013). One-step size-controlled synthesis of functional graphene oxide/silver nanocomposites at room temperature. *Chemical Engineering Journal, 219*, 217–224. https://doi.org/10.1016/j.cej.2012.09.063

Wen, H., et al. (2012). Engineered redox-responsive PEG detachment mechanism in PEGylated nano-graphene oxide for intracellular drug delivery. *Small (weinheim an Der Bergstrasse, Germany), 8*(5), 760–769. https://doi.org/10.1002/smll.201101613

Xu, S., et al. (2017). 'Real-time reliable determination of binding kinetics of DNA hybridization using a multi-channel graphene biosensor. *Nature Communications, 8*, 1–10. https://doi.org/10.1038/ncomms14902

Zhang, L., et al. (2014). Boron-doped graphene quantum dots for selective glucose sensing based on the "abnormal" aggregation-induced photoluminescence enhancement. *Analytical Chemistry, 86*(9), 4423–4430. https://doi.org/10.1021/ac500289c

Zhao, W. (2016). In vitro and in vivo biocompatibility and osteogenesis of graphene-reinforced nanohydroxyapatite polyamide66 ternary biocomposite as orthopedic implant material. *International Journal of Nanomedicine*, 3179–3189.

Zheng, Q., et al. (2015). An electrochemical DNA sensor based on polyaniline/graphene: High sensitivity to DNA sequences in a wide range. *The Analyst, 140*(19), 6660–6670. https://doi.org/10.1039/C5AN01088H

Chapter 13
Mechanical Performance of 2D Nanomaterials Based Advanced Composites

Nazish Alam, Chander Prakash, Sunpreet Singh, and Subhash Singh

1 Introduction

Year 2004, proved to be a turning point in the field of two-dimensional (2-D) material with the introduction of graphene. As a result of excellent properties and its application in the field of biomedicals, optoelectronics, electronics, and electrochemical applications of graphene, comprehensive research is done on 2-D materials. Hence, a vast family of 2-D materials is discovered such as (a) transition-metal dichalcogenids (TMDs), (b) phosphorene (black phosphorous), (c) hexagonal BN (h-BN). (d) silicene, germanene, and many more.

Graphene is a monolayer, having sp^2 hybridization of carbon atoms organized in such a way so that 2-D lattice is exhibited. Graphene has enticed greatly in present days by virtue of its extraordinary mechanical and thermal properties. A flawless monolayer of graphene shows excellent mechanical properties like 130 GPa of fracture strength and 1.0 TPa of young's modulus of elasticity (Lee, 2008). Many methods of manufacturing have been developed to produce monolayer as well as multilayer of graphene in small-scale amount, having goal to search ways to produce Graphene in large amount for utilizing in applications like composites. Graphene nanosheets (GNS) and graphene nanoplatelets created through many graphene layers have shown excellent mechanical properties when compared with single layer of graphene (Chen, 2008; Fang, 2009; Li, 2008), this feature is the reason why it is assumed as extremely good reinforcement of metal matrix composites. Graphene has nanometric nature as

N. Alam · S. Singh (✉)
Department of Production and Industrial Engineering, National Institute of Technology Jamshedpur, Jharkhand 831014, India

C. Prakash
School of Mechanical Engineering, Lovely Professional University, Phagwara 144411, India

S. Singh
Department of Mechanical Engineering, National University of Singapore, Singapore, Singapore

S. Singh et al. (eds.), *Advanced Applications of 2D Nanostructures*,
Materials Horizons: From Nature to Nanomaterials,
https://doi.org/10.1007/978-981-16-3322-5_13

well as large specific surface area permits exceptional association of reinforcement along with matrix. Till now, many researchers have worked on composites of GNS and reported that there is an increase in the mechanical properties of GNS composites is way good in contrast to different composites of polymer having carbon as filler (Ramanathan, 2008).

The composite reinforced by nano-sized particles shows an improved ductility when compared with same material which is reinforced with micro-sized particles (Zhang, 2011). This is the reason why, it is fair to understand that nanoflakes of graphene will increase the ductility of metal matrix composites. The foremost issue regarding fabrication of metal composite with graphene or GNS is to distribute GNS uniformly throughout the metal composite, when dispersion is poor then there will not only decrease in efficiency as reinforcement but also leads to stacking of GNS which causes to slip on application of forces on composites. Furthermore, the generation of interface due to inadequate wettability of metal-GNS is weak, and may considerably decrease the mechanical properties of metal matrix composites/GNS. Hence, a proper distribution of GNSs and better interfacial adhesion of metal-GNS are the dominant problem while fabrication of metal matrix composites/GNS having required mechanical performance. In order find the solution to this challenge, many sincere attempts have been tried but the problem still persists.

2 Mechanical Properties of 2-D Nanomaterials

Theoretical as well as experimental ways are used for the investigation of mechanical properties of 2-D nanomaterials such as GO and Graphene. Lee et al., (2008) studied, the elastic properties as well as breaking strength of monolayer membranes of graphene, with the help of nano-indentation and observed 1.0 ± 0.1 TPa of young's modulus of elasticity. Jiang et al., (2009) probed young's modulus of Graphene by the use of molecular dynamic simulation and also by thermal vibration and observed the modulus of elasticity value varies from 0.95 to 1.1 TPa when temperature ranges from 100 to 500 K. Hence from above it is evident that graphene has excellent mechanical properties, and when this graphene, GO, GNS, FLG, etc., are used as reinforcement to prepare composites then mechanical properties of those composites will be on higher side.

Shin (2015) prepared a composite having FLG as reinforcement and Aluminium as base metal. The method used to fabricate the composite is through hot-rolling of ball-milled powder. The obtained composite is passed through tensile test in order to determine strength imparted to the Al/FLG composites. It is noted that due to grain refinement done by ball-milling, monolithic aluminium yield strength is raised by 2.6 times post-refinement of grain. Furthermore, strength increases proportionally to the percent volume of FLG; precisely on addition of 0.7% FLG by volume yield strength is increased by 1.68 times when compared to monolithic Aluminium. While a common trend is observed that there is reduction in ductility and increase in strength is noticed with the increase in FLG content in composites. In Al/FLG

composites, the strain–to-failure of composite is down by 3–5.5% in contrast to pure aluminium (~13%) which is milled. The outcome also shows that the strain field present throughout the FLGs appreciably alters the plastic flow, generating extremely localized deformation behaviour, as affirmed by the generation of the bands. Yield stress is also dependent on surface area per composite volume, and yield stress is found to be proportional to the surface area per unit volume, and this trend is also found in the composites with the two (FLG/MWCNT) reinforcements. But FLG is proved to be better and more effective reinforcement when compared with MWCNT-reinforced composites having aluminium matrix and the reason behind this is the more surface area per unit volume of FLG with respect of surface area of MWCNT, also FLG have large surface area which is around 12.8 times with respect to MWCNT and this is due to difference in geometry. Moreover, the composite fabricated through approving industrial path using low-cost graphite will improve the probable market opportunity of aluminium FLG composites.

Singh et al., (2018) fabricated aluminium metal matrix composite by introducing SiC decorated with graphene oxide and then they studied the mechanical properties achieved due to the incorporation of graphene oxide. The results achieved are shown in Fig. 1.

As seen from Fig. 1, GO decorated Al/SiC composite shows an increase in the ultimate tensile strength by about 3.4 times in contrast with pure aluminium and about 1.3 times when compared with the tensile strength of the Al/SiC composite with no incorporation of GO on SiC. Also, the yield strength is increased by about 4.2 times in contrast with pure aluminium strength and about 1.4 times when compared with Al/SiC composite. The reason for the improvement in the strength when GO is

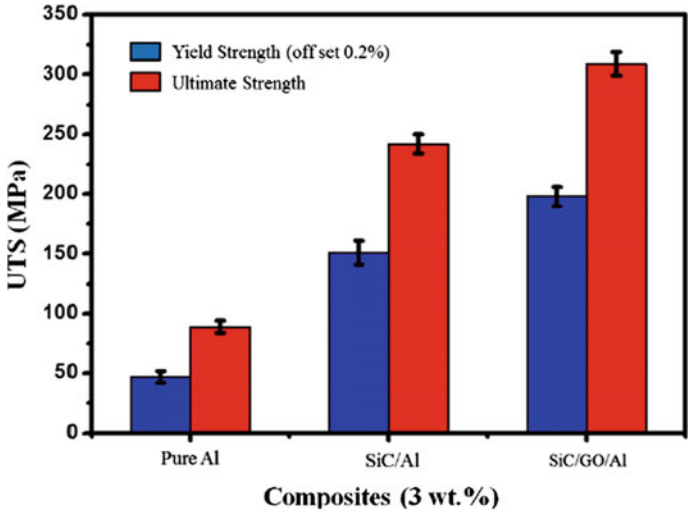

Fig. 1 Tensile strength graph of composite having 3 wt% of GO encapsulated Al/SiC (Singh, Rathi & Pal, 2018)

wrapped around SiC particles is that the GO prevent the agglomeration of particles of silicon carbide and also due to use of GO, grain size of composite is decreased and the strength is increased.

(Li, 2015) in his work fabricated a nanostructured composite with the help of graphene along with aluminium as matrix and for the preparation of composite he used cryomilling with hot extrusion method to fabricate the composite. He found through his work that as he increased the content of GNFs in the composite then the strength of the composite is also significantly increased. For instance, with the introduction of 0.5 wt% of GNFs in the composite, then the strength whether it is yield or ultimate tensile both is increased by 8.8 percent and 17.7 percent respectively in comparison to the original aluminium sample. The result of increased strength can be justified by various factors as follows. First and foremost, it is judicious to accept that GNFs which is having very high strength could be instrumental in providing very high mechanical strength to the composite. On investigation of ductility, it is observed that the ductility of the composite is first retained then decreased with the increment in the percentage of the GNFs. With 0.5 wt percent GNFs, area of contraction as well as elongation of the fabricated composite is not decreased when compared with the pure aluminium metal. This distinctive phenomenon may be illustrated in such a way that, GNFs is having vastly wrinkled structure and this wrinkle is flattened and minimized during plastic deformation, that assist in retaining of ductility of the composite (Yan, 2014). Nevertheless, composite ductility is suddenly decreased as the amount of GNFs is near 1.0 wt percentage. For example, the elongation is decreasing from 17.3 percent for pure aluminium to 8.3 percent for the composite having 1.0 wt percent of GNFs. In order to find the reason behind the decrease in the ductility of Al/Gr composite researcher observed the microstructure of the composite with 1.0 wt percent of the GNFs and the technology used for this is TEM and EDS. The observation suggested that agglomeration of GNFs is distinct especially near the grain boundaries of aluminium matrix and this agglomeration leads to weak bonding at the interface which in turn decreases the ductility of the Al/Gr composite. Contrary to ductility, when we compare the strength of composite having 1.0 wt percent and 0.5 wt percent of GNFs, we found that the strength is increased when the percent of GNFs is increased in the composite. Previously, most of the researchers have focussed their study on composite which is having reinforcement below 1.0 wt percent of graphene but (Li et al., 2015) in his work, investigated the strength of composite having higher amount of reinforcement of GNFs. The result which he found shows that the ductility as well as mechanical strength of the prepared composite decreases concurrently as the amount of GNFs goes beyond 1.0 wt percentage. This decrease in strength and ductility is usually due to increase in content of GNFs as reinforcement, as it becomes very difficult for reinforcement to disperse uniformly into the matrix (Kang & Chan, 2004), particularly the specific surface area and aspect ratio of the GNFs is very high. Hence, the improper dispersion of GNFs results in more amount of clustering and agglomeration of GNFs, which leads to decrease in ductility as well as strength of the composite. So, it is apt to say that the strength of the composite increases up to 1.0 wt percent of reinforcement but its strength is down when the amount of

reinforcement is increased beyond 1.0 wt percent and this downward trend is due to the agglomeration of Graphene at higher level of reinforcement.

The above findings are further strengthened by (Tang, 2014) who in his work investigated the mechanical properties of the composite in which he has taken graphene nanosheets as reinforcement which is decorated by nanoparticles of Nickel (GNS-Ni) and as a matrix he has taken copper. Interestingly, he found that yield strength as well as young's modulus of the GNS-Ni reinforced composite is increased as compared to that of Cu matrix. In case of pure copper, 138 MPa of yield strength and 82 GPa of young's modulus is found. Interestingly, on addition of 1.0 volume percent of GNSs in the copper matrix what they observed is enhancement of yield strength which reaches 268 MPa, an improvement of 94 percent when compared with pure copper. Similarly, an improvement of 61 percent in the young's modulus is obtained when compared with pure copper hence the young's modulus becomes 132 GPa (Fig. 2).

Such tremendous improvement in the mechanical properties is attributed to the fact that intrinsic stiffness is very high and also shearing and rupture of the composite is averted due to the high strength of the GNS, and hence graphene nanosheets provide constraints in the movement of dislocation across interface of Cu-GNS efficiently (Kim et al., 2013). Also, the nanoparticles of nickel which is attached to the GNS warrant the improvement of the strength of the GNS and this is achieved by helping in proper dispersion of GNSs as can be seen in the image of SEM. Nevertheless, the strength of the composite is improved at the cost of ductility. As they increase the content of GNSs in the composite then the ductility of the composite is decreased. This phenomenon is generally attributed to metal matrix composites because of the low ductility of the reinforcement like GNSs. Hence, for the practical purpose, a balance is needed to be maintained between ductility and the strength of the GNS-based composite. Shear-lag model (Fukuda & Chou, 1981) is generally used in case of composite for the calculation of the effective strength, σ_c, and this is obtained from the theory of load transfer between short fibers and metal matrix in case of composites. Some modification is done in shear lag model (Ryu et al., 2003), according to this

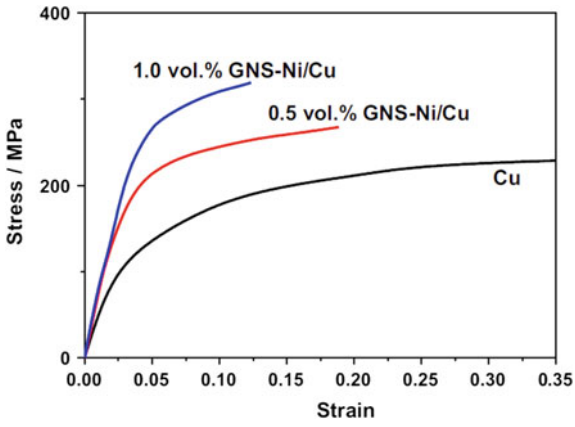

Fig. 2 Stress versus strain curves of Cu/GNS-Ni composite and pure copper samples (Tang et al., 2014)

model, effective strength of the composite, in which GNSs is randomly distributed, is represented as;

$$\sigma_c = \sigma_m(1 + pV)$$

where, σ_m is matrix yield strength, p and V are the aspect ratio and fraction volume of the GNSs, respectively. A fine analysis of results between the experimental and theoretical measurements also back the model of shear-lag and shows that this model is accurate enough to provide a path for the projection of the strength of metal/GNS composites.

Another researcher (Rashad et al., 2014) studied the impact of Graphene naoplatelets when added to the pure aluminium, for this, he has prepared a composite using powder metallurgy technique. On study of density of the composite, he has found that with the inclusion of graphene nanoplatelets, leads to the decrease in the density (theoretically calculated) as compared to the density of the pure aluminium. Interestingly, densities that are calculated experimentally for composite as well as pure aluminium are more than that of theoretical ones. This may be a sign of generation of aluminium oxide formed due to the sintering process. As, aluminium oxide is having higher density with respect to GNPs and aluminium hence, theoretical densities are somewhat less than the densities measured experimentally. On introduction of GNPs in pure aluminium experimental density drops. As, pure Al is having higher density than that of the GNPs, hence density of the composite shows lesser density as compared to pure aluminium. For the determination of hardness of composite vicker's method is used. They conducted Vickers hardness and found that the harness of pure aluminium is less than that of its composite and this increase in hardness is a mark of proper distribution of GNPs in the composite. Similarly, analysis of tensile strength is also done for the nanocomposite. By adding 0.3 wt percent of GNPs in the pure aluminium they get ultimate tensile strength rises by 280 MPa and yield strength is improved by 195 MPa. This rise in strength is due to the presence of graphene nanoplatelets in the composite. GNPs is having thermal expansion of 10^{-6} K^{-1} that is equal to that of graphite, Whereas aluminium has thermal expansion coefficient of 23.6×10^{-6} K^{-1}. So, there is a difference in coefficient of thermal expansion of the composite and pure aluminium and this difference is the reason behind prismatic punching of dislocations at the point of interface, which results in improvement of strength of GNPs/Al composite. Surface area of GNPs particles decides the density of dislocation. Dislocation density is inversely proportional to size of GNPs particles that means strength of the composite is enhanced as the density of dislocation is more and the density of dislocation is more for the smaller size of the GNPs particles (Arsenault & Shi, 1986). Since there is difference in the coefficient of thermal expansion between the composite and the pre aluminium this difference will give rise to the yield strength of composite as well.

Researcher (Chen, 2012) has fabricated a metal matrix nanocomposite in which he has taken magnesium as matrix and GNPs as reinforcement and for the preparation of composite he has used novel processing method which is combination of solid-state stirring and also used process of liquid state ultrasonic processing. The

nanocomposite developed is further investigated to determine the microhardness of the composite. The hardness of the nanocomposite having 1.2 volume percent of GNPs is found to be 66 kg mm^{-2}, a increase of 78 percent in hardness as compared to the pure magnesium. They also analyzed the strength attained due to reinforcement on the magnesium matrix, found on the basis of expression of R;

$$R = (H_c - H_m)/V_f H_m.$$

Here, H_m is the hardness of matrix, H_c represents the hardness of the composite, and also V_f represent the reinforcement in fraction of volume and R represents the strengthening efficiency (Cha, 2005). The strengthening efficiency of GNPs on magnesium is up to 64. The impact of strengthening due to GNPs on pure magnesium may involve limitation in the movement of dislocation and also include bearing of load. The fine bonding between magnesium matrix and GNPs enable the transfer of stress to more strength GNPs by magnesium matrix (Evans et al., 1999). The GNPs provide hindrance in the path of movement of dislocation in the matrix thereby increasing the strength of the composite. As, there is no perfect equation to determine the strength of the nanocomposite so, analysis of strength of nanocomposite is still an issue.

Ashwath et al. (2018) prepared samples of composite in which aluminium alloy AA2900 is selected as matrix and for the reinforcement they have chose nanosized particles of graphene. Composite prepared is further heat treated to study its impact on the mechanical properties. The composite prepared are analyzed for the determination of hardness achieved by composite. For this Rockwell hardness test is performed on the composite samples. In order to minimize the variation in result, approximately 5 readings are considered in the measurement of hardness. Results of Rockwell hardness distinctly reveals that as the weight percent of reinforcement is increased in the composite, hardness is also increased with the increase in the percent of reinforcement. Also, it is evident from the hardness test that as we increase the duration of heat treatment done on the composite, we will get an improvement in the hardness of the composite.

From the above Table 1, it is clear that as we increase the wt% of graphene in the composite having AA2900 aluminium alloy as matrix, then the ultimate tensile strength of the composite is also increased as it can be noted from the test result that with the 0.75 wt% of reinforcement we get tensile strength of 283.7 MPa. Also, it can be seen that as we do heat treatment to the composite its strength increases. If

Table 1 Result of tensile strength for AA 2900 (Ashwath et al., 2018)

S. No.	Reinforcement	Weight %	AA2900		
			As Sintered	1 h Aged	2 h Aged
1	Graphene	0.25	244.5	271.1	312.4
2		0.50	261.2	293.7	337.2
3		0.75	283.7	309.9	351.7

we increase the duration of heat treatment of the composite then with the increase in the duration of heat treatment we get higher strength. For, 0.75 wt% of graphene, if we do 1 h of aging we observed an increase of 10 percent in the strength of the composite and after 2 h of aging we observed an increase of about 25 percent in the strength of the composite. So, we can easily understand that by increasing the wt% of reinforcement in the AA2900 aluminium alloy an increase in the hardness as well as strength is observed.

Ponraj et al. (2017) prepared a composite with GNS as reinforcement and for matrix copper is used. He investigated the proper distribution of GNS in the different morphology of copper powder (Cu). For the purpose of achieving different morphologies of copper milling process is done on the powder of the copper. Hardness of the composite is determined by Brinell hardness test. For Brinell hardness test steel ball is used and a force of 29KN is applied. The composite prepared is having BHN value 60 and in this composite copper in powder form is used having spherical morphology, after milling of copper in spherical form for 8 h BHN value rises to 70, in case of copper in dendritic form is milled for 8 h then (75 BHN) value is even more than the BHN value of copper in spherical form, when copper powder in flake form is milled for duration of 16 h then the BHN value is increased to 83. A 20 percent increase in the hardness of the composite is observed when particles of copper are in flake form and is milled for 16 h. Nevertheless, the maximum hardness (81 BHN) is obtained by the composite when 2 wt% of GNS is used as reinforcement and particles of copper in dendritic form is used as matrix to prepare a composite. The greater hardness is achieved when copper in dendritic form is milled for the time period of 16 h. This increase in hardness is achieved due to the reason of getting finer grain and strain hardening imparted due to the milling operation on the composite. The reason is that the size of particles is inversely related to the hardness of the composite i.e. Hall–Petch effect. The increase in the amount of reinforcement has similar impact to improve the hardness by proper distribution and interfacial strength. If reinforcement is properly and uniformly dispersed then it will have potential to control the transferring of load, and when the reinforcement is not uniformly distributed then it will indicate the failure of the composite.

El-Ghazaly et al. (2017) fabricated a composite in which he has taken AA2124 aluminium alloy in the powder form and graphene as reinforcement. The composite thus prepared by process of milling and hot extrusion were analyzed and its hardness, tensile strength, and wear rate are measured. Vickers hardness test is carried out to measure the macro-hardness of the composite. Macro hardness in the transverse direction is increased by 133% when the composite is reinforced by graphene with 3 wt%. But, when the weight percentage of graphene is increased to 5, then the macro hardness of the composite is increased by 102%. Despite the fact that the microhardness is enhanced with the increase in the percent of the reinforcement, but in case of macro-hardness we see the reverse trends. This may be described by the way of micro-hardness testing is done, which assesses the hardness at the micron level and doesn't include the area of cavitation and porosity. The tensile strength of the nanocomposite is also measured, in each case three samples are tested to get the average value of the strength. Composite with 3 wt percent of graphene and

AA2124 as matrix resulted in enhancement in yield strength by 104 percent and ultimate strength is increased by 20.4%. Whereas when we add 5 wt percent of graphene in the composite then the yield strength is enhanced by 127% and ultimate strength is increased by 21.6%. The young's modulus of elasticity of the composite nearly remains same specifying that there is no significant impact of the addition of graphene as reinforcement of composite. Addition of graphene as reinforcement showed a downward trend in ductility i.e. with 3 wt% of graphene there is a decrease of 58 percent in the ductility whereas in case of 5 wt% of graphene addition there is a decrease of 62% in ductility. This behavior concurs with the enhancement in the hardness of composite achieved owing to the addition of the graphene.

3 Application of 2-D Nanomaterial-Based Advanced Composite

The nanocomposite fabricated finds many applications in the field of structural construction, bio-medicals, and also in the aerospace industry. The extensive use of aluminium in the aerospace and automotive industry, makes of aluminium–matrix nanocomposite a key option to fulfil challenges in the structural design of components. For this, selection of reinforcement is important for maximizing the mechanical properties of the composites. The use of nanosized reinforced material for the fabrication of composites has shown very positive impact on the mechanical properties of final products. Recently, graphene is used as reinforcement particularly in case of aluminium-matrix composite (Bartolucci, 2011; Wang, 2012). The nanosized reinforcement has very large specific surface area which permit tremendous interaction with matrix even when content of reinforcement is very small. As we have seen that in the advance composite the mechanical properties are enhanced tremendously due to the incorporation of graphene or other 2-D nanomaterials as reinforcement that is why it finds application in the aerospace industry. A detailed list of application in the field of aerospace is compiled by (Evans et al., 2011). Some of the application is listed here. Aeronautical metal matrix composites have many applications especially in the aeropropulsion, aerostructural and sub-system group. The items in aerostructural are sleeves of rotor blade, aircraft F-16 fuel door cover, and ventral fins. Components of metal matrix composites that find application in the recreational market are spikes of track, bicycle tubing, and lacrosse stick shaft. In order to impart enhanced wear resistance and smaller stopping distances, the surface of braking on the rims of bicycle is applied with coatings of MMC. Besides, the application in the aerospace industry, these advance composites are used in the construction work in order to provide high strength and stiffness to the structures.

4 Conclusions

Since we have seen the research works of many researchers and from that discussion it can be easily concluded that while fabrication of advance composite, 2-D graphene, TMDs, etc. are used as reinforcement then the strength of the composite is increased tremendously. It is evident that on increasing the amount of reinforcement in the composite we get increased strength. But, when the amount of reinforcement goes beyond a certain level then the strength shows downward trend. Similarly, the hardness and wear resistance of the composite is enhanced with the increase in the percentage of the reinforcement in the composite. However, for macrohardness, hardness of the composite have showed downward trend with increase in the content of the reinforcement, and the reason behind this is that in microardness the focus is at the micron level neglecting the defect and porosity of the composite, but such is not the case with the macrohardness. This increase in hardness, strength and wear resistance of the composite make them right choice for the construction work, aerospace industry, etc.

However, there are still some issues to be sorted out for more effective utilization of the composites. Some of them are non uniform dispersion of the reinforcement in the matrix. This nonuniform distribution of the reinforcement leads to decrease in the mechanical properties of the fabricated composite. That is why uniform distribution is key parameter to be kept in mind while fabrication of composite. Also, there is a need to work on the cost-effective development of the 2-D nanomaterials such as graphene, so, that they can be more commonly used.

References

Arsenault, R. J., & Shi, N. (1986). Dislocation generation due to differences between the coefficients of thermal expansion. *Materials Science and Engineering*. https://doi.org/10.1016/0025-5416(86)90261-2

Ashwath, P., et al. (2018). Heat treating studies of graphene reinforced aluminium metal matrix composite. In *Materials Today: Proceedings* (pp. 11859–11863). Elsevier Ltd. https://doi.org/10.1016/j.matpr.2018.02.157

Bartolucci, S. F., et al. (2011). Graphene-aluminum nanocomposites. *Materials Science and Engineering A*. https://doi.org/10.1016/j.msea.2011.07.043

Cha, S. I., et al. (2005). Extraordinary strengthening effect of carbon nanotubes in metal-matrix nanocomposites processed by molecular-level mixing. *Advanced Materials*. https://doi.org/10.1002/adma.200401933

Chen, H., et al. (2008). Mechanically strong, electrically conductive, and biocompatible graphene paper. *Advanced Materials*. https://doi.org/10.1002/adma.200800757

Chen, L. Y., et al. (2012). Novel nanoprocessing route for bulk graphene nanoplatelets reinforced metal matrix nanocomposites. *Scripta Materialia*. https://doi.org/10.1016/j.scriptamat.2012.03.013

El-Ghazaly, A., Anis, G., & Salem, H. G. (2017). Effect of graphene addition on the mechanical and tribological behavior of nanostructured AA2124 self-lubricating metal matrix composite. *Composites Part A: Applied Science and Manufacturing*. https://doi.org/10.1016/j.compositesa.2017.02.006

Evans, A., San Marchi, C., & Mortensen, A. (2011). *Metal matrix composites in industry*. https://doi.org/10.1007/978-1-4615-0405-4

Evans, R. D., Phaneuf, M. W., & Boyd, J. D. (1999). Imaging damage evolution in a small particle metal matrix composite. *Journal of Microscopy*. https://doi.org/10.1046/j.1365-2818.1999.00631.x

Fang, M., et al. (2009). Covalent polymer functionalization of graphene nanosheets and mechanical properties of composites. *Journal of Materials Chemistry*. https://doi.org/10.1039/b908220d

Fukuda, H., & Chou, T. W. (1981). An advanced shear-lag model applicable to discontinuous fiber composites. *Journal of Composite Materials*. https://doi.org/10.1177/002199838101500107

Jiang, J. W., Wang, J. S., & Li, B. (2009). Young's modulus of graphene: A molecular dynamics study. *Physical Review B—Condensed Matter and Materials Physics*. https://doi.org/10.1103/PhysRevB.80.113405

Kang, Y. C., & Chan, S. L. I. (2004). Tensile properties of nanometric Al_2O_3 particulate-reinforced aluminum matrix composites. *Materials Chemistry and Physics*. https://doi.org/10.1016/j.matchemphys.2004.02.002

Kim, Y. J., Kim, J. W., & Kim, S. S. (2013). Preparation and electrical properties of chemical solution deposited Ho- and Ti-co-doped $BiFeO_3$ thin films. *Ferroelectrics*. https://doi.org/10.1080/00150193.2013.846153

Lee, C., et al. (2008). Measurement of the elastic properties and intrinsic strength of monolayer graphene. *Science*. https://doi.org/10.1126/science.1157996

Li, D., et al. (2008). Processable aqueous dispersions of graphene nanosheets. *Nature Nanotechnology*. https://doi.org/10.1038/nnano.2007.451

Li, J. L., et al. (2015). Microstructure and tensile properties of bulk nanostructured aluminum/graphene composites prepared via cryomilling. *Materials Science and Engineering A*. https://doi.org/10.1016/j.msea.2014.12.102

Ponraj, N. V., et al. (2017). Effect of milling on dispersion of graphene nanosheet reinforcement in different morphology copper powder matrix. *Surfaces and Interfaces*. https://doi.org/10.1016/j.surfin.2017.10.006

Ramanathan, T., et al. (2008). Functionalized graphene sheets for polymer nanocomposites. *Nature Nanotechnology*. https://doi.org/10.1038/nnano.2008.96

Rashad, M., et al. (2014). Effect of Graphene Nanoplatelets addition on mechanical properties of pure aluminum using a semi-powder method. *Progress in Natural Science: Materials International*. https://doi.org/10.1016/j.pnsc.2014.03.012

Ryu, H. J., Cha, S. I., & Hong, S. H. (2003). Generalized shear-lag model for load transfer in SiC/Al metal-matrix composites. *Journal of Materials Research*. https://doi.org/10.1557/jmr.2003.0398

Shin, S. E., et al. (2015). Strengthening behavior of few-layered graphene/aluminum composites. *Carbon*. https://doi.org/10.1016/j.carbon.2014.10.044

Singh, S., Rathi, K., & Pal, K. (2018). Synthesis, characterization of graphene oxide wrapped silicon carbide for excellent mechanical and damping performance for aerospace application. *Journal of Alloys and Compounds, 740*, 436–445 (Elsevier B.V.). https://doi.org/10.1016/j.jallcom.2017.12.069

Tang, Y., et al. (2014). Enhancement of the mechanical properties of graphene-copper composites with graphene-nickel hybrids. *Materials Science and Engineering A*. https://doi.org/10.1016/j.msea.2014.01.061

Wang, J., et al. (2012). Reinforcement with graphene nanosheets in aluminum matrix composites. *Scripta Materialia*. https://doi.org/10.1016/j.scriptamat.2012.01.012

Yan, S. J., et al. (2014). Investigating aluminum alloy reinforced by graphene nanoflakes. *Materials Science and Engineering A*. https://doi.org/10.1016/j.msea.2014.06.077

Zhang, Z., et al. (2011). Mechanical behavior of ultrafine-grained Al composites reinforced with B_4C nanoparticles. *Scripta Materialia*. https://doi.org/10.1016/j.scriptamat.2011.06.037

Conclusion

The new set of materials discovered in the recent decade, initially in the year 2004, has vast expectations in terms of their applications. Termed as two dimensional or 2D materials, they are sheet structured with a thickness of one atom. Though the interest on these materials is on a high from the research perspective, it is absolutely important to thoroughly assess their behaviour by putting them through various tests. Once clarity is obtained on their characteristics, only then can they be employed in social applications. Apart from graphene, the research on other 2D materials is limited to the extent that only partial characteristics knowledge and few manufacturing methods are known. The wide prospects of 2D materials in diverse applications are due to simplified fabrication techniques with good yield and superior material properties that can be effortlessly controlled. Hence, the interest on 2D materials is clearly evident from all science fields since they exhibit exceptional physical, chemical and magnetic characteristics as compared to the conventional materials. The 2D materials may be broadly classified as the graphene family, 2D oxides and 2D chalcogenides. These materials are significant compared to other materials due to their optical, electrical as well as catalytic applications. It is these properties that have been utilized in applications related to bio-sensing, energy production and catalysis. The manufacturing techniques of 2D materials are broadly classified as mechanical and chemical exfoliation methods. The mechanical exfoliation provides versatility and low cost, whereas chemical exfoliation provides chemical homogeneity and molecular-level mixing. The synthesis and fabrication processes control the morphology and size of product which further improves the performance of 2D nanostructured materials in different applications.

Recently, the applications of graphene oxide have gained popularity in electronics, biomedicine, biosensors, water purification and electrochemical sensors. This is due to the plush oxygen-comprising functionalities on the surface of graphene oxide which facilitates easy chemical modification. Moreover, the 2D materials find themselves in nano-coatings and thin films. The nano-films of GO and graphene are in wear resistant, friction applications, electronic applications and bio-applications.

S. Singh et al. (eds.), *Advanced Applications of 2D Nanostructures*,
Materials Horizons: From Nature to Nanomaterials,
https://doi.org/10.1007/978-981-16-3322-5

The structure of graphene obstructs chemical movements and makes it an excellent protector against corrosion. But research also supports corrosive nature of graphene due to graphene's conductivity and forming galvanic cell. The TMDs include materials like MoS_2, WS_2 and the coatings of TMDs, or the thin film applications are used in solid lubricants for space applications. The friction and wear-resistant applications of TMDs include composite films where 2D materials are additives. The h-BN coatings find its applications in corrosion resistant as well as electronic applications. The h-BN proved to have better corrosion characteristics than graphene. One of the recently rediscovered materials is black phosphorous (BP) which has its applications in electronics. There are no other applications of BP apart from electronics. Apart from these, the 2D material coatings enhance the mechanical properties on metal surfaces, and usually, CVD technique is employed for the deposition of uniform 2D material coatings.

A unique 2D material, MXenes, has been discovered since graphene having exceptional electrochemical properties allowing it to be extremely efficient for storing energy in electrochemical devices, especially in the generation where there is increasing dependence on portable electronic devices, electric vehicles and grid-connected power storage units. Research is being done on MXenes and their hybrids for supercapacitors and rechargeable batteries. Novel methods have been adopted for optimum intercalation, exfoliation and to remove inclusions in the thin films of MXenes. Hence, MXenes are also used as transparent conductive electrodes (TCEs). MXenes TCEs are ideal in supercapacitors as they possess immense power density, large volumetric capacitance and exceptional conductive characteristics with superior lifetime. Promising results give a wide future scope for MXenes as TCEs. Apart from the applications of 2D materials in thin films and TCEs, the nanosheets of 2D metal oxides have been found significant in the form of nanocomposites to replace nanoparticles, quantum dots and nanowires/rods in the preparation of thin films for gas sensing. The concept is to utilize the ability of metal oxides (MOs) to detect gas in thin films by employing occurrences like adsorption and desorption of gases in extreme temperature conditions. The chemically exfoliated 2D nanosheets of MOs are flexible, transparent, photosensitive and semiconducting with high ratios of specific surface area to volume. The nanosheets of MOs exhibit unique customizable physiochemical characteristics when combined with other organic/inorganic substances. Hence, they find place in electronics like photodetectors sensors, nanoelectronic/magnetic devices and photovoltaic solar cells (PVSCs). For the practical use of devices having nanosheets of MOs in conjunction with other organic/inorganic biomolecules, appropriate techniques are unavailable to produce identical components in large volumes. Though nanosheets of MOs have regular shapes, it is difficult to densely pack them in thin films and use as building blocks. Novel techniques should be explored.

One important aspect of 2D material analysis is its modeling and simulation. Multiscale simulation methods help the researchers to integrate with analytical tools necessary for understanding the material behaviour. Diverse methodologies of simulation generate an opportunity to analyse the required characteristics of nanomaterials and develop novel nanostructures. This helps in reducing costs associated with

nanomaterial synthesis produced via complex experimental setups. Acute evaluation of these methods might alter or create new algorithms for further evaluation of various nanostructures. The field of nanotechnology has become interdisciplinary and enhanced product development to the next level by the use of nanoparticles (2D nanosheets/carbon nanotubes) which also enhanced the productivity. The conjunction of graphene and carbon nanotubes enhances the material characteristics in terms of strength, load and stress bearing capabilities which allow the fabrication of materials with desired properties. There are associated uncertainties such as enhanced chemical reactivity which need to be sorted out. Hence, superior knowledge is necessary on nanomaterials and their applications for wider prospects. The 2D nanomaterials due to their surface morphology, high surface–volume ratio and anisotropic nature have a wide scope in biomedical and bioengineering fields. The flexible characteristics of 2D materials in terms of construction and design exhibit their suitability in drug/gene delivery, bio-imaging, bio-sensing, antimicrobial activities and various therapeutic applications. Also, 2D black phosphorus with unique characteristics exhibits wide future prospects in this field. Adequate knowledge on the material toxicity ensures use in vitro and in vivo experimentation. The future possibility of 2D material use is for in vivo gene transformation which needs further research. The influencing factors like concentration, size, density and time on 2D materials are being analysed for antibacterial applications. The high strength of nanomaterials leads to their applications in bioimplants and also tissue engineering. The bio-imaging graphene quantum dots are an option as they exhibit low toxicity, but they have low productivity. Hence, it is essential to investigate the biological characteristics exhibited by 2D materials to ensure acceleration in the biomedical field.

Research is also advancing in the manufacturing of composites based on 2D materials (TMDs and graphene) which are applied as reinforcements that enhance the material strength. Optimum quantity of the reinforcement is needed to ensure good mechanical characteristics like high strength, hardness and wear resistance. If not, reduced strength is observed with further increase in the reinforcement levels. Certain aspects need to be sorted before 2D material composites are efficiently utilized. Uniformity in the reinforcement dispersion and cost-effective techniques needs to be established for manufacturing 2D composites. Hence, it can be strongly concluded that 2D materials with unique characteristics and with wide range of applications are a strong prospect for the future. Also, with plenty of information to be tapped, they are certainly of great research interest.